FOG

Freiberg Online Geoscience

FOG is an electronic journal registered under **ISSN 1434-7512**

2021, VOL 60

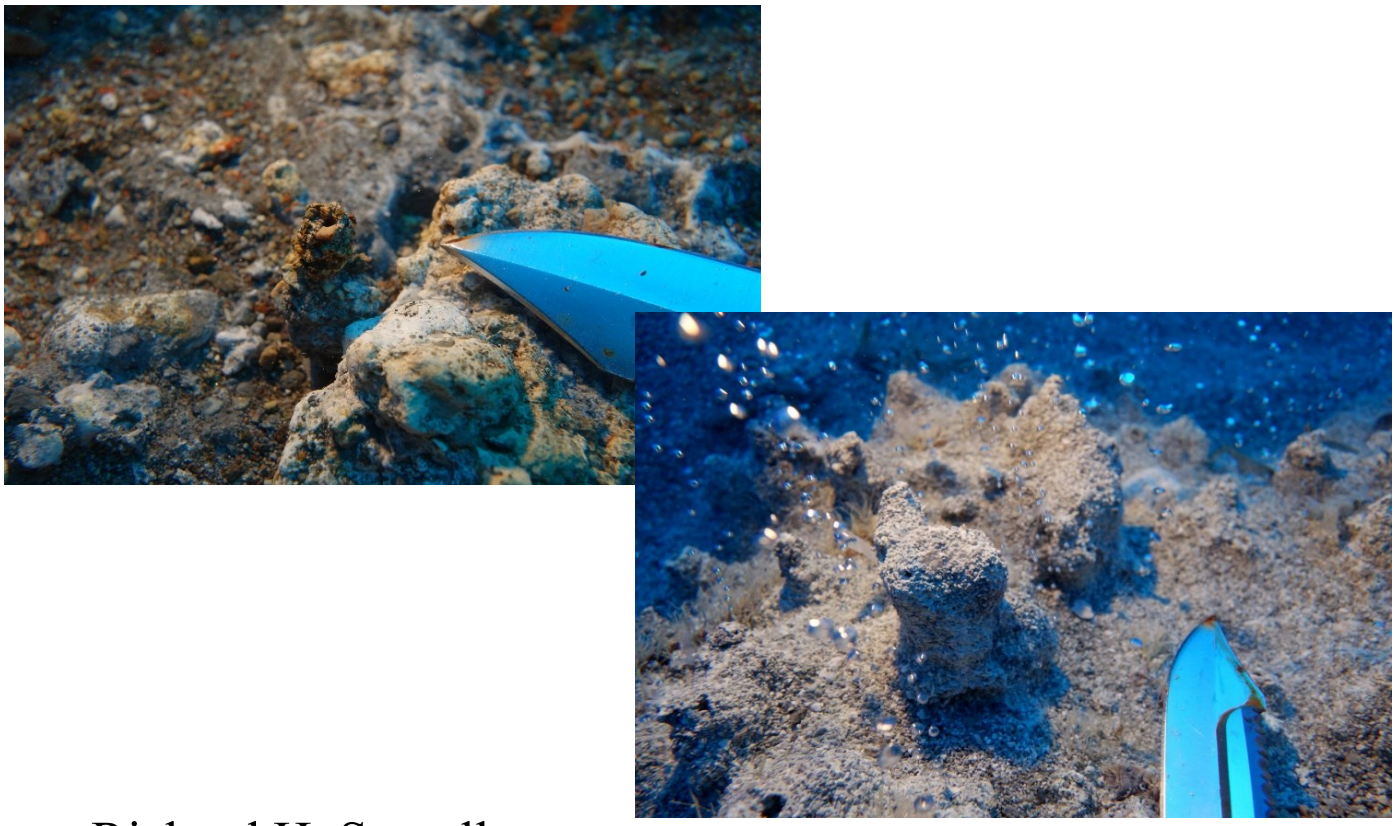

Richard H. Stanulla

Geological and mineralogical investigation of hydrothermal fluid discharge features at the sea bottom of Panarea, Italy

174 pages, 63 figures, 13 tables, 226 references

A. Acknowledgements

At first, I would like to thank my supervisor Prof. Dr. Broder Merkel, who was one of the most important persons during the realization of my research. He enabled me to overcome all bureaucratic issues and always had an open ear for any problems.

My deepest thank goes to Dr. Thomas Pohl, Robert Kühn, Alfred Vinmans and the whole staff of CMAS Scientific Diving Center at TU Freiberg for excellent co-working during the fieldtrips and beyond.

Special thanks go to Judy Adamek for advices not only on language issues, mapping in Panarea and image processing as well as to my students Andreas Prautzsch, Christoph Bender and Victoria Kürzinger who supported my thesis with their projects. Karin Heinzig and Claire Cariven were a great help with bibliographic issues, drawings and video post-production. Furthermore, I thank Christiane Gold, who encouraged me during main parts of the research project and helped with patience, competence and critics whenever needed.

Despite that, this thesis would not have been possible without a variety of support from different institutions. As no research position was funded, a lot of work had to be realized by private capacities. The more complex things got due to this situation, the more grateful I was to receive funding for travel expenses and fieldwork in Italy. Funding was granted by the German academic exchange service DAAD with the program IDIP 4 all. Furthermore, the VFF e.V. and ffg e.V. supported the work by specific funding for the individual fieldtrips.

The fieldwork was supported by Angela from the Hotel Lisca Bianca and her crew who helped the teams of TU Freiberg over more than a decade providing the field laboratory and accommodation. Additionally, the teams of Francesco Sesso (EoloSub Diving Center) and Andrea Fogliuzzi (Amphibia Diving Center) were a great help during the diving campaigns.

I am also very grateful to the personnel of the different laboratories and institutions that helped me with different analysis of my samples. In alphabetic order these are:

Andreas Bartzsch and staff (HIF Freiberg; preparation), Dr. Thomas Leißner (MVTAT TU Freiberg; XCT), Dr. Robert Möckel (HIF Freiberg; XRF), Anja Obst (Institute of Geology, TU Freiberg; REM-EDX), Dr.-Ing. Elsa Qoku, M.Sc. (IKGB, TU Freiberg; XRD), Gitta Schneider (Institute of Geology, TU Freiberg; particle size analysis), Prof. em. Dr. Jörg Schneider (Institute of Geology, TU Freiberg; Paleostructures), Dr. Marcus Schreiner (IEC, TU Freiberg; μXRD) and Prof. em. Dr. Klaus Stanek (Institute of Geology, TU Freiberg; REM-EDX).

Last but not least I thank my reviewers Dr. Sven Petersen and Dr. Francesco Italiano for their review of the thesis.

B. Table of Content

C. List of Abbreviations

Abbreviation	Denotation
3B	3-Bowls
A26	Area 26
AL	alteration
BA	Basiluzzo
BN	Bottaro North
Bo	bowl structure, other
BP	Black Point
BR	Black Rock
BRO	Brodor
BS	bowl structure, sulfurous
BW	Bottaro West
CA	Cave
Cc	cone, consolidated
CE	cementation
CEclay	cement, clay
CEfe	cement, iron
CEo	cement, other
CEore	cement, ore
CEs	cement, sulfurous
CMAS	Confédération Mondial des Activités Subaquatiques, world underwater federation
Cu	cone, unconsolidated
DEM	digital elevation model
FE	fluid erosion
FF	Fumarolic Field
Fo	fracture fill, other
Fore	fracture fill, ore
FS	fracture fill, sulfur
GE	gas erosion
HB	Hot Bowl

Abbreviation	Denotation
HL	Hot Lake
LC	La Calcara
Lo	lineament structure, other
Lpal	lineament structure, paleo/preserved
LS	Lineament Structure (UWIS)
LSs	lineament structure, sulfurous
LT	Lava-Tongue
LWH	length, width, height
m asl/bsl	meter above/below sea level
MBP	Mini-Black-Point
mfo	mixed fluid outlet
MM	Mini-Mouth
MOR	Mordor
MOU	The Mouth
MP	mineral precipitation
MVTAT	Institute of Mechanical Process Engineering and Mineral Processing at TU Freiberg
NR	New Rock
OR	Octopus Rock
P21	Point 21
PAN	Panarea
TFe	tube, iron cemented
To	tube, other
Tore	tube, ore cemented
Tpal	tube, paleo/preserved
TS	tube, sulfurous cemented
TSce	tube, sulfurous cemented
TSpu	tube of native sulfur
UWIS	underwater investigation site

D. Glossary

This glossary aims to give a defined meaning on terms used in this thesis, that have different meanings and might therefore be misunderstood. This list is not an attempt to give any generally accepted definition. It is simply an aid for the reader and serves the harmonization of varying points of reading.

Term	Usage
active	Mostly used in the context of discharges. An active hydrothermal discharge is emitting fluids at the time of investigation, which was witnessed by the author or a cited working group. Sensu “active volcano”: a volcano is called “active” if it has at least one eruption over the last 10 ka.
ancient	Concise evidence is given for a hydrothermal discharge that is permanently inactive/extinct and will probably never again emit fluids.
former	Temporal usage, in terms of “in the past”.
fracture	A crack or fissure in the underground which can act as a pathway for hydrothermal fluids. No structural geological implication.
genetic model	Theoretical scheme of the supposed development of a type of structure/feature.
habitus	Outer appearance of a feature. No mineralogical implication.
hydrothermal feature	Characteristic structure of varying scale that is built by hydrothermal processes such as hydrothermal discharge.
hydrothermal fluid	Mixture of water and gas being influenced by the hydrothermal system. Fluids might either be directly fed by magmatic fluids (direct influence) or consist of ocean water that infiltrated the host rock and is heated by the magmatic body or hydrothermal system (indirect influence).
inactive	On the contrary to an “active” discharge, an inactive discharge does not emit hydrothermal fluids at the time of investigation but could emit fluids in the future.
paleo	Paleo features originate from former times in geological timescales. They are consequently preserved and lithified structures and do not show any activity today.
preservable	Preservable structures may potentially be lithified or preserved in another way to the paleo rock record. However, the necessary conditions have to prevail to realize this process (fossilization).
secondary structure	Geological, sedimentary, or hydrothermal feature, that developed temporarily after the surrounding structures or strata (i.e. mineral precipitation from hydrothermal fluids coating preexisting gravel).
shallow water	Water depths of up to 150 m, that are more or less directly accessible for scientific investigation, i.e. by scuba/tec divers.

E. Abstract

The shallow marine hydrothermal system of Panarea, Italy, is part of the Aeolian Arc and comprises continuous active venting of hydrothermal waters and gases. The hydrothermal discharge causes numerous unique mineral formations as well as sedimentary and hydrothermal features that are in focus of this research.

The interaction of processes at the ocean-sea floor-interface is controlled by a complex suite of factors. These include the hydrothermalism itself and the resulting discharge behavior of the vent sites, marine features such as currents and waves, and geological characteristics like the grainsize of prevailing sediments or the host rock lithology. Regional tectonic processes are responsible for pathway generation inducing hydrothermal fluid migration. Also biological aspects, such as microbial activity (microorganisms) or structural influences of macroorganisms (i.e. macrophytes), belong to the key factors. The complex interaction of those variables results in hydrothermal discharge features that occur in different facies in the Panarea system. Their limited occurrence raises a variety of scientific questions on the processes evolving at the ocean-sea floor-interface. The formation of such hydrothermal discharge features also is of high interest. This includes their genesis and their preservation potential as well as the evolution of single individuals of these structures. Thus, the investigations presented in this thesis focus on lithological aspects, the genesis of hydrothermal discharge features and their facies variations as well as their preservation potential.

To answer the questions concerning facies differentiation and genetic processes, the prevailing work summarizes a broad span of field- and laboratory investigations. Mapping, documentation, and sampling campaigns were conducted on-site. The samples were investigated in form of thin and polished sections by optical microscopy and SEM. Structural and geochemical approaches such as XRD, XRF, XCT and EDX complete the survey in the laboratory.

As a result, a total of 15 lithofacies could be identified in the emergent parts of the Panarea system. Hardrock facies include dacites/andesites, tuffites and dykites. Sandstones, conglomerates and fanglomerates represent the sedimentary facies. Various, mostly recent, sediments occur in the system as well. The findings contradict and update the information given in common literature, which describes only three lithofacies.

STANULLA et al. (2017a) present a first data set on characteristic discharge features and their genesis. Their facies classification is based on the host rock type and distinguishes between hard and soft rock. Hard rocks can form structures induced by gas erosion or formed by mineral precipitation (fracture fills) whereas soft rock facies include different types of cones and tubes.

As this facies classification (based on data from 2010 to 2012) turned out to be partly defective, a completely revised and updated classification is given in the prevailing work, considering a further five years-investigation timespan.

The facies differentiation is now based on the processes involved in the formation of hydrothermal discharge features. Thus, it can be divided into destructive and constructive processes. Destructive processes include subrosion and erosion (by standard agents or fluid dynamics). The term *constructive processes* summarizes mineral precipitation, cementation, alteration, and other aspects such as grain transportation due to the venting flow rates. In most cases, constructive and destructive processes interact very closely and periodically.

Characteristic hydrothermal features can be divided into six major groups: channels, fractures (or fracture fills), tubes, cones, bowls, and lineaments. A final stadium of the proposed evolutionary scheme can potentially form so called “lakes”, which are in fact large-scaled bowls. Each of these groups subdivides into numerous facies types according to the cements or mineral precipitates prevailing. Cements are mostly made of iron or sulfur-bearing minerals, massive sulfide ores or clayish facies. Seldomly also other cements such as quartz or rhodochrosite occur. In single cases, also parameters such as the preservation potential or the general habitus were taken into account for the classification.

To clarify the rather complex formation processes of hydrothermal discharge features, genetic models for each facies are proposed. An integrated evolutionary model is developed considering the temporal evolution of the major types of hydrothermal discharge features in the Panarea system.

Confirming presumptions of former, preliminary data, the first documentation of secure paleo-evidences of hydrothermal discharge features is presented. This testifies the preservation potential of hydrothermal discharge features in the rock record. Beyond doubt, the lithifaction processes necessitate distinct environmental and sedimentary conditions to preserve the fragile features.

Despite the variety of new descriptions and key findings on hydrothermal features, the investigations bring up a number of new scientific questions and research topics. For instance, a comparison to other hydrothermal systems (i.e. Milos Island, Iceland, Caribbean) would help to corroborate the hypotheses of this work. Especially the verification and documentation of yet hypothetical transitional facies in the evolutionary model would clarify the genetic and evolutionary processes in more detail. Also, the documentation of further appearances of hydrothermal discharge features in the rock-record and different types of lithifaction under varying environmental conditions will give new insights in the processes of preservation. Finally, the distinct knowledge of these would enable the subsequent application of lithified discharge features on the identification and characterization of paleo-hydrothermal systems.

Page intentionally left blank due to technical reasons.

1. Introduction

1.1. Preamble

The hydrothermal system of Panarea Island, Italy, is characterized by extreme physico-chemical properties, caused by discharging hydrothermal fluids. It thus comprises unique geological, mineralogical, and ecological circumstances, making it a high-class natural laboratory to investigate topics such as hydrothermalism or ocean acidification. Especially its situation in a shallow marine environment, which is accessible for Scientific Divers, makes it a perfect location to conduct extreme environment analyses using in-situ investigations. Since at least the last phase of major volcanic activity in 2002, the system and its surroundings are in focus of a number of international research groups working on a variety of scientific fields including geochemistry (e.g. ITALIANO & NUCCIO 1991, CARACAUSI et al. 2005b, ESPOSITO et al. 2006, GUGLIANDOLO et al. 2006, TASSI et al. 2009, MERKEL et al. 2011), volcanology (e.g. CALANCHI et al. 2002, ANZIDEI et al. 2005, CAPACCIONI et al. 2007, LUCCHI et al. 2007a, b and 2013a, PECCERILLO et al. 2013), microbiology (e.g. LENTINI et al. 2014, JOGLER et al. 2020, KALLSCHEUER et al. 2020, SANDARGO et al. 2020), ecology (e.g. GUILINI et al. 2017, ESPOSITO et al. 2019, MOLARI et al. 2019) and innovative approaches on energetic usage of geothermics (e.g. BARTH et al. 2010, CASO et al. 2010), to name just a few of them.

The CMAS Scientific Diving Center Freiberg has been working on the system since 2006, approaching a number of topics in interdisciplinary working groups. In this context, a continuous long-term monitoring program was established and has been conducted for over a decade. The working groups covered fields of (hydro-) geology, geochemistry, sedimentology, mineralogy, ecology, (micro-) biology, thermometry, gas-flow measurements, and engineering (development and testing of underwater measuring devices).

During the time since 2006, a huge amount of data has been acquired and analyzed. That way, a more and more detailed base of data and knowledge has grown over the years and a lot of topics discussed in the scientific community were stated to need intense revision or clarification. One of these topics is the general geology of the hydrothermal system of Panarea Island and its macro- and microstructures, which are intensively influenced by the extreme environmental conditions of the system (rock alteration, hydrothermal discharge features, etc.). As most investigations of submarine lithologies have been carried out from the sea surface, they cannot resolve small-scaled variations or structural features.

Therefore, this thesis aims to present accurate information on the geologic inventory of the hydrothermal system and its small-scaled discharge features. The work characterizes all lithologies known to occur in the system and combines the information to facies and genetic models. It presents findings on the evolution of various types of discharge features and their relation to the diagenetic processes affecting and altering the source rocks.

The detailed information on the geological background is the basis for any other investigations related to the rock or sediment material such as hydrochemical investigations (e.g. rock-water-interactions) or fluid dynamics. Also environmental and ecological analyses benefit from detailed information on possible geogenic impacts on the habitats. This thesis thus contributes to the understanding of the hydrothermal system of Panarea Island and consequently to the scientific understanding of geothermalism in general. The general information may be transferred and applied on other systems and comparative studies in different settings in the future as well.

1.2. Research questions, objectives, and hypotheses

The unique setting of the investigated hydrothermal system of Panarea raises a variety of scientific questions being dealt with by researchers from all over the world. The CMAS Scientific Diving Center Freiberg covers numerous fields of science affecting the understanding of the system in general.

Central topics that are dealt with can be summarized to the following superordinate complexes:

Complex 1: Quality and quantity of hydrothermal fluids being emitted at the sea bottom of Panarea including their temporal variations

Despite the basic scientific interest, this topic heavily affects environmental issues connected to climate change and related technical approaches such as carbon capture and storage (CCS). The characteristics of this natural laboratory makes the Panarea system a high-class study site for questions from this field of science.

Complex 2: Interactions at the interface seafloor-oceanwater and effects on geological and sedimentological or mineralogical issues

The highly specific boundary conditions in the system in combination with discharging hydrothermal fluids provoke extraordinary sedimentary and hydrothermal features. The influence of hydrothermal emission furthermore affects the mineralogy of the volcanic strata prevailing. Processes of alteration and recrystallization form the lithology and impact the shape of the seafloor.

Complex 3: Impact of hydrothermalism on the marine ecosystem, biodiversity, and organisms' strategies towards adaption

Events of volcanic activity cause sudden changes in the properties of marine environments. In particular highly specialized organisms may have severe problems in adapting to new environmental conditions in a short time. Therefore, such abrupt

changes often cause either migration of species (to regions, that are comparable to their usual ambience) or the reset of at least parts of the ecosystem by extinction. Prominent fields of research hence deal with the numerous processes of adaption and species migration within the system and beyond.

Complex 4: Threats of volcanic activity and hazard assessment

Hydrothermalism is only one aspect of volcanic activity. Most of the Aeolian volcanoes are recently active in some way. Times of volcanic unrest alternate with hydrothermal emission or phases of dormancy. Volcanic eruptions, earthquakes and other related threats to human population necessitate extensive hazard assessments and reliable risk management procedures for civil defense. A central point is the development of an early warning system for volcanic eruptions and tsunami waves.

Complex 5: Geothermal energy usage

The Aeolian Islands are partly in a remote geographic position. The supply of drinking water and electricity is based on the supply by ships in most cases. Despite the environmental issues being caused by this procedure, the security of supply is a severe problem as waterways may be unpassable due to storms or other events such as supply shortages (fuel). An innovative and environmentally friendly alternative would be the usage of geothermal energy being supplied by the volcano. Therefore, the investigation of new approaches towards a secure and practicable geothermal energy usage considering the local conditions is among the main fields of scientific work.

The prevailing thesis concentrates on the questions of complex 2 involving findings from complex 1. The complexes 3 to 5 are not dealt with in this work.

The focus is set on the direct interaction zone from the seafloor down to about 1 m depth. Drillings or other outcrops were not conducted due to financial limitations.

Ecological aspects, such as the occurrence and activity of microorganisms, have a severe impact on the sedimentological and mineralogical processes at the seafloor. As dealt with in numerous publications by specialized working groups, the information from the literature was used exclusively. The author limits himself to qualitative observations.

Due to the broad aspects of data handled in this thesis the author decided to select major points and fields of interest as superordinate aims to be discussed. Therefore, distinct hypotheses, which will be answered by the prevailing work, are:

1. The seabed interface of the hydrothermal system of Panarea Island is composed of at least 11 lithofacies types of various properties and a complex spatial distribution. Secondary mineralization forms different types of cement.

2. The development of secondary structures and fluid discharge features follows only one complex genetic scheme just varying in the outer shape according to the facies of the discharge feature, the characteristics of the hydrothermal fluids and the type of host rock material.

3. The occurrence of fluid discharges and secondary structures is controlled by regional tectonics in the back-arc basin.

4. Secondary structures and fluid discharge features show a high preservation potential and represent unique marker structures suggesting preserved hydrothermal systems in the paleo rock record.

2. State of research - seafloor hydrothermal systems

2.1. Hydrothermal deposits in general

Hydrothermalism is directly involved in the formation of hydrothermal mineral deposits that are classified by genesis and occurrence. The major types distinguished are vein deposits, scattered deposits (also referred to as epigenetic deposits), and volcanic-sedimentary exhalative deposits (also referred to as syn-sedimentary deposits). In all cases, mineral precipitation is a key process in the formation of the deposit (OKRUSCH & MATTHES 2005).

Due to sudden changes in temperature, the thermodynamic equilibrium overbalances (i.e. in case of the mixing of two different hydrothermal fluids). The determining variable for this process is the saturation index (SI) of the hydrothermal fluid. It forms of the decadic logarithm of the ion-activity product (IAP) and the solubility product (K).

$$SI = log \frac{IAP}{K}$$

If SI < 0, the fluid is undersaturated. If SI > 0, the fluid is oversaturated what may lead to mineral precipitation. However, many minerals are known, which only form above a certain threshold regarding temperature and pressure. Some minerals have exceptionally low kinetics but can be catalyzed by means of bacteria. SI = 0 characterizes the thermodynamic equilibrium.

Vein deposits form if faults and fractures are created by active tectonics. When hydrothermal fluids migrating on these newly formed pathways abruptly cool down or quench, minerals precipitate from the oversaturated fluids. Typical mineral phases are quartz (SiO_2), calcite ($CaCO_3$) and massive sulfides, such as pyrite/marcasite (FeS_2), galena (PbS) or sphalerite (ZnS).

Scattered deposits are formed by hydrothermal fluids migrating through the host rock impregnating the preexisting lithology/structure. Processes of substitution either from the affected host rock or the circulating hydrothermal fluid may occur (metasomatism, OKRUSCH & MATTHES 2005). The typical mineralogy is dominated by massive sulfides, copper (Cu), barite ($BaSO_4$), and fluorite (CaF_2).

Another type of hydrothermal deposits is the volcanic-sedimentary exhalative type. It forms either subaerial at geothermal seeps or fumaroles or submarine at hydrothermal vents or discharges (OKRUSCH & MATTHES 2005). The type of venting depends on the setting of the system. Black smokers occur in deep seas at mid ocean ridges, whereas white smokers are typically related to active subduction zones in shallow waters (e.g. New Zealand, Caribbean). Furthermore, hot spot volcanism may occur in combination with mid ocean ridges comprising prominent venting activities (e.g. Iceland).

The mineralogy of volcanic-sedimentary exhalative systems is dominated by quartz (SiO_2), native sulfur (S) and massive sulfides, such as pyrite/marcasite (FeS_2), galena (PbS) or sphalerite (ZnS). The prevailing thesis mainly focuses on processes that may also be involved in the formation of this type of deposit.

2.2. Deep-sea environments

Deep water hydrothermal (vent) systems, active or inactive, and hydrothermal seafloor deposits seem to be much more abundant than assumed so far. Although they have been intensively studied for many years (c.f. NORTON 1984; VON DAMM 1990; JUNIPER & TEBO 1995; KARL 1995; NELSON & FISHER 1995; SEYFRIED & MOTTL 1995; TIVEY 1995; ZIERENBERG et al. 2000; NORTON & DUTROW 2001; AMILS et al. 2007; BLUMENBERG 2010; KIEL 2010; KIEL & TYLER 2010; LE BRIS & GAILL 2010; VRIJENHOEK 2010; MONECKE et al. 2014; PETERSEN et al. 2016 and many others), only some percent of the area of convergent margins and mid-oceanic ridges have been investigated until today (PETERSEN et al. 2018). About 300 sites showing evidence for significant seafloor hydrothermal activity (past or present) are known (HANNINGTON et al. 2005 and 2011). BUTTERFIELD (2000) presents 35 hydrothermal vent sites which are “confirmed presently active”.

Their location in the deep-sea and the prevailing enormous hydrostatic pressure cause very specific environmental conditions. These extreme habitats comprise both, extreme conditions for adapted organisms and ideal p-T-states concerning mineral precipitation. Therefore, today they are understood as analogues for extraterrestrial environments. These extreme physico-chemical conditions make deep-sea hydrothermal environments excellent hosts for processes involved in the formation of deposits and thus may obtain remarkable economic efforts in the future (e.g. PETERSEN et al. 2016). However, these deep-water systems are hard to access, as logistics and funding basis for research and economic projects provoke major challenges (cf. HANNINGTON et al. 2017).

Deep-sea hydrothermal systems can mostly be found on mid-oceanic ridges. Depending on the dominating fluid-type, the chemical composition varies between alkaline and acidic, what naturally determines the mineralogy of the system.

A prominent example for an alkaline system is the Lost City Vent Field in the Atlantis-Massif (approx. 30 ° N, 42 ° W, Mid-Atlantic). This serpentinite-hosted system seems to have been active for about 30 ka and is built up of carbonates precipitating on a peridotite lithology being characterized by intense serpentinization (e.g. FRÜH-GREEN 2003; KELLY et al. 2005 and 2007). It comprises numerous hydrothermal features, which are well comparable to the ones described in this thesis in terms of their morphology and structures (cf. BELL et al. 2012).

However, a comparison of deep-sea and shallow marine environments is difficult in general: ambient pressure, temperatures, illumination, and many other physico-chemical and biological parameters vary significantly (e.g. TARASOV et al. 2005). Although the overall appearance (“habitus”) as well as some geometric data (height of chimneys) might be comparable, the mineralogical and (hydro-) geochemical properties are completely different.

Acidic environments are characterized by low pH-values in the hydrothermal fluids resulting metalliferous mineral precipitation. Prominent examples are the warm springs on the Galapagos Rise (CORLISS et al. 1979), the massive sulfide occurrence on the East Pacific Rise (EPR) at 21 ° N (FRANCHETEAU et al. 1979; HEKINIAN et al. 1980;

CONVERSE et al. 1984) or the 350 °C “black smoker” vents and massive sulfide “chimneys” at 21 ° N EPR (SPIESS et al. 1980). Also the PACMANUS hydrothermal field in the Manus basin, Papua New Guinea, is known for its hydrothermal features (e.g. BINNS 2014). Furthermore, the high-metal-grade deposits at TAG site on the Mid-Atlantic Ridge (MAR; a.o. HUMPHRIS et al. 1995; PETERSEN et al. 2000), the Middle Valley site on the northernmost Juan de Fuca Ridge, the 13 ° N site on the East Pacific Rise, and the Atlantis II Deep, Red Sea (SHANKS & BISCHOFF 1980; FOUQUET et al. 1996; ZIERENBERG et al. 1998; SHANKS 2019) are well studied locations.

2.3. Shallow-water systems and their preservation potential

Hydrothermal systems in shallow marine environments are mostly connected to convergent plate-boundaries and active volcanic systems.
In contrast to deep-sea environments, shallow marine systems can be investigated comparatively easily as they are accessible by diving scientists. Their physico-chemical conditions vary significantly from deep marine systems. Not only the ambient pressure, but also illumination, temperatures, and material fluxes (sedimentation) are naturally on different scales. Nevertheless, both types of hydrothermal systems may have similarities, for example in the type of exhaled hydrothermal fluids and their fluid flow patterns. For this reason, hydrothermal features such as hydrothermal chimneys may be structurally well comparable patterns, both in deep-sea environments as well as in shallow marine systems, respectively (STANULLA et al. 2017b; ESPOSITO et al. 2018), as their genesis follows the same physics. However, the different physico-chemical situations during the processes of their genesis must be taken into consideration while comparing both features.
Geologically preservable parameters are microbial mats and microbially induced sedimentary structures, fluid escape structures including "abiotic micro-tunnels" (MCLOUGHLIN et al. 2010) or "pipes" (POHL et al. 2010; STANULLA et al. 2017a and c) and biological aspects (c.f. DANDO 2010).
Microbial mats and their lithification by sedimentary processes is one typical proxy for the preservation potential and a common feature in hydrothermal features. General information about parameters, processes and resulting geological structures is given by KRUMBEIN et al. (1979), NOFFKE & KRUMBEIN (1999), GERDES et al. (2000), NOFFKE (2000, 2007, 2009 and 2010), NOFFKE et al. (2001a, 2001b, 2003b), GINGRAS (2002), SCHIEBER et al. (2007), KRUMBEIN (2008), NOFFKE & PATERSON (2008) and REITNER & THIEL (2011). Microbial mats occur commonly in recent environments. WITTE et al. (2004) describe microbial mat occurrences at the Baltic Sea coast of Germany whereas CUADRADO et al. (2011) deal with microbial mats of the Bahia Blanca estuary (Argentina). Findings of geologically preserved microbial mats are relatively abundant. Microbially induced sedimentary structures and stromatolites can be found in the Devonian Muth Formation (NW Himalayas) for instance (DRAGANTIS & NOFFKE 2004). Examples from the Mid-Proterozoic Belt Supergroup, Montana, U.S.A., are given in SCHIEBER (1998). NOFFKE & KNOLL (2002) report mat-preservation from the Upper

Neoproterozoic Nama Group in Namibia. Microbial mats from a siliciclastic marine environment of the Mozaan Group, South Africa, are documented by NOFFKE et al. (2003a) and tidal microbial mats in the Moodies Group (South Africa) are given by NOFFKE et al. (2006a) and HEUBECK (2009). Microbial mats in siliciclastic storm deposits of the Witwatersrand Supergroup, South Africa, are presented in NOFFKE et al. (2006b). SUR et al. (2006) found indicative structures at the Precambrian Rampur and Bijaigarh Shale in the Vindhyan basin (India).

Another important aspect concerning the preservation potential of hydrothermal systems is related to escape structures. FREY et al. (2009) and STANULLA et al. (2017a) discuss their morphology and genesis. Examples for recent gas escape structures in the northwestern Sea of Okhotsk, Russia, are given by LÜDMANN & WONG (2003) and SHAKIROV et al. (2004). Paleontologically preserved escape structures from a Middle Devonian carbonate mound (Hollard Mound) at the Hamar Laghdad (Antiatlas, Morocco) are shown by PECKMANN et al. (1999). RÖßLER et al. (2009) present degassing structures in the Permian volcanites of the Leukersdorf-Formation in Chemnitz, Germany.

Features being relevant for the preservation potential of ecosystems are also described in the literature as a subtopic of case examples (e.g. CAMPBELL 2006).

Besides venting activities in the Caribbean (FINK 1972; MCCARTHY et al. 2005; KOSCHINSKY et al. 2007; JOSEPH et al. 2011), the Mediterranean Sea comprises hydrothermalism as a common feature as well (DANDO et al. 1999). The volcanic provinces of Italy are among the most prominent examples of shallow-water hydrothermal systems. The recently most active shallow marine areas are located in the Tyrrhenian Sea: the Aeolian Arc, among many others described by ITALIANO & NUCCIO (1991), ESPOSITO et al. (2006), LUCCHI et al. (2013a), PECCERILLO et al. (2013) (see chapter 3.1. for further information on Panarea Island), and the Pontine Archipelago (Zannone Island), recently investigated by MARTORELLI et al. (2016), ITALIANO et al. (2019), and INGRASSIA et al. (2020).

The hydrothermal system of Milos, Greece, represents a widely investigated system that will be taken into account as one of the best examples given in scientific literature. Previous work was done here by a number of scientists from different disciplines. FYTIKAS (1989) gives an overview of parts of this work and the prevailing subaerial geology. Recent geographic work is done by KHIMASIA et al. (2020) which present a detailed map in small scale (1:3.300) of the Paleochori Bay. UGUR et al. (2003) present a radiometric dating of sediment cores from a hydrothermal vent in Milos. Volcanological and sedimentological data is given and interpreted by STEWART & MCPHIE (2004), ANASTASAKIS & PIPER (2005) and STEWART & MCPHIE (2006). FONTAINE et al. (2003) summarize the acting hydrothermal processes and mechanisms of compaction-induced phreatic eruptions, whereas LIAKOPOULOS et al. (1991) investigated drilling cores and cuttings to gain insights into the deep structure of the system. Geochemical approaches are used by BOTZ et al. (1996), FITZSIMONS et al. (1997), CHRISTIDIS (1998), KARAGOERGIS et al. (1998), MARINI et al. (2002), NADEN et al. (2003), NADEN et al. (2005), VALSAMI-JONES et al. (2005), VARNAVAS & CRONAN

(2005), and PRICE et al. (2013a) to characterize the hydrothermal system. BOTZ et al. (1996) report of hydrothermal gas exhalations offshore Milos. DANDO et al. (1994) and DANDO et al. (2000) try to characterize the hydrothermal system through the measurement of heat fluxes and the distribution of chemicals, fluids and bacteria from hydrothermal exhalations and their effects on the biodiversity. SIEVERT (1999), PANSINI et al. (2000), BIASI et al. (2004), and PRICE et al. (2013b) study biological features including macro- as well as microbiological investigations. DANDO et al. (1995) and ALIANI et al. (2004) investigate the connections between the volcanic environment and the hydrothermal system. The influence of seismic and volcanic activity on the hydrothermal system and periodicities of pressure and water/sediment temperatures are analyzed and compared with the degree of volcanic activity.

3. Panarea Island - the area of investigation

3.1. The hydrothermal system of Panarea Island

Generals

The island of Panarea is part of the Aeolian Archipelago, located in the central Mediterranean Sea. This group of seven volcanic islands is situated about 50 km north of Sicily in the Tyrrhenian Sea. The main islands are Volcano, Lipari, which is the largest island in the group, Salina, Alicudi, Filicudi, Panarea and Stromboli. They form an arc of about 200 km in length, framing the Marsili basin and Marsili seamount ringlike to the south. It separates the Marsili basin from the uplifting continental crust of the Calabrian Arc to the east and the continental slope of northern Sicily to the west (Figure 1; CALANCHI et al. 1995; PEPE et al. 2000; PETERSEN & MONECKE 2009; FABRIS et al. 2010; LUCCHI et al. 2013b; PENNINIO et al. 2014).

With an area of 3.4 km² Panarea Island is the smallest of the Aeolian Islands, situated about 30 km southwest of Stromboli. This emergent portion of a submarine composite volcano (ESPOSITO et al. 2018) of a length of approximately 18 km elevates 421 m asl. at its highest point, Punta del Corvo. The cone-shaped volcanic edifice rises approximately 1,600 m from the sea floor to this point (GABBIANELLI et al. 1990; GAMBERI et al. 1997; ANZIDEI et al. 2005; FAVALLI et al. 2005; FABRIS et al. 2010).

There are different approaches on the activity of volcanic systems. Volcanoes are typically classified to be active, erupting, dormant or extinct. In the following a volcano is denoted to be active if it has at least one eruption over the last 10 ka. Active volcanoes can be erupting (at the moment) or dormant (not erupting but will probably erupt again in the future). If a volcano has had no eruption over the last 10 ka and is not expected to have one in comparable time scales, it is classified extinct. Because most of the volcanoes in the Aeoloian Arc have recently been active, as eruptions of Stromboli and gas emissions on Volcano and Panarea Island show, intense work has been done with respect to continuous seafloor monitoring and consequently volcanic hazard assessments (i.e. ROMANO et al. 2019).

The calc-alkaline volcanism and the connected hydrothermal systems result from the subduction of the African under the Eurasian plate (SAVELLI et al. 1999; SERPELLONI et al. 2007; ESPOSITO et al. 2010). The eruptive history of the Panarea system is quite simple. It can be divided into seven successive periods of volcanic activity (eruptive stages) intermitted by quiescence stages between 155–149 ka and 24–8.7 ka (LUCCHI et al. 2007a, b and 2013b; ESPOSITO et al. 2018).

In fall 2002, a period of increased volcanic activity caused a heavy gas eruption in the submarine crater about 2.5 km east of Panarea (a.o. CAPACCIONI et al. 2007, CARACAUSI et al. 2005a). During this active phase, a lateral collapse of the Sciara del Fuoco at Stromboli happened, which caused a Tsunami-wave in the Mediterranean Sea (e.g. TINTI et al. 2005a, b; WALTER et al. 2009).

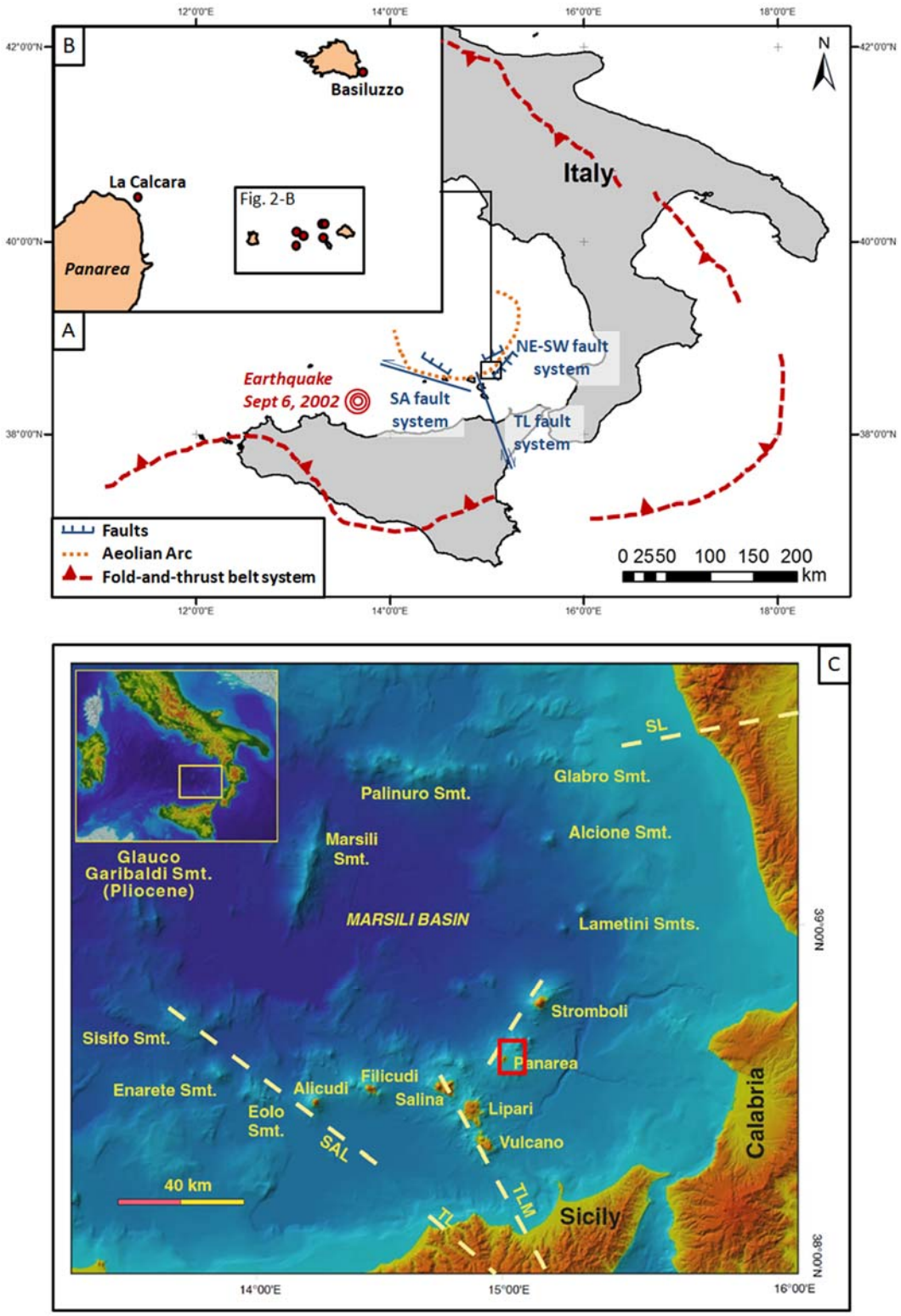

Figure 1: Geographic position of the area of investigation. **A –** Overview map of south Italy and Sicily including the Aeolian Islands in the north (Europe coastline shapefile from the European Environment Agency; available: http://www.eea.europa.eu/data-and-maps/data/eea-coastline-for-analysis/gis-data/europe-coastline-shapefile). Main structural elements are illustrated: TL Tindari–Letojanni fault system, SA Sisifo–Alicudi fault system (based on ESPOSITO et al. 2006; modified after STANULLA et al. 2017a). **B –** Map sketch of Panarea Island and its surroundings (generalized). The submarine locations Basiluzzo and La Calcara are situated apart from the central locations. **C** – Overview map showing the Marsili basin and the Aeolian Arc including the area of investigation marked with red square and major tectonic elements (modified after PECCERILLO 2017).

Since November 2002, the degassing activity in the area has decreased. However, nowadays the discharges within the submarine crater between the islets of Dattilo, Lisca Bianca, Bottaro, and Lisca Nera are among the most active ones in the system (Figure 2). Furthermore, intense hydrothermal activity is reported for the location *Smoking Lands* on the plateau between Panarea Island and Basiluzzo at water depths of about 70 – 80 m (ESPOSITO et al. 2018) recently. Here, a hydrothermal chimney facies with specimen of one to four meters in height and up to four meter in diameter evolved (SPAGNOLI 2019). Massive sulfide ore mineralization (pyrite, sphalerite, galena) was found in this area in the late 1990's (MARANI et al. 1997).

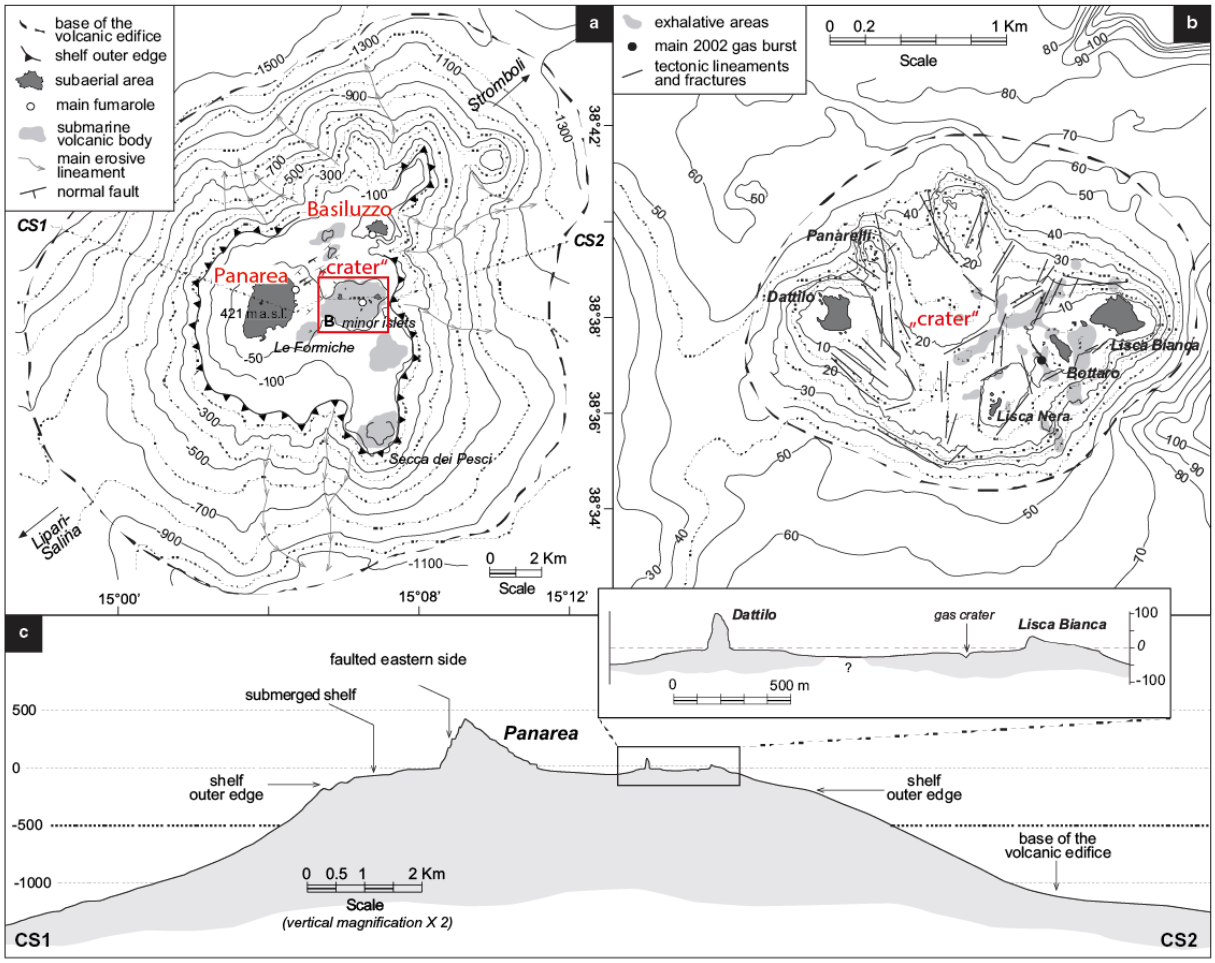

Figure 2: A – Bathymetric map sketch of Panarea and its islets including Basiluzzo. Locations of interest are marked in red. **B –** Bathymetric map sketch of the "crater" of Panarea including most of the underwater investigation sites (cf. chapter 3.3.). **C –** Cross section through the volcanic edifice of Panarea showing the submerged slopes and their development. All depth in m bsl. (modified after GABBIANELLI et al. 1993; CHIOCCI & ROMAGNOLI 2004; ESPOSITO et al. 2006; TASSI et al. 2009; LUCCHI et al. 2013b and ROMAGNOLI et al. 2013).

Regional geology

The mostly andesitic to dacitic or rhyolitic rocks of Panarea and its surrounding islets occur in lava domes, volcanic plugs and coulees being interbedded with pyroclastic deposits (ESPOSITO et al. 2010). Materials belong to the calc-alkaline, high-K calc-alkaline, shoshonitic and alkaline potassic associations (CALANCHI et al. 2002; FAVALLI et al. 2005; CHIODINI et al. 2006).

The subaerial portion of the isle was formed 149 to 124 ka ago by effusive activity and the emplacement of domes (CALANCHI et al. 1999). Pyroclastic activity dominated a second genetic portion between 59 and 13 Ka (LOSITO 1989).

Investigations of paleo-coastlines show varying sea level changes or up- and down-lift of the island during the past 150 ka. Nowadays, a total of five major staircased paleo-shorelines can be observed up to approximately 120 m asl. After LUCCHI et al. (2013b), the corresponding terraces are nowadays located at an elevation of

- 115 m asl: paleoshoreline I
- approx. 100 m asl: paleoshoreline Ib)
- 60–65 m asl: paleoshoreline II
- 35 m asl: paleoshoreline III
- 12 m asl: paleoshoreline IV
- 10–12 and 5 m asl: paleoshorelines Va–Vb).

A sea level rise of approximately 129 m compared to nowadays' sea level was calculated. This fact witnesses a tectonic rise of the isle of Panarea of several meters over the years (LUCCHI et al. 2007b and 2013b and references therein; cf. BENJAMIN et al. 2017). A total subsidence rate of 2.05 ± 0.1 mm/yr^{-1} is calculated by ANZIDEI et al. (2014). A volcano-tectonic contribution of 1.43 ± 0.1 mm/yr^{-1} was estimated therein for the last 2 ka. Consequently, it can be assumed that the documented underwater investigation sites where subaerial in the Upper Pleistocene. This has to be taken into account when interpreting geological processes.

The common literature distinguishes between a total of five lithofacies in the "crater" of Panarea. Materials include hypo abyssal lava, basaltic-andesite lava with xenolithes and vein hydrothermal alteration to alunite plus sands, gravel and conglomerates laterally transitional to breccia (ESPOSITO et al. 2006; DOHERTY et al. 2015). Local vent hosted massive sulfide ore bodies such as the shallow water grey smoker "Black Point" are prominent outcrops of secondary formation within this lithology (cf. BECKE et al. 2009; CONTE & CARAMANNA 2010). Furthermore, ongoing mineral precipitation and cementation are common features, which has formed iron-ooids (DI BELLA et al. 2019) or hydrothermal discharge features (STANULLA et al. 2017a) recently.

The Aeolian Arc is formed by three major tectonic structures (cf. Figure 1; DE ASTIS et al. 2003; ESPOSITO et al. 2006; ACOCELLA et al. 2009; PECCERILLO et al. 2013; ROMAGNOLI et al. 2013; VENTURA 2013):

1. the NE – SW trending faults in the eastern sector including the islands of Panarea and Stromboli. The tectonic regime is extensional in this region.
2. the NNW – SSE trending Tindari–Letojanni fault system (TL) in the central sector (Salina, Lipari, and Volcano) exhibiting right lateral regimes.
3. the WNW – ESE orientated Sisifo–Alicudi fault system (SA) of the western sector (Alicudi – Filicudi) where compressive strains prevail.

Recent investigations show that the tectonic inventory in Panarea is much more complex than given in the literature. ADAMEK et al. (2019) describe additional NNW – SSE and N – S trending structures.

A decrease of volcanic activity from the most active eastern parts (Panarea, Stromboli) to the extinct western parts of the Aeolian Arc (Alicudi, Filicudi) is remarkable. The central sector (Salina, Lipari) is nearly dormant at the moment.

Hydrothermalism

Data on water and gas chemistry and discharge behavior is presented by ITALIANO & NUCCIO (1991), GUGLIANDO et al. (2006), BAUER et al. (2009), ITALIANO (2009), HEINICKE et al. (2009), SIELAND (2009), STEINBRÜCKNER (2009), VOLTATTORNI et al. (2009), ANDALORO et al. (2010), CAPACCIONI et al. (2010), HAMEL (2010), HEINICKE et al. (2010), PONEPAL et al. (2010), MERKEL et al. (2011), PETERS et al. (2011), SCHIPEK & MERKEL (2011), TUDINO et al. (2013), BAGNATO et al. (2017), GROS et al. (2019) and others.

Gas-dominated hydrothermal discharges are classified with respect to the major elements emitted. Sulfur dominated vents are named solfatara, whereas outlets dominated by water vapor are called fumarole. The discharges in Panarea are mostly dominated by CO_2 and are therefore referred to as mofetta.

TASSI et al. (2014) distinguish three major types of gasses being emitted in the Panarea hydrothermal system:

1) H_2- and CO-rich gases, which also show relatively low Ar concentrations
2) H_2S-rich gases, having variable CO/CH_4 ratios, and
3) Ar-rich gases, having relatively low H_2 concentrations.

However, all investigated outlets always emit a mixture of hydrothermal water and gas. They are therefore generally referred to as “mixed fluid outlets” (mfo). However, they mostly show a domination of either water or gas discharge. Respectively, gas-dominated outlets are also named “gas vents” in the following (and water dominated accordingly).

The fluid composition is comparable to that of deep-sea hydrothermal vents (ITALIANO 2009). The most dominant gas is CO_2 (94 to 99.5 %) followed by H_2S (0.5 to 6 %) and trace gases. O_2, CH_4, CO and H_2 as well as some inert gases (N_2, Ar, He) appear in variable concentrations. The pH of the thermal waters ranges between 1.9 and 5.7 (ITALIANO & NUCCIO 1991; CARACAUSI et al. 2005b; SIELAND 2009; MEINARDUS 2016; DI BELLA et al. 2019).

The chemical composition of the discharging hot geothermal groundwater (80 to 130 °C), expressed in enrichment factors (EF) with respect to Mediterranean Sea water, is given in Table 1. The highest enrichment factors over all sampling points were measured for Mn with EFs from 40,000 in Point 21 to 369,000 in Hot Lake. The individual locations show significant differences in the enrichment factors > 1000, which were identified for the elements Pb, Cs, Y, Cd, Tl, Ba, Fe, Zn, and the species NO_2^- and NH_4^+ (STANULLA et al. 2017a).

Table 1: Extreme values of hydrochemical parameters and enrichment factors (EF) with respect to Mediterranean ocean water for elements and species at 5 example locations.
Key: blue – hydrochemical data (extreme values measured from 2006 to 2018); O_2 is given in [%] referred to the atmosphere. Thus, ocean water at the atmosphere – ocean water interface is defined as 100 %. **dark brown** – EF ≥1000; **brown** – EF ≥100; **pale brown** – EF ≥10; **white** – EF <10. The concentrations measured are given by STANULLA et al. (2017a).

Black Point		Hot Lake		Area 26		La Calcara		Point 21	
pH (25 °C)	2.4	pH (25 °C)	4.4	pH (25 °C)	4.5	pH (25 °C)	4.6	pH (25 °C)	4.7
EC [mS/cm]	82.0	EC [mS/cm]	118.3	EC [mS/cm]	68.7	EC [mS/cm]	64.8	EC [mS/cm]	61.0
O_2 [%]	1.1	O_2 [%]	0.0	O_2 [%]	0.4	O_2 [%]	2.2	O_2 [%]	0.4
T [°C]	134.1	T [°C]	78.7	T [°C]	64.2	T [°C]	134.3	T [°C]	74.0
Species	**Factor**	**Species**	**Factor**	**Species**	**Factor**	**Species**	**Factor**	**Species**	**Factor**
Mn	282,000	Mn	369,200	Mn	117,700	Mn	230,400	Mn	40,400
Pb	11,000	NO_2^-	30,000	Sulfide	12,000	Cs	4,500	Sulfide	24,000
Cs	7,800	Sulfide	19,300	Y	5,500	NH_4	1,900	NH_4	1,300
Cd	5,800	Cs	17,200	Cs	2,600	Tl	1,700	Tl	1,000
NH_4	4,800	NH_4	9,700	Tl	1,600	Ba	792	Ba	871
Y	4,000	Tl	3,300	NH_4	1,500	Sulfide	733	Cs	422
Sulfide	4,000	Ni	710	Dy	809	As	474	Y	390
Zn	2,900	Ba	707	Gd	611	Pb	370	Ni	385
Tl	2,900	Fe	512	Er	472	Sb	360	Fe	228
Fe	1,800	Y	475	Yb	346	Y	251	Cr	170
Ni	974	Cr	433	Sm	273	Fe	240	Bi	143
Ba	952	Bi	219	Ho	171	Eu	98	Sn	135
Dy	646	Li	210	Pb	140	Si	95	NO_2^-	110
As	630	Sn	200	Nd	127	Li	65	Eu	99
Gd	464	Co	194	Ba	124	Ni	65	Pb	75
Er	396	Rb	191	Eu	121	Al	59	Gd	70

Black Point		Hot Lake		Area 26		La Calcara		Point 21	
NO_2^-	375	Si	109	Tb	120	Rb	47	Dy	62
Yb	351	Pb	94	Fe	118	Sn	44	Ce	57
Sn	339	Dy	87	Ni	107	Dy	44	Si	51
Cr	291	I	79	Si	106	Gd	43	Sm	40
Sm	226	Ce	76	Sn	91	Zn	34	Cd	37
Eu	212	Gd	76	Tm	60	Sm	29	Nd	36
Si	184	B	75	Bi	53	NO_2^-	27	Co	36
Bi	160	Eu	73	Lu	51	Er	26	Sc	32
Al	150	Sm	49	Pr	50	Yb	22	Er	30
Ho	135	Sc	47	Al	48	Nd	20	Yb	25
Nd	120	Cd	43	Li	43	Co	15	As	20
Tb	105	Er	41	Rb	36	I	15	Pr	18
Li	104	Nd	33	Ce	36	Ce	11	Ag	16
Rb	96	Yb	31	Cr	33	B	11	Cu	16
I	91	Be	30	NO_2^-	19	Pr	11	Ho	12
Sc	82	As	27	Cu	14	Ho	9.3	Tb	12
Ce	74	Ga	25	Zn	13	Cd	8.4	Al	12
Co	61	Cu	24	Sc	12	Sr	7.7	TIC	11
Pr	58	Al	24	I	12	Ca	7.1	Li	9.7
Tm	55	Te	23	TIC	11	TIC	7.0	Zn	8.7
Lu	53	Ag	20	Be	11	Tb	6.9	Rb	5.4
In	29	Pr	18	B	9.4	Ga	5.8	I	5.0
V	26	Ca	18	As	8.1	In	5.3	Be	4.9
Ag	25	Sr	18	Co	7.8	V	3.7	Lu	4.1
B	22	Tb	18	Ag	4.9	Sc	3.5	Tm	4.0
Cu	19	Ho	18	Cd	4.5	Tm	3.4	B	3.9
Sb	18	Sb	16	In	4.3	Lu	3.3	In	2.7
Ga	17	In	14	Ga	4.0	Bi	2.6	V	2.4
Be	17	TIC	9.1	Ca	3.9	Cr	2.3	Ga	2.2
Sr	12	Zn	8.1	V	3.6	K	2.1	F	2.1
Ca	11	F	7.5	Sr	3.2	Be	2.1	Te	2.0
F	7.8	K	6.9	K	2.0	Th	2.0	Sr	1.5
TIC	7.6	Lu	6.0	Br	1.8	Mo	2.0	Ca	1.5
Te	4.4	Tm	5.6	F	1.7	Te	2.0	Br	1.4
K	4.0	V	4.0	Te	1.3	Br	1.6	Sb	1.4
Br	2.2	Mo	3.7	Cl	1.3	Se	1.3	SO_4	1.2
Th	2.0	Br	3.3	Sb	1.3	F	1.3	K	1.2
Mo	1.6	Cl	2.4	Mo	1.2	Cl	1.2	Cl	1.1
Cl	1.5	Se	2.3	Na	1.1	Na	1.1	Na	1.1
Se	1.3	Na	1.6	SO_4	1.0	SO_4	1.1	Mg	1.1
SO_4	1.1	Mg	1.0	Mg	0.9	Mg	1.0	Se	1.0
Na	1.1	SO_4	0.9	Se	0.9	U	1.0	U	0.9
Mg	1.1	U	0.9	U	0.3	Cu	0.8	Mo	0.9
U	1.0	Th	0.5	Th	0.3	Ag	0.4	Th	0.7
La	0.5	La	0.1	La	0.2	La	0.1	La	0.2

Table 2: Classification of the submarine hydrothermal venting in Panarea Island, Italy, according to STEINBRÜCKNER 2009. *) standard liter

Class	A	B	C	D	E
Range of gas flow rate [L/min]*)	< 2.1	2.1 – 3.6	3.6 – 7.2	> 7.2	> 40
Number of vents observed	23	8	6	11	10
Mean [L/min]	1.06	3.04	4.86	9.89	n.a.
Standard deviation [L/min]	0.53	0.74	1.18	2.13	n.a.

The gas emissions in Panarea Island's submarine hydrothermal system can be subdivided into five classes (A - E) according to their specific gas flow rate (STEINBRÜCKNER 2009, Table 2).

There are different models describing the hydrothermal system below Panarea Island. The initial attempt was made by ITALIANO & NUCCIO (1991). Among others, PRICE et al. (2015), MEINARDUS (2016), STANULLA et al. (2017c), DI BELLA et al. (2019) and KÜRZINGER (2019) give updated summarizing models on the components and processes in the underground.

Recent investigations brought knowledge on the appearance of completely different, contradicting hydrothermal facies within short lateral distances of only several meters (STANULLA et al. 2017c; cf. chapter 5.2.9). One reasonable explanation might be, that the hydrothermal fluids are subject to processes of phase separation (basically mentioned by WHITE 1964; for the Panarea system a.o. discussed by CARACAUSI et al. 2005b) during their ascent from the hydrothermal reservoir to the surface. Hydrothermal fluids are rich in elements such as CO_2, HF, HCl, H_2S, H_2 and SO_2. Temperatures near the geothermal heat source are estimated to over 300 °C. Changing physico-chemical conditions as well as a supersaturation of the hydrothermal fluids may cause a splitting into different fluid-types migrating on different pathways through the rock (Figure 3). Most branches undergo different evolutions including processes such as fast lift, supersaturation, and mineral precipitation before being discharged at the submarine vent. A high mineralization comparable to the initial fluid composition may be obtained resulting in the respective type of mineral precipitate. Mixing of the initial hydrothermal fluid with local seawater causes dilution. A different (hydro-)chemical composition and consequently different mineralogical properties in the hydrothermal facies are the results (Figure 4). However, the mineral formation during the discharge is also subject to the physico-chemical conditions at the emanation point (e.g. redox potential). Depending on the geological and depositional conditions, the secondary mineral phases will overlay in the vertical profile or form laterally different lithologies (shift of facies).

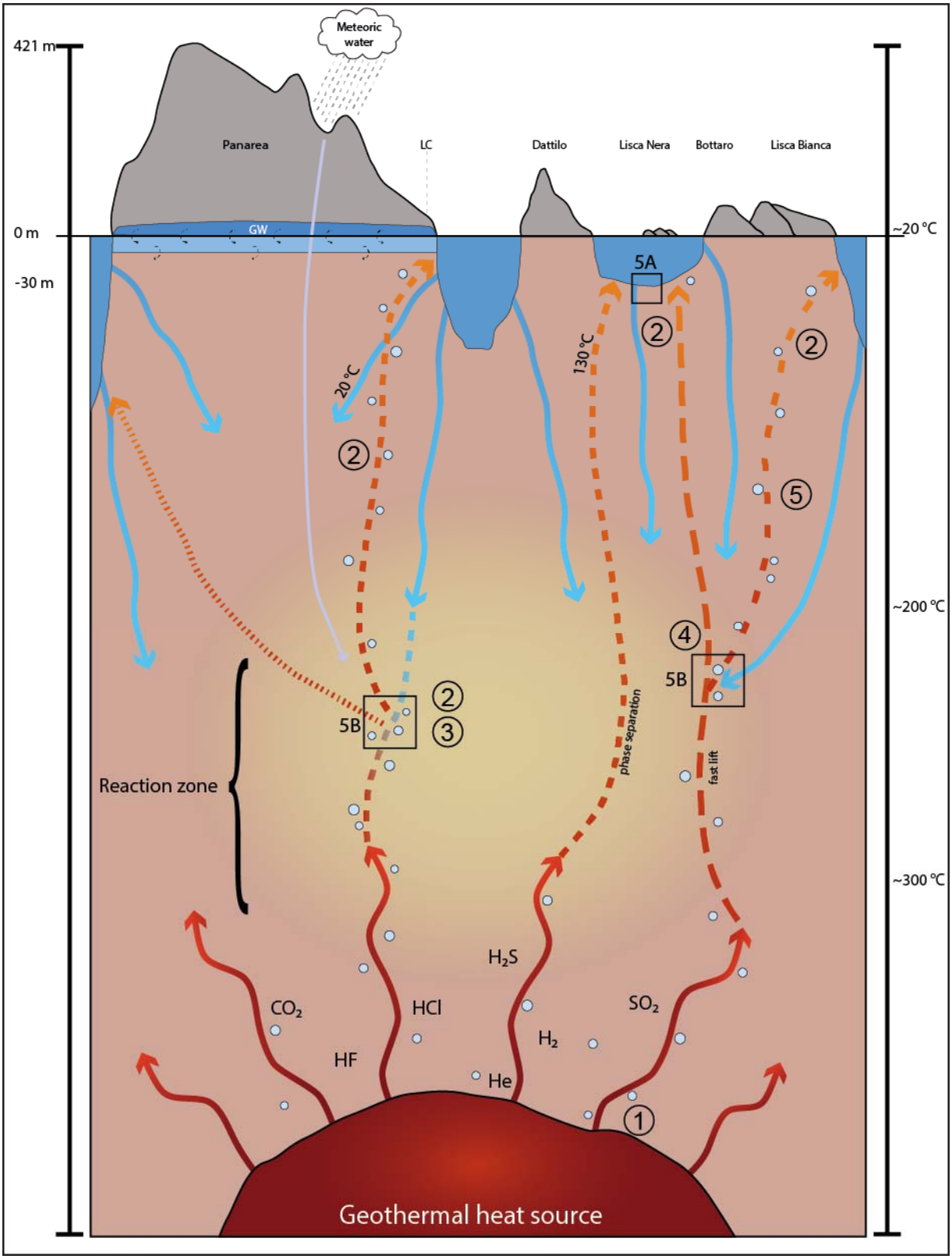

Figure 3: Simplified schematic section through the hydrothermal system of Panarea. The model includes basic topography, bathymetric data, temperature distribution as well as the major migration patterns of local meteoric water, sea water and hydrothermal fluids plus their interaction under different physico-chemical conditions. Combined from and modified after ITALIANO & NUCCIO (1991), MEINARDUS (2016), STANULLA et al. (2017c), DI BELLA et al. (2019), KÜRZINGER (2019). Detailed close-ups (5A and 5B) and key given in Figure 4. Processes indicated by encircled numbers: 1) degassing of magma, 2) water-rock interaction, 3) phase separation, 4) fast lift, 5) condensation.

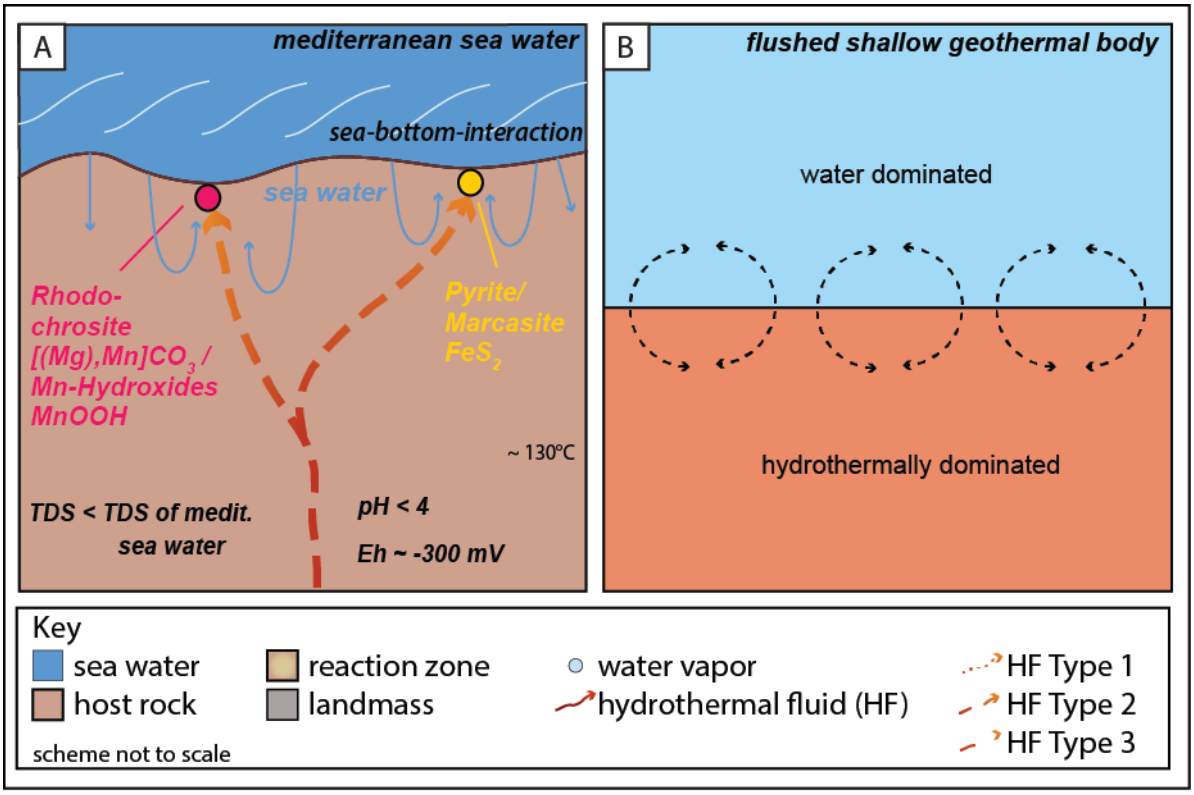

Figure 4: Close-up views to Figure 3. **A –** Processes at the sea-bottom-interface. Ambient seawater infiltrates the sediment and mixes with uprising hydrothermal fluids. Processes of phase separation may lead to the precipitation of apparently contradicting mineral phases such as carbonates and sulfides as is the case in La Calcara (cf. STANULLA et al. 2017c). **B –** The "reaction zone" is also referred to as "flushed shallow geothermal body". The main process here is the complex mixing and reaction of hydrothermal fluids with infiltrating water phases originating either from meteoric or ocean water.

The volcanic and hydrothermal conditions heavily impact the submarine ecology. Low pH values as well as elevated temperatures cause an extreme environment. Especially the presence of extremophile bacteria and other adapted species witness an enormous dynamic system. Typical mass occurrences of whitish and yellowish biomats (*Thiobacillus*; GUGLIANDOLO et al. 2006) are concentrated around the discharge points of hydrothermal vents, where hot water with high H_2S concentrations discharges. The adaption of these thio- and ferro-bacter is a good example for the inhabitation of extreme environments. Their occurrence is reported for several shallow-water hydrothermal systems, i.e. Zannone Island, Italy (INGRASSIA et al. 2020) and the deeper areas around Basiluzzo Island (BORTOLUZZI et al. 2017; *Smoking Lands* - ESPOSITO et al. 2018). However, both systems are located at intermediate water depths between 70 and 150 m.

As the local seawater dilutes the discharged hydrothermal fluids, wide areas with nearly standard ocean water qualities are common. However, robust species such as *Posidonia sp.* can tolerate a certain stress (LAURITANO et al. 2015) due to low pH-values and high sulfide concentrations in the water. Thus, they also inhabit near-discharge regions, if also a decelerated growth behavior can be observed at locations with active venting nearby (SEEBAUER 2015, NOÈ et al. 2020). The elevated CO_2 content in the

seawater near CO_2-dominated vent sites is known to enhance the seagrass productivity. However, massive CO_2 discharge as during gas outbursts (like in 2002 near Bottaro) can stress the individuals and lower the seagrass production due to elevated temperatures and turbidity (VIZZINI et al. 2010, NOÈ et al. 2020). Especially *Posidonia sp.* even seems to support the formation of discharge features (cf. type TFe).

Just after the 2002 gas eruption, when conditions were most extreme, severe ecological incisions were reported. However, a remarkable recovery of the ecosystem was observable during a time span of about 10 years. Today the ecosystem more and more normalizes (e.g. NOÈ et al. 2020). This shows clearly, how ecological evolution and specific adaption may be enforced by single events such as gas outbursts.

3.2. Fluid discharge features in Panarea

STANULLA et al. (2017a) describe eight different types of hydrothermal discharge features in the system of Panarea (Table 3, Figure 5). The classification is based on genetic and/or morphologic characteristics.

The superordinate classification distinguishes between erosive processes, mainly dominated by fluid flow, and constructive processes such as the cementation and mineral precipitation from hydrothermal fluids. The occurrence of different mineralogical facies such as carbonates and sulfides supposes processes of phase separation in the hydrothermal fluid as described by STANULLA et al. (2017c). Erosive patterns mostly manifest in complex, irregular and multidirectional networks of open channels above recent or ancient discharge points. Standard agents of erosion may lead to abstraction during time. The cementation or mineral precipitation in hydrothermal discharge features show a variety of facies depending on the geochemistry of the discharging fluids and the physico-chemical situation at the emanation point.

Discharge features can be tube-shaped and composed of iron, sulfur, or other mineral precipitates. A biogenic influence is discussed in the context of their formation but can neither be proven nor neglected definitely (plant roots, worms, etc.). The formation of network structures is supposed, based on the presence of ancient junctions on single individuals.

Additionally, cemented (consolidated; mostly sulfurous) or unconsolidated cone-shaped structures are common. Both are reported to be active and inactive discharges. Obviously, this facies is characteristic for gas-dominated discharges (cf. MCLOUGHLIN et al. 2010). It is also known to occur in other systems (e.g. Milos, Greece; cf. KHIMASIA et al. 2020: Figure 3-C).

Furthermore, fracture-fills are typical. They consist mainly of laminated massive sulfides (cf. DEKOV et al. 2013), such as pyrite or marcasite, or of laminated native sulfur precipitates. Fracture-fills occur preferably in hardrock lithologies.

Discharge features generally underly a continuous interplay of constructive and destructive processes, sometimes even acting isochronic. They therefore develop depending on the type and amount of hydrothermal activity. Indicators might be fluid flow, elevated temperatures and consequently the (mass-) occurrence of thermophile microorganisms (bioindicators; bacterial mats). Discharge features shall show a high preservation potential due to their remarkable shape and internal structure. Nevertheless, this could not yet be proven certainly.

Ongoing investigations show that the suite of facies of hydrothermal discharge features is much more complex than presented by STANULLA et al. (2017a). Excavations brought knowledge on new, still undescribed types of structures and features occurring in other rock facies as known up to now. Therefore, the classification scheme must be updated which is one aim of the prevailing work.

Table 3: Types of discharge features in Panarea after STANULLA et al. (2017a).

Facies	Description	Location
Erosion by hydrothermal fluids		
GE (gas erosion)	Gas erosion due to kinetic energy of fluid flow. Irregular, multidirectional network of open channels above recent or ancient discharge point. Possibly abstraction during time.	Hot Lake
Cementation by hydrothermal fluids		
TFe (tube, iron cemented)	Precipitates cementing sand or gravel along the pathway of hydrothermal fluids in the sediment; tube-shaped; multistory genesis resulting in characteristic layering of the precipitates	Basiluzzo, La Calcara
TS (tube, sulfur cemented)	Precipitates of (native) sulfur in sediments or hard rocks; tube-shaped; sometimes bio-induced	Point 21, La Calcara
To (tube, other)	Tube-shaped discharge features neither TFe nor TS; multistory genesis possible; sub-types I – III depending on the morphology	La Calcara
Cc (cone, consolidated)	Cone-shaped discharge feature; consolidated by precipitates of (native) sulfur in sediments; concentrating along fractures	Area 26
Cu (cone, unconsolidated)	Cone-shaped discharge feature; unconsolidated in sediments; concentrating along fractures	La Calcara, Area 26
FS (fracture fill, sulfurous)	Fracture-fill of (native) sulfur in hard-rocks; multistory genesis resulting in characteristic layering of the precipitates	Point 21
Fo (fracture fill, other)	Fracture-fill with other minerals; layering of the precipitates likely	Black Point

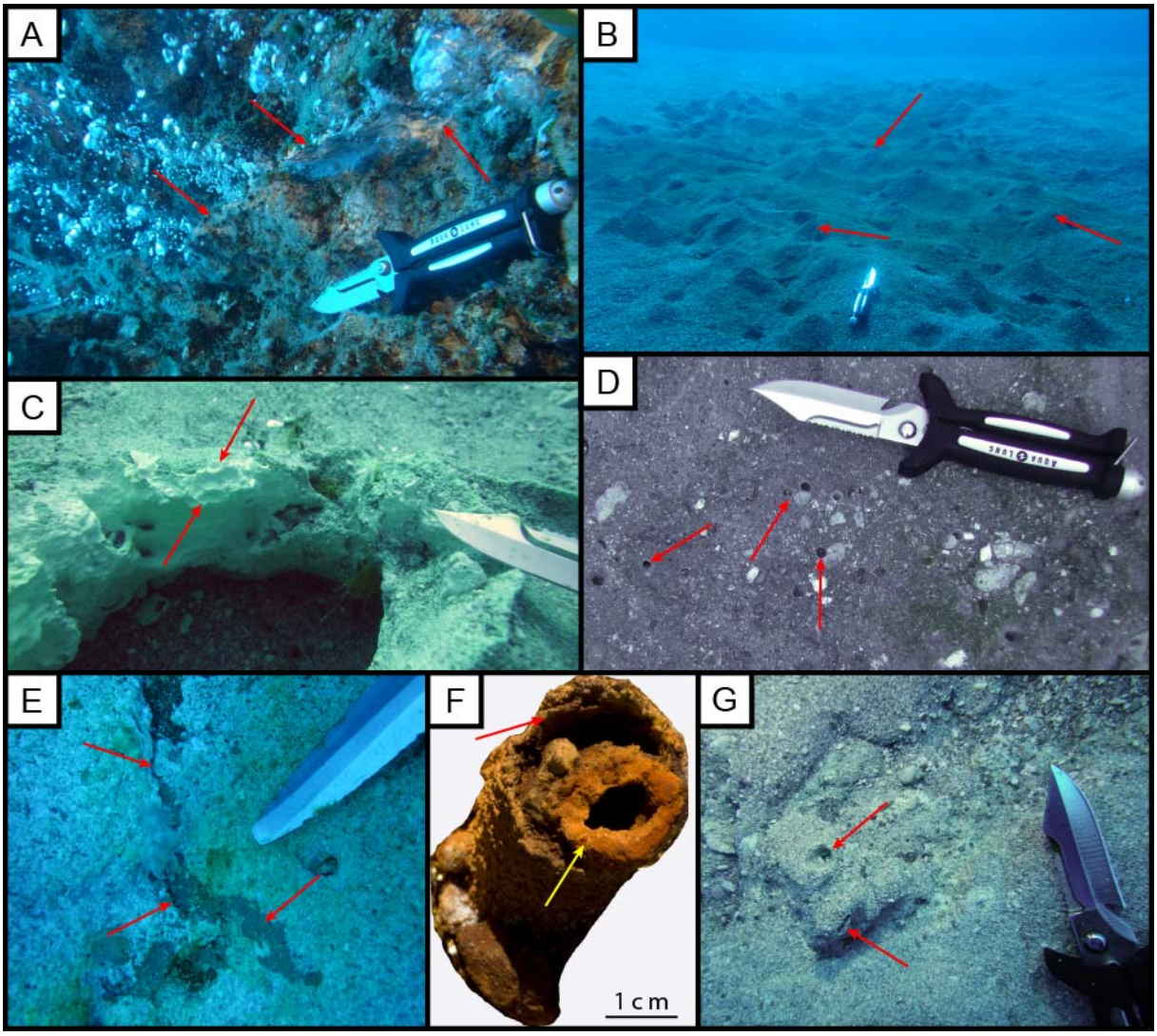

Figure 5: Hydrothermal discharge features described by STANULLA et al. (2017a) as given in Table 3. **A –** Type FS at Point 21. Fracture fill builds the typical ridge-structure (red arrows). **B –** Large field of type Cu discharge features (red arrows) in La Calcara. **C –** Sulfurous features are common in Area 26. Here, type TS discharge feature at Lineament Structure. The red arrows mark emanation points. **D –** Type To features in La Calcara. Their cementary fabrics are not clearly identified up to now. The red arrows mark emanation points. **E –** Fracture fills can be built up of various types of mineral precipitates, here of massive sulfides (red arrows) in La Calcara. **F –** Characteristic sample of TFe facies (Basiluzzo). The sample shows complex genetic structures (cf. STANULLA et al. 2017a). The red arrow marks the outer/older part of the tube. The yellow arrow marks the recently active inner tube. **G –** Complex structure of Cc discharge features in Area 26. The red arrows mark emanation points.

3.3. Study sites

The study area is located about 2.5 km east of Panarea Island and shows a spatial extent of 2.3 km². The maximum water depth is 30 m (ESPOSITO et al. 2006). The average water depth ranges between 10 and 30 m. The seafloor is much deeper in the north western and (south-) eastern regions where depths of more than 100 m occur (Figure 6). These regions are followed by deep-sea abyssal plains (e.g. ANZIDEI et al. 2005; ESPOSITO et al. 2006).

The investigations were carried out at ten different locations spread over the shallow shelf of Panarea by scientific divers. The central parts are referred to as “the crater”, whereas other locations are located at the shorelines of the islands of Panarea and Basiluzzo. The underwater investigation sites La Calcara and Area 26 were divided into sub-locations due to their spatial extent.

Some of the locations show a higher potential for the preservation of discharge features than others and are thus more in focus of this work. This is mainly controlled by the preservation potential and the occurrence of appropriate preexisting geological structures in the underground. Only at shallow depths of less than 10 meters tide and wind driven currents may transport sediments in certain areas (e.g. channel between Lisca Bianca and the islet of Bottaro) and may form the morphology of the sea bottom. The impact of waves on the sea bottom morphology decreases with water depth, but especially high waves during winter storms have an impact of the sea bottom morphology even in depths of 30 m and more. Geothermal water and gas discharges are the major force shaping the sea bottom morphology during low wind periods in summer.

The investigation sites include (alphabetic order; Figures 1, 2 and 6, Table 4):

Area 26

Investigations at this location in the central part of the “crater” started in 2010 at Buoy 1 and were spatially extended over the years. Important sub-locations are Hot Bowl, Lineament Structure, Brodor, and 3-Bowls. All of them are characterized by important structures in the area, which are mostly eponymous.

The sandy plains of Area 26 extend over several hundred square meters at a water depth of 26 m. The site comprises a large variety of secondary sedimentary structures being consolidated by sulfurous cements. Discharges are both, water- and gas-dominated. Most structures are naturally covered by recent wave-transported sands and can only be identified with the help of bioindicators such as microbial mats highlighting the structures.

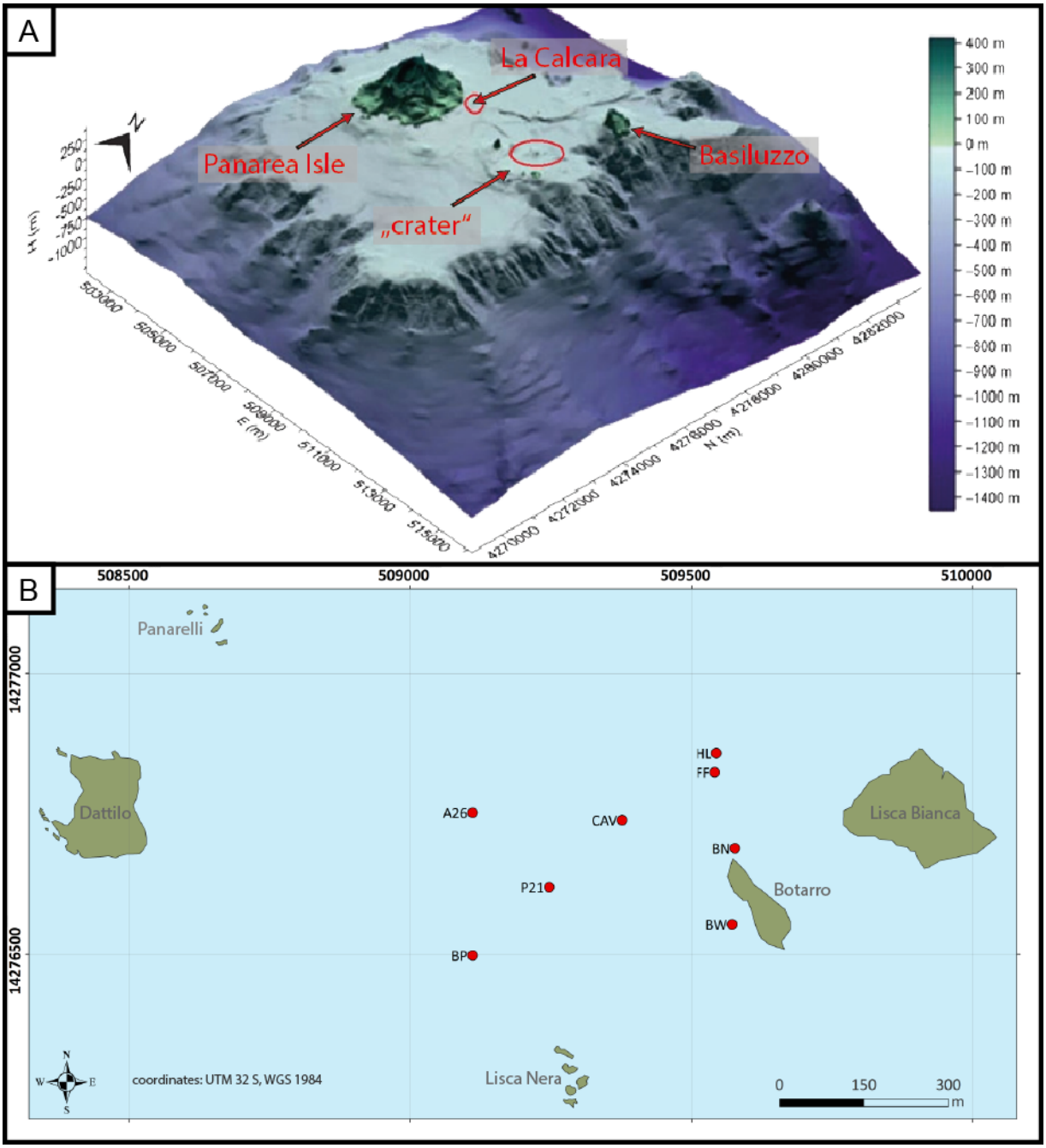

Figure 6: Geographic position of the area of investigation. **A –** DEM of Panarea and its surrounding islets. Areas of investigation marked in red. The submarine locations Basiluzzo and La Calcara are situated apart from the “crater” locations illustrated in B. Bathymetric data grid: 10 m (modified after FABRIS et al. 2010). **B –** Map of the locations in the “crater“: Area 26 (A26), Black Point (BP), Bottaro North (BN), Bottaro West (BW), Cave (CAV), Fumarolic Field (FF), Hot Lake (HL) and Point 21 (P21), where the strongest gas vents occur. Modified after ADAMEK (2021) based on Google Earth (2020; version 7.3.2.5776; orthophoto taken on 2019-07-07).

Basiluzzo

This underwater investigation site is situated at the south-east slope of the islet Basiluzzo (near Punta Levante) about 4 km northeast of Panarea Island. Investigations started in 2011. The steep hard-rock cliffs and blocks of the shoreline continue down to a water depth of about 15 m. In greater depth wide sand slopes dominate the topography.

Exploration was conducted only down to a depth of 40 m due to dive technical reasons, although the slopes obviously continue far deeper. The site is one of the type localities for TFe-type discharge features described by STANULLA et al. (2017a).

Black Point

Black Point is one of the key locations in the submarine geothermal system of Panarea. It comprises a shallow water grey smoker at a water depth of only 23.5 m. This unique structure allows scientific divers to carry out in-situ measurements and the investigation of topics from all fields of geo- and biosciences.

Black Point itself is built up of massive sulfide ore aggregates (galena, sphalerite, pyrite/marcasite) growing around the main emanation point of hydrothermal fluids (BECKE et al. 2009). The elongated block shows several minor discharges and elevated fluid temperatures. The surroundings are characterized by gravel fields being covered with Posidonia.

Bottaro North

The location is situated in the channel between the islets of Bottaro and Lisca Bianca.

The underwater investigation site at the slope of Bottaro is characterized by lots of apparently gas-dominated hydrothermal vents: "*The Ting*" in the central part is a ring of several strong vents at water depths of about 9 m.

The flat slopes are covered with large blocks and gravel. Mineral precipitates are mostly built of native sulfur.

Bottaro West

Situated west of the islet of Bottaro, this site was a central point of the 2002 gas eruption. The "boilltore" formed a well visible, large crater structure in the slope of Bottaro (cf. CARACAUSI et al. 2005a).

This location had changed dramatically in the years 2006 to 2010. Sediments continuously filled the "boilltore" and abstracted the crater structure. Today, only several small gas-dominated vents can be observed. The area is covered by gravel and Posidonia.

Cave

The underwater investigation site Cave is situated in the central parts of the “crater”. Investigations started in 2015. A depression of about ten meters bears a small cave at its eastern rim, showing remarkable hydrothermal fluid discharge. Due to the sheltered location, the inner parts of the cave are completely covered by bacterial mats. The depression is intersected by a large dyke and comprises some interesting outcrops of the underlying geological strata. Water depth reaches 23 m.

Fumarolic Field

This wide field of gravel lies close to Hot Lake at a water depth of 17 m. It shows a number of small gas-dominated vents, mostly arranged in parallel lines along fracture zones. The surroundings are covered with Posidonia.

Hot Lake

This meter-deep depression is situated at a water depth of 17 m north of Fumarolic Field. For years it has been one of the best investigated sites in the area as it was characterized by hot hydrothermal water with the highest electrical conductivity (two-fold seawater) and only very few and weak gas discharges within the depression. Due to its geometry, the seawater within the depression showed higher temperatures (approx. 35 °C) than the surrounding seawater what gives the site its name. During the last years, this phenomena of “hot” water in the depression has disappeared. Measurements in 2017 and 2018 showed no increased temperatures anymore. Furthermore, the bacterial mats in the small grotto disappeared completely. The location also comprises lots of secondary sediment structures. It is surrounded by large fields of Posidonia.

La Calcara

Except Basiluzzo, La Calcara is the only documented underwater investigation site outside the “crater” area. It is situated at the bay of La Calcara at the shore of Panarea Island. Due to its large lateral extent, several sub-locations were defined. In addition to the two buoys, there are Black Rock, New Rock, n.n.-Area, The Wall, Fix Point 9, Octopus Rock and Mordor. The water depth in the investigated area varies between 10 and 24 m.

The location is characterized by wide, recent sandflats with single boulders/rocks. The underlying sands in the underground are characterized by a large amount of clayish matrix.

Hydrothermal vents are mostly small and gas-dominated showing continuous exhalation. They cause typical secondary structures in the sediment (cones, tubes).

Point 21

The discharges of Point 21 are among the strongest vents in the system. The emanations at the base of a scarp wall which was probably caused by a tectonic structure can be located even from distance. The hardrock wall shows sulfurous mineral precipitates as well as massive sulfide ore mineralization. The surroundings are characterized by blocks and boulders lying on gravel or being covered with diverse biota. The deepest point is 21 m below the ocean surface.

Table 4: Locations and sub-locations in the area of investigation. Coordinates are given mainly for the reference points (buoys). Further spatial references are given in the location maps of SDC Freiberg.

Location [abbr.]	Coordinates [UTM 33 S]	Water-depth [m]	Discharge [classes after STEINBRÜCKNER (2009)]	Rock facies/special features
Area 26 [A26]				
Buoy 1	509111 4276753	26	Class A to B vents gas-dominated few water discharges	Sand, gravel, mass flow deposits; sulfurous cementations; flat morphology
Buoy 2/Mouth [MOU]	509141 4276771	26	Water-dominated	Pre-subrosion state
Hot Bowl [HB]	509124 4276699	26	Gas/water	Subrosion structure
Lineament Structure [LS]	509157 4276719	26	Gas/water	Elongated hydrothermal feature forming a variety of structures
Brodor [BRO]	509146 4276713	26.2	Gas-dominated	Tubes, cones
3-bowls [3B]	509171 4276702	26	Gas/water	Subrosion structures
Lava-tongue [LT]	509170 4276742	26	Gas-dominated	Gas erosion; isolated volcanic bomb
Basiluzzo [BA]	510216 4279357	> 40	Class A to B vents gas-dominated	Sand, silt; iron(hydr-)oxide cementations; tubes; wide slopes
Black Point [BP]	509111 4276498	24	Class A to C vents gas/water	Shallow water grey smoker; massive sulfide ore mineralization
Bottaro Nord [BN]	509578 4276690	9	Class A to E vents gas/water	Coarse sediments: gravel, boulders; sulfurous cementations
Bottaro West [BW]	509573 4276555	14	Class A to C vents gas/water	Main crater of 2002 gas eruption; coarse sediments: gravel, boulders; sulfurous cementations

Location [abbr.]	Coordinates [UTM 33 S]	Water-depth [m]	Discharge [classes after STEINBRÜCKNER (2009)]	Rock facies/special features
Cave [CA]	509376 4276740	23	Class A to D vents gas/water	Large scale subrosion structure
Fumarolic Field [FF]	509542 4276825	17	Class A to C vents gas/water	Coarse sedimentary facies: gravel, conglomerates
Hot Lake [HL]	509545 4276859	17	Water-dominated	Large-scale subrosion structure, filled with medium to fine-grained volcanoclastics (> 3 m sediment depth)
La Calcara [LC]				
Buoy 1 [B1]	506616 4277411	23	Class A to C vents gas/water	Sand, silt; massive sulfide mineralization; alunitic and iron(hydr-)oxide cementations; tubes, cones; flat morphology, slopes;
Buoy 2 [B2]	506615 4277480	23	Class A to B vents gas/water	
FP 9	506609 4277596	23		Iron(hydr-)oxide cementation and crusts
Black Rock [BR]	adj. B2	21	Class A to B vents gas/water	Massive sulfide ores
Mordor [MOR]	adj. B1	21.6	Class A to C vents gas/water	Iron(hydr-)oxide cementations; tubes, cones
New Rock [NR]	adj. B2	23		
Octopus Rock [OR]	506714 4277078	23		Tubes of different facies
Point 21 [P21]	509247 4276621	21	Class B to E (4x) vents gas-dominated	Dacites/andesites, scarp wall
Subaerial 1	506575 4277293	48 m asl.	n.a.	Paleo -lineaments
Subaerial 2	505821 4277197	130 m asl.	n.a.	Brown tuff; paleo-tubes;

4. Materials and methods

4.1. Underwater research

Generals

Any research at underwater locations raises complex and specific demands on the workflow, on occupational safety and the special training status of the scientists. Among many other procedures such as laboratory standards or sampling routines, methods of Scientific Diving are necessary to carry out underwater research. However, the diving itself has to be understood as one single research tool the scientist uses. It is only a supporting method to make the underwater sites accessible. Scientific methods itself have to be carried out in their usual way, although adapted to a special environment. If possible, standardized measuring and sampling procedures should be adapted to the application under water to conduct in-situ measurements.

Due to the work in a hyperbaric ambiance, a number of safety regulations have to be followed while doing underwater research. This complex topic touches different fields such as technical design of diving equipment, maintenance procedures, dive planning and routines as well as health requirements of the divers and documentation obligations. Thus, a specific working instruction for “Scientific Diving” must be considered and strictly carried out. It defines central points, such as decompression procedures and diving methods. Normally, scientific diving is realized using high quality diving equipment without permanent surface supply. It is therefore limited by the parameters time (tanks size), temperature (cooling of the diver), decompression and a combination of these.

The work for this thesis was carried out using 15 L, 200 bar standard scuba-tanks, redundant cold-water regulator technics (Apeks) and semi-dry-suits. All dives were realized with compressed air but neither Nitrox nor Trimix, which is normally not available on the isle of Panarea. Dive planning did not consider decompression as typical for trimix diving. However, all dives were realized using redundant diving computers and their decompression calculation. Deco-stops longer than 30 minutes were avoided.

The campaigns were planned with three dives per day, but normally each diver had only two dives a day. Two five-day blocks of diving were separated by a one- or two-day diving break in order to optimize the N_2-desaturation of all divers.

The underwater investigation sites are about 2.5 km offshore Panarea (harbor). Thus, a Zodiac with a capacity of 16 divers from a local diving center (Eolo Sub Diving Center or Amphibia Diving Center Panarea) was used.

Drawing and mapping was realized using PVC writing tables and graphite pens.

Water depth measurements were conducted using the diving computers which theoretically give values at a ± 10 cm accuracy.

4.2. Field methods

Rock sampling and sample treatment in the field

The underwater techniques of rock sampling (hammer, chisel; transport box or sampling bag), drilling (hardground; pneumatic drilling alignment; crown: D=112 mm; L=300 mm) and liner sampling (soft sediment; PVC liner; D=50 mm, L=1 m) proved to be most appropriate for this research. If necessary, geological structures were excavated by a mobile airlift pump as described by STANULLA et al. (2016).

Rock samples from subaerial locations were gained by hammer and chisel. All samples were geologically described and documented with photos. Afterwards, they were cleaned and washed directly in the field to avoid secondary mineralization. Fragile rock samples were stabilized in the field lab using epoxy resin.

For some samples, handling under a protective nitrogen atmosphere was realized to avoid the oxidation of certain minerals such as pyrite or galena. The procedure included the on-spot isolation of the sample to the protective atmosphere. The rock was placed into PVC-bags and washed repeatedly with boiled water. Afterwards, the bags were inflated with nitrogen and firmly closed by cable ties (cf. KÜRZINGER 2019). At the surface, the samples were immediately transferred to a mobile field glovebox with N_2-atmosphere and treated therein just as “normal” samples.

The transport of samples and sampling equipment was conducted with transport nets if their weight was less than 6 kg. Weights larger than 6 kg were handled using lifting bags (50 or 100 lbs).

Mapping

All maps and sketches were developed directly on-spot. Distances were measured related to fixed points from shot-lines (downline to a buoy), which were measured with a Garmin GPSmap 64 ST at the water surface. The accuracy of the device is given with ± 3 m by the manufacturer. However, a remarkable deviation of several meters must be considered as the buoy at the surface might not float orthogonally above the anchor point at the sea-bottom (depending on current and wind). This effect is hard to quantify and increases with water depth. Additionally, also an underwater-GPS arrangement equipped with a Garmin GPSmap 276c (accuracy: ± 3 m) was applied to gain data (cf. GANSS 2013).

Although measured repetitively by different persons in different years using different GPS devices, an inexplainable shift was detected in all GPS coordinates during post-processing. The degree of shifting varies daily and cannot be named precisely. Any coordinates given in this thesis are corrected by a daily shift acquired by the deviation of reliable topographic points (e.g. the mole of Panarea). If this was not possible, the read data from the fieldtrips is denoted.

The underwater positions were determined by their distance to the fixpoint (buoy) and the respective compass-course. For (sub-) locations, where no coordinate has been measured, the values were calculated from this distance-direction-dataset. In

combination with the before mentioned accuracy values, an estimated overall accuracy of approximately ± 10 m can be assumed.

The working groups created a number of different map sketches of various scales and contents which have been combined to the largescale overview maps.

Structural geodata is given as striking „from-to“ in cases, where no dipping angle was measurable or a great error was to be expected due to sediment cover or outcrop properties (cf. ADAMEK 2021). Otherwise, the form “strike/dip sector” is given for underwater sites: e.g. 330/70 NE describes a 330 ° strike direction and a dipping angle of 70 ° to the northeast. For subaerial measurements, the form “inclination/dip” is presented. Consequently, the values 000/75 indicate an inclination of 0 ° and a dipping angle of 75 °. Strike direction and inclination angle are perpendicular to each other.

Fluid discharge features were classified according to STANULLA et al. (2017a). Where indicated, the classification scheme was updated in the context of the prevailing work. The respective nomenclature is given in chapter 6.

To map the different types of discharge features which are covered by sediments they had to be cleaned off from sediments (sand, silt, clay). The covering sediments were removed both by whirling up the sediment by hand or using a mobile airlift pump (cf. STANULLA et al. 2016). A cleaned off discharge feature remained uncovered for several days (or sometimes only hours, depending on the currents). However, it has to be pointed out, that removing the surrounding sediment is a massive impact on the boundary conditions in the case of an active discharging system (both gas and water discharge). Thus, any physico-chemical measuring or water and gas sampling must be done before the cleaning procedure.

Photo and video documentation

The visual documentation was carried out using different camera systems according to the aim of the documentation. Most of the images and videos were taken with a compact camera system type Sony DSC-RX 100 MII combined with an Ikelite polycarbonate underwater housing. The AVCHD-format with rates of 50 half-images per second was used. Images were created at 20 MP using the RAW format. For special video-sequences, a Broadcast HD camera type Sony PMW EX1R XDCAM combined with an external HD/4K Recorder Video Device PIX-E5 was used. The system is waterproof by an underwater housing type Gates EX1R and equipped with a wide-angle objective type Phantom SWP44C. The scenery was illuminated by special HQ LED video lights with a color temperature of 3200 K. The respective white balance was adjusted in the camera. A scale is given by diving knifes (usually Aqualung Scissor Knife, black; complete length: 22 cm; “Aqualung”-label: 8 cm), pens or scale bars.

Video-postproduction was carried out using the software Avid Media Composer 5.5 and Adobe Premiere Pro CS 6. Image manipulation was conducted with the Adobe Creative Suite CS 6. Panoramas were stitched using the software autostich64 from the University of British Columbia.

Selected images are given in the photo documentation in appendix 1. Appendix 2 gives a selection of video scenes on central issues in the context of the presented research questions.

Fluid sampling

Geothermal fluids discharging at the sea bottom were sampled with polypropylene syringes (i.e. SIELAND 2009) of different types (40 ml, 100 ml, and 450 ml; e.g. GeoWiD SaSy) being equipped with three-way-valves and tubes (Teflon) attached. The tubes were flushed three times with the sampling fluid. The diver has to consider possible degassing of the fluid in the syringe and expansion of gas bubbles to avoid popping out of the plunger of the syringe when ascending to the surface. Sea water samples were taken either with the above-named technique or by the use of water samplers (GeoWiD DOBB; cf. BRÜMMER et al. 2013).

Gas sampling was done with a funnel (stainless steel or teflon: GeoWiD DeGaS) with a gas trap at the top and a sidewise outlet of water placed on the discharge point collecting the emitted gas phase (MERKEL et al. 2011). The gas is transferred to a gas-collecting-tube directly at the point of sampling.

Gas flow rates were measured over longer periods at Point 21 by a flow meter (FSVG; PONEPAL et al. 2010). Small gas flow rates were measured by means of displacing water in a glass bottle by discharging gas and reading the time. Using the depth from the diving computer, measured gas volumes were recalculated to normal conditions (1 bar, 25 °C; cf. STEINBRÜCKNER 2009). All gas flow rates given in this thesis were estimated according to the classification given by STEINBRÜCKNER (2009).

Sample preparation in the lab includes the sample-filtration with 200 nm syringe filters for IC and ICP-MS analysis. Samples for cation IC and ICP-MS were acidified with ultrapure HNO_3 to a pH < 2. All samples were stored in a refrigerator until analytical procedures.

Measuring of physico-chemical parameters

Physico-chemical parameters were measured in-situ as well as in the field laboratory. In-situ measurements included electric conductivity using the GeoWiD CoMeD equipped with an Ahlborn Almemo 2590 and temperatures of the discharging water measured with a GeoWiD HEAT. Temperature measurements were also conducted with thermogradient probes, thermo-flux devices and a variety of thermo-probes combined with a GMH 3350 (cf. BARTH et al. 2010; MÜLLER 2011).

The field parameters pH, Eh, EC and O_2 were measured either directly with a multiparameter probe (YSI) or a WTW MultiLine handheld which was housed in a custom-made waterproof housing and/or within 1 to 2 hours after underwater sampling using HACH and WTW field devices.

4.3. Laboratory methods

This chapter only refers to solids (sediment and rock samples) as they are the host for hydrothermal discharge features, which are in focus of this thesis. However, continuative (geochemical) analysis such as isotope ratios have not been in scope of this work and are subject to further analyses. The treatment of fluid samples was conducted in the laboratory of the Hydrogeology Department of TU Bergakademie Freiberg in the context of other theses (e.g. MEINARDUS 2016).

Sample preparation

Numerous thin and polished sections were prepared. Due to the highly fragile material, most of the samples were stabilized with epoxy resin (multiple applications under vacuum conditions). Thin sections have a standard size of 28 x 48 mm and a thickness of 30 µm. Larger formats of 50 x 75 mm were prepared when necessary to map a complete structure. Powder samples were prepared for XRF and XRD analysis at a fraction of < 63 µm.

Sample analysis

Optical microscopy was carried out using different types of Zeiss polarization microscopes and binoculars. Scanning electron microscopy (SEM) analyses were carried out using a Jeol JSM-7001 F Field Emission Scanning Microscope at the Institute of Geology of TU Bergakademie Freiberg. Measurements were kindly realized by Mrs. Anja Obst. The polished thin sections were coated with graphite before the investigation to ensure a homogenous conductivity of the sample.

X-ray computed tomography (XCT) was kindly conducted by Dr. Thomas Leißner of MVTAT at TU Bergakademie Freiberg with a ZEISS Xradia 510 Versa. Measurement and reconstruction parameters for samples BA-4, LC-1 and BK_ A26-2010 are given in Table 5.

After acquiring the projection images, reconstruction of the volume data was done using the software XRM Reconstructor (Zeiss). This software uses the “back filtered projections“-algorithm. The parameters of the reconstruction are listed in Table 6.

Quantitative analysis of microstructures and illustration was carried out using the software MAVI 3D (Fraunhofer Institut für Techno- und Wirtschaftsmathematik, ITWM, 2015).

Table 5: Parameters of the XCT scan using a Zeiss Xradia 510 Versa X-ray microscope.

Parameter	[ ]	Sample		
		As	LC-1	A26-2010
Source position	mm	-150	-150	-150
Detector position	mm	110	110	55
Objective		0.4X	0.4X	0.4X
Mode		Widefield	Widefield	Vertical stich
Binning		2	2	2
Pixel size	µm	39.5	39.5	50
Voltage/power	kV/W	160/10	160/10	140/10
Filter		HE2	HE3	HE2
Exposure time	s	3	2.5 (var., strength 3)	4
Secondary reference		None	None	None
Angle	°	360	360	360
Projections		1601	1601	2001
Scan time	h:mm	2:40	2:40	3:30

Table 6: Reconstruction parameters used in the Zeiss XRM Reconstructor software.

Parameter	Sample		
	BA-4	LC-1	A26-2010
Smoothing filter	Gaussian, 0.7	Gaussian, 0.7	Gaussian, 0.7
Beam hardening correction method	Standard	Standard	Standard
Beam hardening const.	0.1	0.1	0.1
Secondary reference	None	None	None
Center shift	Automatic	Automatic	Automatic
Byte scaling	Automatic	Automatic	-79.0687/2194

Parameter	Sample		
	BA-4	LC-1	A26-2010
Ring removal	None	None	High contrast
Defect correction	Disabled	Disabled	Bright and dark spots

Energy dispersive X-ray spectroscopy (EDS) was performed with a BRUKER EDS during SEM microscopy with a Jeol JSM-7001 F Field Emission Scanning Microscope. Thin sections were sputtered with graphite before the investigation.

The XRF analysis used a Spectro Xepos spectrometer with a standardless routine. All values are normalized to CI-Chondrite concentrations after MCDONOUGH & SUN (1995). Values below the detection limit were eliminated from the dataset. The elements were sorted empirically by the mean element concentration of the dataset, from the lowest concentrations (left) to the highest (right).

X-ray diffraction (XRD) patterns were measured with a Panalytical X'PERT Pro MPDPW 3040/60 diffractometer in reflection geometry using powder samples (Table 7). For reflection measurement the sample was prepared by using the Back-Loading technique. µ-XRD analysis was applied to small-scaled structures using a Bruker axs D8 Discover. The phase identification was performed using the X'Pert HighScore Plus software. Investigations using XRF and XRD were kindly conducted by Ms. Elsa Qoku (IKGB) and Dr. Markus Schreiner (IEC) at labs of TU Bergakademie Freiberg.

Table 7: Parameters of the XRD analysis using a Panalytical X'PERT Pro MPDPW 3040/60 diffractometer.

Parameter	Setting
Angular range	7.5 – 80 ° 2θ
Step size	0.013 ° 2θ
Step time	30 s
Radiation	Copper
Tube Power	40 kV/40 mA

Granulometric analysis was kindly conducted by Mrs. Gitta Schneider in the sedimentological laboratory of the Institute of Geology at TU Bergakademie Freiberg. Grainsize measurements were realized according to DIN 18123-5.

5. Results

Information given in this chapter partly include findings from other working groups (bio, fluid flow, gas-/water-chemistry, geo, thermo) of the Scientific Diving Center Freiberg.

Names of local features at certain UWIS which are discussed in this chapter are highlighted with *Italic* letters.

5.1. Prevailing lithologies

Investigations show, that the three lithofacies given in common literature for the submergent parts of the “crater” of Panarea are not sufficient to describe the suite of rocks in that system. Some of the areas shown as homogeneous lithology in current maps (cf. ESPOSITO et al. 2006), exhibit a much more complex architecture. However, it was not aim and purpose of this work to map the underwater shelf area of Panarea in detail.

The rough descriptions in the following chapters should deliver a basic knowledge on the rocks and sediments distinguished (Figures 7 - 19). However, neither a sedimentological nor a petrographic study were in scope of this thesis and are thus subject to further investigations.

5.1.1. Hardrocks

Three major types of hardrocks were documented in the submarine system of Panarea (Figures 7 - 8, Table 8):

(1) Dacite/Andesite

Dacites/Andesites are the dominating volcanic hardrock in the system (Figure 7-A and -B). They are characterized by porphyritic texture and large phenocrysts or volcanic inclusions.

As any other lithology, this facies is heavily affected by hydrothermal alteration which makes mineral identification nearly impossible. According to the shape of minerals, plagioclase, biotite, and some heavy minerals could be identified (Figure 8).

Colors range from white to reddish brown depending on the degree of alteration.

Type locality: Point 21

(2) Tuffite

This lithology appears in limited local extent near Hot Lake and in Area 26 (*Lava-Tongue*). The grains appear as fine to medium sand in grain size. The lithology shows washy surfaces which is probably enhanced by the impact of the seawater movement (waves, current; Figure 7-C and -D). Colors appear beige to (pale) grey.

Type locality: Hot Lake, Area 26 (*LT*)

(3) Dykite

Several dykes intersect the “crater” roughly in a main strike direction of 330 ° (personal communication J. Adamek). Concise measurement of single geometries was not in scope of this work.

The material is strongly silicified and thus extremely hard. It therefore appears dominant as cliffs or ridges with smooth surfaces at the seafloor (cf. *Dragon Tooth* at Bottaro West, Figure 30-D, or “honeycombs” at Cave, Figure 32-A). Especially in Cave, the rock is interspersed with small tube-like channels that act as gas pathway. It is mostly greyish colored (Figure 7-E and -F).

Subaerial analogues can be found on land at the islet of Bottaro and in the bay of La Calcara (Subaerial 1). Additionally, CAS et al. (2011) present hydrothermal breccia textures, that show similar structures. However, the veins of the here described dykite appear much harder and brittle wherefore these lithologies cannot be compared. The breccia facies was not found in the documented underwater investigation sites.

Type locality: Cave

Table 8: Hard rock lithologies in the submarine hydrothermal system of Panarea and their main occurrences.

Lithology	Description	Type Locality
Dacite/Andesite	Porphyritic texture, large phenocrysts or volcanic inclusions white to reddish brown depending on the degree of alteration	Point 21
Tuffite	Grain size: fine to medium sand washy surfaces beige to pale grey	Hot Lake, Area 26 (*LT*)
Dykite	Extremely hard and strongly silicified lots of small channels mostly greyish	Cave

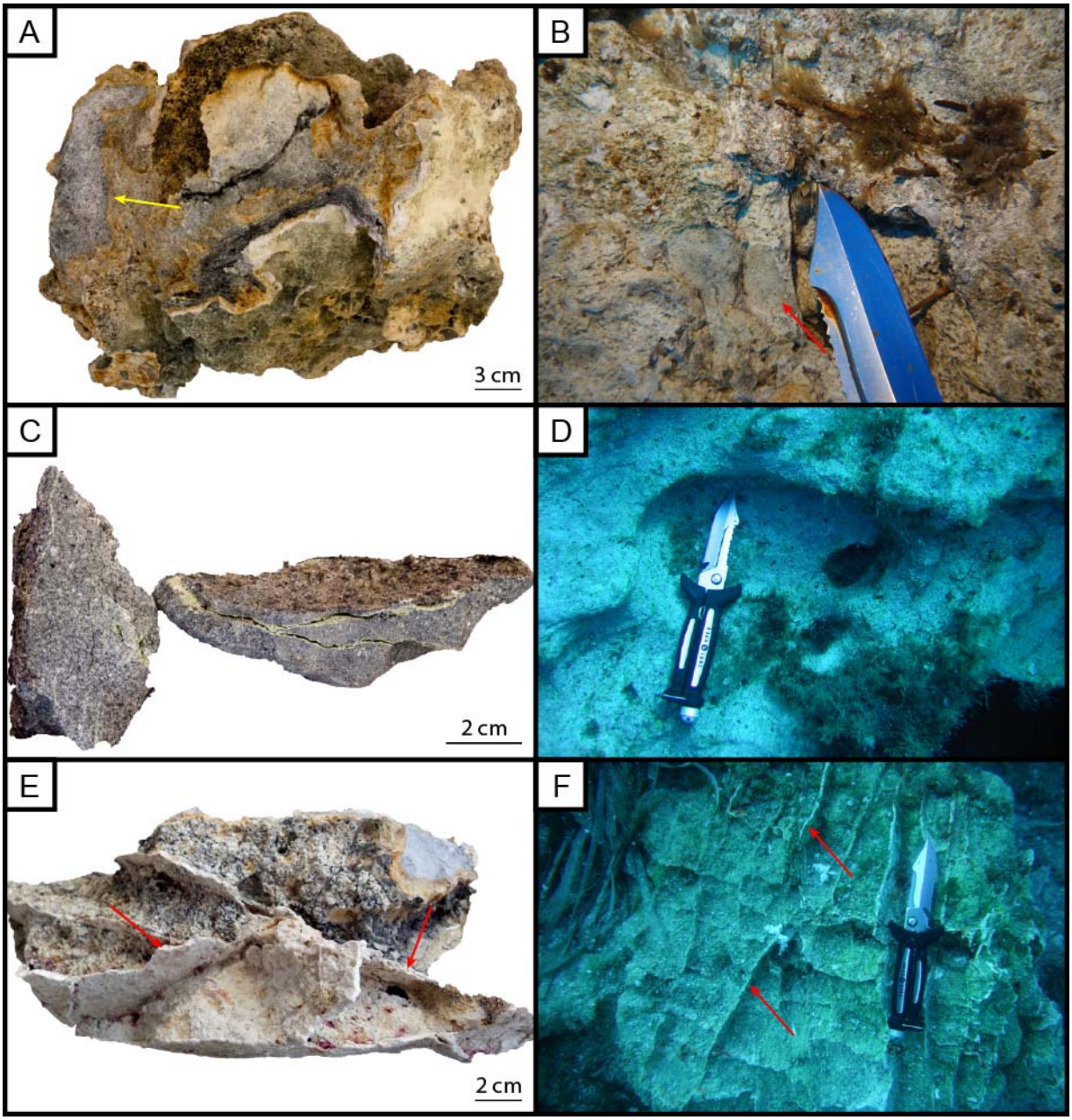

Figure 7: Hard rock lithologies – samples and in-situ documentation. **A –** Sample of the highly altered Dacite/Andesite taken near Hot Lake. Iron-bearing secondary mineralization on fractures is marked by the yellow arrow. **B –** Strongly altered Dacite/Andesite in-situ at Point 21. The red arrow marks a prominent phenocryst. **C –** Tuffite sample from Hot Lake. The material is intersected by small fractures with sulfur filling (FS). **D –** Outcrop near Hot Lake showing the Tuffite lithology. Erosion by waves and currents caused washy surfaces. **E –** Dykite of Cave. The silicified "honeycomb" structures are well visible. They incorporate different materials such as Dacites/Andesites and Clays. The red arrows mark degassing channels. **F –** Block of an in-situ Dykite near Cave. Some discharging ridges are marked by the red arrows.

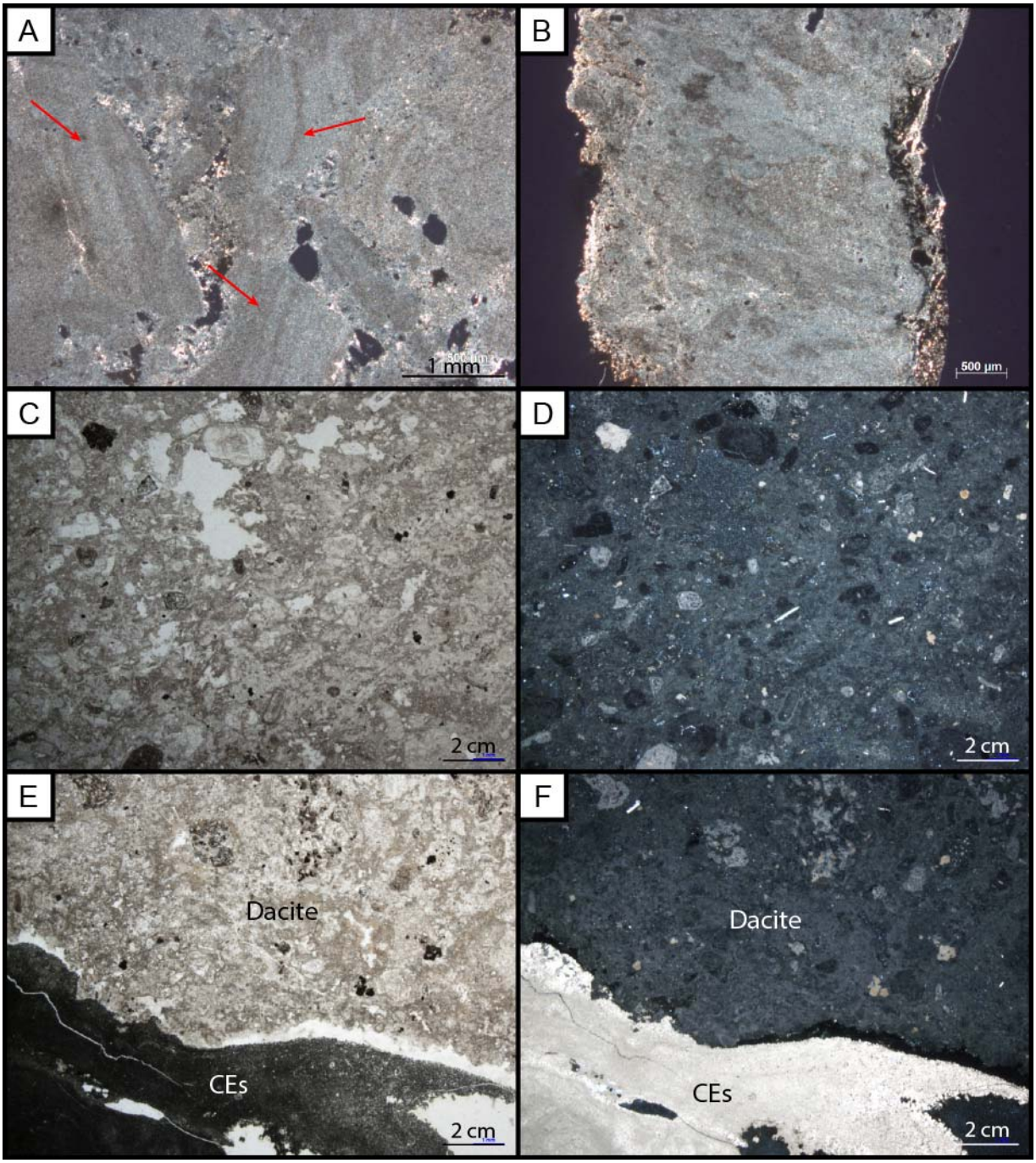

Figure 8: Hard rock lithologies – thin sections. **A –** Thin section of strongly altered hardrock from Cave. Single minerals can be distinguished concerning their shape (red arrows). However, mineral and rock identification failed due to the degree of alteration. X-Pol., 2,5x. **B –** Overview image of the thin section shown in A. Despite secondary mineralization at the outer rims, a remarkable silicification appears in the whole thin section. Further mineral identification is not possible due to severe alteration. X-Pol., 2,5x. **C –** Strongly altered Dacite/Andesite from Point 21. Compared to the material from Cave, the degree of alteration is moderate. Single minerals can be identified by their outer shape. Rock identification based on the overall composition is not possible. II-Pol., 2,5x. **D –** Same as C but X-Pol. In combination of II- and X-Pol., single minerals can be identified as amphibole, quartz, and biotite. Some volcanic glasses can be assumed. **E –** Native sulfur crust (CEs) on highly altered Dacite/Andesite (Dacite) from Point 21. The Dacite/Andesite shows xeno- to idiomorphous crystals, mainly feldspar, biotite, and volcanic glasses. Erosional structures on the crystals surface are common. The material shows a high degree of alteration. II-Pol. **F –** Same as E but X-Pol. Mineral residuals dominate the thin section.

5.1.2. Sedimentary rocks

All investigated locations obtain sedimentary material, which either is a primary sedimentary rock or a recent cover of sand and/or gravel. A good example is Area 26: the outcropping lithology is a typical volcanoclastic sandstone (sedimentary rock). It is mostly covered by recent sands (sediment), which appear quite similar on the first view.

The following chapter describes the consolidated sedimentary rocks (Table 9). The loose sediments are described in detail in chapter 5.1.3.

The sedimentary rocks can be distinguished by their cements that mainly consist of secondary mineral precipitates such as native sulfur, iron(hydr-)oxides or massive sulfide ore minerals. Furthermore, clayish cements occur. The cements and their facies are described in chapter 5.1.4.

Typical sedimentary rocks in the system are:

(1) Sandstone

Typically, the sandstones of the Panarea system are medium grained, polymict and mostly poorly sorted. The grains are angular to sub-rounded. Most strata can be interpreted as mass flow deposit (Area 26; Figure 9-A and -B). Cements are predominately built up of (native) sulfur or iron(hydr-)oxides (Figure 10).

Type locality: Area 26

(2) Conglomerate

The conglomerates are quite comparable to the sandstones, despite their grain size, which is coarse sand to coarse gravel. The mode is polygenic, and the sorting is poor. Most grains are (sub-)rounded to well-rounded in this lithology (Figure 9-C and -D). Cements contain (native) sulfur or iron(hydr-)oxides.

Type locality: Fumarolic Field

(3) Fanglomerate

The fanglomerates are quite comparable to the conglomerates. They differ concerning their rounding which is angular to sub-rounded. The mode is polygenic, and the sorting is poor. Cements consist of (native) sulfur. This lithology was only documented in Area 26 and it hints on a deposition by a mass-flow event (Figure 9-E).

Type locality: Area 26

Table 9: Sedimentary rocks in Panarea and their main occurrences.

Lithology	Description	Location
Sandstone, sulfurous cements	Grain size: medium sand polymict, poor sorting grain shape: angular to sub-rounded	Area 26, Black Point
Conglomerate, sulfurous cements	Grain size: coarse sand to medium gravel polygenic, poor sorting grain shape: (sub-) rounded to well-rounded	Fumarolic Field, Cave
Fanglomerate, sulfurous cements	Grain size: coarse sand to medium gravel polygenic, poor sorting grain shape: angular to (sub-) rounded	Area 26
Sandstone, clayish cements	Grain size: medium sand polymict, poor to medium sorting grain shape: angular to sub-rounded	La Calcara
Sandstone, iron cements	Grain size: medium sand polymict, poor to medium sorting grain shape: angular to sub-rounded	La Calcara, Basiluzzo
Sandstone, ore cements	Grain size: medium sand polymict, medium sorting grain shape: angular to sub-rounded as reworked clasts in Bowls or incorporated in sulfurous sandstones and fanglomerates	Area 26
Conglomerate, ore cements	Grain size: coarse sand to coarse gravel polygenic, poor sorting grain shape: angular to rounded	Black Point, Cave

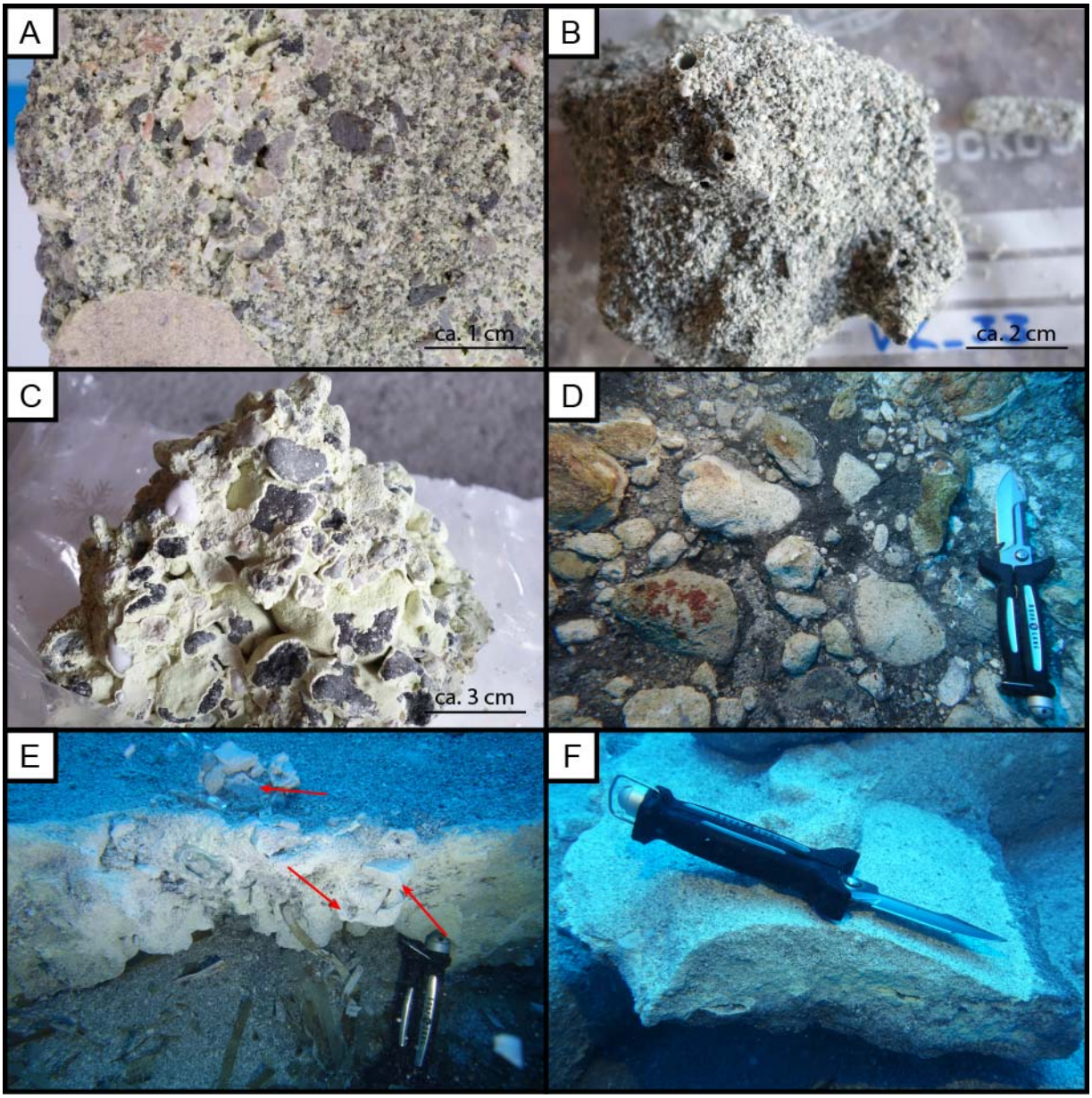

Figure 9: Sedimentary rocks. **A –** Drilling core in sulfurous sandstone from Area 26. Total core diameter is 100 mm. Angular to sub-rounded grain shape is well visible. Sulfurous cements dominate the lithology. **B –** Sulfurous sandstone of Area 26 showing the poor sorting and general habitus. At the top of the sample, two discharge features are visible. **C –** Conglomerate with sulfurous cement from Fumarolic Field. Sub-rounded grain shape and polygenic mode are obvious. **D –** Conglomerate of Cave with cements of massive sulfide ore mineralization. Coarse and sub-rounded grains dominate this facies. **E –** Fanglomerate with sulfurous cements from Area 26. The red arrows mark prominent angular to sub-angular grains that are typical for mass flow deposits. **F –** Typical sandstone from Area 26 with native sulfur cements. Sample taken from the sidewall of Bowl B at *3-Bowls* in Area 26.

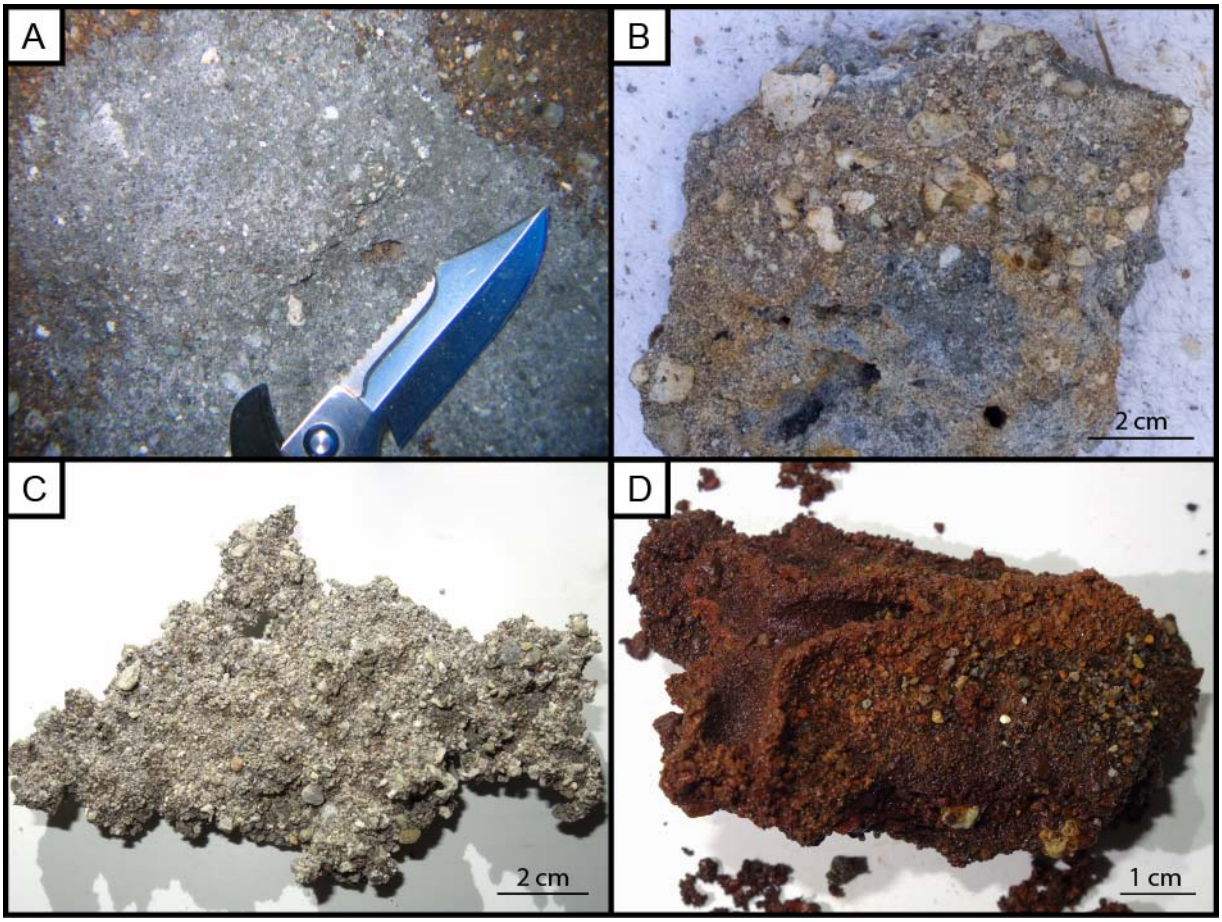

Figure 10: Sedimentary rocks. **A –** Sandstone with clayish cements (Alunite) in LC. The grains are affected by a high degree of alteration. **B –** Coarse sandstone with clayish cements from LC. Rounding varies from sub-angular to sub-rounded. Poor sorting is well visible. **C –** Sandstone from LC with massive sulfides (pyrite/marcasite) cementing the grains. Moderate sorting and sub-angular to sub-rounded grains are typical. **D –** Iron cemented sandstone from Basiluzzo. Again, a poor rounding and moderate sorting hint in short transportation. The sample obtains a prominent junction (Y-type) of TFe-type tubes in the left part.

5.1.3. Sediments

There are different types of soft sediments in the system, that mainly appear as recent sand cover at the seafloor. In some cases (e.g. Area 26), the material consists mainly of reworked particles of the prevailing sedimentary rock. The modes and the grain shapes seem similar. Additionally, the presence of isolated massive sulfide ore sheets in the sediment (or incorporated in the cemented sandstone) of Area 26 witnesses the reworking of former strata (Figure 11). However, this reworking must have been before recent neotectonics processes, as fractures intersect some of the ore sheets.

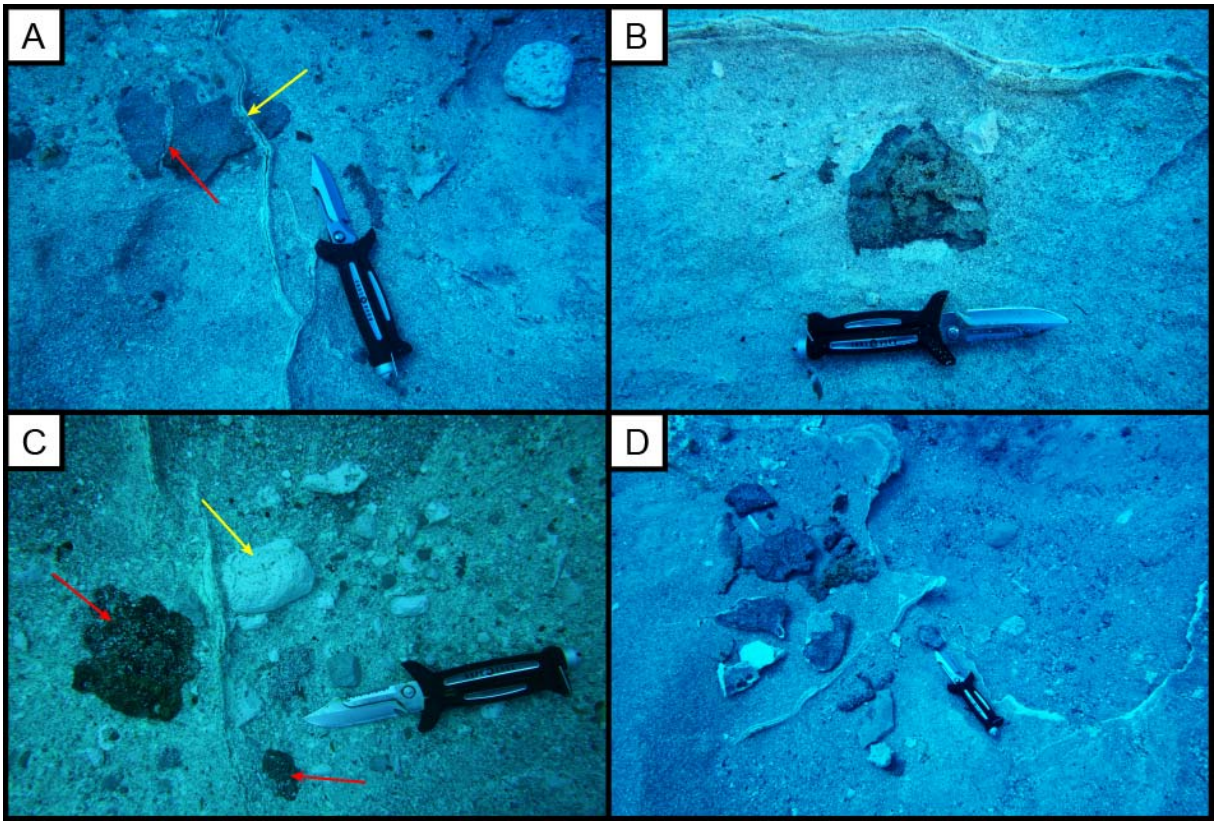

Figure 11: Ore sheets in Area 26. **A –** Clast of massive sulfide ore is intersected by two fractures (red and yellow arrows). In case of the one marked by the yellow arrow, a hydrothermal discharge feature (type FS) formed after deposition. **B –** Major clast of massive sulfide ore in the middle of *Lineament Structure* at Area 26. The clast is completely incorporated in the sedimentary rock. **C –** Set of clasts of massive sulfide ores (red arrows) and highly altered volcanites (yellow arrow). The polymictic material must have been transported before deposition as the rounding in the sedimentary context implies. **D –** Set of ore sheets from the excavated bowls at *3-Bowls* in Area 26. The material was not yet lithified. However, a transport into the bowls is likely, as in-situ mineralization would not produce such isolated clasts.

Other locations obtain different materials: in La Calcara, a mostly iron-bearing sand covers the clayish strata near Octopus Rock. The same situation can be observed in Basiluzzo. In contrast, also gravel occurs as covering layer for instance in Fumarolic Field and Black Point (Figure 12).

Figure 13 gives the results of granulometric analysis on samples from Fumarolic Field, La Calcara, Area 26, Black Point and Hot Lake. All materials show grainsizes of coarse medium sand and coarser. The only exception is the material from Area 26, where also fine- to medium grained sand prevails. All materials show a good grading and can be classified as “narrow graded” sand or gravel. Due to the finer components of the materials from Area 26, this material is the only one to be classified as “intermittent”. Permeability coefficients vary between 1 x 10^{-1} m/s in case of the Fumarolic Field gravel and 5.8 x 10^{-5} m/s for the sand of Area 26. All other samples show values of about 10^{-3} m/s.

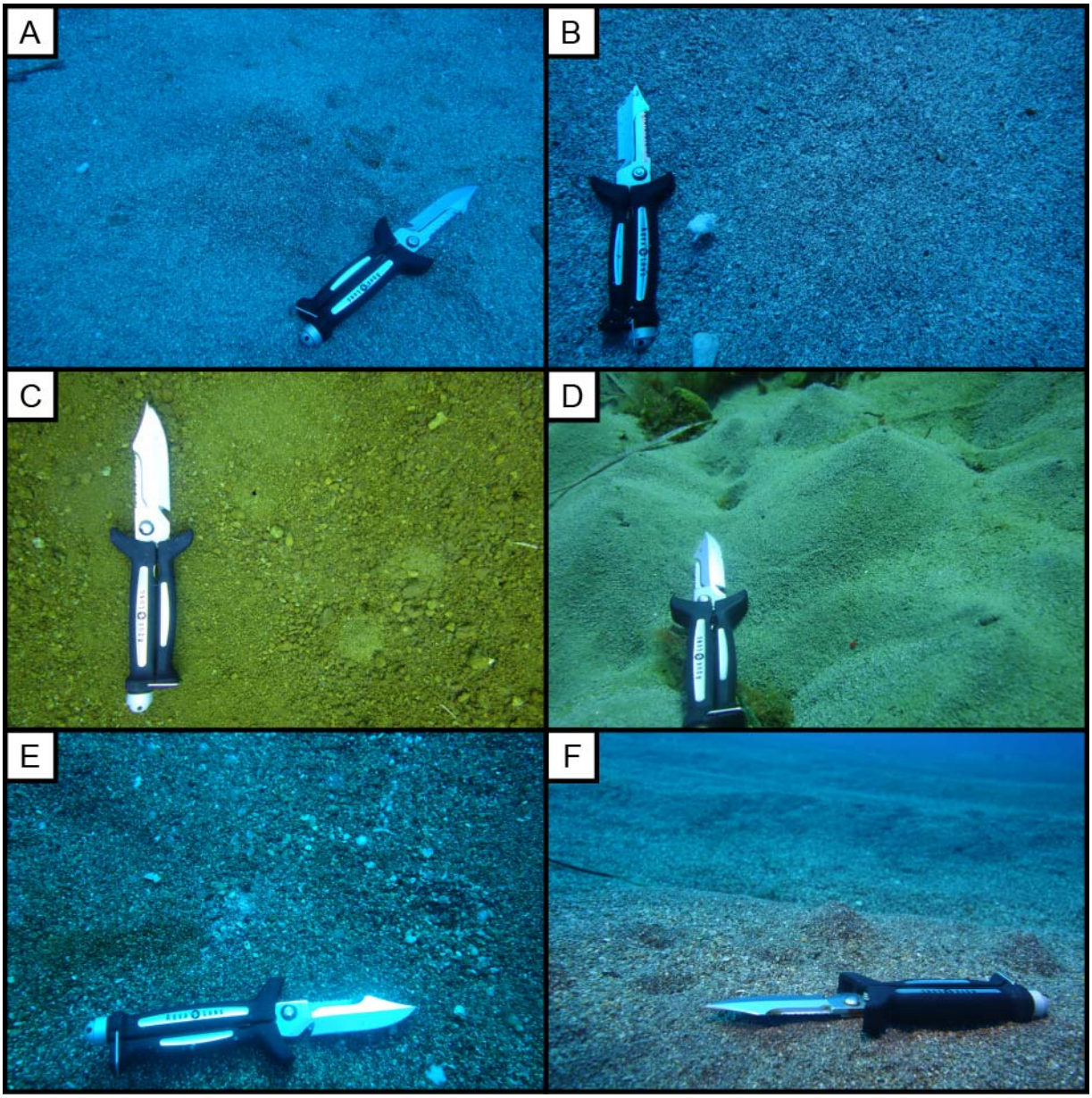

Figure 12: Recent sediments. **A –** Recent sand cover in Area 26. The material is polymict and comparably well sorted. It consists mainly of reworked material of the underlying strata. **B –** Recent cover sand filling the Hot Lake depression. The material shows a rather good sorting and seems to be allochthonous. **C –** Recent sand cover from Basiluzzo at about 35 m water depth. The grains are mostly coated by iron(hydr-)oxides. The sorting is poor and secondary mineralization form consolidated layers (iron(hydr-)oxide cemented crusts). **D –** Well sorted cover sands in Basiluzzo at a water depth of about 10 m. The material overlies the dacitic/andesitic hardrock facies and is probably heavily impacted by physical forcing of waves and tides (rounding, sorting). **E –** Coarse grained sand cover in La Calcara near *Mordor*. The material is poorly sorted and consists of a variety of materials. Secondary mineralization of iron(hydr-)oxide and other cements forms coarser aggregates. **F –** Fine grained cover sands in La Calcara. In contrast to E, nearly no secondary mineralization can be observed. Furthermore, the material is far better sorted and rounded, what hints on a higher level of energy at this site (south of Buoy 2).

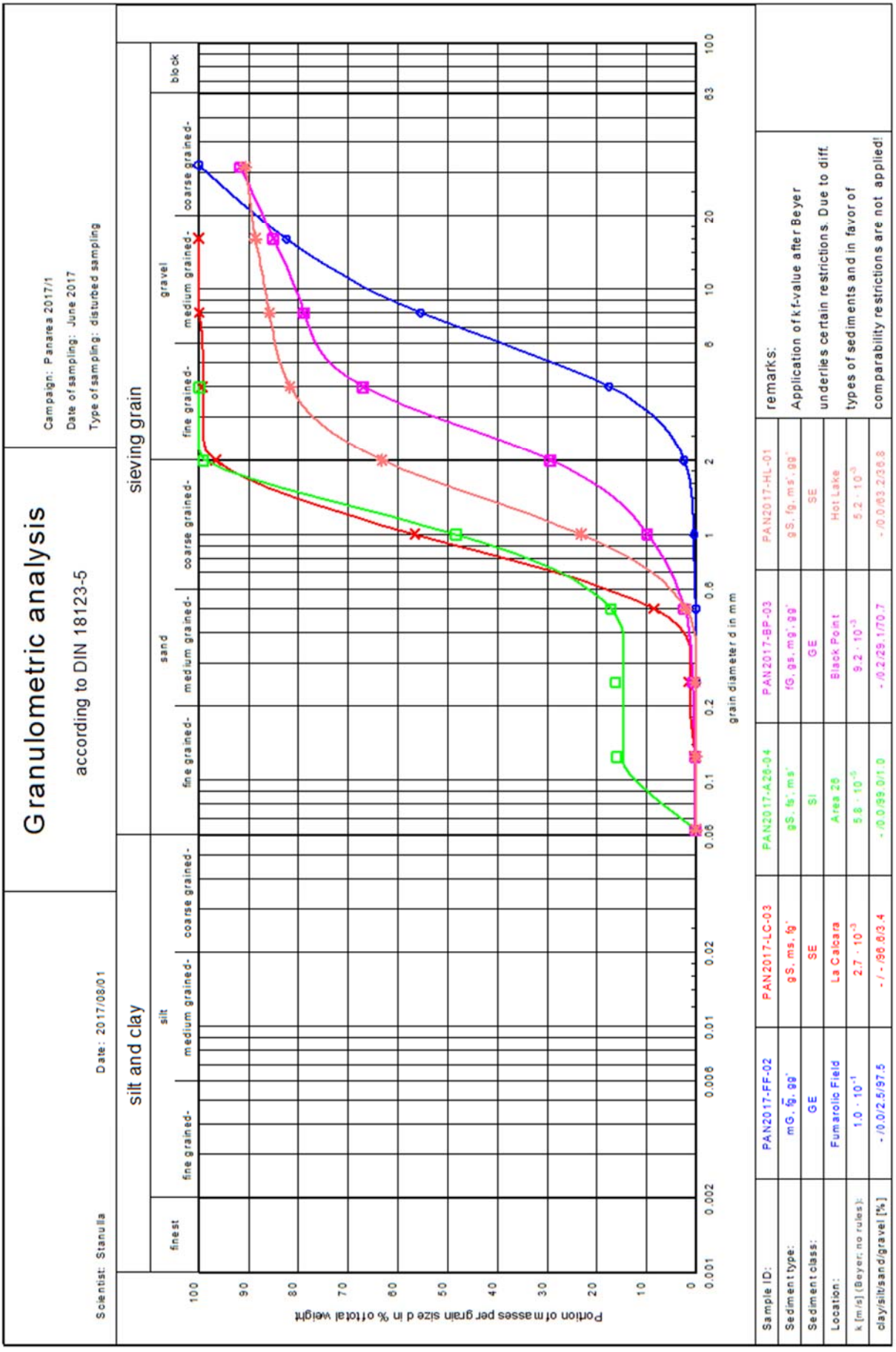

Figure 13: Granulometric analysis of recent sands from different locations.

5.1.4. Cements

Cementation is a common feature in the system of Panarea. This secondary mineralization occurs as isolated feature at hydrothermal discharges as well as rock forming process in larger scales. Anions and cations are mainly derived by hydrothermal fluids and rock-water-interactions such as leaching and weathering (a.o. DEKOV & SAVELLI 2004).

Materials are mainly made of iron(hydr-)oxides, sulfur bearing minerals or massive sulfide ores such as marcasite and pyrite (Table 10). Alteration processes may also form clayish cements that originate from the degradation of volcanic hardrock facies (cf. KÜRZINGER 2019). The following types of cements were found in the Panarea system (Figures 15 – 19):

(1) Cements of iron-oxides or iron-hydroxides (CEfe - cement, iron)

Iron-bearing cements are mostly occurring as fine-grained groundmass or coating (Figures 14, 15 and 16; cf. ESPOSITO et al. 2018). Lamination is a typical feature. The dominating minerals are Goethite and Hematite.

DI BELLA et al. (2019) and FERRETTI et al. (2019) also report from iron precipitates from Panarea having been investigated recently.

Type localities: Basiluzzo, La Calcara

(2) Cements of (native) sulfur (CEs - cement, sulfurous)

Commonly occurring as fine-grained coating or compact, crystalline fabrics (Figure 14 and 17). Rhythmic precipitation is a typical feature forming characteristic laminations. Mostly associated to colder vents.

Visually similar materials are reported by PETERSEN et al. (2014) from Palinuro seamount (north of Panarea) at a water depth of 600 – 650 m.

Type localities: Area 26, Fumarolic Field, Cave

(3) Cements of massive sulfides (CEore - cement, ore)

This type of cement appears as impregnations of (massive) sulfide ore minerals or individual aggregates (Figure 18). Rhythmic precipitation is a common feature forming characteristic laminations. Mostly associated to high temperature vents. The dominating minerals are marcasite, pyrite, sphalerite and galena (cf. PRAUTZSCH 2012).

Type localities: Area 26, Black Point, La Calcara

(4) Cements of clay minerals (CEclay - cement, clayish)

This facies is mostly occurring as weathering relicts that are forming the groundmass of sandy loams (cf. KÜRZINGER 2019; Figure 19). The characteristic mineral is Alunite.

Type locality: La Calcara

Table 10: Types of cements in Panarea and their typical mineralogy (exemplary).

Type	Description	Mineralogy	Type locality
CEfe (cement, iron)	Cements of iron-oxides or iron-hydroxides. Mostly occurring as fine-grained groundmass or coating (cf. ESPOSITO et al. 2018).	Goethite, hematite	Basiluzzo, La Calcara
CEs (cement, sulfurous)	Cements of (native) sulfur. Mostly occurring as fine-grained coating or compact, crystalline fabrics. Mostly associated to colder vents.	Sulfur	Area 26, Fumarolic Field, Cave
CEore (cement, ore)	Impregnations of (massive) sulfide ore minerals. Mostly associated to hot vents.	Pyrite, marcasite, sphalerite, galena	Area 26, Black Point, La Calcara
CEclay (cement, clayish)	Cements of clay minerals. Mostly occurring as weathering relicts forming the groundmass of sandy loams.	Alunite	La Calcara
CEo (cement, other)	Subordinated or unidentified cements. Mostly occurring isolated under special conditions.	Rhodochrosite, certs/quartz	La Calcara, Cave

Chemical analysis of the cements was carried out with XRF, (µ-)XRD and REM-SEM. The materials show varying chemical compositions. Figure 14 shows exemplarily the composition of iron(hydr-)oxide and sulfurous precipitates. The iron(hydr-)oxides are characterized by high concentrations of As, Br, Sr, Cl, Nb, Zr, K, and Rb. Y, Si, and Ca are common, while the Zn-, Pb-, W-, and Ni concentrations are low (cf. STANULLA et al. 2017a). Sulfur cements show high concentrations of Br, Cl, K, Ta, and S. Si, Pb, Mn, and Ni concentrations are low while concentrations of As, Nb, Zr, and Al are below the detection limit. However, the preferably laminated character of the cements must be considered while interpreting the chemical compositions (cf. STANULLA et al. 2017a). A physical separation of single laminae was not possible.

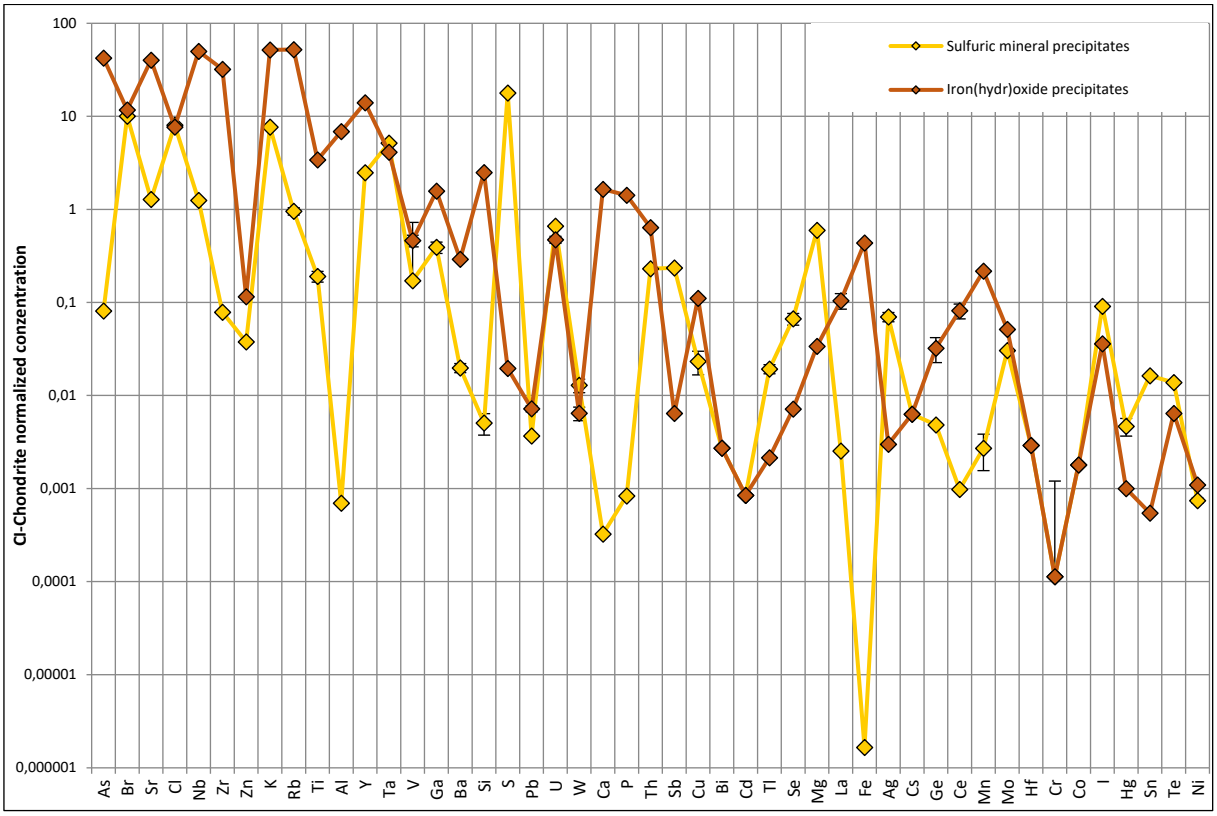

Figure 14: XRF analysis of the iron(hydr-)oxide and sulfurous cements. The brown curve represents the iron(hydr-)oxide precipitates. The lamination sometimes incorporates single manganese laminae resulting in a prominent peak in the spider diagram. The yellow graph shows the chemical composition of the sulfur cements (dataset given by STANULLA et al. 2017a).

The cements mostly grow in open spaces, either in the pore space or at the free surfaces. They form netlike structures (Figure 15) that condense to massive aggregates. Thus, the precipitates grow as matrix between single grains of sediments or as crust on larger particles. Influenced by discharging hydrothermal fluids, they contribute to the formation of hydrothermal discharge features.

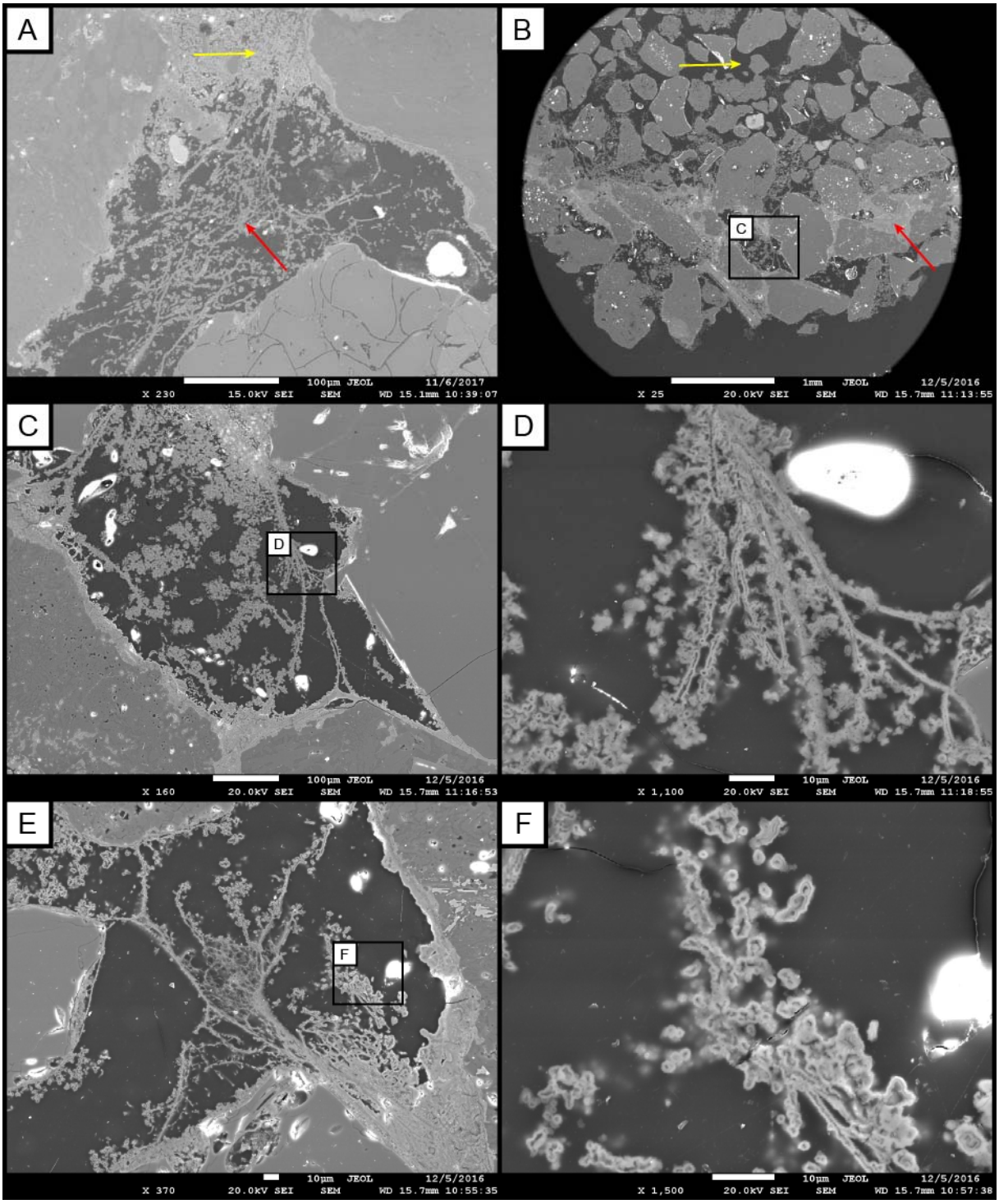

Figure 15: Growth of cements. **A –** SEM image of an iron(hydr-)oxide cement from Basiluzzo. The image shows two regions: a) is a loose network of cement aggregates representing an early-stage genetic stadium (red arrow); and b) where the cement forms a compact mass between the grains acting as matrix (yellow arrow). **B –** Iron(hydr-)oxide crust in TFe tube from Basiluzzo. The inner parts are not cemented (yellow arrow), whereas the cemented parts are solidified (red arrow). **C –** Detail of B zooming in to an early genetic region of the cement. **D –** Detail of B and C. The ongoing cementation can be well observed at the slender aggregates at the branches of the net. **E –** Early-stage iron(hydr-)oxide cement from Basiluzzo. Ongoing cementation fills the pore space and solidifies the sediment. **F –** Detail of E zooming in to a growing branch of the net.

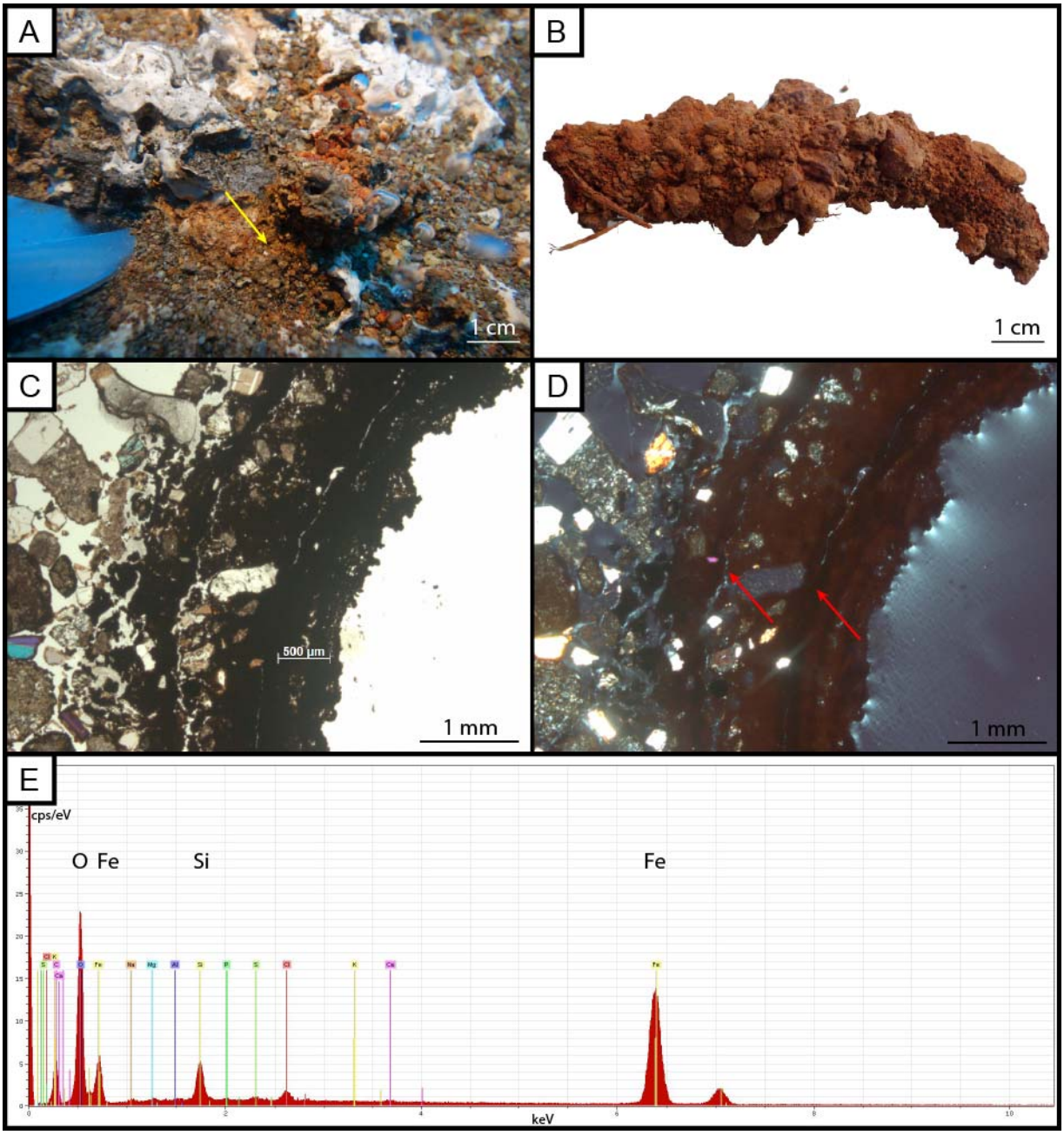

Figure 16: Iron(hydr-)oxide cements. **A –** Hydrothermal discharge feature at La Calcara. Iron(hydr-) oxide cements stabilizing the tube (yellow arrow). **B –** Cemented sediment from Basiluzzo. The precipitates stabilize all grain sizes and form massive crusts within the sediments. **C –** Thin section of a TFe tube from Basiluzzo. Iron(hydr-)oxides are coating the inner parts of the tube. II-Pol; 2,5x. **D –** Same as C but X-Pol. A multistory deposition is obvious. The cement shows at least three genetic stadia. The borders are marked by the red arrows. **E –** EDX measurement of an iron(hydr-)oxide cement. The material is predominantly built up of iron and oxygen. Minor amounts of silicate probably stabilize the material.

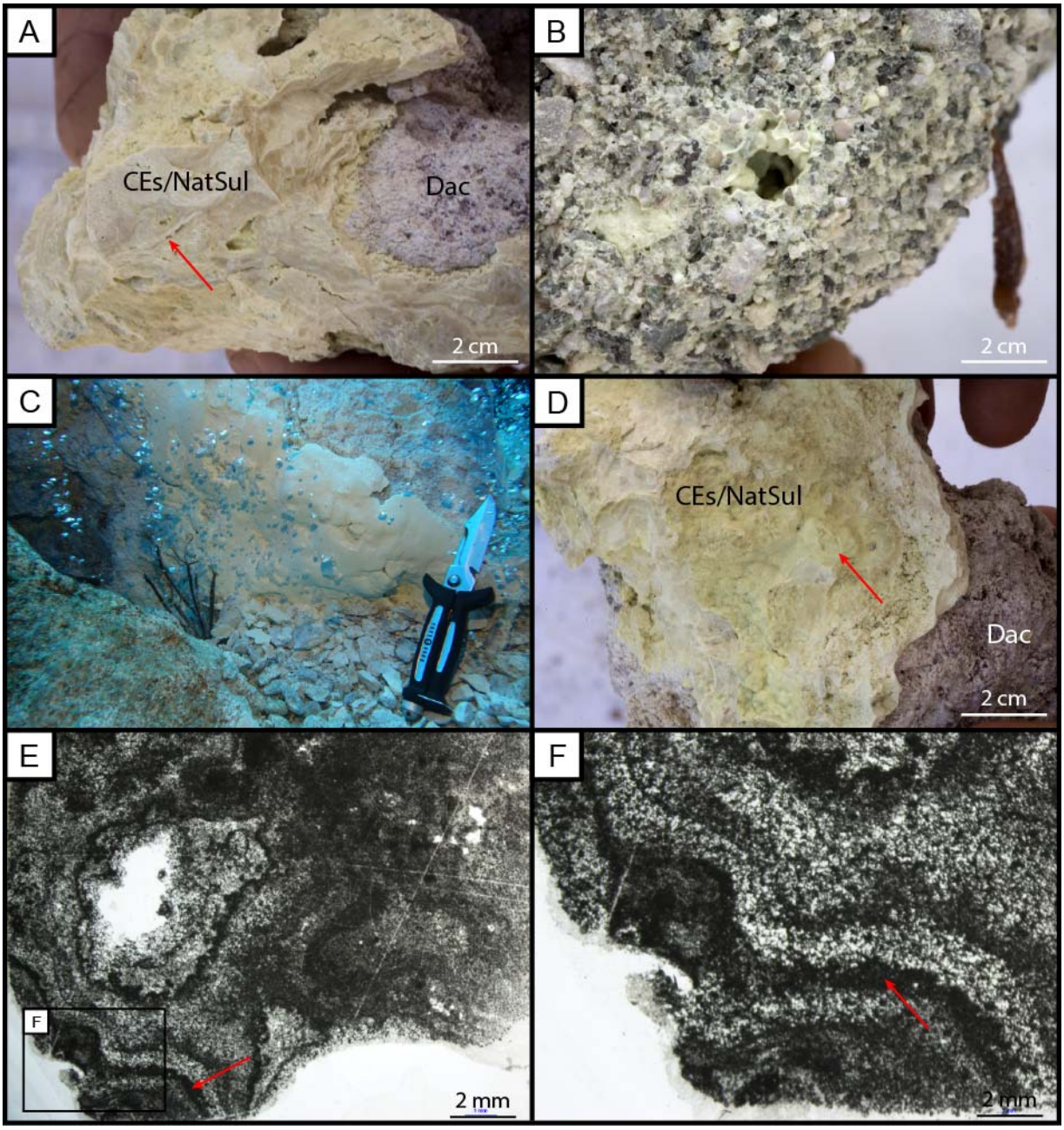

Figure 17: Sulfur cements. **A –** Crust of native sulfur (CEs/NatSul) on Dacite/Andesite (Dac) from Point 21. Lamination and multistory genesis are well visible (red arrow; cf. Figure 8-E and -F). **B –** Sulfur cemented sandstone from Area 26 showing a hydrothermal discharge feature (type Cc). **C –** Crust of native sulfur on a block of Dacite/Andesite near Point 21. The active emanation causing the precipitation is well visible. **D –** Crust of native sulfur on Dacite/Andesite as in A. The red arrow marks laminated, reniform aggregates. **E –** Overview on thin section of sulfur crusts from Point 21 showing hydrothermal discharge features of type TS (white hole; modified after STANULLA et al. 2017a). The red arrow marks the prominent lamination. **F –** Close-up on the thin section shown in E. The intense layering (red arrow) witnesses a cyclic deposition (modified after STANULLA et al. 2017a).

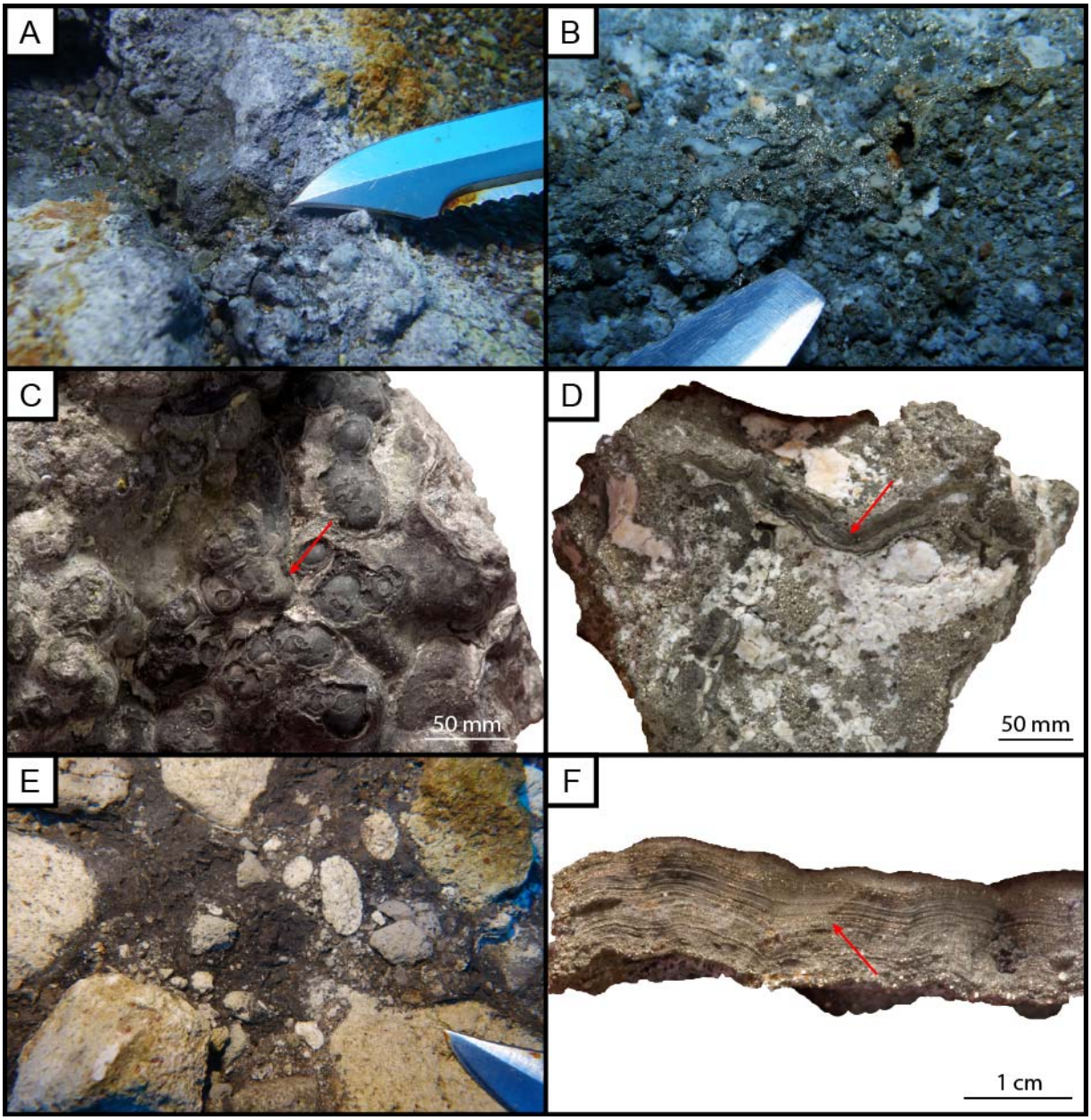

Figure 18: Massive sulfide cements. **A –** Massive sulfide impregnation near Black Rock in La Calcara. Disperse mineralization on clayish sediments is common at this site. Single, isolated larger mineral specimen were found. **B –** Typical cementation by massive sulfide ore in sediments of la Calcara. The single grains are well visible. **C –** Sample of a large mineral specimen. The lamination is well visible (red arrow). Minerals often show a reniform habitus. **D –** Prominent sample from La Calcara showing different types of precipitates. Pyrite, marcasite, and sphalerite are common. **E –** Massive sulfide ore mineralization cementing the conglomerate in Cave. **F –** Sample of a large mineral specimen (from La Calcara). A laminated deposition is obvious (red arrow).

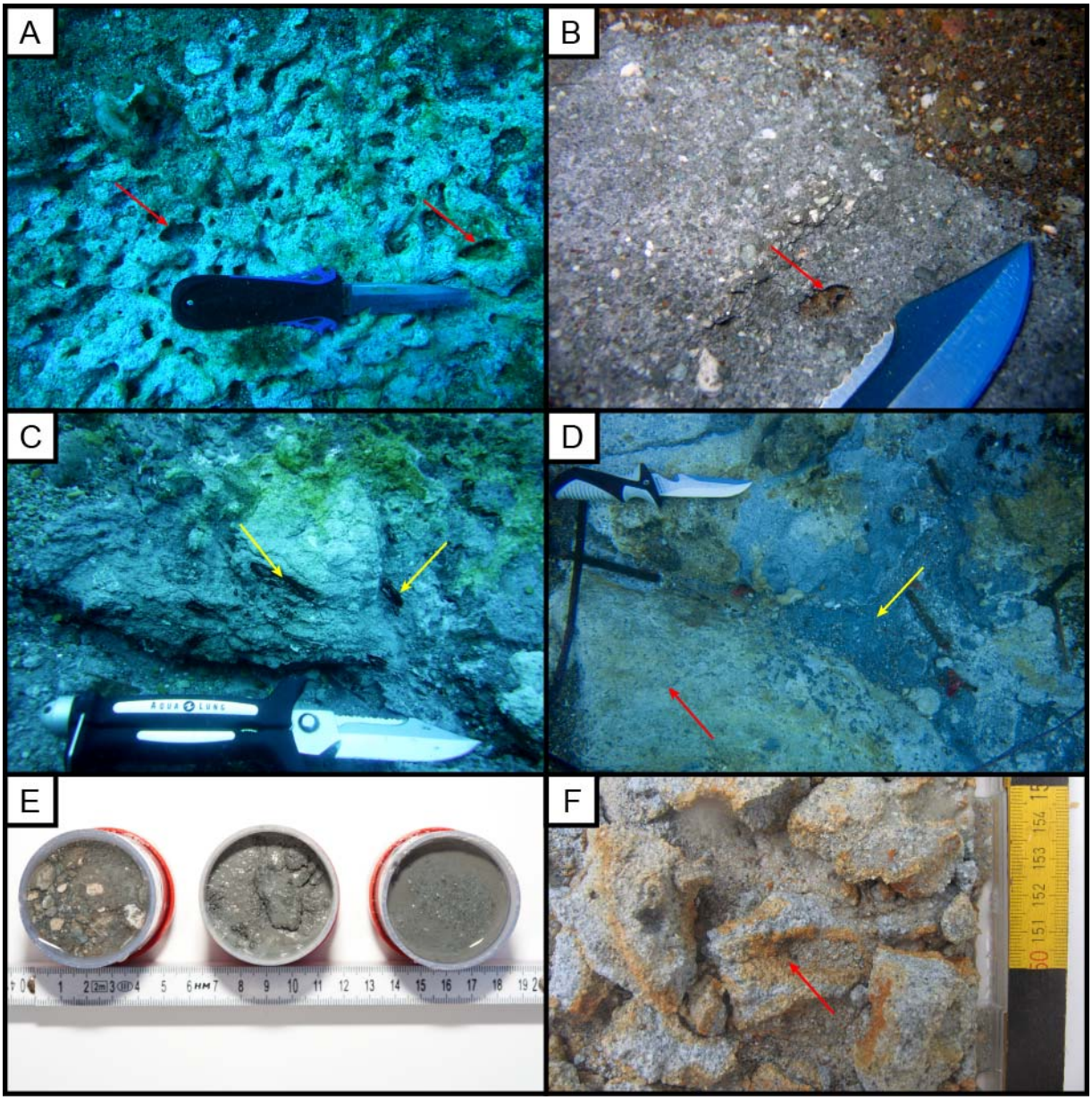

Figure 19: Clayish cements. **A –** Clastic sediments with a pale colored clayish matrix near *Octopus Rock* in La Calcara. Numerous hydrothermal discharge features (red arrow) hint on intense emanations in the past (cf. STANULLA 2012 and STANULLA et al. 2017a). Consequently, clayish facies such as alunites and smectites can develop due to hydrothermal alteration processes. **B –** Hydrothermal discharge feature (red arrow) in an alunitic clay facies from La Calcara. The fine-grained material cements the clastic components of the sediment. This lithology is often covered with recent sands (upper right corner). **C –** Alunitic cements near *Black Rock* in La Calcara. Plant remains (yellow arrow) are incorporated in the sediment. However, these ones show a completely different type of preservation than the ones from Area 26. **D –** Outcrop of two different clayish facies near *Black Rock* in La Calcara. The yellow arrow marks the greyish alunites whereas the red arrow indicated the pale colored facies (?smectite). **E –** Samples from the alunitic facies in La Calcara. The clastic components are well visible. **F –** Sample from the clayish facies near *Octopus Rock* in La Calcara. Red arrow marks one example of commonly occurring hydrothermal discharge features (iron bearing cements in the direct vicinity; cf. PRAUTZSCH 2012).

5.2. Underwater investigation sites and findings

5.2.1. Area 26

Location

Area 26 is situated in the central parts of the “crater”. It is characterized by large sand flats with eight sub-locations (Figure 20).

3-Bowls describes a set of three cavities in the southern parts of Area 26 (Figure 21). The structures were excavated using an airlift down to about 1.5 m below seafloor. However, only one of the structures’ bottoms was reached. The cavity filling shows typical materials such as pyroclastites, massive sulfide ore aggregates and clayish alteration products. However, the ore-sheets reached sizes of several dm² or form massive layers.

The sub-location *Brodor* was excavated first in the year 2017. This nearly circular spot (excavated: 1 x 1.2 m) of intense hydrothermal fluid discharge shows gas-dominated fluids being emitted from a complex network of tube-shaped secondary structures in the sand (total height: 0.3 m; Figures 22 and 23). The network was found several dm below the surface sand cover and incorporated different types of subrounded clasts of up to 10 cm diameter.

Hot Bowl is a 330 ° orientated steep depression of 1.80 m x 0.75 m in the southern part of Area 26 (Figure 24; cf. POHL et al. 2010). The cavity was excavated using an airlift pump down to 1.5 m below the seafloor still not reaching the bottom of the structure.

Lava-tongue describes a flat block of several square meters in the north of Area 26. In contrast to its name, it is homogeneously built up of tuff being secondarily impregnated by massive sulfide ore aggregates. The outer parts of the block are affected by gas-erosion processes resulting in lots of small tubes and channels on the surface of the hard rock.

The *Lineament Structure* is an elongated feature of about 10 m length and some cm to dm in width along the main fault direction of 310 ° - 330 ° in the area (Figure 25). Located in the central parts of Area 26 it intersects the location from near *3-Bowls* in the South in direction to *The Mouth* in the North. Along the structure, there are several water and gas emanations. The structure was excavated down to approximately 1 m without reaching the bottom. The rims of the cavity show different types of discharge features. In 2015, the first appearance of a tube-facies exclusively composed of sulfur-bearing minerals in Area 26 was reported. Documentation was not possible during that campaign. At the following attempt in 2016, no tubes were found neither at the same location nor elsewhere. This fact outlines the high dynamics during constructive genetic processes and in the system in general.

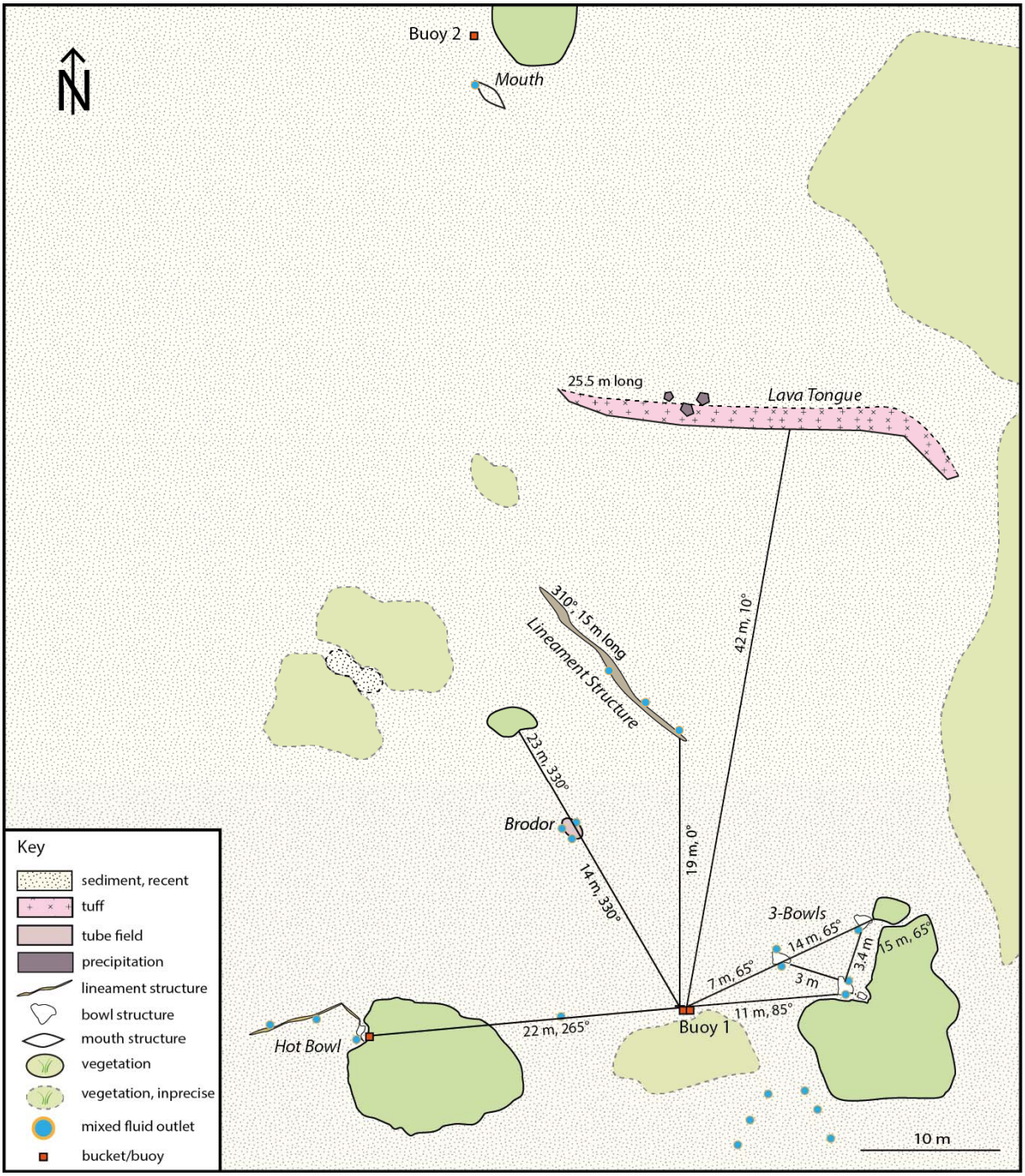

Figure 20: Map sketch of the UWIS Area 26 showing all described locations. The investigations concentrate on the sublocations *Hot Bowl*, *3-Bowls*, *Lineament Structure* and *Brodor*. Modified after ADAMEK (2021).

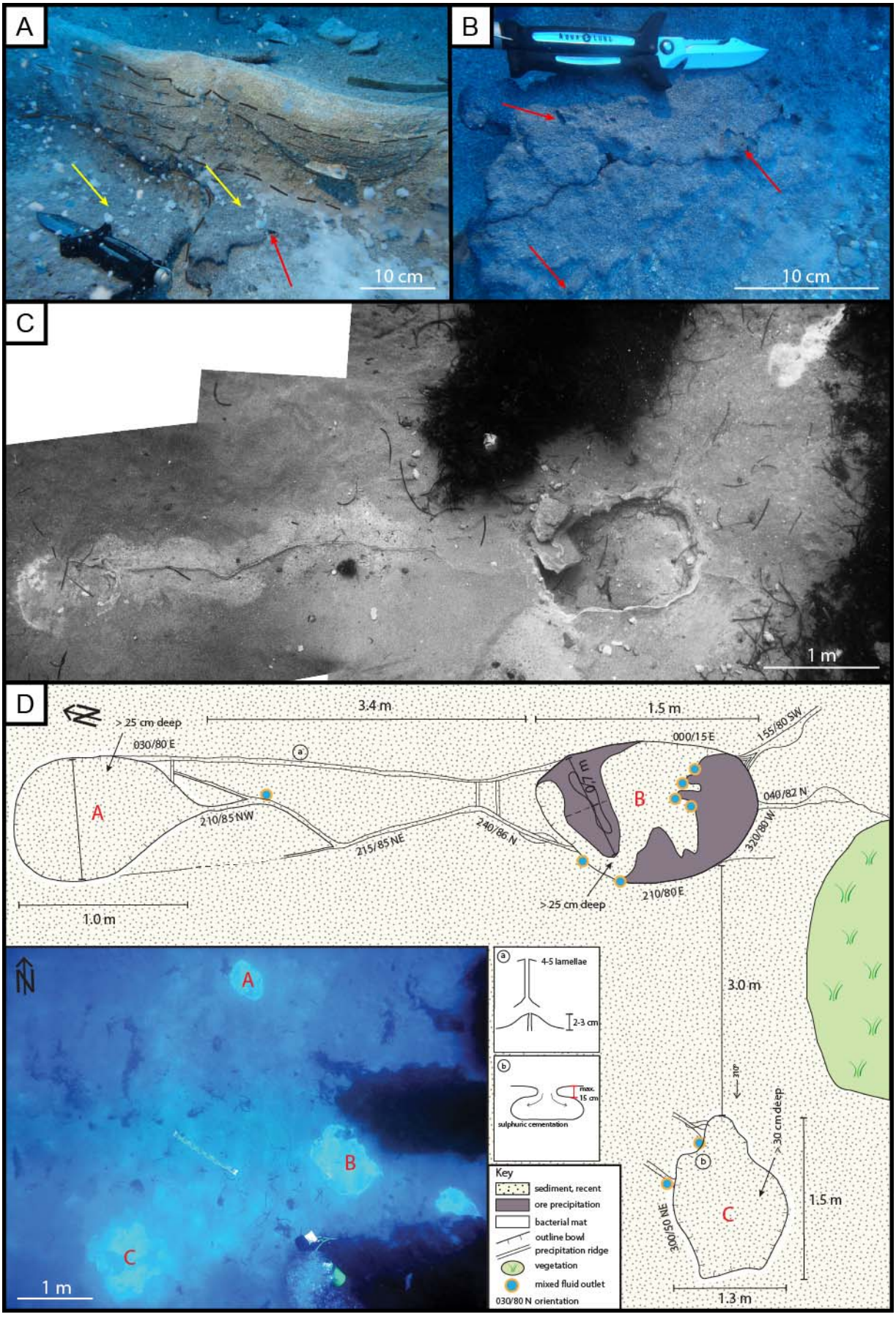

Figure 21: *3-Bowls* (3B). **A –** The sidewalls of the bowl-structures show the multistory deposition of the volcanoclastic lithology. Dashed lines highlight distinct layers. However, also massive sulfide ore mineralization takes place in-situ, as the presence of such layers at the bottom of the bowls show (yellow

arrows). Post-genetic hydrothermal discharge can be assumed based on the discharge features within the ore-layers (red arrows). **B –** Layer of massive sulfide ore mineralization at the top of Bowl B. Discharge features of the Tore-facies are clearly visible (red arrows). **C –** Stitched panorama-image of *3-Bowls* showing the Bowls A and B as well as the neo-tectonic features in the surrounding structures. **D –** Map-sketch of the complete structure including neo-tectonics features, hydrothermal fluid emanations and structural elements. Map view image for orientation (modified after ADAMEK et al. 2019).

Geology

Area 26 is characterized by polymict sand to gravel facies. Despite the typical volcanoclastic sulfurous cover-sands, there are sandstones and fanglomerates, being cemented by native sulfur. Both sediment types show typical characteristics of mass-flow-deposits such as poor sorting and angular grain shapes.

Massive sulfide ore mineralization is a common feature in this location. It occurs as impregnations, clasts, or former crusts, which build ore-sheets within the sedimentary fill of cavities. This phenomenon commonly corresponds to discharge features as explained in chapter 3.2. The occurrence of the ore-sheets supposes a multiphase deposition including erosive processes.

Some of the cavities show at their deeper parts (e.g. excavation of HB down to 1.5 m depth) whitish to greyish fine-grained sediments (silt to clay) which are comparable to materials documented at Octopus Rock, La Calcara. It cannot be stated beyond doubt, whether these are materials from the underlying strata or in-situ-decay-products of single blocks or clasts.

Temperature distribution

Thermo-measurements were carried out at pre-explored discharges with elevated temperatures. These are mostly connected to the secondary sedimentary structures being orientated along the general fractures system. Fluid temperatures vary from 27 °C to 75 °C (e.g. MÜLLER 2011; CANZLER 2012).

Fluid discharge

The fluid discharges in Area 26 are mostly dominated by geothermal water. The rather aggressive gases are emitted with low gas flow rates from distinct emanation points. In some locations lots of small vents discharge at high gas flow rates but in defined areas. The sub-location *Brodor* for instance is restricted to about 1.5 m², where about 30 small vents are discharging.

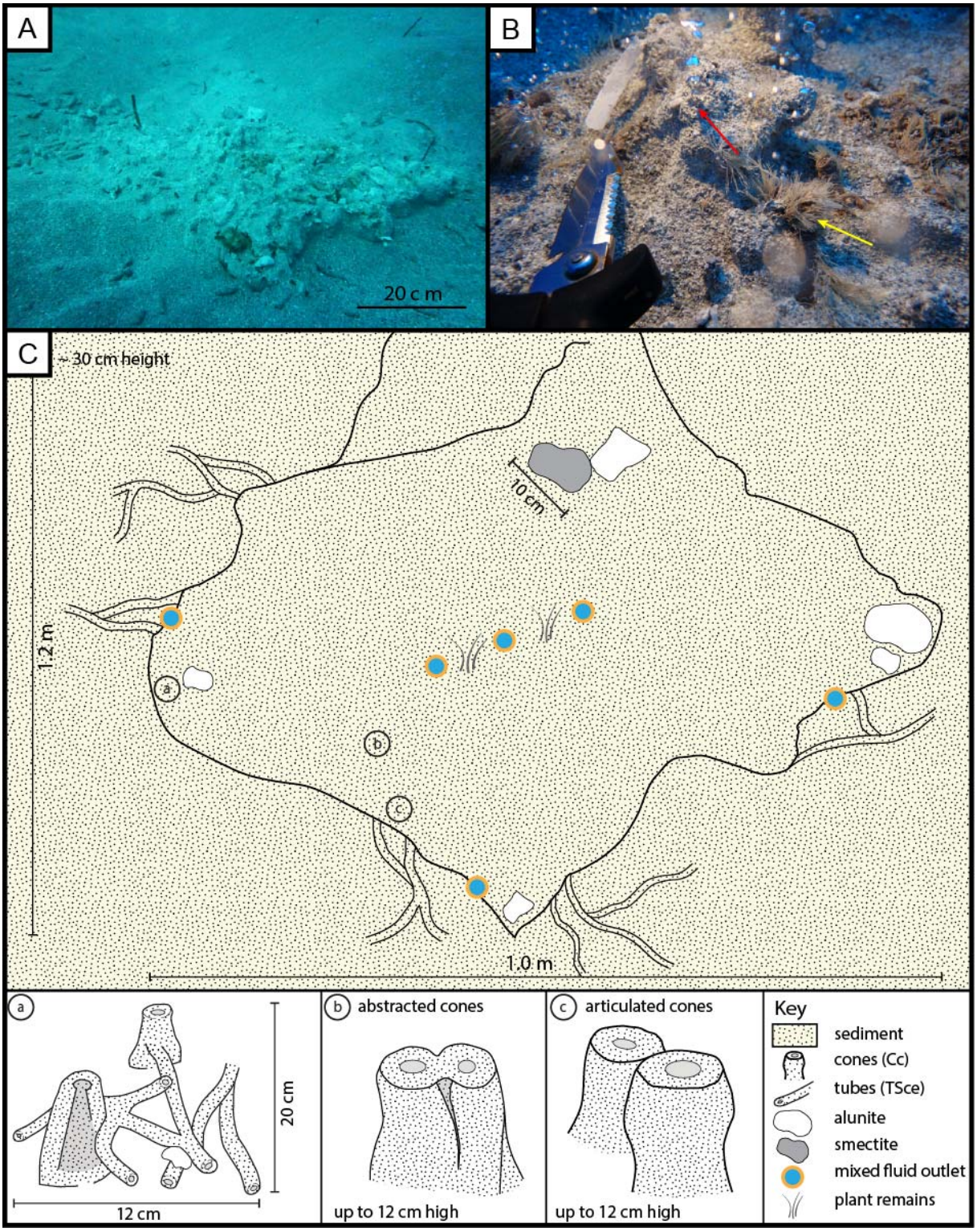

Figure 22: *Brodor* (BRO). **A –** Overview of the excavated area. Lateral extend is 1.0 x 1.2 m while height is ca. 0.3 m. **B –** Active discharge (red arrow) with high biogenic influence of *Posidonia sp.* (yellow arrow). **C –** Generalized map-sketch of the location BRO. Single features are given in Figure 23 for comparison (sketch - V. Kürzinger, 2017; digital drawing - J. Adamek, 2020).

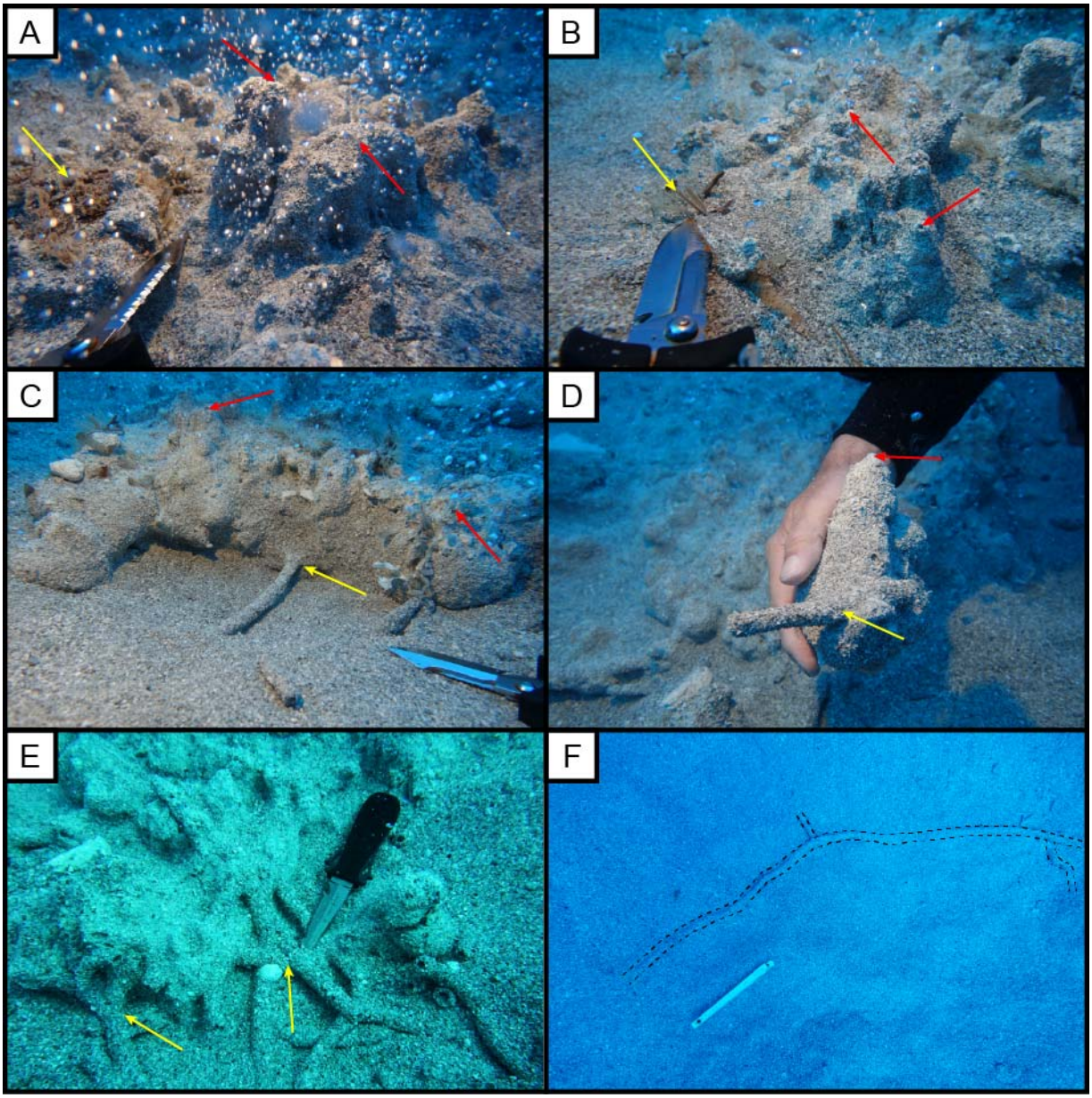

Figure 23: *Brodor* (BRO). **A –** Highly abstracted cones (type Cc) at the central parts. Active discharge out of well-defined emanation points (EMP) is highlighted by the red arrows. Posidonia remains are incorporated in the structure what hints on a severe biogenic influence in early-stage genesis. **B –** Close-up on active hydrothermal discharges. The red arrows mark EMPs. The yellow arrow hints in Posidonia remains (cf. chapter 6.1.1.2. – stages 1a – 5a). **C –** Excavated sidewall of the central consolidated part of the structure. Active emanation at the top is well visible (red arrows). At the lower parts, numerous junctions of long tube specimen (type TS) are obvious. **D –** Prominent specimen of Cc from the central part (red arrow – EMP). The junction between tube and cone (yellow arrow) witnesses the complex genetic processes as well as their direct interaction. **E –** Complex set of tubes (type TS) at the outer rim of the structure. Numerous junctions witness the complexity of the network what makes it difficult to trace the fluids pathway. **F –** Dashed line highlights the longest tube (type TS; ~1.2 m) ever documented in Panarea in this project. The main tube crosses two junctions and probably continues further in the sediment. Further excavation was not possible due to time limitations.

Discharge features

Depending on the specific lithology at the discharge point, a number of discharge features occur in Area 26.

In loose sands, the Cu-type is a common feature. They are mostly arranged irregular, with no obvious orientation. Their size varies between several centimeters to some decimeter in height.

Within the precipitates, predominately Cc-type discharge features evolve. They appear mostly along the main fractures and build ridges of several meters. Active and inactive discharges can be found nearby.

For example, the central parts of *Brodor* are built up of intensively abstracted consolidated cones (facies type Cc) which are up to 12 cm high and unusually overstepped (aspect ratio ~ 1:4; cf. Figures 22 and 23). The outer regions of the excavated area consist of comparably long, poorly consolidated tubes cemented by typical sulfur cements as documented at the underlying sandstones. Single segments measure from few centimeters to over a meter. Most segments were about 50 to 60 cm long, showing outer diameters of about 1.5 cm and inner diameters of 0.7 cm. Junctions were mostly bidirectional covering angles of 90 to 120 °. Generally, more horizontal tubes were documented in comparison to vertical tubes (horizontal-vertical-ration: ~ 4:1). Massive gas-dominated discharge directly out of these tubes was documented (see Appendix 2). However, a several decimeter long worm was documented living in one of the tubes as well.

Cavities of different scales are the most prominent discharge features in Area 26. Sizes vary between some centimeters to over one meter. At their rims, sometimes a second generation of discharge features evolves (mostly tube facies). *Hot Bowl* and *3-Bowls* are the most prominent discharge features of this bowl facies that have been documented over the years.

The *Lineament Structure* is among the most prominent features in the Panarea system and the type locality for the lineament facies type. This feature of about 10 m length crosses major parts of the central sandflats in Area 26. A lot of smaller lineaments of up to several meters developed for instance near *Hot Bowl*. Lineaments connect single bowls to larger structures by (open) fractures.

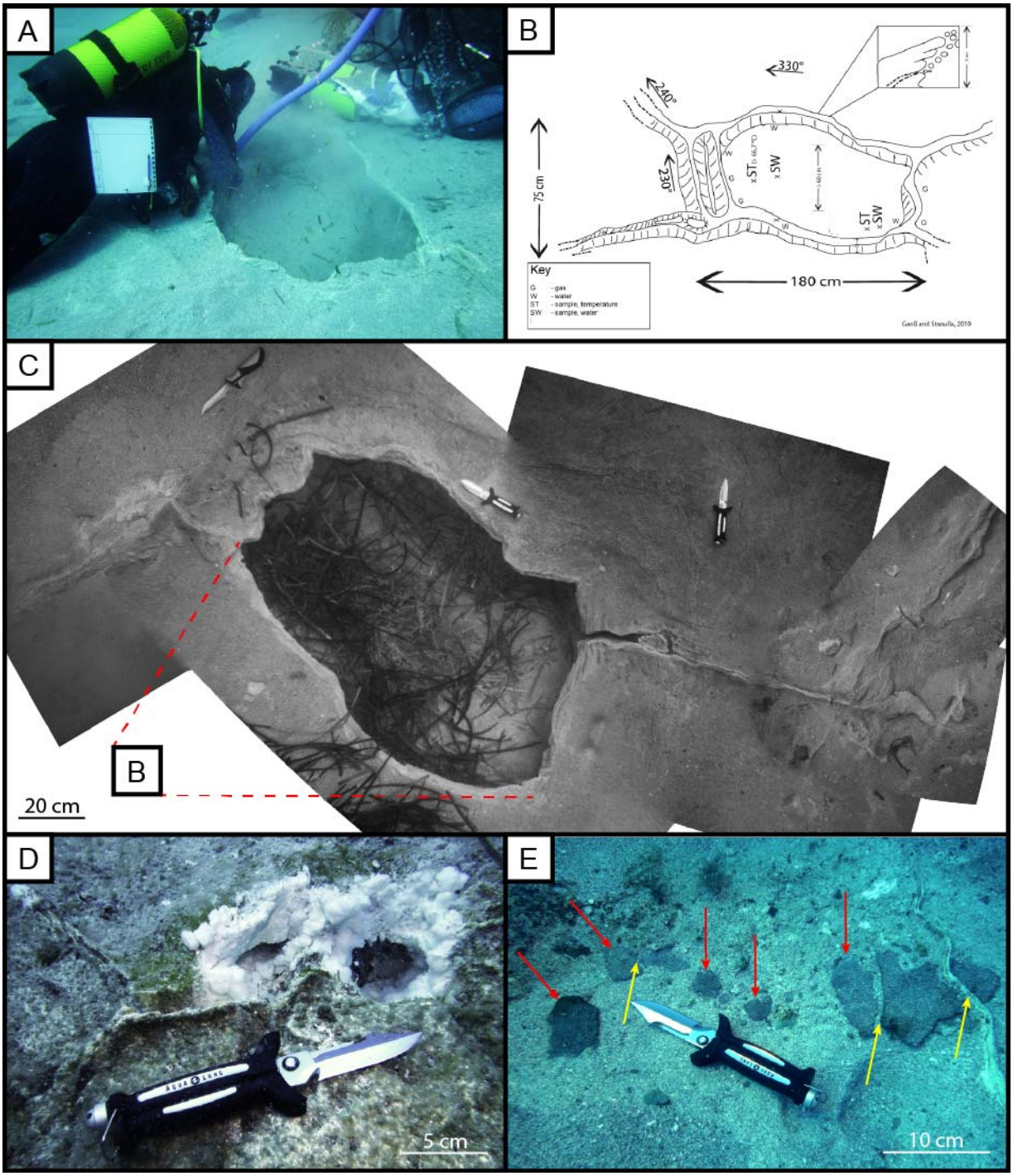

Figure 24: *Hot Bowl* (HB). **A –** Excavation of *Hot Bowl* in 2015. The sediment cover was cleaned off using a mobile airlift pump as described by STANULLA et al. (2016). **B –** Map-sketch of the central part of *Hot Bowl* showing the main dimensions and hydrothermal discharges (modified after POHL et al. 2010). **C –** Stitched panorama-image of *Hot Bowl* showing the central depression as well as the neo-tectonic features in the surrounding structures. **D –** Typical discharge of hydrothermal waters near *Hot Bowl*. Significant amounts of discharged fluids and constant flowrates cause typically concentric cavities and structures being highlighted by thermophilic whitish algae-bacteria-mats. The most prominent discharges are always found at the crossings of faults or cleavages. **E –** Massive sulfide ore mineralization is a common feature in Area 26 (red arrows). The ore aggregates show neo-tectonic disturbances witnessed by intersecting recent cleavages (yellow arrows).

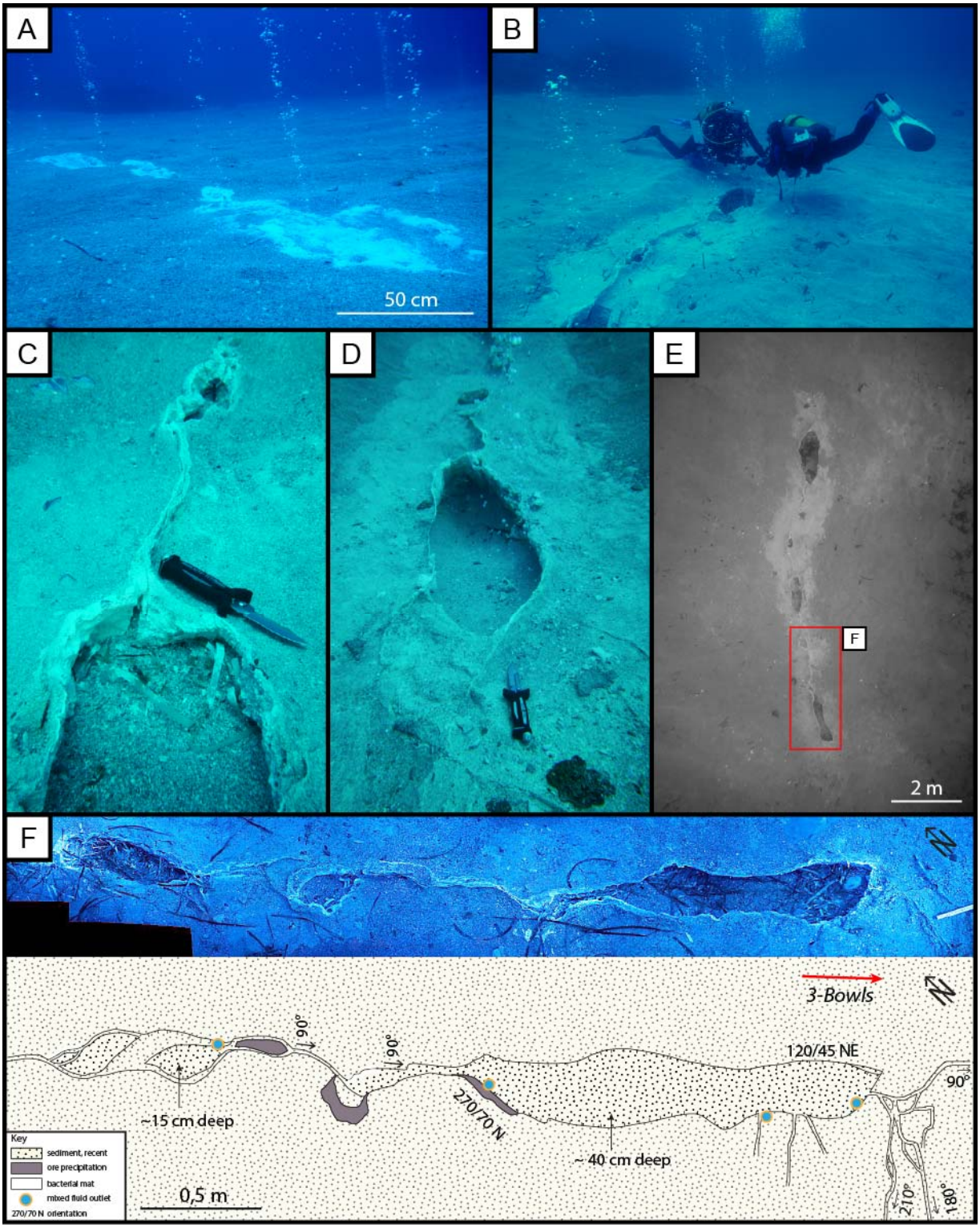

Figure 25: *Lineament Structure* (LS). **A –** *LS* covered with recent sand before excavation. Biomats are highlighting the outlets. **B –** Divers mapping the structure after excavation. **C –** Single bowl within *LS*. Massive precipitation of native sulfur is well visible. Single bowls are connected by small ridges built up of precipitates following the fault direction. **D –** Main bowl in the western part of *LS*. Oversteepening of the walls is well visible hinting on a relatively old structure (cf. chapter 6). At the lower portions of the image, a large ore clast is well visible witnessing the presence of reworked ore strata. **E –** Complete structure from above. Red square marks the mapping area given in F. **F –** Map-sketch of the eastern part of *LS*. Mapping was carried out in 2017. Modified after ADAMEK (2021).

5.2.2. Basiluzzo

Location

The islet of Basiluzzo is situated northeast of Panarea. The underwater investigation site covers the southeastern shore north of Punta Levante. The rocky shoreline changes to sandy slopes at about 15 m depth. The slopes were investigated down to 40 m below sea level but continue much further.

Geology

The island of Basiluzzo itself is built up of massive tuffs (Punta Torrione Formation) and rhyolithes of the Basiluzzo-Formation (CALANCHI et al. 1999).

Mineral precipitates are mostly built up of iron(hydr-)oxides forming large networks of tube-shaped discharge features (TFe-type; STANULLA et al. 2017a) and thin coats around single sand grains or massive crusts, pure or around biomaterials (e.g. roots).

The location is characterized by mostly unconsolidated, medium-grained, polymict sands forming large sandflats that host and cover the secondary discharge features.

Temperature distribution

No elevated temperatures were documented in this location. However, investigations on that topic were at first of exploratory character. Supposing, that highly elevated temperatures are mainly caused by hydrothermal waters, this site was not considered as a geothermal hotspot (nowadays).

Fluid discharge

The discharges in the area are small and mostly gas-dominated. During the investigations it was not possible to sample any active fluid outlets. However, the TFe-type discharge features clearly witness a stronger discharge of hydrothermal fluids in former times.

Discharge features

The most prominent discharge features at this site belong to the type TFe (Figure 26). In case of ongoing hydrothermal venting, TFe-type discharge features form large networks of several meters (cf. chapter 3.2.). Some of the tubes reach several cm above the sand-surface. Also incrusted roots or boulders were observed. Subordinately also Cu-type discharge features occur, supposedly covering TFe-tubes in the sand.

Similar features of type TFe were found in 2018 at the north-western shoreline of the islet of Dattillo. However, neither sampling nor documentary work could be realized during that single explorational dive.

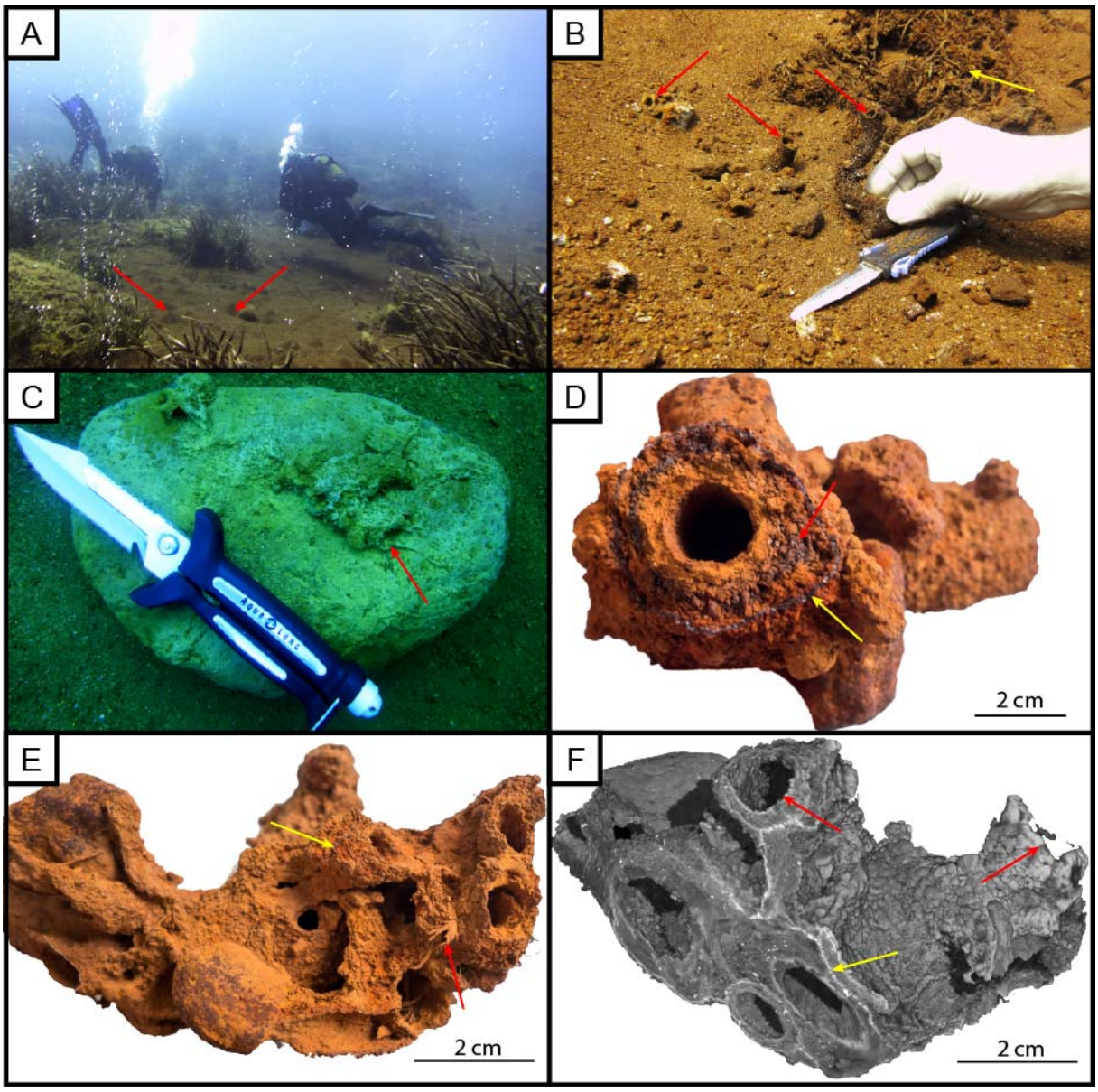

Figure 26: Basiluzzo (BA). **A –** Scientific divers sampling in BA. The wide slopes covered with recent iron-bearing sands comprise small fields of cones (type Cu). **B –** In-situ tubes of type TFe (red arrows). Recent sands cover the discharge features. Image modified after STANULLA et al. (2017a). **C –** TFe-type tubes incrustate large pebbles on the slopes of BA (red arrow). Such formations hint on a relatively fast or event-triggered genesis. **D –** TFe tubes mostly show a multi-story genesis (red arrow). Single events may cause changes in the composition of the hydrothermal fluids what leads to isolated "event-layer" in single tubes. A prominent Mn-layer is a common feature in the BA-tubes (yellow arrow). **E –** Set of tubes (type TFe) showing an enormously complex network structure. Multiple junctions and crossings allow hydrothermal fluids to migrate in nearly all directions within the network structure. The prominent Mn-bearing event layer (yellow arrow) hints on a far-reaching event. Remains of *Posidonia sp.* (red arrow) hint on an early-stage biogenic trigger as explained in chapter 6.1.1.2. **F –** XCT-image of the sample shown in E. Light colors show (heavy) metalliferous materials (e.g. massive sulfide ores, Mn-layer; yellow arrow). The internal structure of the sample is as complex as their outer shape. The red arrows mark prominent outer tubes of the sample. A video documentation of XCT data is given in Appendix 2.

5.2.3. Black Point

Location

The shallow water grey smoker Black Point is located in the central parts of the “crater”. It is one of the most interesting locations by means of hydrochemistry and thermodynamics in the system. The main discharge point lies in a shallow depression of 26 m (N-S) x 24 m (E-W) extend (BECKE 2009) at 23.5 m water depth (Figure 27). The depression is supposed to be an ancient outburst crater comparable to Bottaro West. The massive sulfide ore body “Black Point” is about 2.7 m long (N-S), approximately 1 m wide and 0.5 m high (BECKE 2009).

Geology

The discharge point of Black Point itself is built up of nearly pure sulfide ore material being dominated by pyrite and marcasite, but also galena and sphalerite are common (cf. BECKE 2009).

Besides the ore bodies, the depression is covered by gravel and blocks of Dacite and Andesite (subrounded to rounded, poor sorting). They may occur as conglomerates cemented by the sulfide ores or native sulfur.

Temperature distribution

Fluid temperatures reached up to 132 °C at the emanation point of the grey smoker. Observations over a 12-year-period show a cooling-trend of fluid temperatures. However, the discharge still shows the highest fluid temperatures measured in comparison to all other sites and is close to or at the boiling point.

Fluid discharge

Black Point intensively discharges highly mineralized hot fluids. The emitted fluids are water-dominated. The discharges are among the most acidic ones in the system showing pH-values as low as 2.6. Measurable gas emanations were not documented.

Discharge features

Due to the continuous discharge of highly mineralized hot fluids, a continuous mineral precipitation can be observed. The constant growth-rates of the precipitates hinder the development of typical discharge features. Only small-scaled structures of the To/Tore type can be documented (mostly microscale).

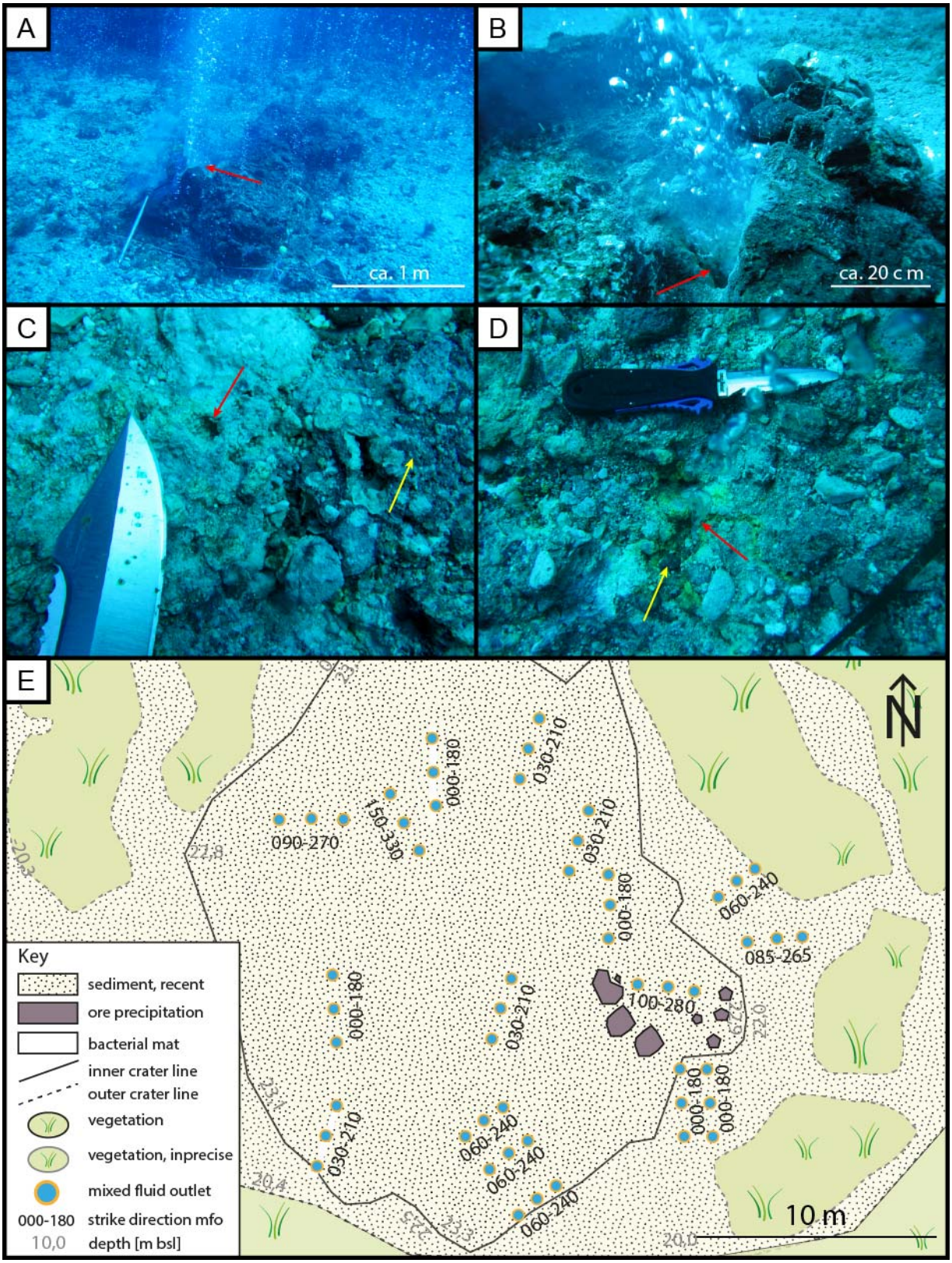

Figure 27: Black Point (BP). **A –** The shallow water grey smoker "Black Point". The red arrow hints on the main emanation point where the greyish precipitation plume is visible in the water column. **B –** Close-up on the main EMP. The ore body consist mainly of massive sulfide ore minerals. Pictures A and B: SDC (2008). **C –** Abstracted tube (To/TS) near Black Point (red arrow). There is no active discharge detectable at this point. Massive sulfide ore mineralization (MSO) is a common feature in this site (yellow arrow for example). **D –** MSO (yellow arrow) near an active discharge (red arrow). Precipitation can be observed nearly in real time. **E –** Map sketch of the UWIS Black Point. Modified after ADAMEK (2021).

5.2.4. Bottaro North

Location

The location in the channel between the islets of Bottaro and Lisca Bianca is characterized by a number of strong gas-dominated vents (class E). In the central parts five of them are arranged in a ring of several meters in diameter. They are therefore referred to as "*The Ting*". The slopes of Bottaro are covered by large boulders (rockfall) and decrease gently to a water depth of about 10 m. At the shoreline, there is a rock cliff of about 5 m height.

Geology

The site is mostly characterized by loose blocks and boulders of different compositions. They cover sulfur-cemented polymict conglomerates or fanglomerates which can also be found in Fumarolic Field, Cave and Area 26. Especially the fanglomerates show large, angular clasts of sulfide ores (cf. Area 26). Cementation is sulfur-dominated in the whole area (Figure 28).

Temperature distribution

Fluid temperatures were measured mostly at ~ 30 °C (27.9 – 33.7 °C). Two emanations in the shallower parts showed temperatures of 45.7 °C in 2009. The highest temperature was determined at 56 °C.

Fluid discharge

The vents in Bottaro North are mostly gas-dominated and of classes A-E. The most prominent ones were classified as class E vents. Gas flow rates were estimated to about 60 L/min by ESPA et al. (2010) and appear nearly constant in the observation period from 2006 to 2018.

Discharge features

Most mineral precipitates consist of native sulfur and occur as cements, crusts or discharge features such as TS and FS. Due to the intense venting, discharge features are rather common in this location.

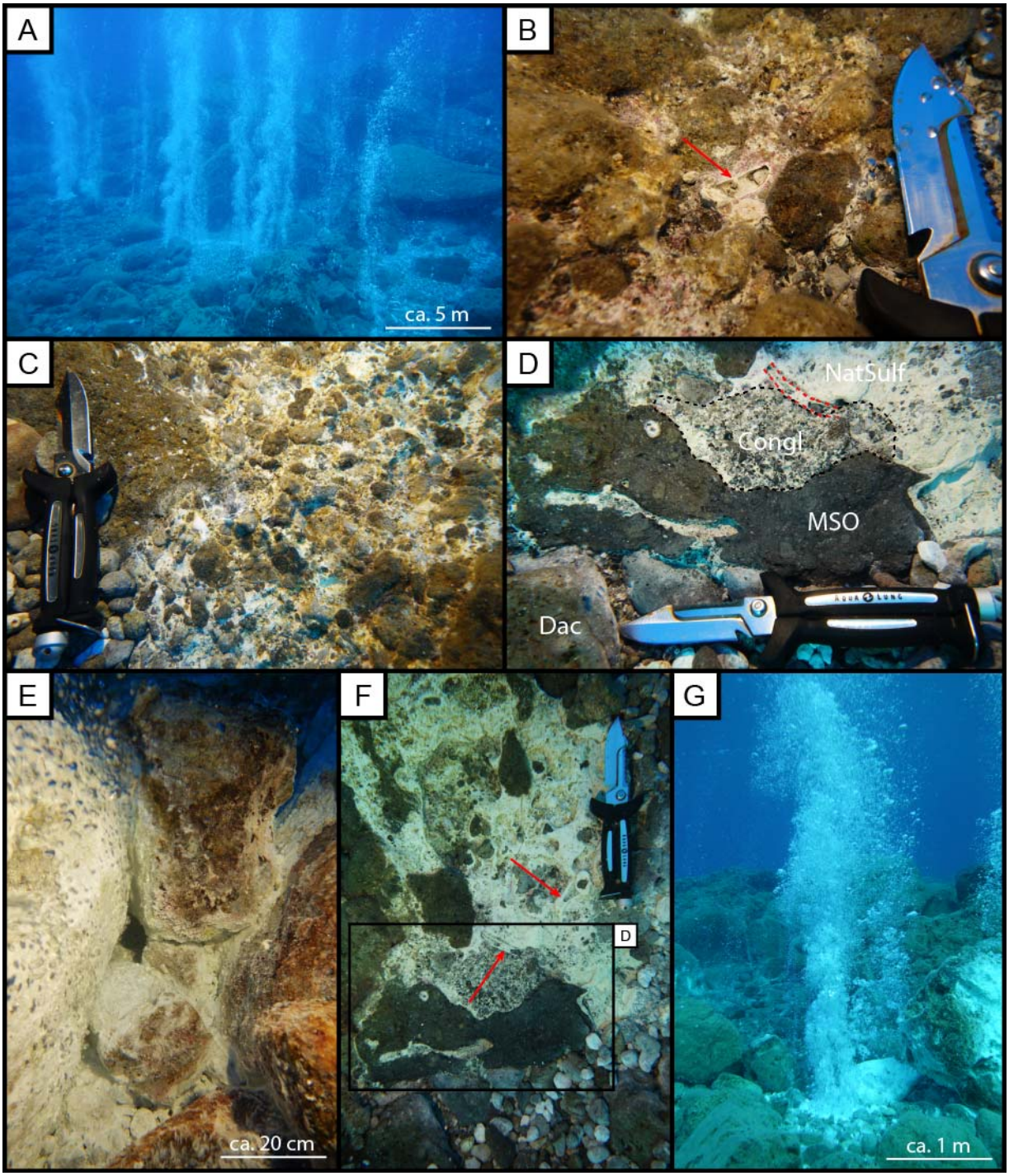

Figure 28: Bottaro North (BN). **A –** Overview image of *The Ting* at BN. Discharges of class E belong to the most powerful in the Panarea system. **B –** Well defined in-situ tube of type TS consisting of nearly pure sulfurous cements (red arrow). **C –** Typical conglomerate cemented by native sulfur. (Sub-) rounded clasts hint on a relatively high energetic environment. **D –** Close-up of image F. The different lithologies of this location are well visible. Dac – Dacite/Andesite; MSO – massive sulfide ore; Congl – conglomerate; NatSulf – Native sulfur. **E –** Close-up on an active hydrothermal discharge emitting a gas-dominated hydrothermal fluid. However, remarkable water fibrillation witnesses the water-portion within the fluid. Recent native sulfur precipitation is obvious at the rock-surfaces. **F –** Overview image of D. Further pure TS tubes are indicated by the red arrows. **G –** One of the major vents in *The Thing.* Gas bubbles sometimes are even remarkable at the sea-surface.

5.2.5. Bottaro West

Location

Bottaro West is located at the western shore of Bottaro Islet at a water depth of 7 – 10 m. The central part of the site is the crater of the 2002 gas eruption which transported an estimated amount of 4,000 m³ of rock material. Originally the crater showed an ellipsoidal shape in NW-SE orientation (ca. 40x25 m) and a depth of 7 m (8 to 15 m water depth; ANZIDEI et al. 2005). In the year 2018 it is still well visible at the seafloor at about 12 m (Figures 29 and 30). In the years after 2006 the crater has been more and more affected by sedimentation (cf. ALIANI et al. 2010) and abstraction driven by tide and wind induced currents and wave dynamics.

Geology

In Bottaro West the volcanites are mostly covered by loose blocks and boulders of different compositions. Due to their high level of alteration, a precise determination of the rock- or lava-types is not possible. The materials show relictic structures in the thin sections, but mineral identification fails in most cases. It is only possible based on characteristic outer shapes of the minerals (e.g. plagioclase).

Single dykes intersect the location. One prominent example is a single, triangular rock (sometimes referred to as "*Dragon tooth*") in the northern parts. It shows a high level of silicification and can be compared to the "honeycomb"-material in Cave.

Temperature distribution

Fluid temperatures generally varied from 29.4 to 31.0 °C in 2009. Only single measurements showed elevated values up to 43.6 °C. Temperatures up to 65 °C were documented in 2010 (MÜLLER 2011).

Fluid discharge

The site was characterized by lots of class A gas discharges in 2009. Until 2017, the number of vents has decreased constantly. The vents are mostly gas-dominated.

Discharge features

Due to the coarse grain sizes no discharge features could have been documented in or at the crater.

However, the gravel and Posidonia fields west of the crater showed single early-stage discharge features, e.g. on Posidonia roots in sheltered positions. These were exclusively the sulfurous types FS and TS.

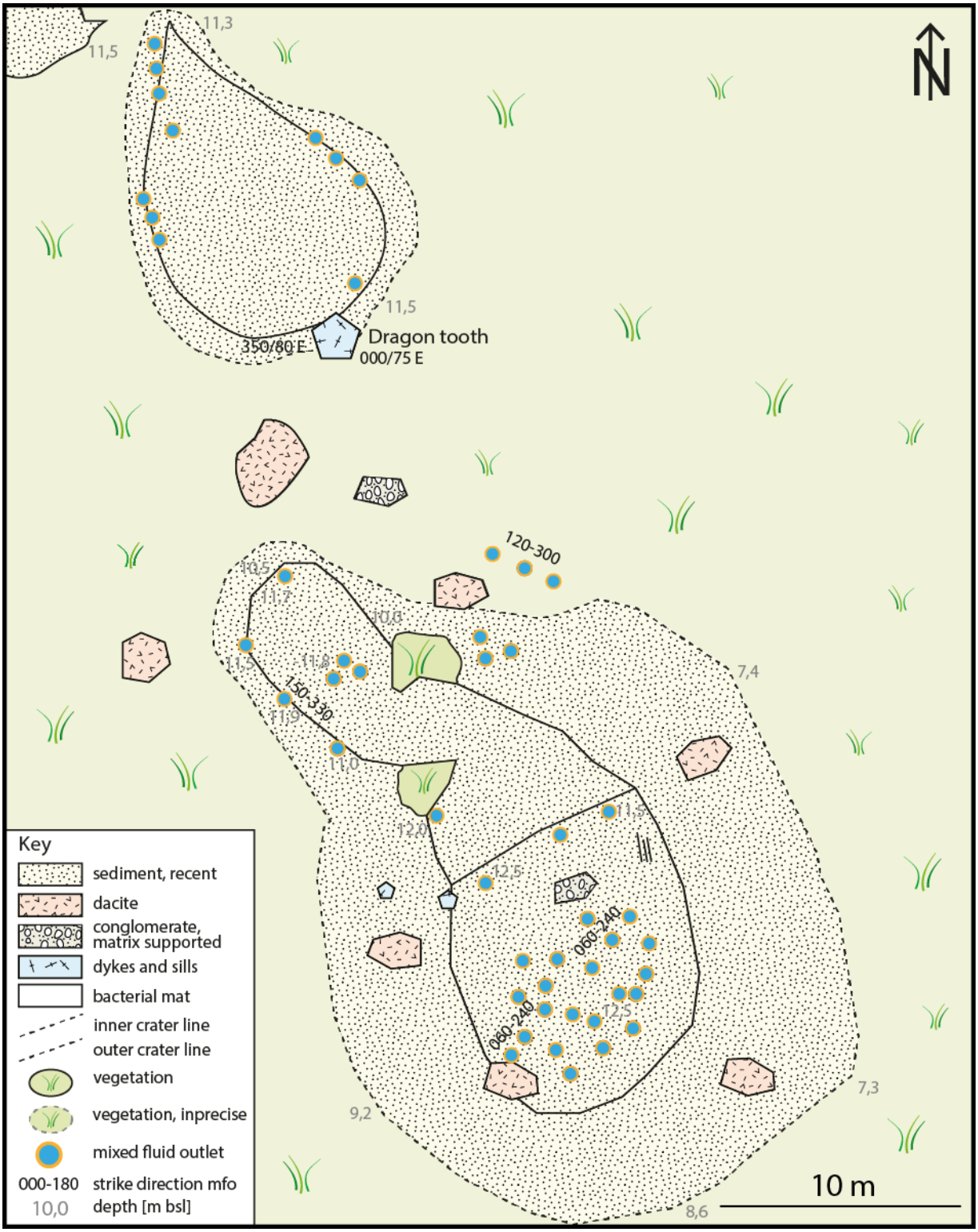

Figure 29: Map sketch of the UWIS Bottaro West showing all described locations. The main crater was the center of the 2002 gas outburst. Modified after ADAMEK (2021).

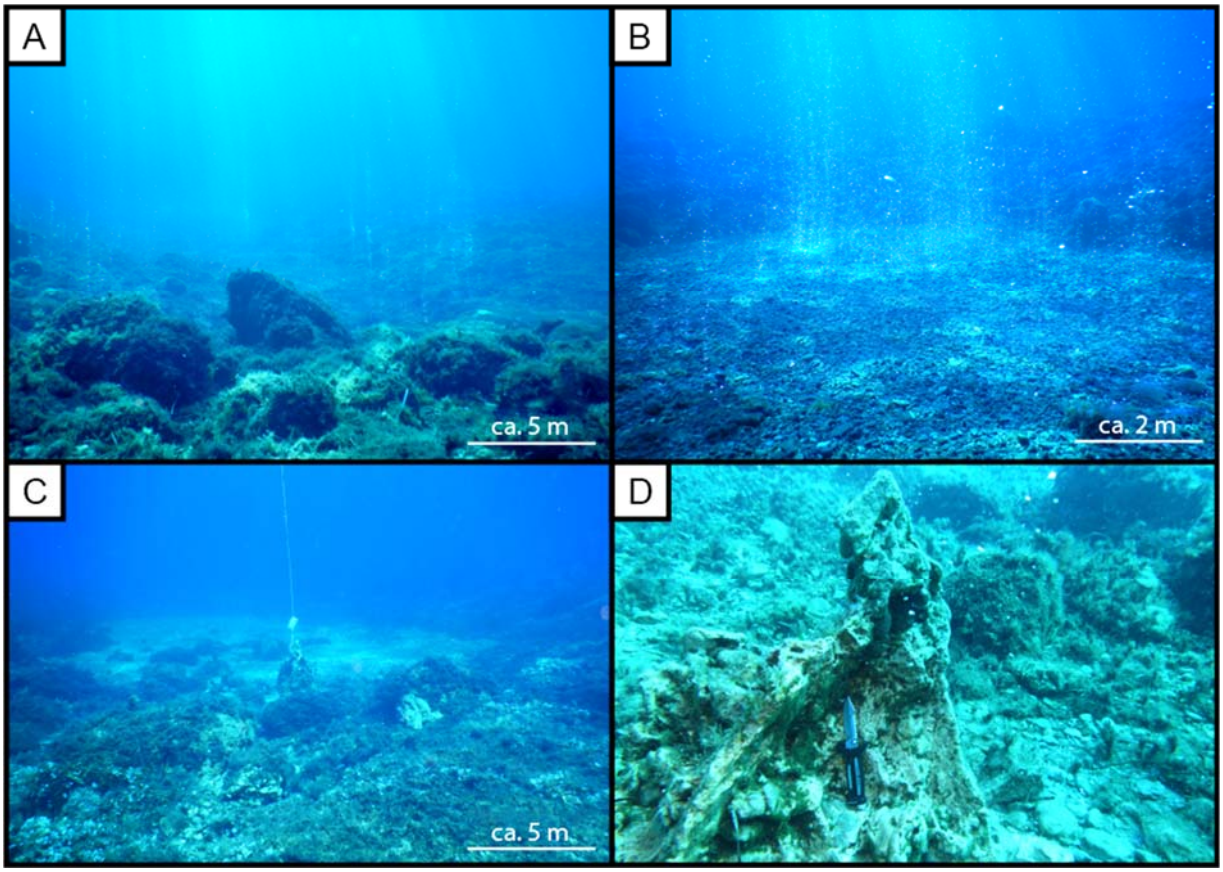

Figure 30: Bottaro West (BW). **A –** Overview image of main crater of BW. This depression is supposed to be the center of the 2002 gas outburst. **B –** The central part of the main crater still shows continuous discharge of mainly gas-dominated vents. **C –** Overview image of the smaller crater near "*Dragon tooth*". The shot line is fixed to this small outcrop. **D –** Close-up on the "*Dragon tooth*". The rock consists of Dykite comparable to those from Cave and on land of Bottaro Island (cf. chapter 5.1.1 and Figure 7-E).

5.2.6. Cave

Location

The underwater investigation site Cave is situated north of Point 21 at a water depth of 23 m (Figure 31). It is dominated by a grotto of 8 x 4 x 1.5 m (LWH) which is, due to massive hot fluid emanations, completely covered by microbial mats. In front of the cavity there are several boulders framing the depression the cavity lies in.

Geology

The grotto and the boulders in the direct vicinity are built up of the typical volcanites (Dacites/Andesites). A precise rock-type determination is not possible due to the extremely high level of alteration. At the bottom of the depression a polymict conglomerate crops out. It is characterized by sulfurous cementation and incorporates numerous sulfide ore clasts. Grains and clasts are mostly sub-rounded to rounded. The material is comparable to the conglomerates in Bottaro North and Fumarolic Field. Asides, some areas show a cementation of pure sulfide ore mineral precipitates. They incrust volcanite clasts with grain sizes of coarse gravel to rock (Figure 32-E). A prominent dyke intersects the location. It shows intense silicification. In combination with weathering and erosive processes, this leads to a noticeable outer shape of the rock material. It is intersected internally by hard ridges of only few millimeters in width sticking out some centimeters. The networks form polyhedral structures referred to as “honeycombs” (Figure 32-A) due to their outer shape.

Temperature distribution

As the site was first investigated in 2015, there are no long-term observations. Discharging waters showed temperatures up to 60 °C.

Fluid discharge

Discharges are small (class B), mostly gas-dominated, and flowrates are low and irregular in the area of the conglomerates. In contrast, the discharge at the dyke structure emits continuously and at higher flowrates (class B – C). The mass occurrence of whitish bacterial mats in the grotto witnesses a high discharge of hydrothermal waters with high sulfide concentrations. However, these discharges occur disperse and are therefore hard to sample (cf. Hot Lake).

Discharge features

Due to the diverse host-rocks, a number of discharge features can be observed. As the grotto itself is completely covered by bacterial mats, no discharge features could be observed in-situ. Their presence can be assumed but an investigation would

necessitate intense work to remove the bacterial mats beforehand. However, an early-stage development within the microbial mats was observed (Figure 32–D). If not lithified, this type of discharge feature cannot be preservable.

Depending on the type of cements, Tore and TS discharge features were documented in the respective type of conglomerate. Due to the low discharge, the individual features were not well developed.

The dykite shows lots of small tubes (mm-scale), vertical on the silicified ridges (Figure 32-A). The tubes are well visible and can be traced within the rocks. Diameters were measured from 0.3 to 2.0 mm. Active, gas-dominated emanation was observed in-situ. This still undescribed type of discharge feature is classified as To.

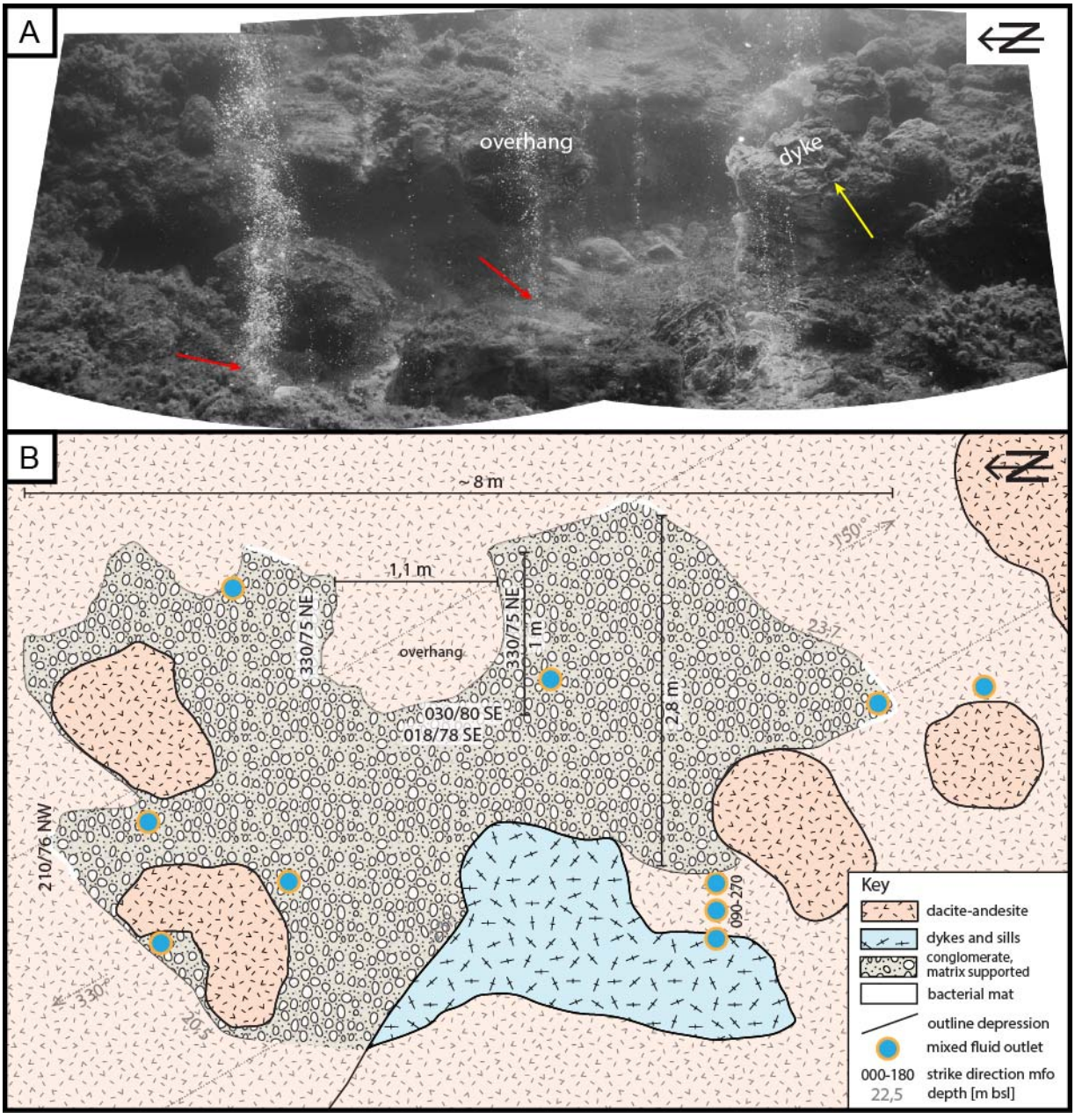

Figure 31: Cave (CA). **A –** Panorama view on the UWIS Cave. The prominent rock overhang represents the main grotto in the central part. Inside the grotto there are mass occurrences of algae-bacterial-mats

and numerous small discharges (cf. Figure 32). The site is intersected by a large dyke comprising strong silicifications, with respect to their outer shape described as “honeycombs” (yellow arrow, cf. Figure 32). The red arrows mark prominent discharges of type B to C. **B –** Map sketch of the UWIS Cave. The main strike of the location is 150-330 °. Modified after ADAMEK (2021).

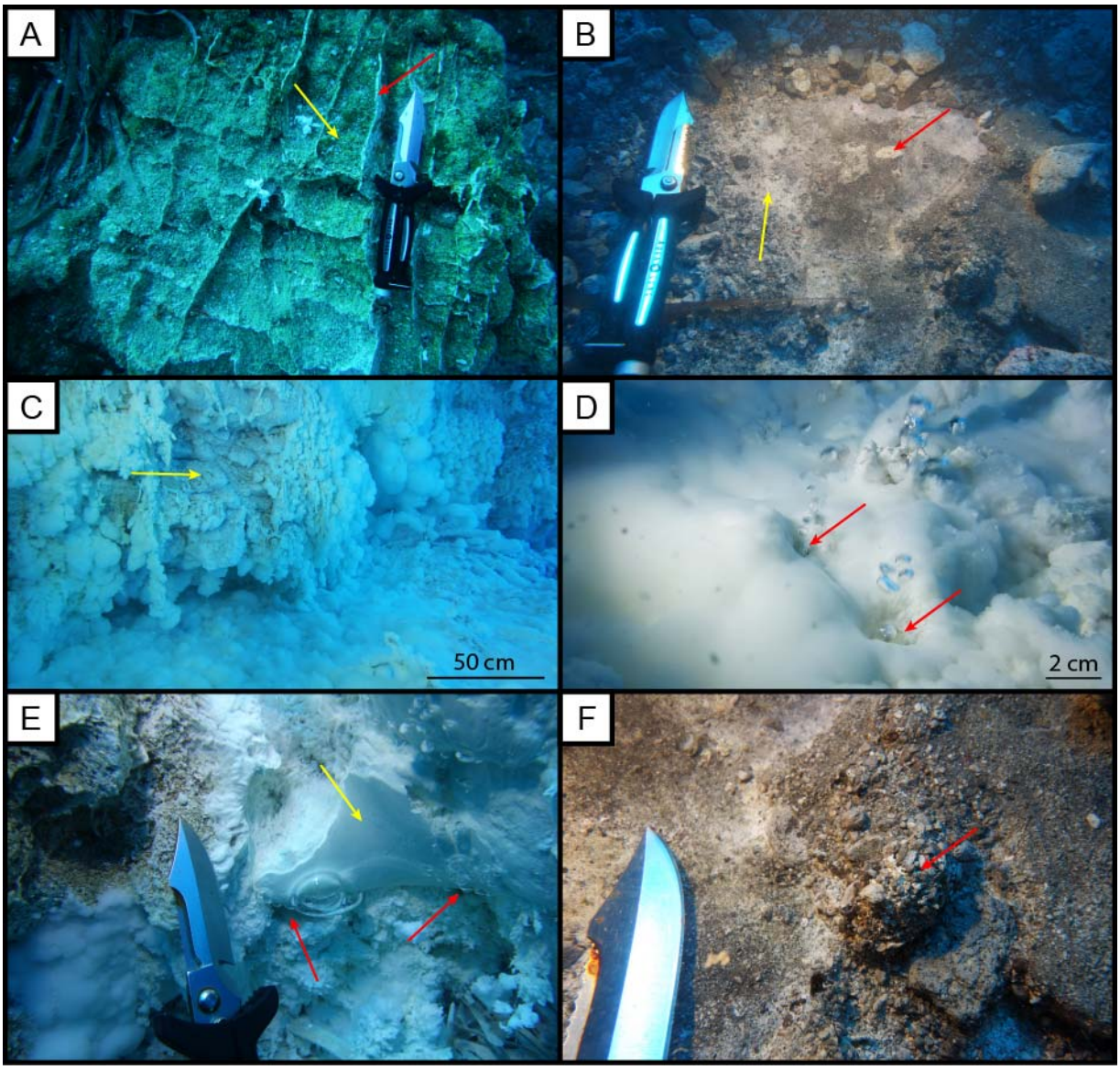

Figure 32: Cave (CA). **A –** Block of Dykite referred to as “honeycombs”. The silicified ridges (red arrow) comprise numerous small-scaled discharge channels of less than 1 mm. Active discharge can be observed visually. The interspace is filled with highly altered volcanites (Dacite/Andesite; yellow arrow). **B –** Excavated lithological border between the volcanites and the underlying conglomerate (sulfurous cements; yellow arrow). The red arrow marks a prominent sub-rounded volcanite clast. The material is comparable to those from Hot Lake and Area 26. **C –** Typical mass occurrence of whitish biomats within the grotto (*Thiobacillus*; GUGLIANDOLO et al. 2006). Yellow arrow marks the inhabited rock showing the prominent outer shape of small pillows. This outer shape is probably the result of weathering of the Dykite shown in A. Further investigation would require intense clean off, what causes very bad visibility for hours. It was therefore not carried out. **D –** Close-up on active discharging (red arrows) through the biomats. The fluids cause typical forms of discharge features (here: To) even in the recent biomats. **E –** Active discharges (red arrows) recently causing mineral precipitates (type CEs; cf. Table 10; yellow arrow). **F –** Active discharge (red arrow) forming discharge features of type Cc. There occurrence is quite rare in this location due to the main lithology.

5.2.7. Fumarolic Field

Location

The underwater investigation site is situated in the northeastern part of the “crater” 40 m south of Hot Lake. The water depth measures 17 m (Figure 33).

Geology

Fumarolic Field comprises polymict gravel overlying conglomerates with sulfurous cementation. In 2017, the occurrence of black coatings on gravel in distinct areas of several meters was documented. Their appearance changed very rapidly, both spatially and temporally. The precipitates were identified as MnO_2 (KÜRZINGER 2019). The phenomenon seems to depend on distinct events, probably influencing the hydrochemistry of the discharging fluids.

Temperature distribution

Fluid temperatures varied between 26 and 30 °C at class A to B vents in 2009. This fact hints on a gas-dominated fluid-type as the measured temperatures equal nearly the ocean-seawater-temperature. Single increased values of slightly above 30 °C were measured at stronger vents of class C in 2009. Since 2015 only one single discharge (water dominated) was documented that showed increased temperatures. The highest temperature was determined with 57.6 °C.

Fluid discharge

Fumarolic Field is characterized by lots of small vents (predominately class B) showing constant moderate flowrates. Over the years a decrease of flowrates was observed. In 2017, only single discharges were documented. Most of these small vents are arranged along regular subsurface lineaments. The three dominant strike directions of 000-180 °, 030-210 ° and 150-330 ° correspond to the fracture system (ADAMEK 2021). At the rims of the gravel flat, single stronger vents (class C) occur.

Discharge features

Most mineral precipitates consist of native sulfur and occur as cements or crusts. However, typical discharge features such as TS and FS are not common at this location.

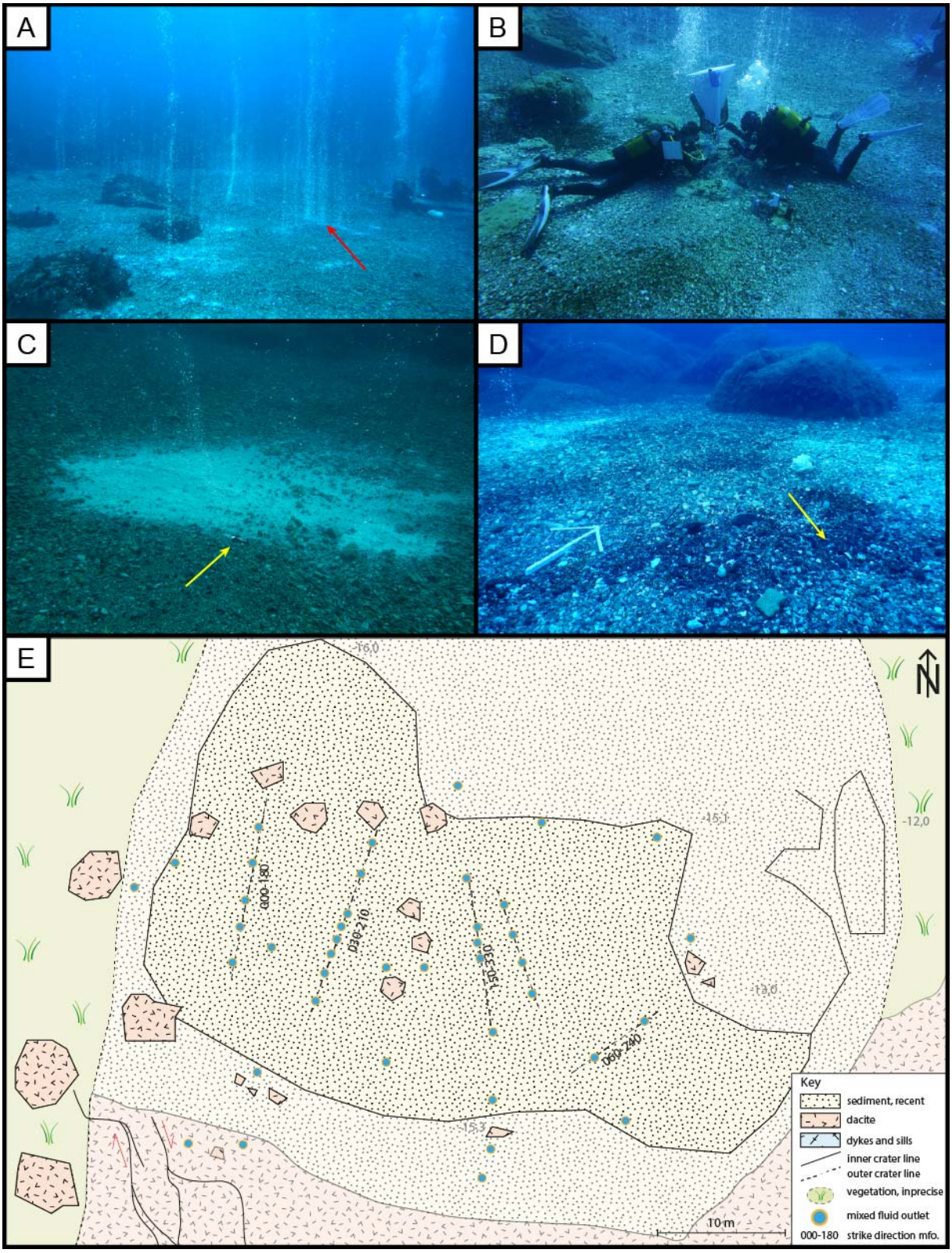

Figure 33: Fumarolic Field (FF). **A –** Overview of the location FF. The red arrow marks prominent discharges in the central part. The vents are arranged along fractures in the underground. **B –** Scientific divers conduct sampling under a protective atmosphere (nitrogen) of mineral precipitates. Results are presented by KÜRZINGER (2019). **C –** One of the major discharges in FF. Whitish biomats highlight the emanation area. The yellow arrow marks knife for scale (22 cm). **D –** Appearance of black coatings on gravel, probably resulting in short-term changes in the hydrochemistry of the discharging fluids. The yellow arrow marks coated gravel. The white arrow shows north direction and scale. **E –** Map sketch of the UWIS Fumarolic Field. Modified after ADAMEK (2021).

5.2.8. Hot Lake

Location

This 2 to 3 meter deep depression north of Fumarolic Field measures 8,6 m (NNE-SSW) x 6,5 m (WNW – ESE) and is situated at a water depth of about 17 m (Figure 34). At the rims there are lots of volcanic boulders. It is surrounded by large fields of Posidonia.

Combined with the hot fluid emanations its geometry caused increased water temperatures compared to the surrounding seawater. Consequently, dense bacteria mats grew in the adjacent grotto.

During the last years, discharges decreased constantly and the phenomena “hot” disappeared over time. Today’s measurements show no increased temperatures of the ocean water in the depression anymore, but the chemistry of the hydrothermal water is still very different from seawater.

Geology

The site is characterized by tuffites and large boulders built up of dacites and andesites. Additionally, sulfurous sandstones comparable to Area 26 occur.

The depression is filled with a more than 3 m thick layer of recent sands and gravel. Breakdown of blocks and boulders is visible at the sidewalls of the structure. With ongoing erosional impact, the depression is supposed to slowly grow over time. However, detailed investigations concerning this hypothesis are still object to further research, as recent photogrammetric data is missing. An estimation of growth rates would necessitate precise data over several years.

Cementations consist of native sulfur appearing as disperse cements (matrix) or fracture fills. They can be found predominantly at the sidewalls and the discharge features therein.

Temperature distribution

For several years, this local depression showed fluids discharging at about 70-80 °C. In 2011/2012 values between 30 and 80 °C were measured (CANZLER 2012). However, temperatures have been cooling constantly. In 2017, only minimally increased temperatures were observed.

Fluid discharge

Discharge features hint on former active degassing. No recently active gas emanation was observed during the time period 2006 to 2018. However, water-dominated discharge is reported to have been a common feature. The fluids are highly saline and

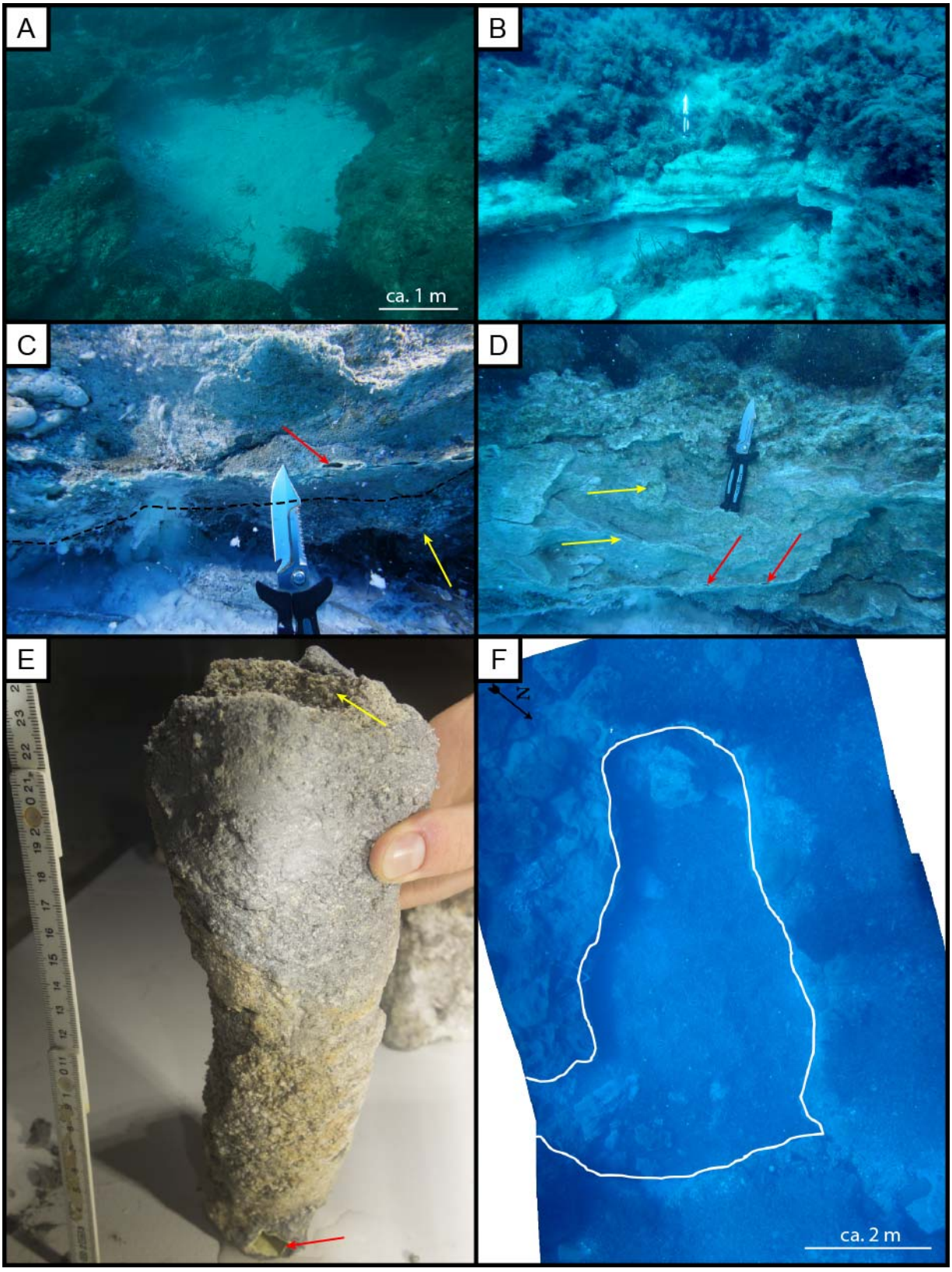

Figure 34: Hot Lake (HL). Knife for scale is 22 cm. **A –** Overview image of the location HL. **B –** Outcrop of the typical Tuffite near HL. **C –** Discharge features (type FS – TS; red arrow) at the sidewall. Dashed line marks the lithological boundary between the underlying conglomerate (red arrow) and the Tuffite strata at the top. **D –** Recent (red arrows) and ancient (yellow arrows) discharge features at the sidewall. The different states of abstraction indicate the temporal succession. **E –** Prominent discharge features of type To from the sidewall of HL. The feeder channel is well visible and coated with native sulfur (red arrow). At the emanation point, a clear coarsening of the grains due to the fluid flow is noticeable (yellow

arrow). **F –** Panorama image of the location. White line highlights the contours of HL (photography: SDC, 2007).

rich in CO_2 and H_2S (GUGLIANDOLO et al. 2015). As temperature measurements show, these emanations are cooling and will eventually disappear.

Discharge features

The sandy filling of the depression hinders the development of discharge features in the central parts of Hot Lake. However, the rims of the depression show different types of sulfurous discharge features, such as FS and TS.

Single prominent individuals of yet unclassified discharge features were documented and sampled in the rim-wall. The tube-shaped structure of ca. 20 cm height showed a diameter of approx. 10 cm (Figure 34-E).

5.2.9. La Calcara

Location

Situated at the northern shore of Panarea Island, the bay of La Calcara is one of the underwater investigation sites outside the central area of fluid discharges. It is adjacent and directly linked to the onshore hydrothermal area of Panarea. The moderate slopes show complex neo-tectonic features and several discharges, both in subaerial and submarine settings, respectively. Due to its large extension, the site was subdivided into a northwestern part (Buoy 1) and a southeastern part (Buoy 2). Water depth ranges from 23 m in the deepest regions up to 12 m at the sub-location *The Wall* (Figure 35). Severe currents are typical due to the exposed setting of the spot.

The area around *Black Rock* (BR) and *New Rock* (NR) comprises numerous massive sulfide ore mineral precipitations. Mineralogical investigations of these are given by KAKUK (2014 and 2016).

In 2015, intense excavation work was conducted some meters north of the rocks (sometimes described as *FP 9*). In this outcrop, intense iron cementation was documented. A clear stratification in the underground hints on a cyclic evolution of the La Calcara strata (Figure 36). Preserved networks of inactive TFe-tubes gave insights on the preservation potential of these typical hydrothermal discharge features.

The sub-location *Mordor* was first excavated in the year 2017. This nearly circular spot (excavated: 1.7 x 2 m) comprises numerous intense hydrothermal fluid discharges which show both, gas- and water-dominated fluid emanations (Figures 37 and 38). The discharges of classes B to C form a complex network of tubes (facies type TFe and To) and cones (facies type Cc) which are in parts highly abstracted. The network was covered by several centimeters of recent cover sands. Cements are mainly iron-bearing or some kind of chert/quartz (cf. Table 10). The latter occur as white mineral crusts, which could not be identified mineralogically with the applied techniques. Some cones in the central part are intensively abstracted showing heights of up to 14 cm and unusual oversteepening (aspect ratio ~ 1:4; cf. Figure 38-D). These cones are well comparable to the ones in Area 26 – *Brodor*. They are built up of coarse sand to fine gravel what witnesses the typical depletion of fines in this facies (cf. chapter 6). Dimensions of tubes range about 2.5 cm in the outer diameter and up to 2 cm in the inner diameter. Junctions were mostly abstracted but appear to follow the same properties as in other TFe type facies (~90-120 °). Massive gas- and water-dominated discharges directly out of all discharge features were documented (see Appendix 2).

Octopus Rock was intensely investigated in 2010 and 2011. The area is characterized by numerous small tubes (facies type To) in large scale networks of several meters. The findings from these campaigns build the main basis for the descriptions given by STANULLA et al. (2017a) and the classification therein.

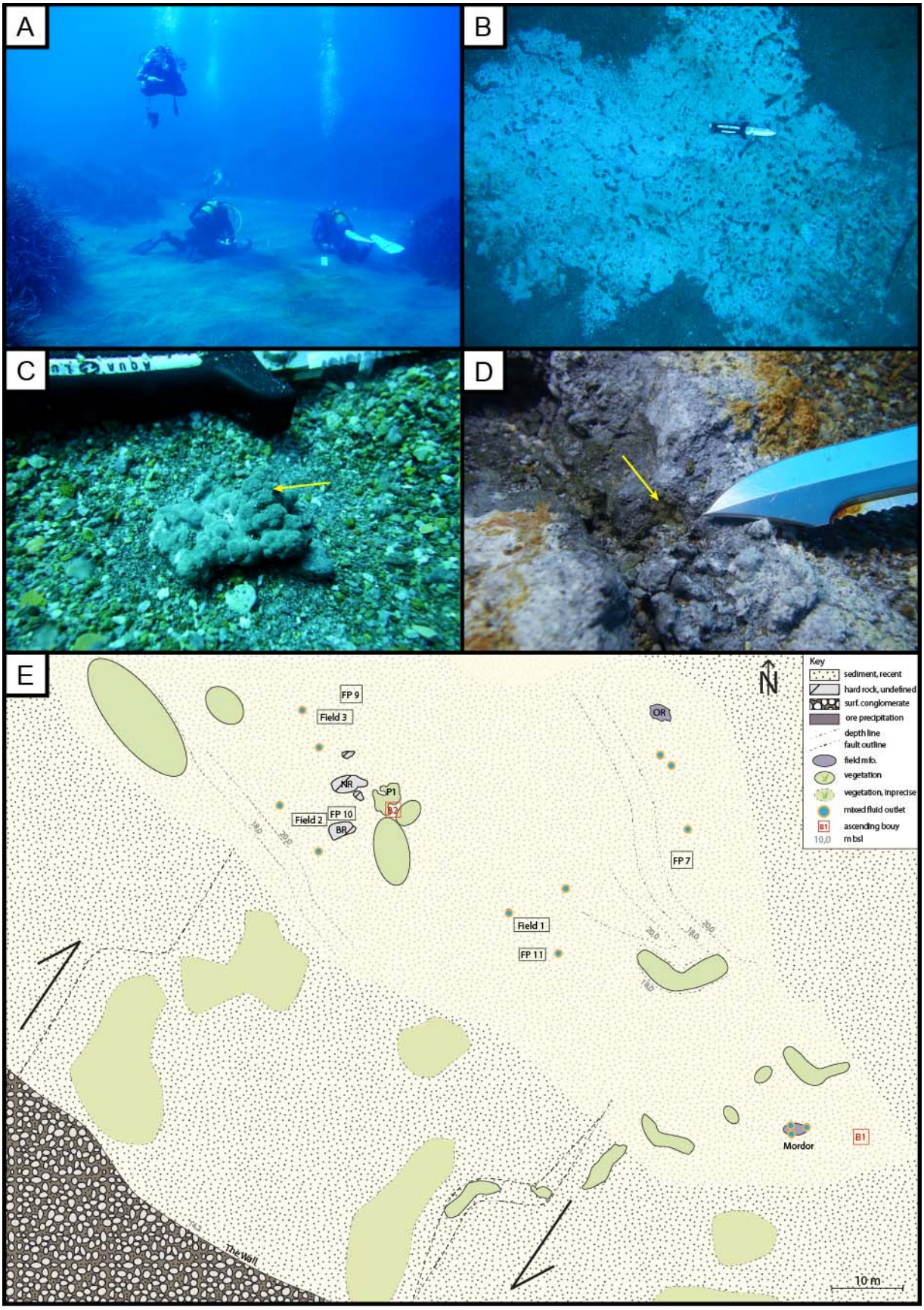

Figure 35: La Calcara (LC). **A –** Overview image of parts of the location. Large sandy flats intersect with wide fields of Posidonia. **B –** Excavation site near OR. This meter-scaled network of tubes (facies type To) is one of the earliest indications for large-scaled networks and builds the basis for the classification given by STANULLA et al. (2017a). **C –** Prominent massive sulfide ore precipitation (pyrite/marcasite; FeS_2) found near BR. **D –** Massive sulfide ore precipitation (pyrite/marcasite; FeS_2)

as fracture fill near BR. **E –** Map sketch of the UWIS La Calcara. The main investigation sites are listed. Modified after ADAMEK (2021).

Geology

La Calcara prevails polymict sandy facies. The uppermost layer of about 10 to 40 cm is a recent cover sand. Underlying sandy facies appear mostly with a fine-grained matrix. In contrast to Area 26, the fine-grained components are neither rigid nor crystalline. They consist mainly of weathering products of the hard rock lithologies (Dacites/Andesites) such as Alunites and Smectites. The sediments seem to be mostly homogeneous and show no stratification in the uppermost meter. Exceptions are the preserved discharges such as FP9 where a clear stratification within the mineral precipitates is obvious. In most areas, large rocks and boulders are incorporated. They are predominantly well-rounded remains of the typical hardrock facies. Theories concerning the genesis of this sandy facies are proposed by KÜRZINGER (2019). Secondary alteration and mineral precipitation (e.g. of pyrite, marcasite or iron(hydr-) oxides) by hydrothermal fluids play an important role in this highly active location.

La Calcara provides another astonishing fact: potentially contradicting mineralogical facies appear within short distances. Magnesium-rich manganese carbonates such as rhodochrosite ($MnCO_3$) interchange with iron disulfide mineral phases like pyrite and marcasite (FeS_2) in distances of only 5 m. Two different types of sediment were described by STANULLA et al. (2017c): Sediment 1 is characterized by plagioclase and potassic feldspar ($KAlSi_3O_8$), gypsum ($CaSO_4$) and quartz (SiO_2). Cements are built up predominately of marcasite and pyrite (FeS_2). Sediment 2 contains various types of feldspar, hornblende ($(Ca,Na,K)_{2-3}$ $(Mg,Fe,Al)_5$ $[(OH,F)_2/(Si,Al)_2Si_6O_{22}$), apatite $(Ca,Ba,Pb,Sr)_5$ $(PO_4,CO_3)_3$ (F,Cl,OH)), titanaugite ((Ca,Na) (Mg,Fe,Al,Ti) $(Si,Al)_2O_6$) and quartz (SiO_2). The cement consists of rhodochrosite ($MnCO_3$). A plausible explanation for these quite contradicting findings is the process of phase separation of the hydrothermal fluids (cf. chapter 3, Figure 3) as supposed by STANULLA et al. (2017c).

Temperature distribution

Morphologic conditions in La Calcara such as large sand flats exhibiting clearly defined thermal hotspots enabled a consequent long-term monitoring of the geothermal state in the area. Among numerous single-spot, heat flux and thermogradient measurements (BARTH et al. 2010; MÜLLER 2011 a. o.), a transect monitoring was realized showing the thermal patterns at the seafloor.

Temperatures range from about 20 °C (seawater infiltration) to 134 °C, what nearly equals the boiling point at this depth. Over the years, quite constant geothermal conditions have been measured in the area. Any temperature data in La Calcara has to be interpreted considering possible disturbances due to iron(hydr-)oxide crusts in the sediments (cf. Figure 36, *FP 9*). These crusts may have severe impact on the hydrothermal fluid flow and thus potentially buffer or shift the temperature values.

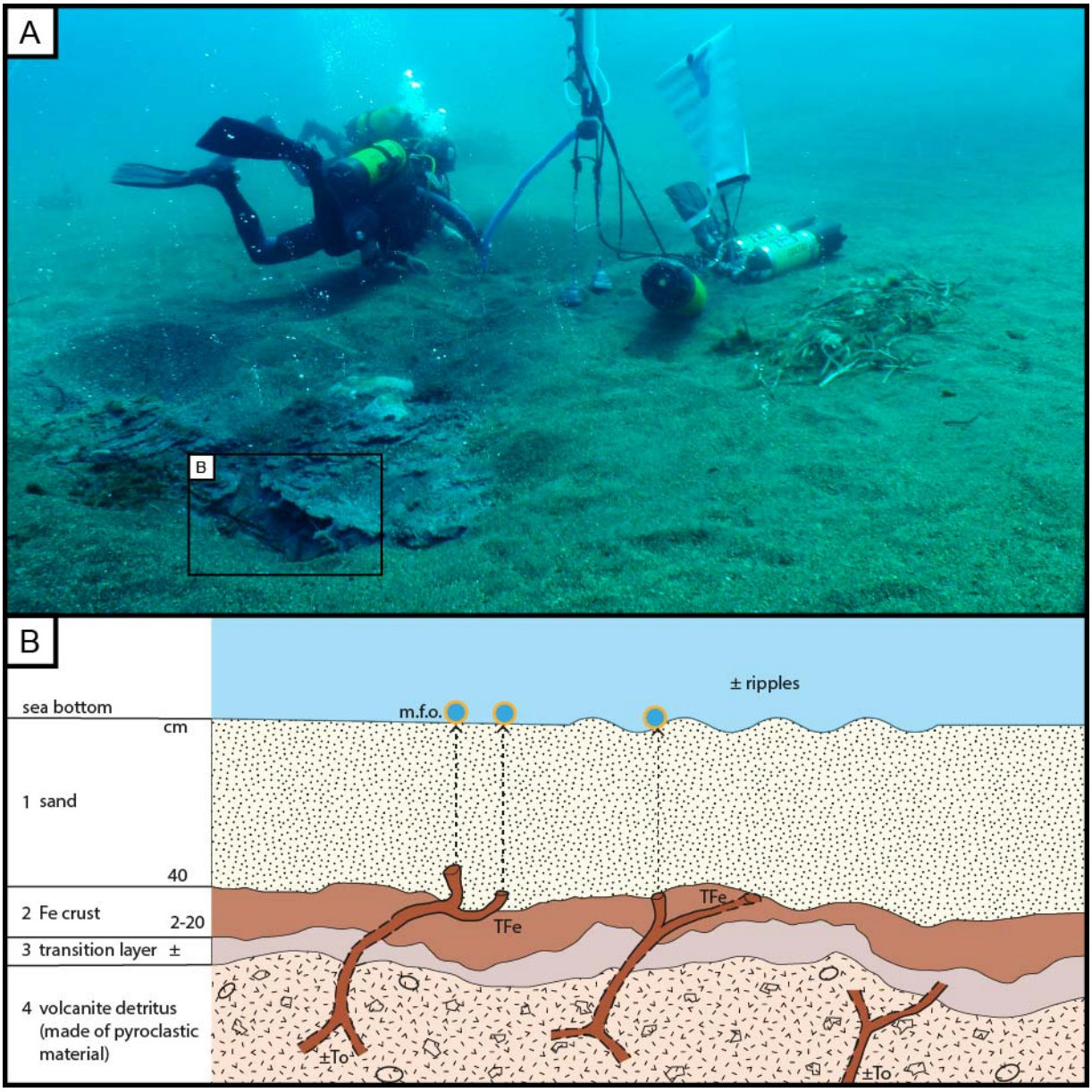

Figure 36: La Calcara – *FP 9*. **A –** Overview image of the location *FP 9*. Scientific diver conducting excavation work using a mobile airlift pump (cf. STANULLA et al. 2016 and 2017c). Square indicates the area of detailed mapping given in B. **B –** Detailed map sketch of the excavated outcrop at *FP 9*. The recent cover sand (1) overlies a massive crust of iron(hydr-)oxide mineral precipitates (2). Discharge features of type TFe intersect the crust. A transition layer (3) of varying thickness is the link to the underlying soft sediments built up of altered volcanite detritus (4). Here, the discharge features appear in facies type To due to the different host lithology.

Fluid discharge

In contrast to locations with single major vents, La Calcara is characterized by lots of weak and sometimes unsteady discharges (class A-B). However, isolated spots (e.g. sub-location *Mordor*) show constant class-C-discharges with simultaneous emissions of gas and water.

The presence of paleo-discharges is proven by mineral precipitation and discharge features in the sediment (e.g. FP 9, Figure 36). Their widespread occurrence witnesses a potentially periodic and complex development of the discharges over time.

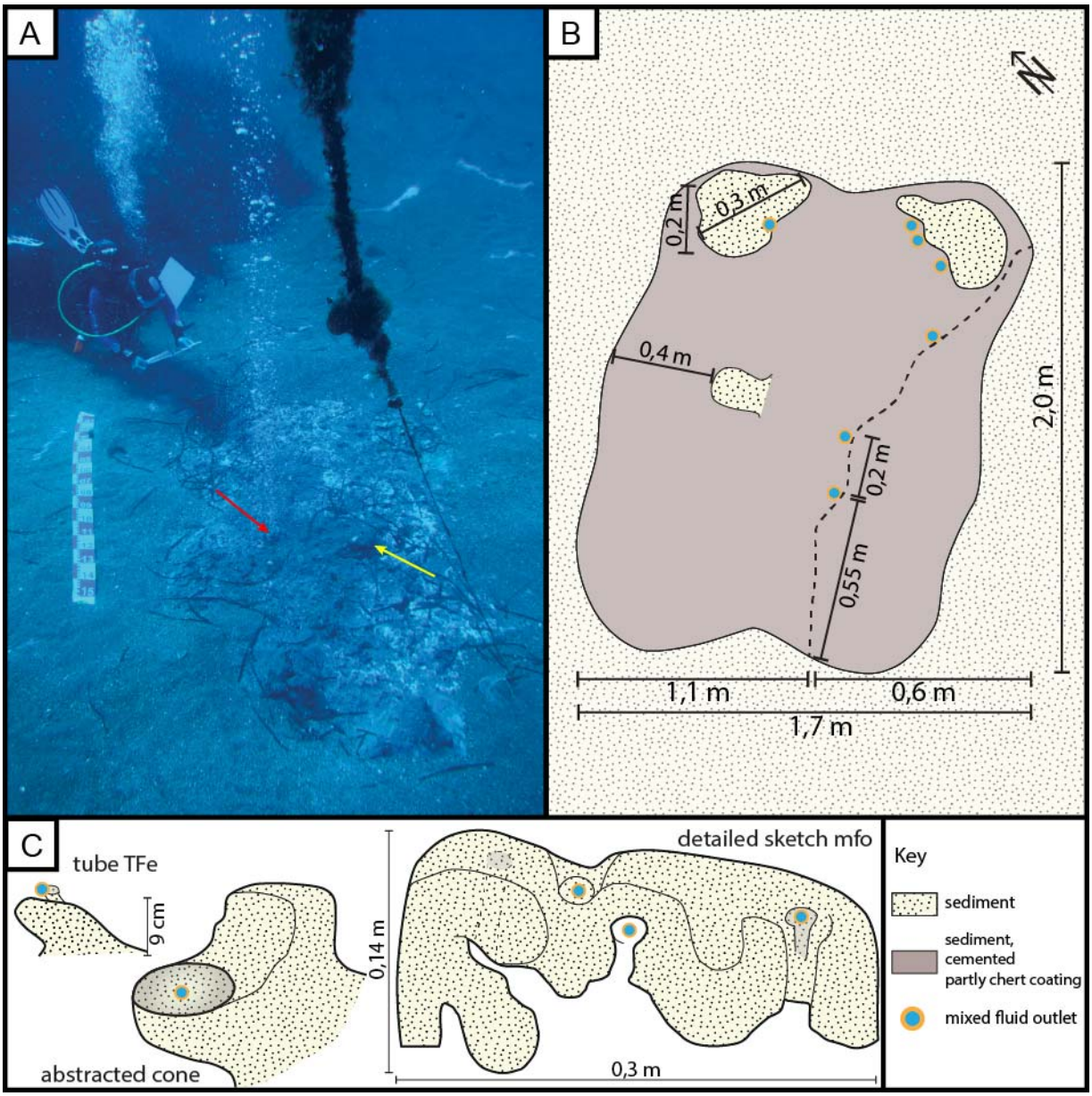

Figure 37: La Calcara - *Mordor* (MOR). **A –** Overview image of the excavation site at MOR. Scale is 1.5 m. The yellow arrow marks central discharge feature (cf. Figure 38-D). The red arrow marks active emanations. **B –** Map sketch of the sublocation. Prominent discharge features are given as details in C. **C –** Details of prominent discharge features. The structures involve a mixture of typical features such as cones and tubes.

Discharge features

Numerous different discharge features make the site a key locality for the understanding of those structures. Some of them are described as type To or TS by STANULLA et al. (2017a) occurring within the semisolid surface of the bedrock clays.

Being covered with recent sands, these tubes can only be found with the aid of secondary markers such as biomats or mineral precipitates at the recent sediment surface. When uncovering the bedrock-(cover-)sand-interface, an unexpected diversity of structures can be found in most cases (cf. STANULLA et al. 2017a).

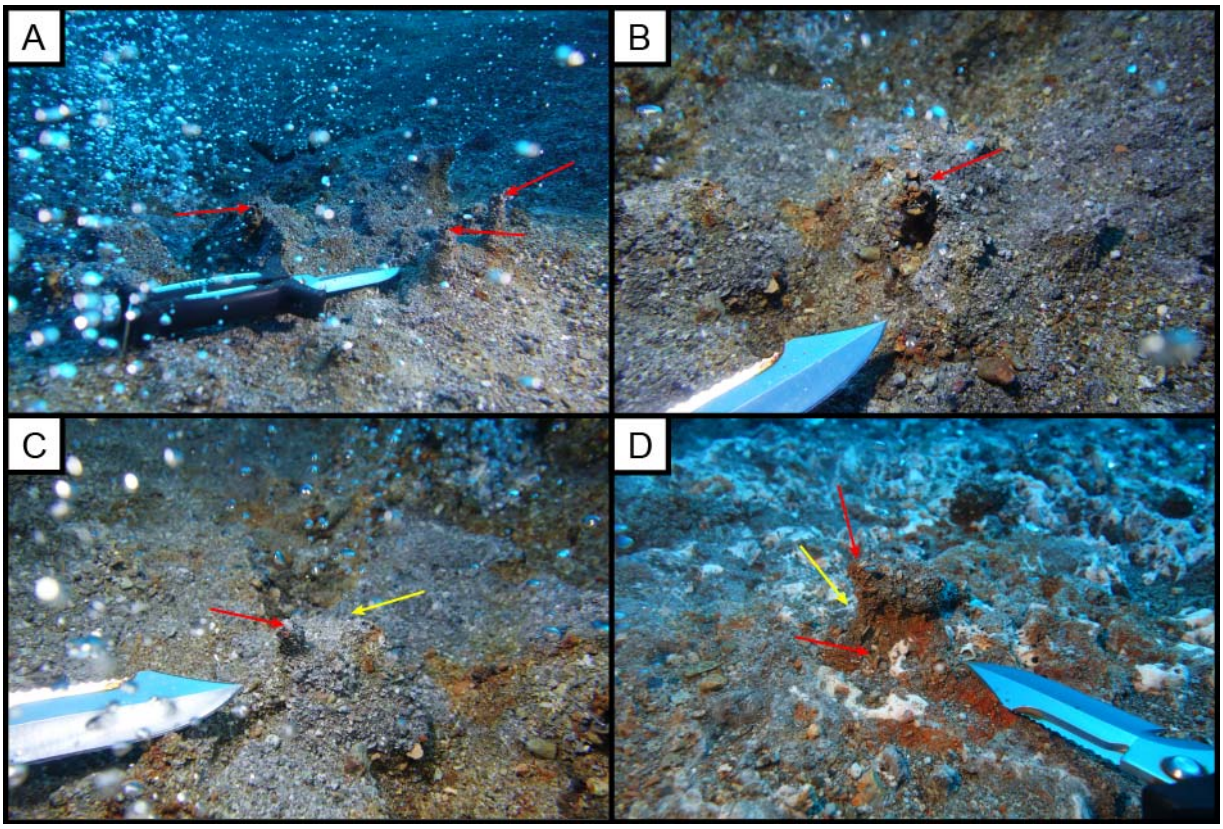

Figure 38: La Calcara – *Mordor* (MOR). **A –** Overview image of the location MOR. The red arrows mark prominent tube specimen. Most of them are actively discharging. **B –** Tube specimen showing massive grain coarsening at the emanation point. Iron bearing cements are common. **C –** Discharge features (type TFe; red arrow) at the central part. Intense fibrillation of the water column witnesses hot water emanation (yellow arrow). **D –** Highly abstracted cone specimen (Type Cc) at MOR. The cementation with iron(hydr-)oxides is a relatively rare feature. Active discharge is both, gas- (gas bubbles; red arrow) and water dominated (fibrillation of water column; yellow arrow).

Several irregular structures being cemented by iron(hydr-)oxide mineral precipitates were excavated on different sub-locations (e.g. *Mordor*, *FP 9*). They are classified as TFe discharge feature according to STANULLA et al. (2017a). Although unconsolidated, they are comparable to the well-defined tubes from Basiluzzo (cf. Figures 5 and 26). In other cases, these structures occur as irregular bodies within the sediment. They often represent paleo-discharges or active venting areas.

Furthermore, discharge features in soft sediments are common (type Cu; STANULLA et al. 2017a). The cones mostly occur in random patterns showing heights of 10 to 15 cm and diameters of about 20 cm. Aspect ratios vary from 1:2 to 1:3. In some areas, the cones are aligned along 060 °-240 ° or 000 °-180 ° lines, indicating fractures underneath the recent sediment cover (cf. ADAMEK et al., 2019).

5.2.10. Point 21

Location

Point 21 is dominated by a large scarp wall which is one of the most dominant structures on the shelf of Panarea (Figure 39). It is about 4 - 5 m heigh and extends approximately 30 m from NW to SE. The hydrothermal vents at its bottom rank to the strongest in the system. These outlets were chosen for the installation of the gas flow rate measuring device FSVG (cf. BARTH et al. 2010; PONEPAL et al. 2010). Intense biomat growth can be observed in the vicinity of the hydrothermal emanations. Spacious fields of Posidonia surround the location.

Geology

The scarp wall consists of Dacites/Andesites showing various degrees of alteration. It comprises complex neo-tectonic structures of different degrees. Some fractures are oriented 030-210 ° or 000-180 °. The strike directions of 150-330 °, 090-270 ° and 060-240 ° are remarkably common. However, no dominating fault direction can be determined (ADAMEK 2021).

Disperse fluid discharge within the scarp wall causes massive sulfide mineral precipitation which is witnessed by a number of ore crusts covering the hard-rock or filling small fractures (cf. ORDRUSCH 2016).

Furthermore, native sulfur is a common mineral precipitate occurring as fracture-fill or crust in the vicinity of hydrothermal fluid emanations.

Temperature distribution

The FSVG is equipped with temperature measuring devices (cf. PONEPAL et al. 2010). Thus, mid-term temperature data is available for this location. Temperature values of the emitted gas are constantly measured at about 65 °C.

Fluid discharge

At and in the wall, there are numerous gas-dominated emanations. Three of them are among the strongest gas vents in comparison to all other sites in the system. The measurements of fluid discharge rates (FSVG) show average flowrates of 30 to 70 L/min in 2010. A distinct tidal influence on the discharges is remarkable (PONEPAL 2011; cf. LI et al. 2019). A subjectivly decreasing gas volume flow has been noticeable since 2015.

There is a number of more disperse discharges in the wall itself and in the vicinity. As the measuring of gas flow rates is a lot more difficult in a steep wall, there is no numerical data on these up to now.

Discharge features

The underwater investigation site Point 21 shows diverse discharge features. Especially gas erosion is well observable in the SE parts of the wall. Furthermore, a lot of fracture fills, mostly built up of native sulfur, can be observed (cf. STANULLA et al. 2017a). The typical lamination proves the cyclic character of the hydrothermal discharges (cf. chapter 3.2.).

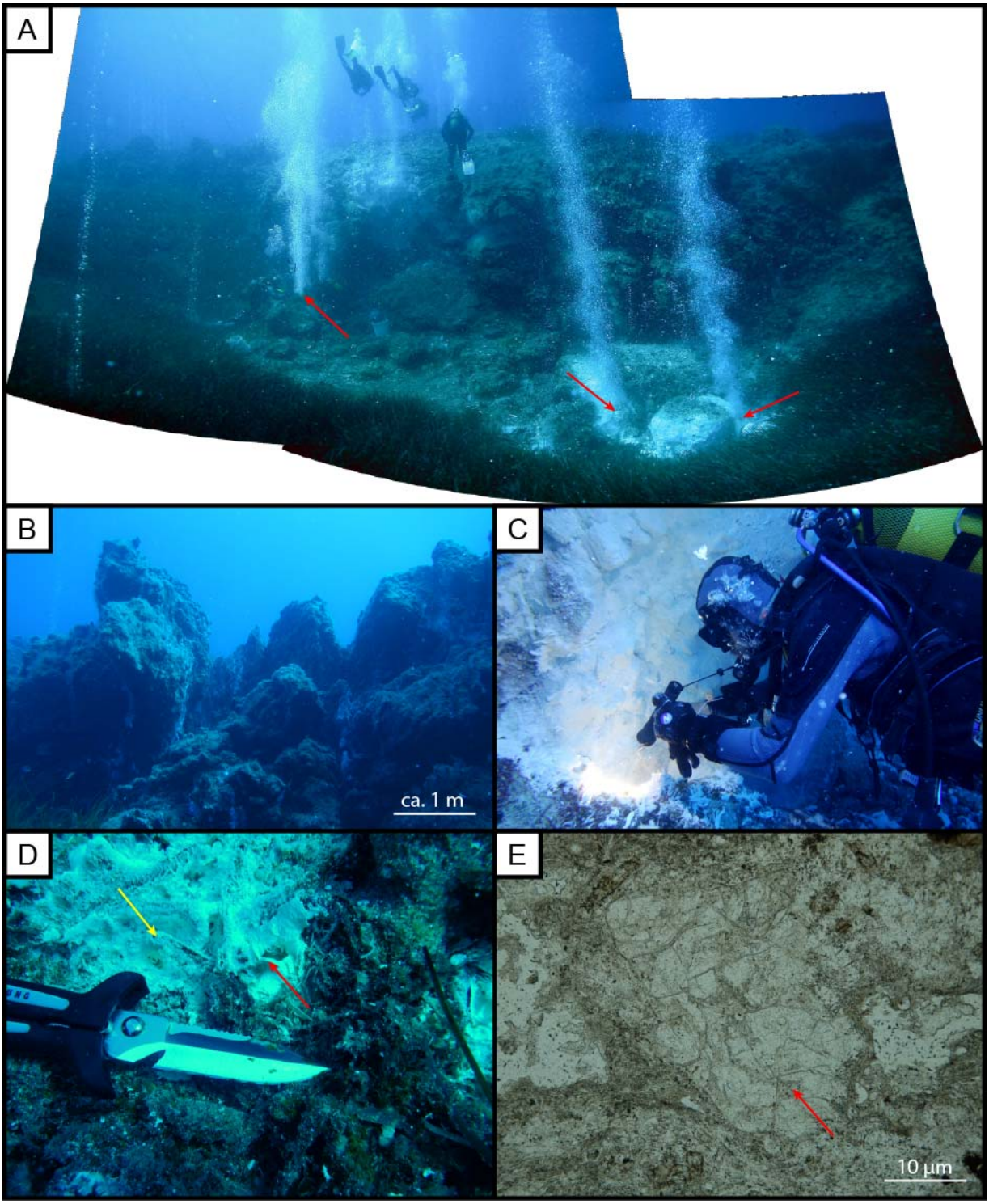

Figure 39: Point 21 (P21). **A –** Overview panorama of the location P21. The red arrows mark the most prominent discharges. **B –** Erosion channels at P21. Active emanation is forcing erosional processes.

C – Scientific diver measuring temperatures (here: 55.7 °C) at the wall of P21. **D –** Recent sulfurous mineral precipitates (red arrow) near P21. The cements are incrustating plant roots (yellow arrow) which possibly form gas pathways (cf. chapter 6). **E –** Thin section of the prevailing hardrock lithology. The Dacite/Andesite is hard to identify. Mineral phases appear very altered and may only be identified by characteristic grain shapes. The red arrow marks relictic mineral specimen.

5.2.11. Subaerial locations

Location

Despite the submerged portions of the Panarea volcanic system, preliminary results on the subaerial parts of Panarea deliver important knowledge on the paleo-development of discharge features in the system. Therefore, some prominent examples with outstanding genetic relevance are presented in this thesis.

The two main locations that were investigated on land are the following:

Location subaerial 1:

near the path between ancient Bronze Age settlement and the bay of La Calcara

(UTM-coordinates: 33S 506575.17 4277293.33; ca. 48 m asl)

The outcrop is some tens of meters wide and 3 to 4 m high. It is located right beside the path down to the bay. It is a defined location with sharp borders (Figure 40).

Location subaerial 2:

beside the street S. Pietro – Heliport Air Panarea – North End

(UTM-coordinates: 33S 505821.265 4277197.2; ca. 130 m asl)

This site is located approximately 500 m up the street from the Air Panarea heliport in the north of the island. The outcrop is 1.5 m long and approx. 0.5 m high at the left side of the street coming from the heliport (Figure 41).

Geology and paleo-discharge features

Location subaerial 1:

This location shows intense hydrothermal alteration, both, iron-dominated (reddish colors) and clayish (whitish to greyish colors) types. Different cooling features such as pillars and shrinking structures are visible. In large portions, the overall lithological

impression is similar to the dykes in the underwater investigation site Cave (honeycombs). However, two different types can be distinguished here: a) a whitish, vesicular, hard and brittle material forming the rims of the combs and b) an also whitish, but loose and chalk-like material which probably represents the alteration products of volcanites. The honeycombs mostly show dacitic inclusions.

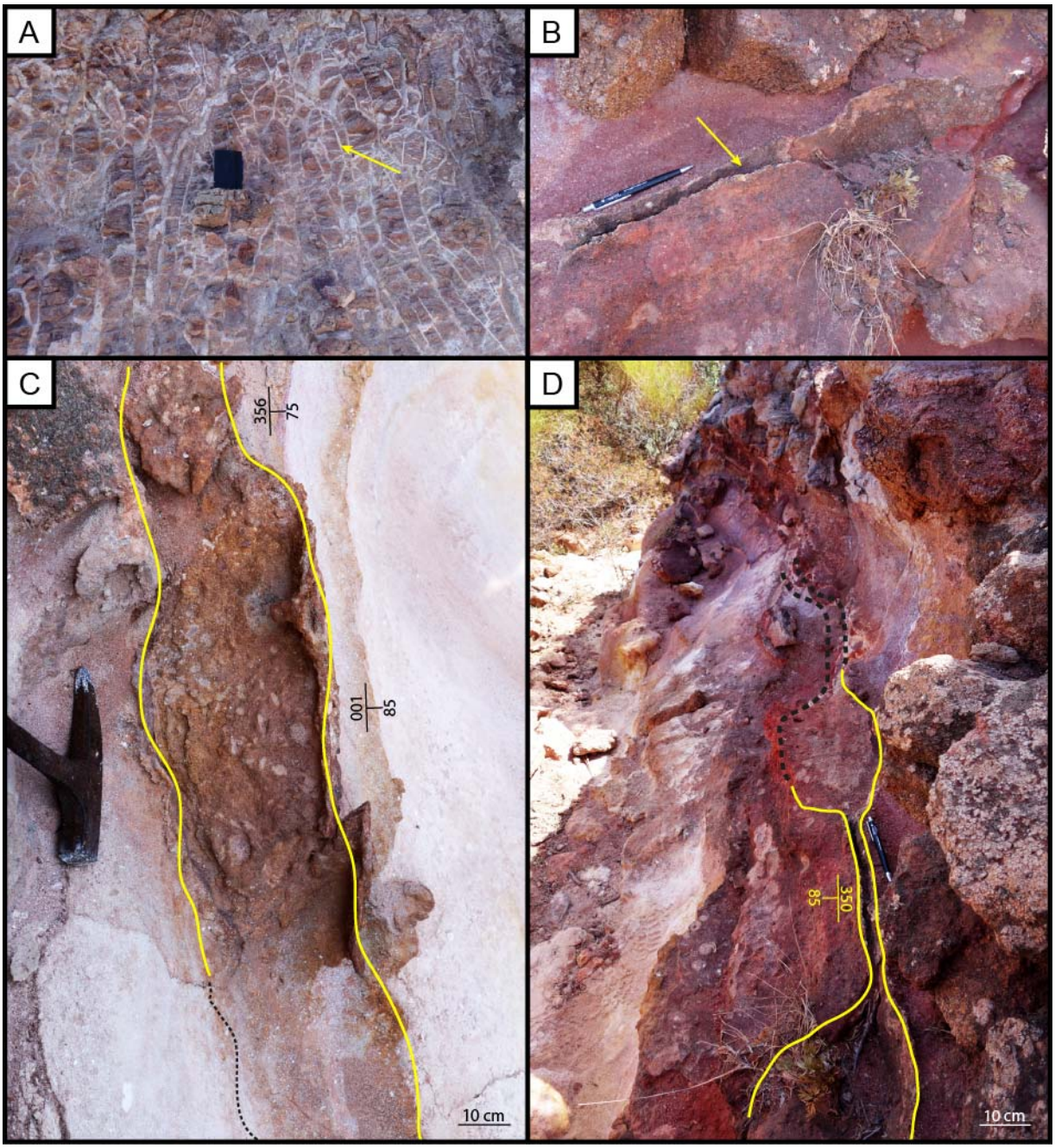

Figure 40: Subaerial 1. **A –** "Honey comb" structures at the subaerial 1 outcrop. The structures seem to be well comparable to the ones in Cave. However, the massive silicification documented in the submarine location could not be proven here. The yellow arrow marks a characteristic vein. **B –** Typical preserved fracture feature of type Fo (yellow arrow). **C –** Part of a preserved lineament structure. The structural data fits well to the underwater measurements. The secondary fill probably originates from the overlying strata. **D –** Overview of the preserved paleo-lineament structure (see also ADAMEK 2021). Shape and structure of the feature is similar to the ones in Area 26. This is the first evidence for the preservation of lineament structures as described in this thesis.

At most 20 m west of the described structure, the transition between two tuff-strata can be observed. In this weakened zone, large-scaled discharge features could develop. The structure is about 10 m long and opens about 1 – 20 cm to a depth of 10 – 50 cm. A laminated or stratified architecture as in the underwater investigation site Area 26 can be observed (Figure 40-C and -D). The structure is oriented along the main fault system (350/85) and cemented by iron(hydr-)oxides. The erosion cuts off single discharge ways (tubes). The structure is well comparable to the lineament structures in Area 26. It represents the first evidence for the occurrence of such structures in a subaerial environment. However, their genesis must be discussed concerning the sea level fluctuation and tectonic processes in the region according to which the location probably was submerged in former times (cf. chapter 3.1). The mapped coastlines by LUCCHI et al. (2013b) suppose a remarkable uplift of the island of Panarea as sea level fluctuations cannot explain the presence of paleo-coastline in a height of up to 115 m asl considering the age of the island. Consequently, the occurrence of preserved hydrothermal discharge features in the described elevation is also a good evidence for sea level fluctuations and the uplift of the island by tectonic processes.

Location subaerial 2:

The outcrop is built up of a brownish, massive tuff representing the Punta Torrione strata (CALANCHI et al. 1999). According to this geological map it shows a CA basaltic andesite-andesite composition and is strongly reworked and stabilized by millimetric glass fragments. The material is part of the eruptive epoch 4 and contains to the Lower Brown tuffs (bt) as described by LUCCHI et al. (2008, 2013b).

The tuff shows large-scaled networks of tube discharge features (Figure 41-A and -B). The networks show an extend of several decimeters. The tubes show similar shape, habitus, and orientation as the TFe-type tubes of Basiluzzo. Although well preserved, no laminae can be documented. Their obviously post-genetic formation seems to be the same as recently active in La Calcara or Basiluzzo. The presented network of tubes (Figure 41) is the first evidence for the preservation of tubes as described in this thesis. This second, independent evidence for the formation of discharge features in general in former settings confirms the statements given for the location subaerial 1 and the relevance of paleo sea level changes as well as tectonic processes (uplift of the island). This fact has to be taken into account while interpreting today’s submarine strata.

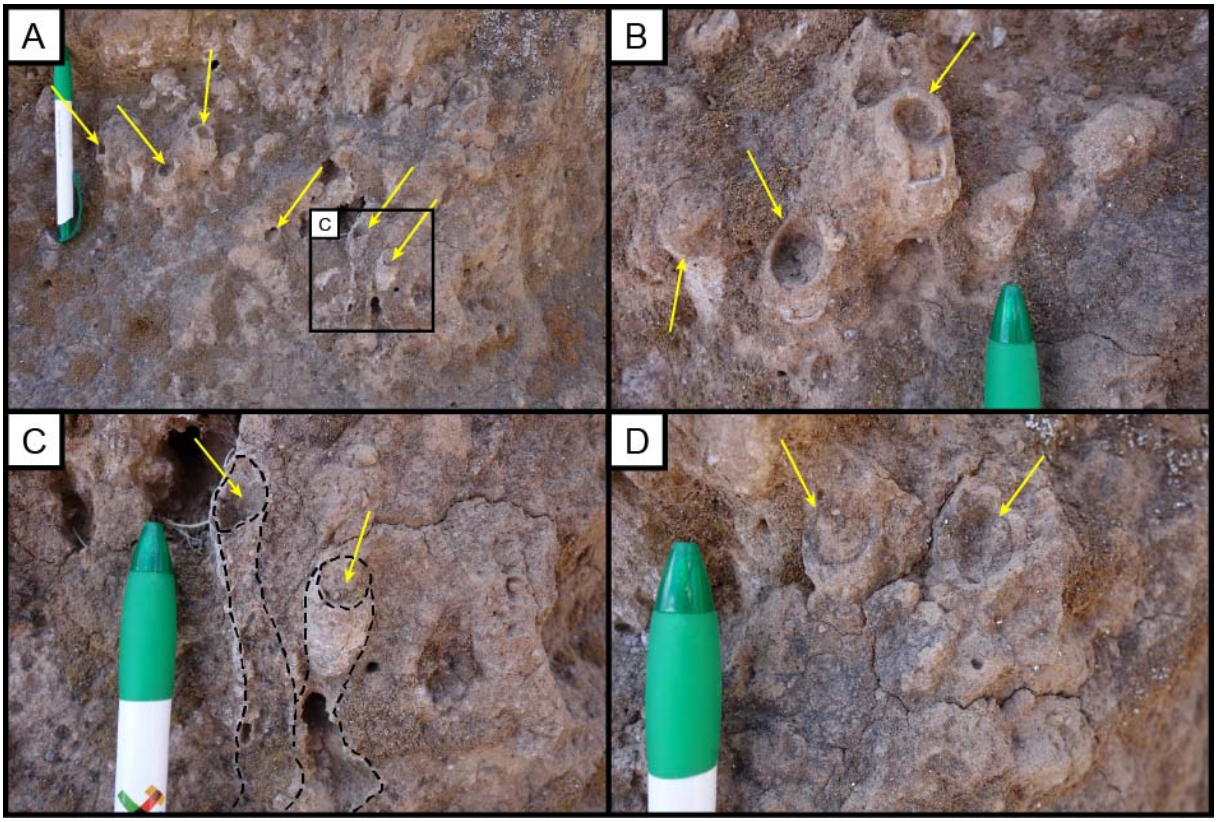

Figure 41: Subaerial 2. **A –** Overview of parts of the outcrop. The site comprises well preserved paleo-tubes. A large-scale network of several dm is well visible. **B –** Close-up on typical preserved tube features (yellow arrow). Their shape, habitus and orientation are similar to the tubes from Basiluzzo. **C –** Detail of A. Two prominent tube specimens (dashed lines) connected to a network of tubes what is a typical feature of this type of discharge feature. **D –** Two quite abstracted tube specimen. Different stages of abstraction are the result of erosional processes. Here, tiny relicts of former laminae could be supposed (yellow arrow). It cannot be stated without doubt, whether these are in fact laminae.

5.3. Summarizing tables

The main results given in chapter 5.1 and 5.2 are based on the investigations carried out in the years 2010 to 2018. The following tables 11 and 12 sum up the analyses realized during that period by the author and its supervised students (bachelor or master theses). Data collected by other members of the SDC-team is not listed.

Table 11: Summarizing table on field investigations during the project.

Analysis	Description	Aim	Number
Field investigations			
Scientific dives	Total number of scientific dives realized by the author.	Exploration and underwater investigation.	73
Investigation sites	Investigated locations at the Panarea volcanic complex.	Representative locations.	13
Diving time	Minutes underwater to realize the investigations (author only).	Exploration and underwater investigation.	3890
Photographs (underwater)	Number of scientific under-water pictures taken by the author.	Illustration of scientific outcome and basis for imaging methods.	1629
Videos (underwater)	Number of scientific under-water videos taken by the author.	Illustration of scientific outcome and basis for imaging methods.	43
UW-excavations	Number of underwater excavations carried out.	Exploration of covered or filled geological structures.	5
On-land fieldtrips	On-land fieldtrips to study comparative sites.	Comparison with subaerial locations and estimation of preservation potential.	6
Total time abroad	Number of days in the area of investigation (author only).	Exploration and underwater investigation.	70

Table 12: Summarizing table on laboratory investigations during the project.

Analysis	Description	Aim	Number
Laboratory investigations			
Samples taken	Total number of samples taken by the author.	Basis for laboratory investigations.	324
Photographs (analytical)	Number of scientific pictures taken in the laboratory.	Illustration of scientific outcome and basis for imaging methods.	1783
Granulometric analysis	Sieve analysis according to DIN 18123-5.	Sediment characterization.	5
Polished sections	Total number of polished sections analyzed.	Investigation and illustration of discharge features and other geological properties.	20
Thin sections	Total number of thin sections analyzed.	Investigation and illustration of discharge features and other geological properties.	77
Point counting	Quantitative analysis using imaging methods.	Quantification of parameters such as cement ratio, pore space distribution or extend of discharge features.	3
XCT	Total computed tomographic investigations realized.	Investigation and illustration of the inner parts of selected samples. Approach on pore space distribution and pathways.	3
SEM	Total SEM investigations realized.	Investigation and illustration of discharge features and other geological properties.	21
EDX	Total EDX investigations realized.	Chemical characterization of selected features.	23
XRF	Total XRF investigations realized.	Chemical characterization of selected materials.	38
XRD	Total XRD investigations realized.	Mineralogical characterization of selected materials.	25
µXRD	Total µXRD investigations realized.	Mineralogical characterization of selected materials.	61

6. Interpretation

6.1. Discharge features and secondary processes

Discharge features are among the most abundant sedimentary structures in the system of Panarea. Although they are common features in every depositional system being influenced by fluid discharge, they still are barely investigated and raise a number of scientific questions. These include topics such as “dependence on physico-chemical parameters”, “temporal rates of growth and development” as well as “host rock and fluid-type influence”, and “biological impacts”. However, the findings of STANULLA et al. (2017a) are the basis for the description of this complex suite of structures being connected with each other by several constructive and destructive processes (Table 13).

Destructive processes are mainly caused by the flow of gas and water from the hydrothermal vents. The flow acts in combination with chemical rock-fluid-interactions leading to rock destabilization by leaching and chemical weathering. The destabilized rock can then be eroded by the abrasion of the fluid flow (STANULLA et al. 2017a). This process is referred to as **fluid erosion** (FE). Ongoing FE might lead to subrosion in sedimentary lithologies (pathways for FE) if the constructive processes do not dominate the depositional behavior.

Constructive processes include any material building process in the system. Especially **mineral precipitation** (MP) and **cementation** (CE) play an important role (cf. KÜRZINGER 2019). MP describes the formation of minerals at the surface of a rock or structure. It depends on the flowrate and physico-chemical parameters such as pH, Eh, T or p and both chemical composition of the hydrothermal water phase and gas composition (in particular H_2S content). Additionally, environmental properties like seawater temperature, waves, tides, or currents play an important role. In contrast, CE occurs intergranular in sediments and is the main process for consolidation (e.g. of cones or tubes). In both cases, mineral formation out of hydrothermal fluids is the key factor. Especially quenching and consequent mineral precipitation out of hot fluids contacting cold seawater is typical. Furthermore, **alteration** (AL) and recrystallization due to geochemical influences impact the rocks.

Constructive and destructive processes always interact very closely and periodically in most cases. This complex interaction forms characteristic laminated aggregates in different facies types of discharge features.

Table 3 and STANULLA et al. (2017a) give a classification for discharge features having been known until 2012. New investigations and findings make a general update of this classification necessary. The column “changes” in tables 14 – 19 describes reason and background for single adaptions. The updated classification represents all types of discharge features, that were observed in the hydrothermal system of Panarea until 2017. It makes no claim to be complete as further exploration might bring up further facies types.

Table 13: Processes influencing the facies types of discharge features in Panarea.

Process	Description	Type locality
Destructive processes		
FE (fluid erosion)	Erosion due to the kinetic energy of the fluid flow. Forms irregular, multidirectional networks of open channels above recent or ancient discharge point. Possibly abstraction during time. Erosional processes inside discharge features interact with MP.	Hot Lake, Area 26 (bowls and lineament structures)
Subrosion	Major destructive process beneath the seafloor forming cavities and overlaps. Occurring mostly in macro-structures.	Hot Lake, Cave
Erosion	Standard erosion by mechanical and chemical agents such as currents, waves, tides, temperature changes, …	Bottaro West
Constructive processes		
MP (mineral precipitation)	Formation of minerals at the surface of a rock or structure triggered by hydrothermal fluids. Occurring in various facies (cf. Table 10).	Point 21, Bottaro North
CE (cementation)	Intergranular crystallization in sediments. Main process for consolidation of cones and tubes. Occurring in various facies (cf. Table 10).	Area 26, La Calcara
AL (alteration)	Change of mineralogy due to rock-fluid-interactions. Re-crystallization may occur. Very common: weathering of volcanites to clay minerals (Alunites and Smectites in LC).	Point 21, La Calcara
other	e.g. grain transport due to flow rate.	Area 26, La Calcara

Table 14: Updated classification of facies types of discharge features in Panarea – **channels**. The classification given in Table 3 and STANULLA et al. (2017a) is the basis for the given structure.

Facies	Description	Changes	Type locality
Channels			
NCi (network of channels, irregular)	Irregular, multidirectional network of open channels above recent or ancient EMPs. Erosion of hard rock or MP due to fluid erosion (FE). Possibly abstraction during time.	Formerly referred to as “gas erosion”. Despite the mixture of “process” and “facies”, the emitted fluids are always a mixture of gas and water. Therefore, this nomenclature must be updated.	Hot Lake, Area 26 (bowls and lineament structures)

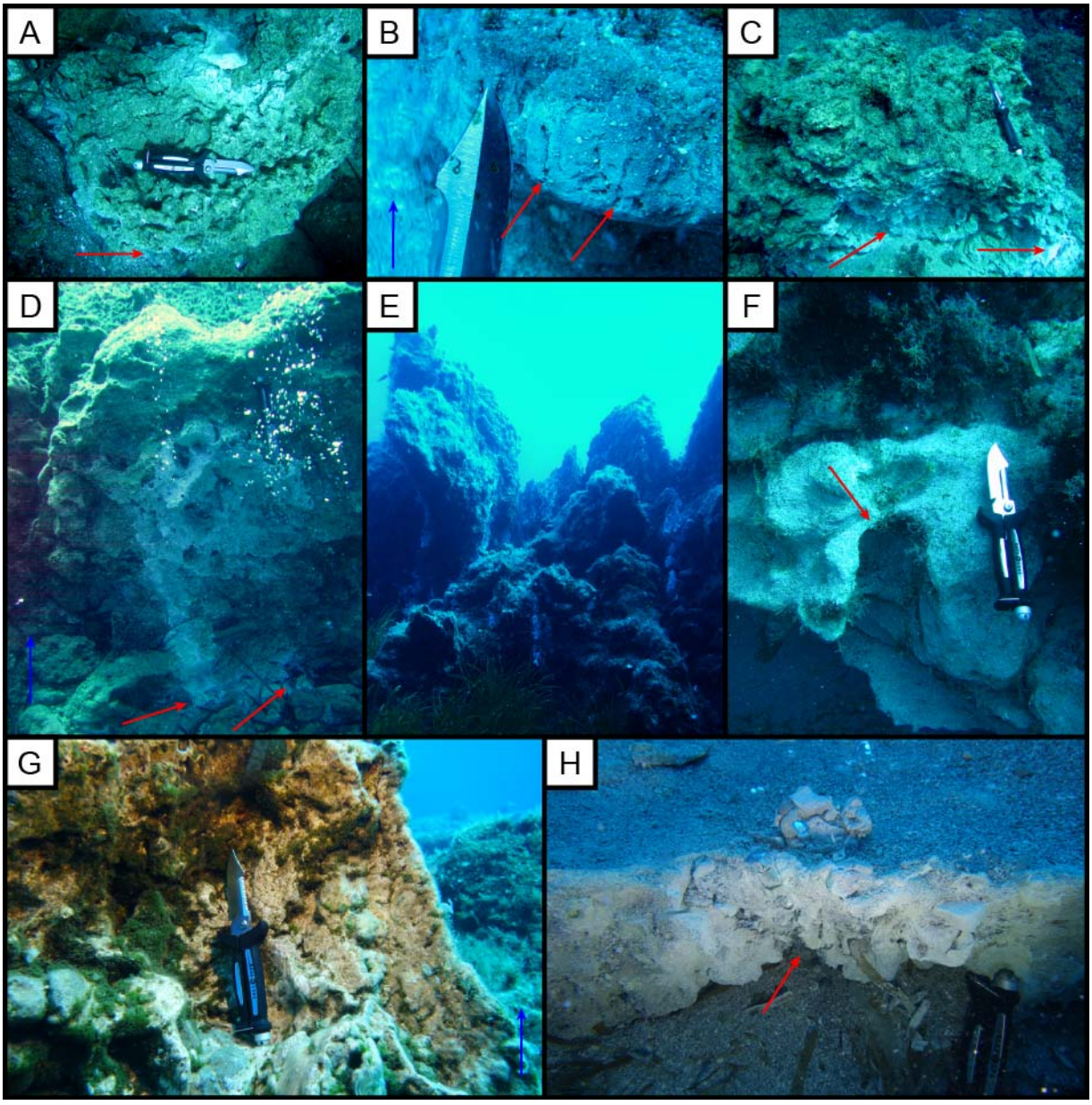

Figure 42: Examples for erosive processes forming hydrothermal features - type NCi in various lithologies. All pictures: knife/pen for scale. **A –** NCi at Hot Lake. Massive erosive processes manifest as hydrothermal features. The red arrow marks active discharge. **B –** Massive discharge at Lava-Tongue in Area 26. The fluid flow erodes the volcanoclastic rock. Process is highlighted by characteristic rills marked by the red arrows. The blue arrow indicates the flow direction. **C –** NCi eroding large volcanite boulder at Hot Lake (see A). The red arrow marks active discharge point highlighted by biomats. **D –** Active discharge forming large irregular networks of open channels (NCi). The blue arrow indicates the flow direction. The red arrow marks active discharge. **E –** Large scale channels at Point 21. Erosive features may evolve to large dimensions at powerful outlets. Height of wall approx. 4 m. **F –** The shape of NCi varies over time. After the formation, the channels can be eroded and abstracted by standard erosional processes. The red arrow marks ancient part of NCi. **G –** NCi in Bottaro West. Active hydrothermal discharge eroding a large block of volcanite forming NCi. The blue arrow indicates the flow direction. **H –** NCi develops at the sidewall of a larger lineament structure in Area 26. The red arrow marks active discharge.

Table 15: Updated classification of facies types of discharge features in Panarea – **fractures**. The classification given in Table 3 and STANULLA et al. (2017a) is the basis for the given structure.

Facies	Description	Changes	Type locality
Fractures			
FS (fracture fill, sulfurous)	Fracture-fill of (native) sulfur in hard-rocks; multistory genesis resulting in characteristic layering of the precipitates	n.a.	Point 21
Fo (fracture fill, other)	Fracture-fill with other minerals; layering of the precipitates is likely	n.a.	Cave
Fore	Fracture-fill of (sulfide) ore minerals in hard-rocks; multistory genesis resulting in characteristic layering of the precipitates	Undescribed	Black Point

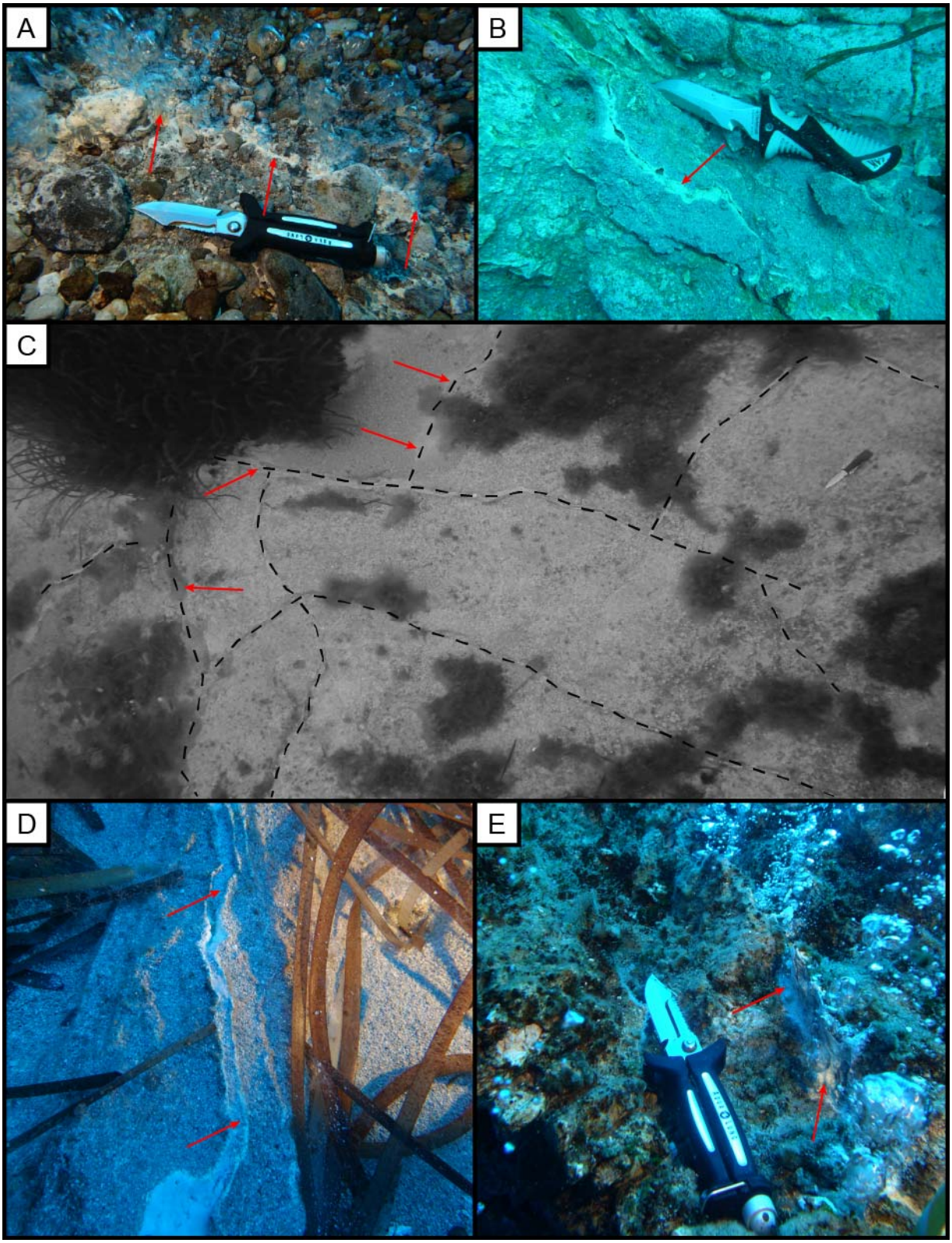

Figure 43: Fractures. All pictures: knife/pen for scale. **A –** FS in Bottaro North. The red arrows mark the fracture that is filled with native sulfur precipitates. Active discharge is obvious. **B –** Sulfur fracture fill near Hot Lake. **C –** Panoramic image of a fracture system near *The Mouth* in Area 26. Red arrows mark initial bowl structures. The scheme shows typical main and minor fracture structures. All fractures show sulfur mineralization. **D –** Open fracture (FS) in Area 26. No active discharge is visible. However, biomats indicate the release of hot water. **E –** Major fracture near Point 21 showing intense discharge and typical sulfur precipitation.

Table 16: Updated classification of facies types of discharge features in Panarea – **tubes**. The classification given in Table 3 and STANULLA et al. (2017a) is the basis for the given structure.

Facies	Description	Changes	Type locality
Tubes			
TFe (tube, iron cemented)	Precipitates cementing sand or gravel along the pathway of hydrothermal fluids in the sediment; tube-shaped; multistory genesis resulting in characteristic layering of the precipitates	n.a.	Basiluzzo, La Calcara
TSpu (tube of pure, native sulfur)	Precipitates of (native) sulfur in sediments or hard rocks; tube-shaped; partly bio-induced (roots of *Posidonia sp.*)	Formerly described as facies-type TS. New findings brought know-ledge on different types of sulfur tubes.	Point 21, La Calcara
TSce (tube, sulfur cemented)	Tube-shaped aggregates of sand or silt being cemented by sulfur bearing precipitates; mostly covered by recent sands; partly bio-induced (worms; roots of *Posidonia sp.*)	Undescribed	Area 26 (*Brodor*)
Tore	Precipitates of massive sulfide ore minerals in sediments or hard rocks; tube-shaped;	Undescribed	La Calcara (*Mordor*), Black Point
To (tube, other)	Tube-shaped discharge features neither TFe nor TS; multistory genesis possible; sub-types I – III depending on the morphology	n.a.	La Calcara (*OR*)
Tpal	Preserved individuals in the rock record; further classification at the moment only possible on major structures (dependent on the style of preservation)	Undescribed	Panarea (subaerial 2)

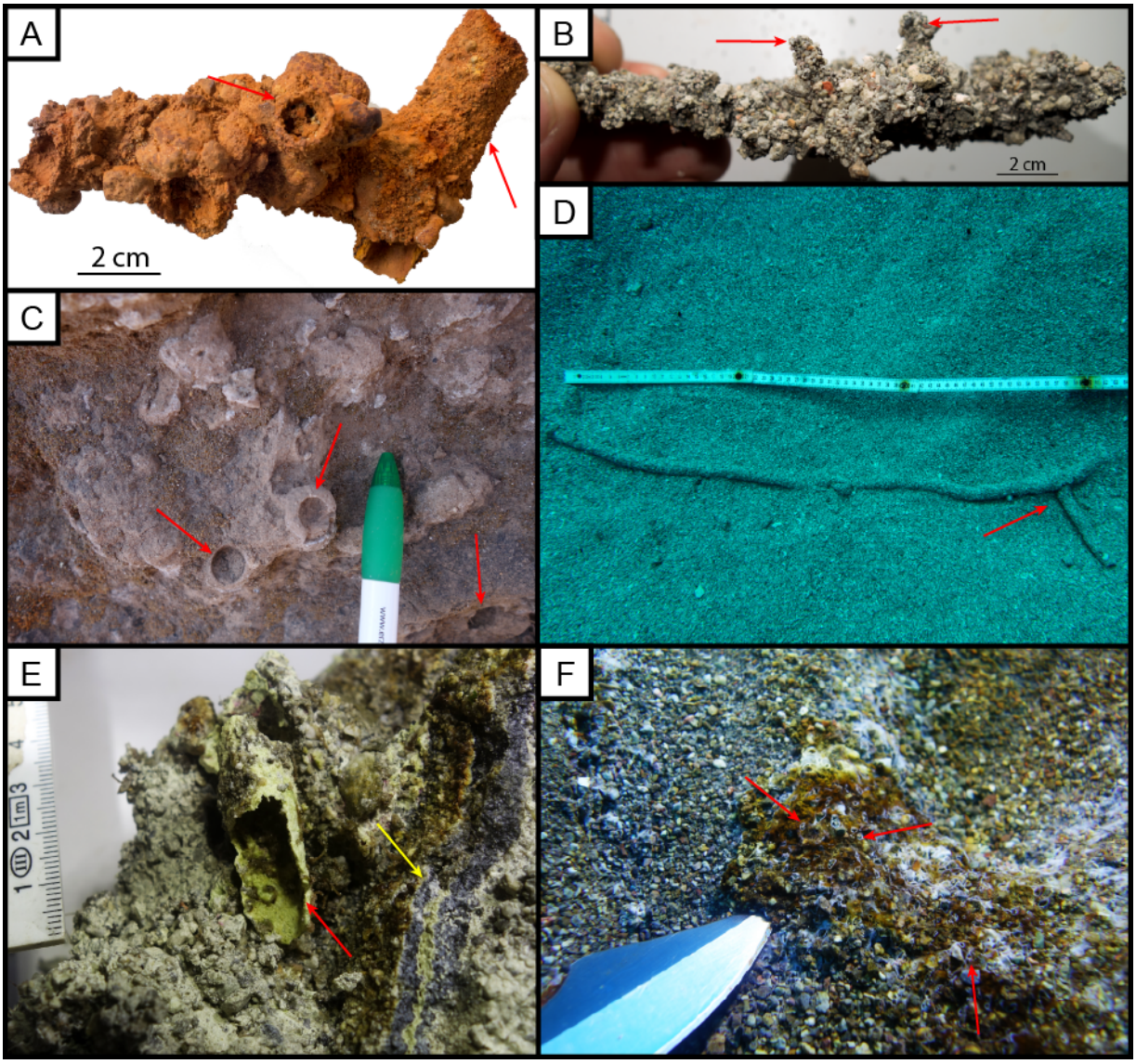

Figure 44: Discharge features occurring in Panarea. All pictures: knife/pen for scale. **A –** Type TFe from Basiluzzo, typically forming complex network structures. The red arrows mark single multidirectional tubes. **B –** Type Tore from La Calcara. The massive sulfide ore mineralization forms hard crusts in and on the sediments, exhibiting cm-scaled ore-tubes. The red arrows mark the emanation points. **C –** Tpal at subaerial location 2 near Panarea Airport. This is the first report on geologically preserved tubes in Panarea. The red arrows mark single individuals. The outcrop situation indicates the typical network structure. **D –** Large-scaled TSce in Area 26. This tube facies forms networks extending for several meters. **E –** Typical TSpu facies (red arrow). The yellow arrow marks adjacent Fore facies. **F –** Tubes of Fo facies in La Calcara. Whitish biomats hint on elevated temperatures and thus hydrothermal fluid discharge.

Table 17: Updated classification of facies types of discharge features in Panarea – **cones**. The classification given in Table 3 and STANULLA et al. (2017a) is the basis for the given structure.

Facies	Description	Changes	Type locality
Cones			
Cc (cone, consolidated)	Cone-shaped discharge feature; consolidated by precipitates of (native) sulfur in sediments; varying aspect ratios from 1:1 to 1:4 depending on the maturity of the cone; forming mass occurrences along fractures	n.a.	Area 26
Cu (cone, unconsolidated)	Cone-shaped discharge feature; unconsolidated in sediments; varying aspect ratios from 1:1 to 1:3 depending on the maturity of the cone; forming mass occurrences along fractures	n.a.	La Calcara, Area 26

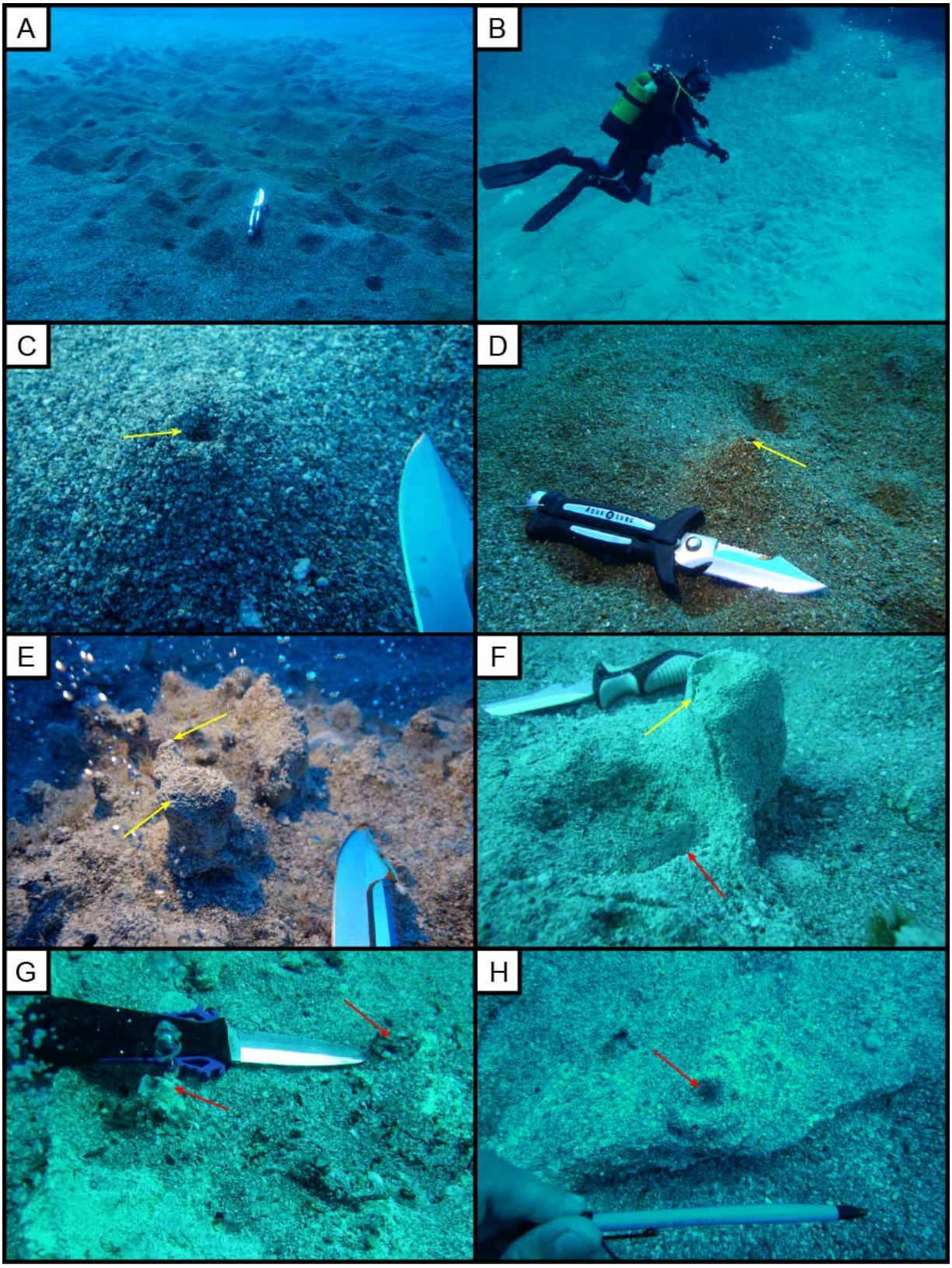

Figure 45: Cones in Panarea. All pictures: knife/pen for scale. **A –** Field of Cu in La Calcara. **B –** Field of Cu in Area 26. Features are similar to the ones in La Calcara. **C –** Cu in Area 26. The yellow arrow marks emanation point. **D –** Cu in La Calcara. The yellow arrow marks emanation point. **E –** Cc in Area26-*Brodor*. The yellow arrows mark emanation points of active discharge. **F –** Cc in Area 26-*Hot Bowl*. The yellow arrow marks ancient emanation point. The red arrow marks prominent ore clast in the lithology. **G –** Coarse specimen (red arrows) of Cc in Area 26-*Hot Bowl*. **H –** Cc in Area 26-*Hot Bowl*. The red arrow marks ancient emanation point.

Table 18: Updated classification of facies types of discharge features in Panarea – **bowls**. The classification given in Table 3 and STANULLA et al. (2017a) is the basis for the given structure.

Facies	Description	Changes	Type locality
Bowls			
BS (bowl, sulfurous)	Cm to dm large cavities along fractures potentially connecting single individuals. Often active discharge at the sidewalls and resulting second generations of discharge features (e.g. TSpure). Host rock is sulfurous cemented	Undescribed	Area 26
Bo (bowl, other)	Similar cavities as BS but with other cement facies	Undescribed	n.a.

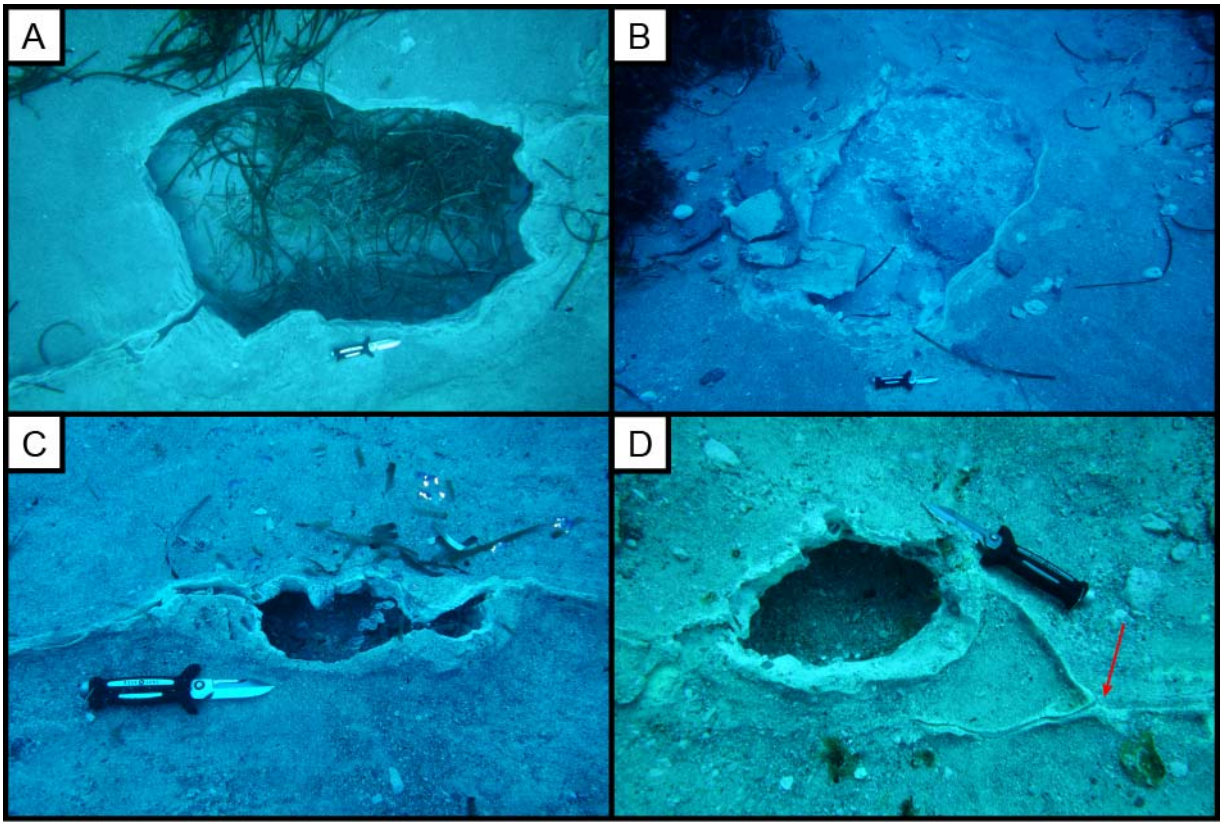

Figure 46: Bowls in Panarea. All pictures: knife for scale. **A –** *Hot Bowl* in Area 26 is one of the most prominent bowl structures in the system. Connected fractures cross the bowl. **B –** Bowl B at *3-Bowls*. This major bowl is directly connected to the two other bowls in the direct vicinity by fractures. The complex of *3-Bowls* is linked to the *Lineament Structure* nearby. **C –** Small bowl which is part of the *Lineament Structure*. Active discharge enhances the growth of the structures. **D –** Small bowl in Area 26. Red arrow marks adjacent fractures.

Table 19: Updated classification of facies types of discharge features in Panarea – **lineament structures**. The classification given in Table 3 and STANULLA et al. (2017a) is the basis for the given structure.

Facies	Description	Changes	Type locality
Lineament structures			
LSs (lineament structure, sulfurous)	Elongated structures linking up bowls, cones and fractures of different scales. Structures are often several meters in extend. Mostly active discharge at the sidewalls of individual bowls and resulting second generations of discharge features (e.g. TSpure). Host rock is sulfurous cemented.	Undescribed	Area 26
Lo (lineament structure, other)	Similar to LSs but in other host rock facies.	Undescribed	Yet undefined; potentially La Calcara
Lpal (lineament structure, paleo)	Preserved individuals in the rock record; further classification at the moment only on single structures possible (dependent on the style of preservation)	Undescribed	Panarea (subaerial 1)

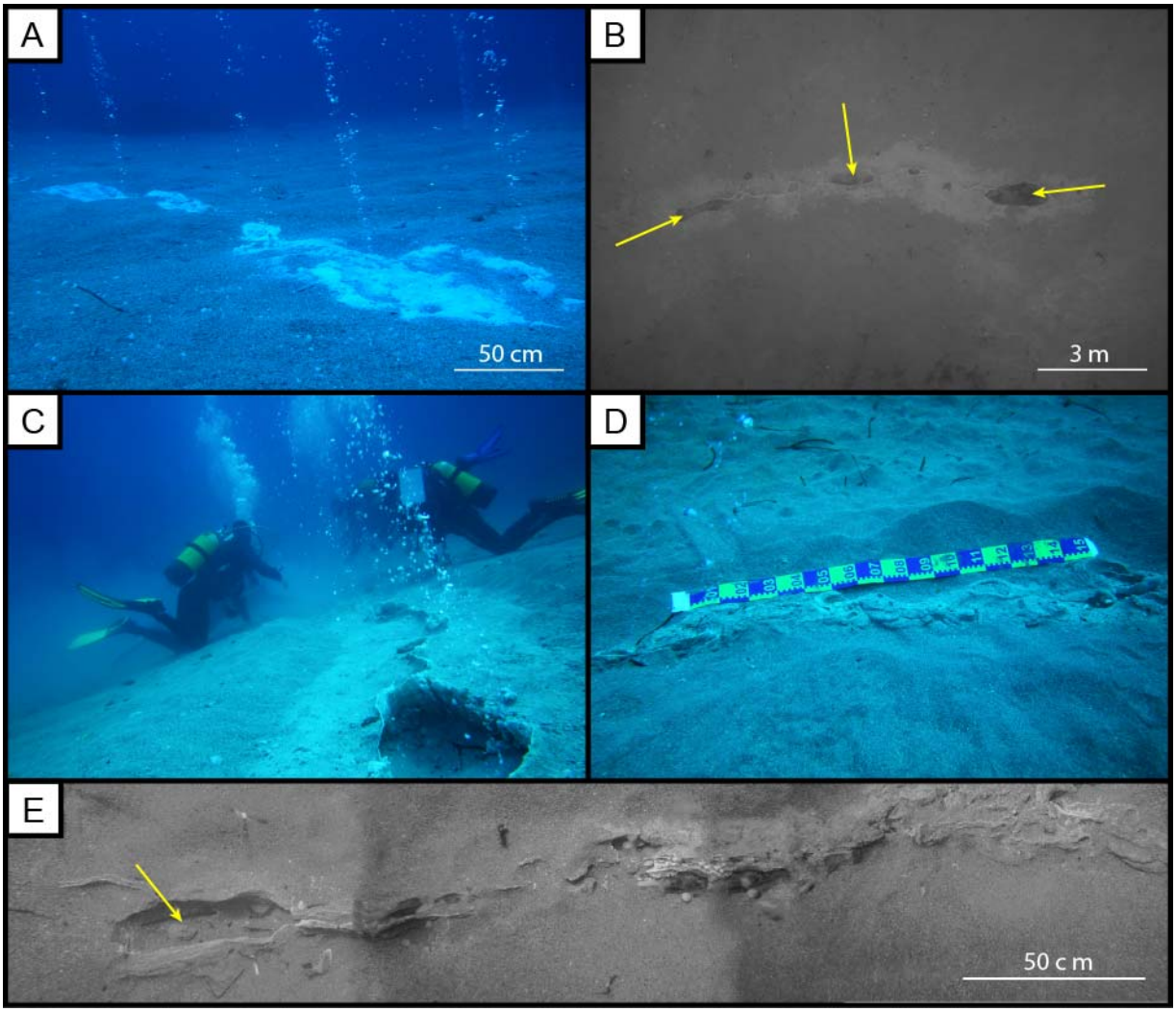

Figure 47: Lineament structures. **A –** Lineament structures are often highlighted by intense growth of biomats. This bioindicator is the most effective marker when starting to map these features. **B –** Excavated *Lineament Structure* in Area 26. This prominent feature is the type locality for this facies type. The yellow arrows indicate major bowls along the lineament. **C –** Scientific Divers measuring at *Lineament Structure*. The feature can be tracked for over 10 meters. **D –** Part of the lineament structure adjacent to *Hot Bowl*. The variety of small discharge features indicates the complex genesis of this facies type. **E –** Lineament structure adjacent to *Hot Bowl.* This feature is with about 3 m extend a lot smaller than the structure described in B. It comprises a lot of Cc-type cones and FS-type fractures. Bowls are not yet a dominant feature, what hints on a relatively young discharge feature.

6.1.1. Complex genesis and development of discharge features and their occurrence throughout the system

6.1.1.1. Cones, bowls, and lineament structures

The mapping of a variety of different locations in Panarea showed that genetic relations between different types of discharge features can be assumed and that the same processes can end up with different structures. A good example for this is the evolution of bowl- and lineament-structures. Their development is dominated by a complex interaction of constructive and destructive processes which affect the present state of the feature. The genetic evolution can be interpreted according to the following model (Figures 48 - 53 and pages 119 - 127):

Stage 1: initial fracture – starting point
An initial fracture in the bedrock acts as pathway for hydrothermal fluids. During their ascent from the hydrothermal reservoir, the fluids undergo phase separation as explained by STANULLA et al. (2017c; cf. Figures 3 and 4).

Dominant process: neotectonics causing fractures in the underground

Type locality: Point 21

Stage 2: widening and mineral precipitation (Fo, FS)
The initial fracture is widened by a constant fluid flow and consequent fluid erosion processes such as rock alteration and abrasion.

Dominant process: fluid erosion

Type locality: Point 21

Stage 3: interaction of fluid erosion and mineral precipitation
Starting of mineral precipitation from hydrothermal fluids by oversaturation or quenching. Ongoing interaction between constructive and destructive processes leads to cyclic growth of mineral precipitates and closure of the fracture.

Dominant process: fluid erosion, mineral precipitation

Type locality: Point 21

Stages 4a - 7a: influence of sediment cover - development of cone facies (Cu/Cc)
Development of a sustaining sediment cover. Formation of escape structures (cf. FREY et al. 2009) of facies type Cu and Cc as described by STANULLA et al. (2017a). Persistent interaction of constructive and destructive processes inside the ascent channel of the cone. Cementation (mostly sulfurous cements) solidifies the cone.

Dominant process: cementation, grain transport

Type locality: Area 26, La Calcara

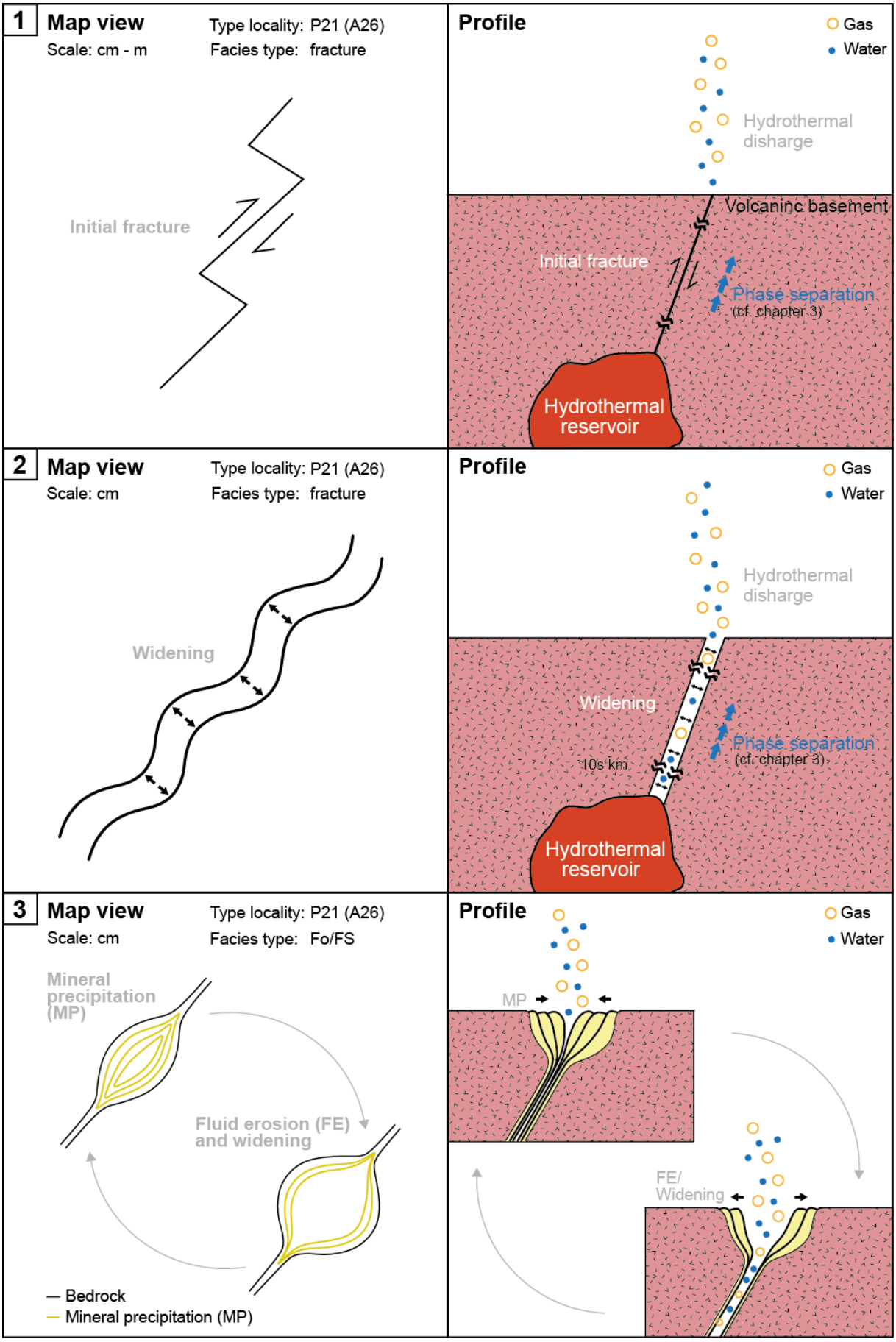

Figure 48: Genetic model of cones, bowls, and lineaments – Stages 1 to 3.

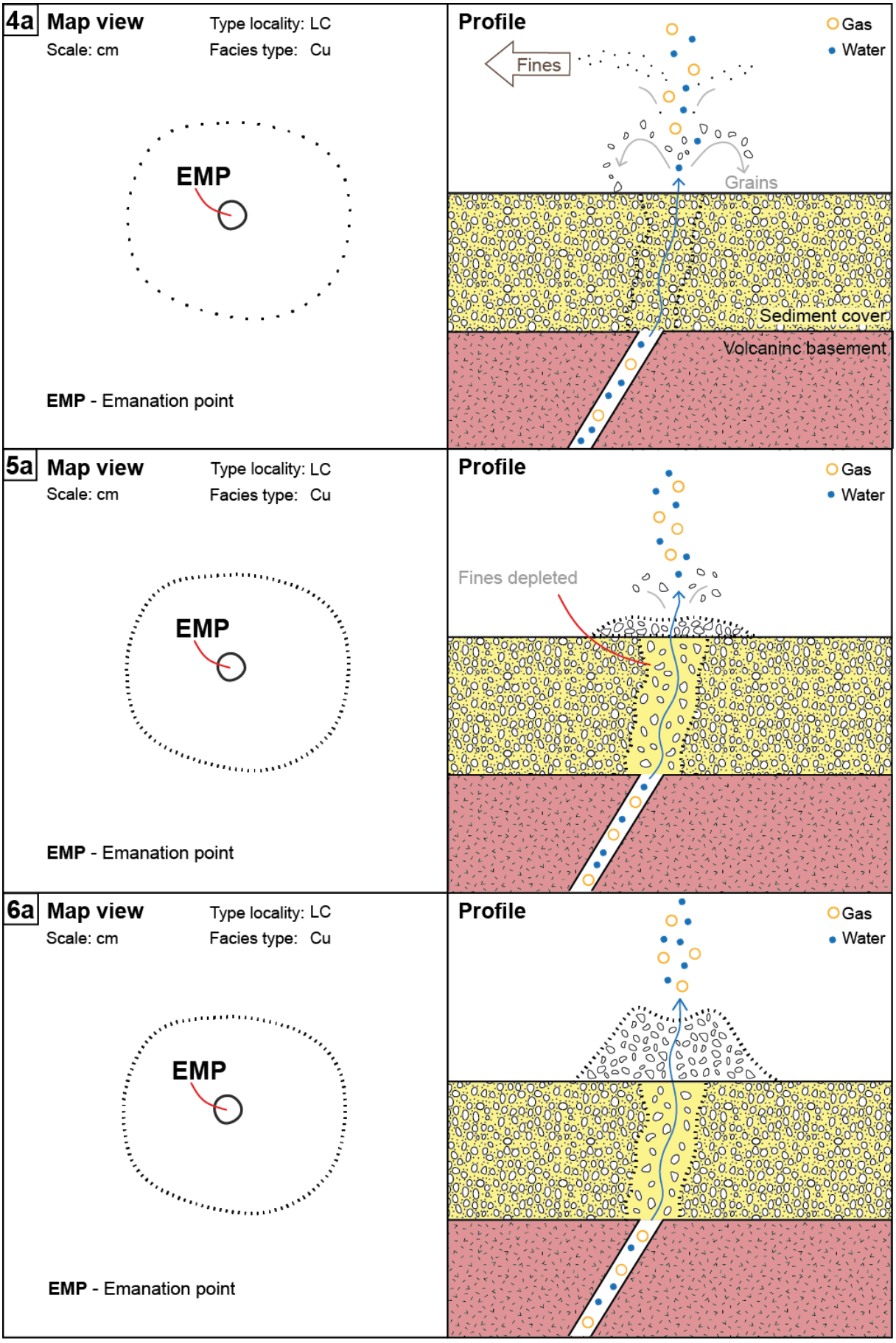

Figure 49: Genetic model of cones, bowls, and lineaments – Stages 4a to 6a.

Stage 4: unhindered evolution and growth of mineral precipitates (Fo, FS)
Evolution without sediment cover. Ongoing mineral precipitation leads to accretion of fractures. Formation of facies types FS, Fo and Fore. Mineral precipitation is always a cyclic process leading to internal lamination of crusts and fracture fills.

Dominant process: mineral precipitation

Type locality: Point 21

Stage 5: ongoing evolution and formation of small-scaled cavities
Persistent interaction of fluid erosion and mineral precipitation with slight domination of fluid erosion leads to the formation of small cavities with crusts of mineral precipitates at the walls. Potentially formation of new generations of discharge features within these crusts. Periodic evolution occurs.

Dominant process: fluid erosion, mineral precipitation/cementation

Type locality: Area 26

Stage 6: structure collapse after ongoing fluid erosion
Collapse of the walls of cavities due to domination of fluid erosion processes leads to a consequent (over-)steepening of the sidewalls (in combination of rock destabilization by leaching and chemical weathering).

Dominant process: fluid erosion

Type locality: Area 26

Stage 7: post-collapse evolution and initial bowl formation
Abstraction of collapsed cavities and widening of these structures forced by erosional processes.

Dominant process: erosion

Type locality: Area 26

Stage 8: post-collapse evolution: abstraction and cementation of breakdown
Collapsed material is cemented by mineral precipitation forming new, smooth surfaces in primitive bowl structures. Interaction with ongoing fluid erosion is likely.

Dominant process: mineral precipitation/cementation

Type locality: Area 26

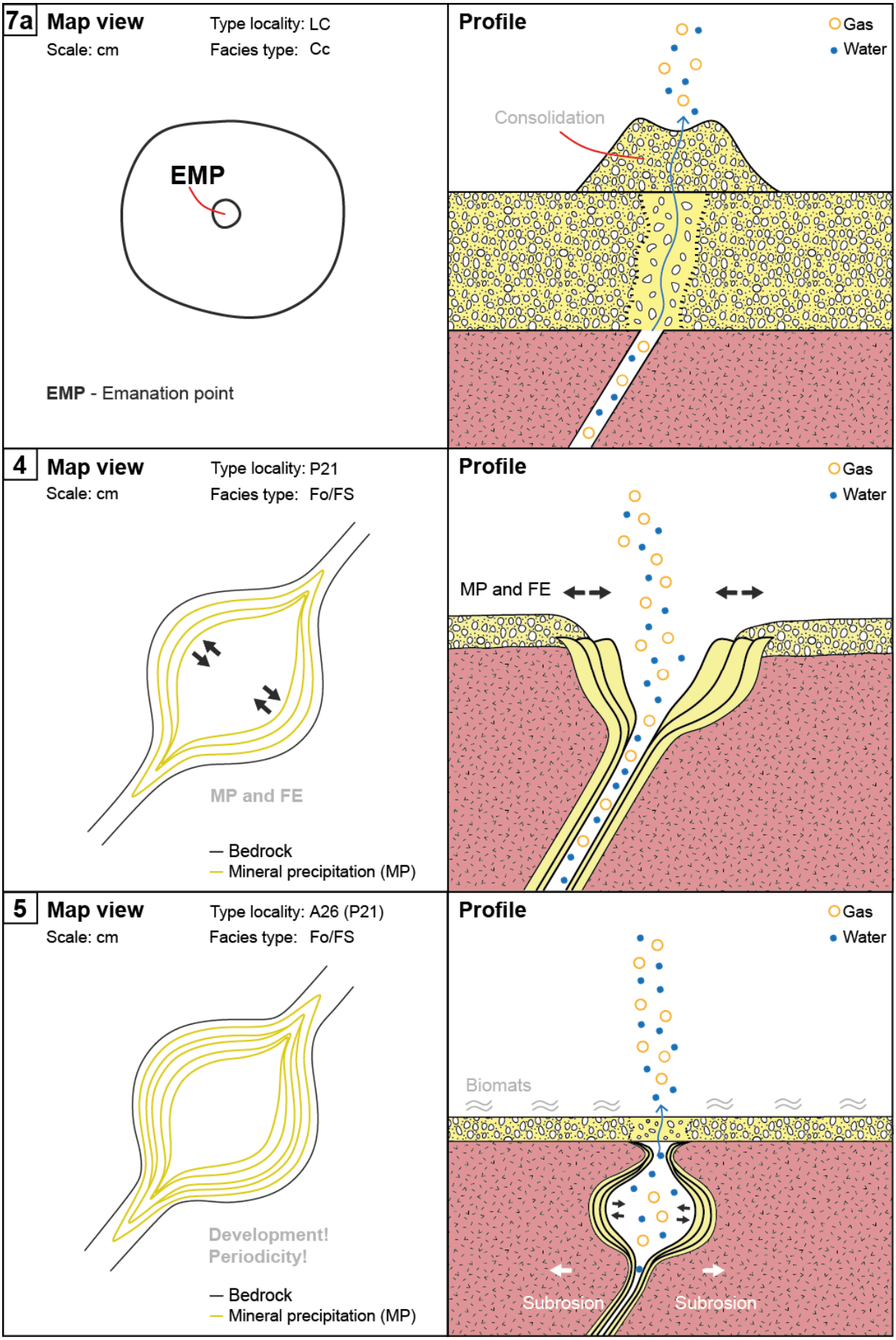

Figure 50: Genetic model of cones, bowls, and lineaments – Stages 7a to 5.

Stage 9: subrosion of bedrock and formation of bowl facies
Fluid erosion processes dominate and subrode the lithology beneath the seafloor. Formation of larger bowl structures analogue to stage 5. Solidification by mineral precipitation. Permanent discharge of hot waters leads to elevated temperatures within the bowls and thus isolated microenvironments (e.g. mass occurrence of bio mats).

Dominant process: fluid erosion, mineral precipitation

Type locality: Area 26

Stage 10: growth of discharge features and evolution of lineament facies
Periodic interaction between fluid erosion, subrosion, collapse and mineral precipitation leads to growth of bowl structures. Connection of single individuals by fractures or merging of defined bowls. Formation of lineament-structures (several meters) is the consequence. Discharge of hot waters leads to elevated temperatures within the bowls and thus isolated microenvironments (mass occurrence of bio mats).

Dominant process: fluid erosion, mineral precipitation

Type locality: Area 26

Stage 11: Hot Lake stadium – growth and evolution of macrostructures
Structures grow further to scales of several tens of meters. Permanent discharge of hot waters forms submarine hot water ponds (e.g. Hot Lake). Complex suite of processes as shown in stages 1 – 10.

Dominant process: subrosion, mineral precipitation

Type locality: Hot Lake

Stage 12: Hot Lake stadium – abstraction
Connection of single individuals by faults or merging of defined lakes. Macro structures comparable to lineament structures in Area 26 develop.

Dominant process: subrosion, mineral precipitation

Type locality: Hot Lake

Stage 13: final stadium
As all described processes and evolutionary stages are mostly periodic, a well-defined final stage would be hard to identify. Observations of cones and bowls imply that a permanent abstraction is the most plausible process. The ebbing of hydrothermal discharge would enforce this, as the cycle of fluid erosion and mineral precipitation would be interrupted. An abstraction by standard erosional processes is likely.

Dominant process: erosion

Type locality: n.a.

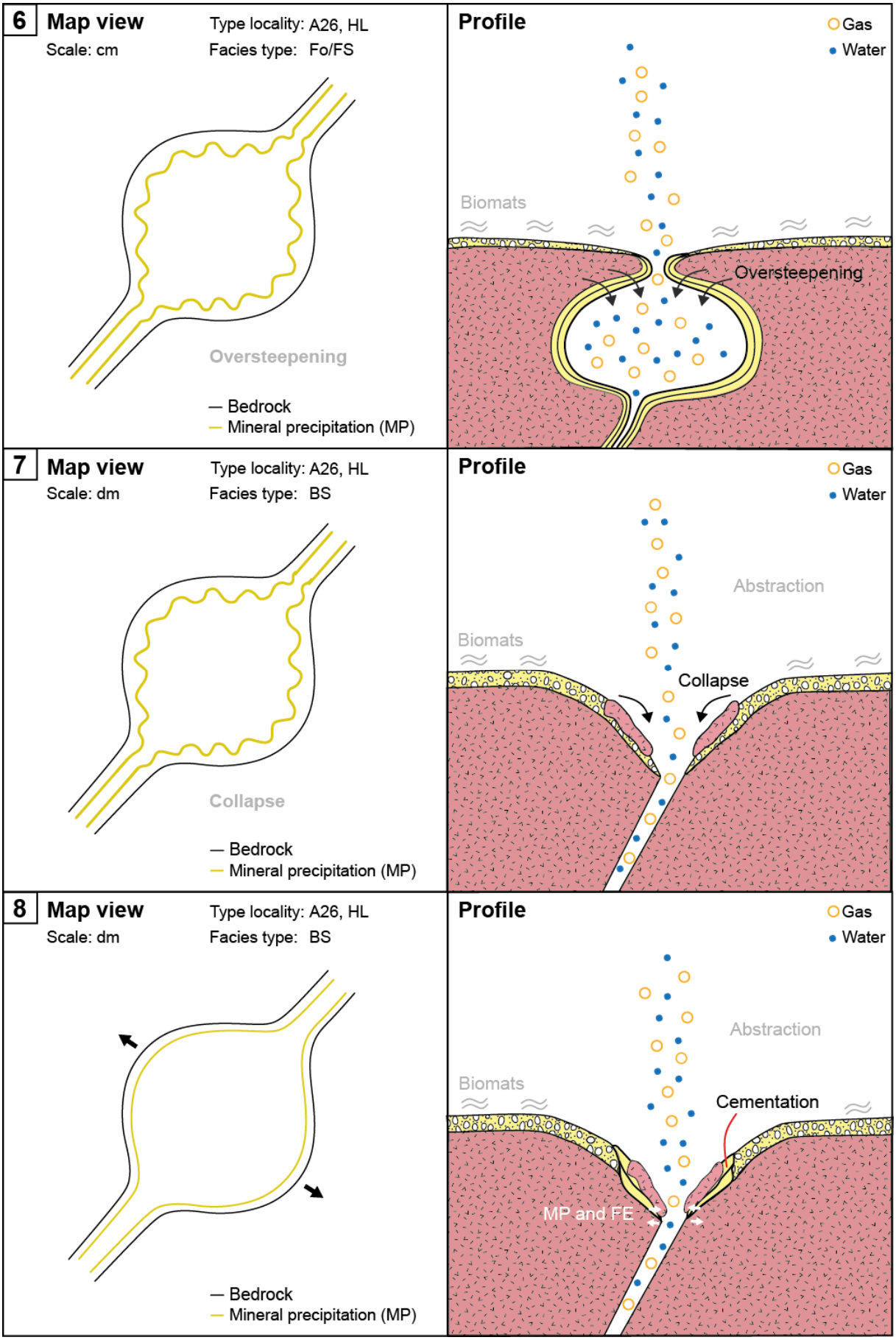

Figure 51: Genetic model of cones, bowls, and lineaments – Stages 6 to 8.

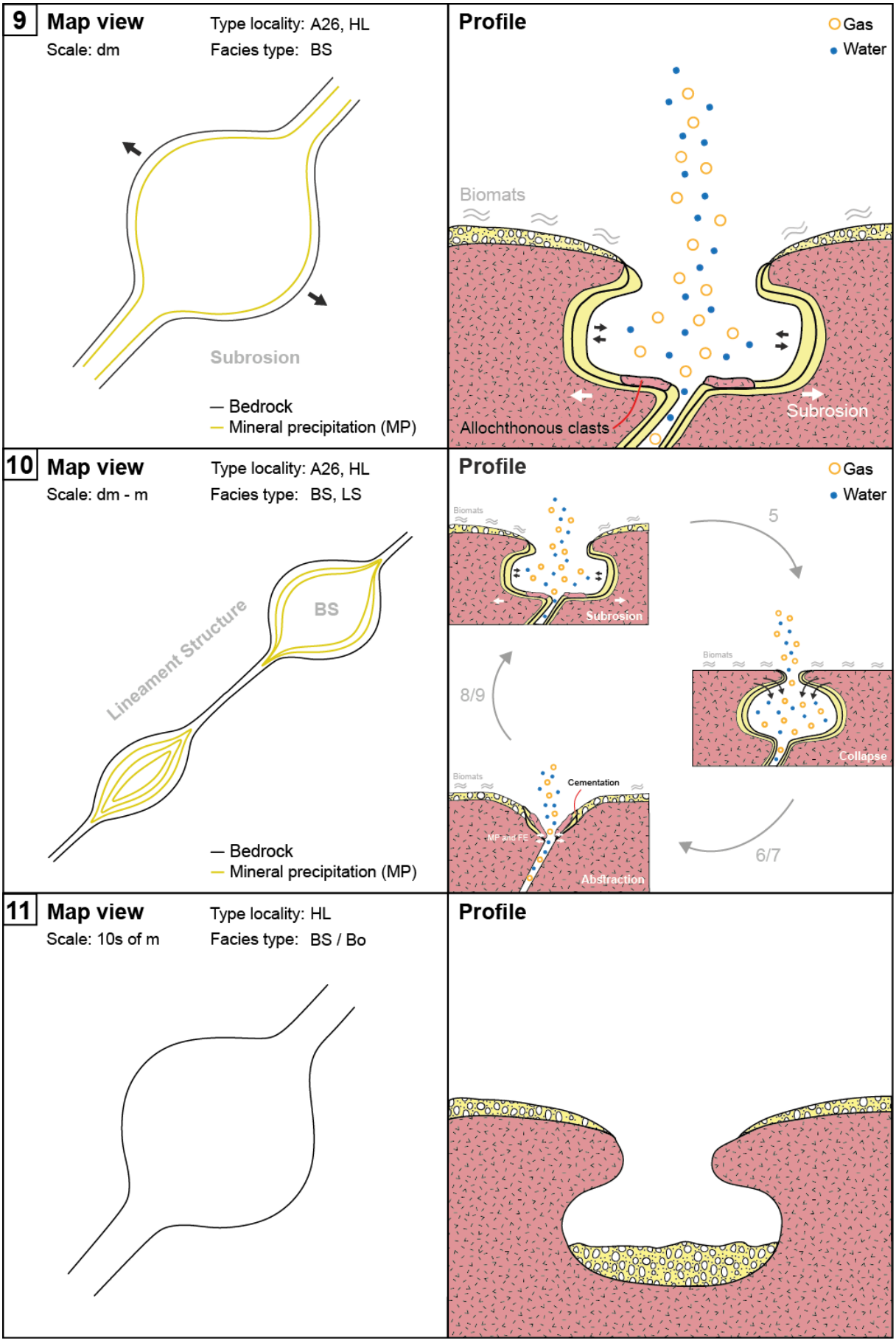

Figure 52: Genetic model of cones, bowls, and lineaments – Stages 9 to 11.

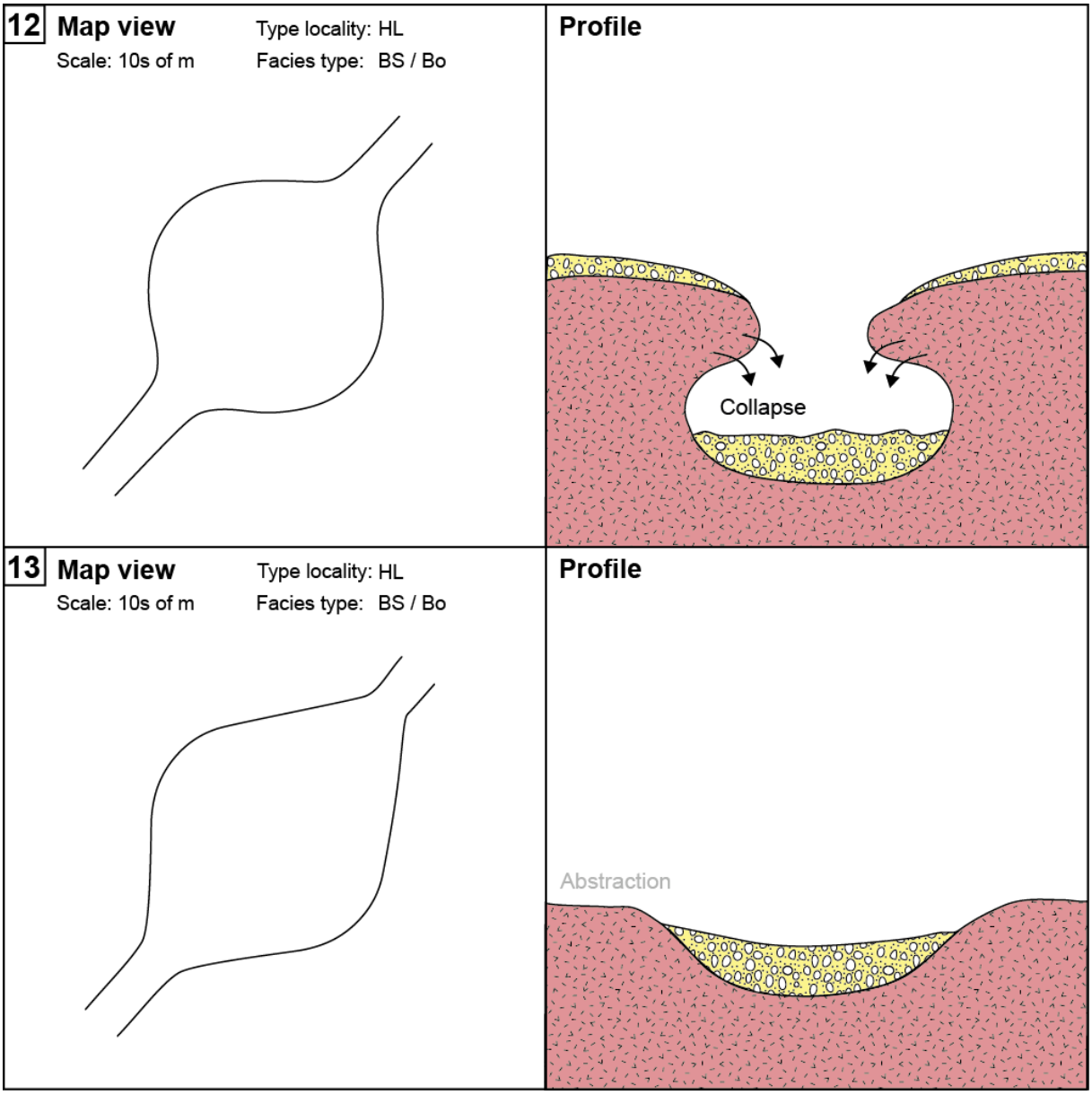

Figure 53: Genetic model of cones, bowls, and lineaments – Stages 12 to 13.

6.1.1.2. Tubes

Another typical feature in Panarea is the tube-shaped discharge feature which occurs in different, mostly sand-dominated locations. Although of comparable outer shape, there are enormous differences between the facies.

A basic model of genesis is suggested by STANULLA et al. (2017a) dealing with tubes from Basiluzzo. Meanwhile samples from Area 26, La Calcara and Hot Lake witness the presence of other facies types. They vary in size, shape, cement, and environment. However, a comparable genesis is likely. The following scheme assesses their formation with no dominant biogenic influence or trigger (Figures 54 - 57 and pages 128 - 134):

Stage 1: initial fracture – starting point
An initial fracture in the bedrock acts as pathway for hydrothermal fluids. During their ascent from the hydrothermal reservoir, the fluids undergo processes of phase separation as discussed for the underwater investigation site La Calcara by STANULLA et al. (2017c).

Dominant process: n.a.

Type locality: Point 21, Area 26

Stage 2: first mineral precipitation
Hydrothermal discharge causes the formation of ring-shaped bodies of mineral precipitates within the sediment above the initial fracture.

Dominant process: mineral precipitation

Type locality: Basiluzzo, La Calcara

Stage 3: depletion of fine-grained fabrics
The fluid flow transports fine-grained fabrics into the oceanwater. The tube-shaped precipitate body becomes depleted of fines which are carried away by currents and other water movements (waves). Coarser grains remain within the precipitate body.

Dominant process: fluid flow

Type locality: Basiluzzo, La Calcara

Stage 4: primitive tube
Ongoing hydrothermal discharge with supposedly increased flow rates transports also coarser grains out of the precipitate body. A primitive tube is formed within the sediment. The wall consists of one single layer of mineral precipitate (e.g. iron oxides).

Dominant process: fluid flow

Type locality: Basiluzzo, La Calcara

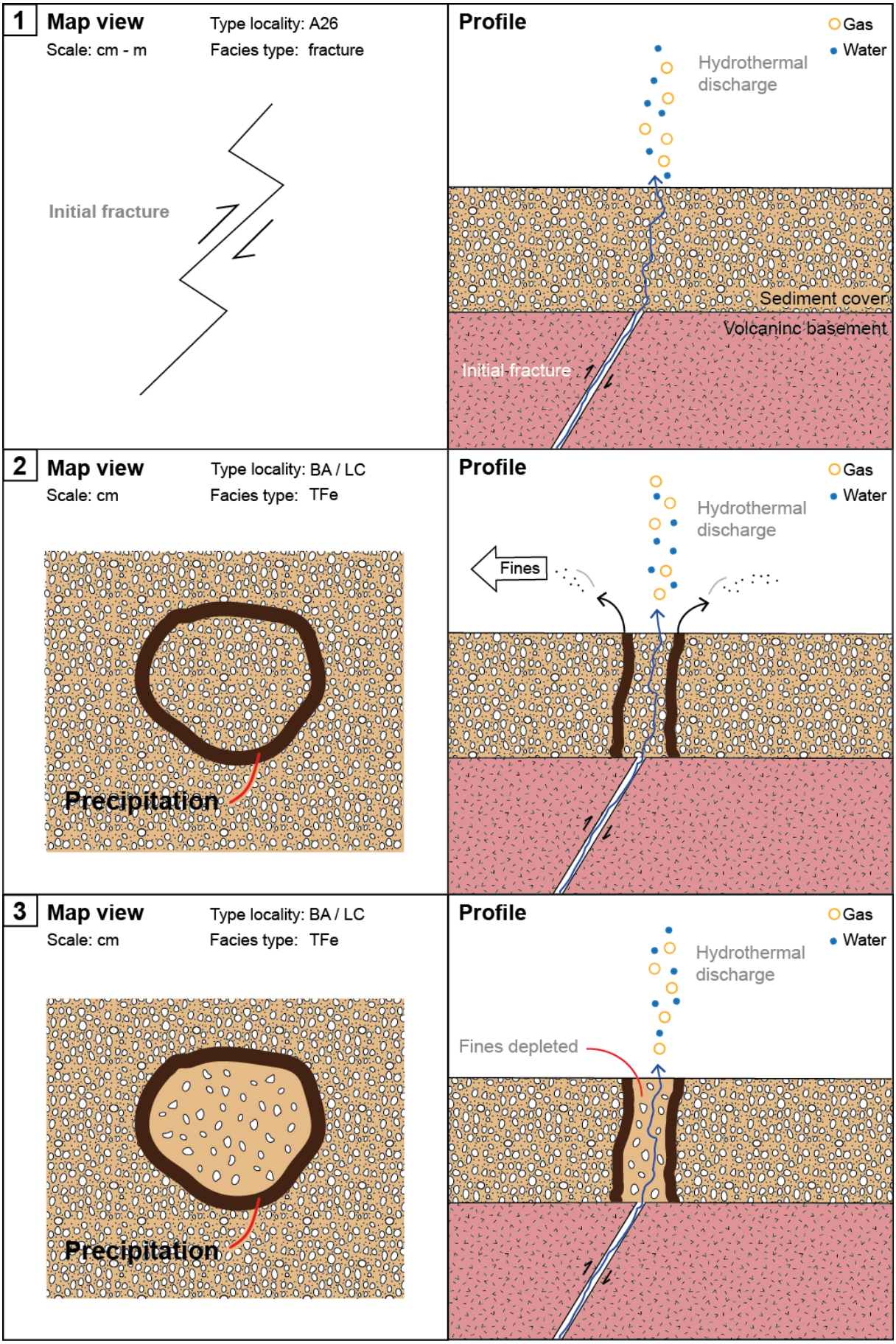

Figure 54: Genetic model of tubes – Stages 1 to 3.

Stage 5: forming of event layers
In case of sudden changes in the physico-chemical properties of either the hydrothermal fluids or the surrounding ocean waters (e.g. due to volcanic activity), single event layers may form. A common observation is the presence of manganese layers in the tubes (cf. STANULLA et al. 2017a).

Dominant process: mineral precipitation

Type locality: Basiluzzo, La Calcara

Stage 6: multi-layer tubes
Ongoing mineral precipitation leads to the formation of further layers at the inner parts of the tube. The supposably cyclic process is forming multi-layer tubes over time. Typically, four or five layers were documented (cf. STANULLA et al. 2017a).

At the same time, fluid erosion resulting from the hydrothermal discharge counteracts the process of mineral formation.

Dominant process: mineral precipitation, fluid erosion

Type locality: Basiluzzo, La Calcara

Stage 7: clogging
The amount of precipitated minerals exceeds the effects of fluid erosion. The resulting positive mass balance leads to a clogging of the tube and consequently to a rise of pressure within the tube.

Dominant process: mineral precipitation

Type locality: Basiluzzo, La Calcara

Stage 8a / 8b$^{1-2}$: the formation of reservoirs and junctions
The rising pressure can form two different patterns:

(1) the pressure releases sideways due to structural deficits potentially forming a new tube according to stages 1-6 (stage 8a). The resulting complex of tubes is connected at the so-called “junction”.

or

(2) the pressure cannot leak from the clogged tube and thus widens the structure. The resulting spherical body is referred to as “reservoir” (8b^{1}). If the pressure exceeds the plastic potential of the reservoir, the latter may crack at points of structural deficits. A new tube may form according to stage 8a. This is the typical situation documented in complex networks up to now (8b²).

Dominant process: mineral precipitation

Type locality: Basiluzzo, La Calcara

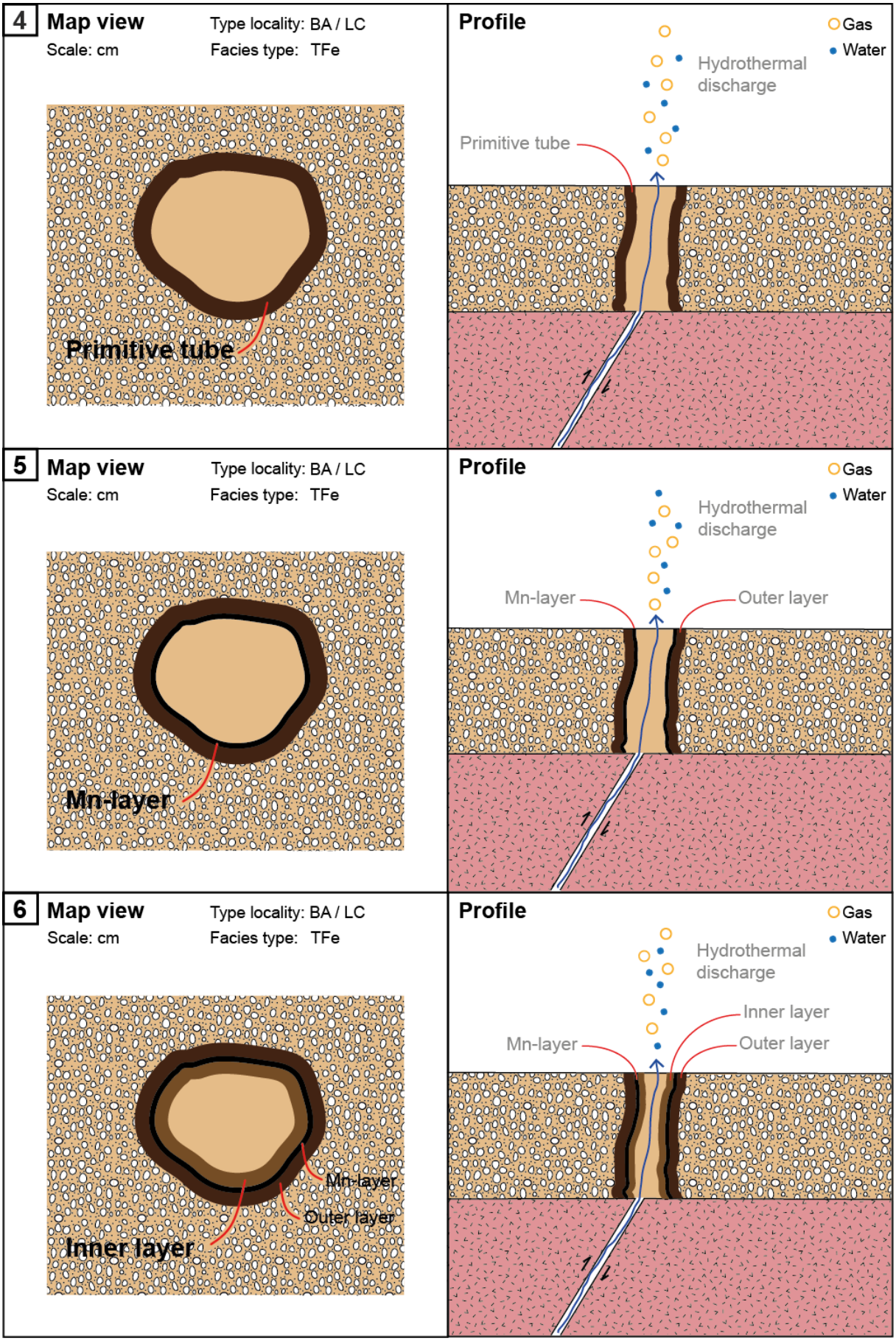

Figure 55: Genetic model of tubes – Stages 4 to 6.

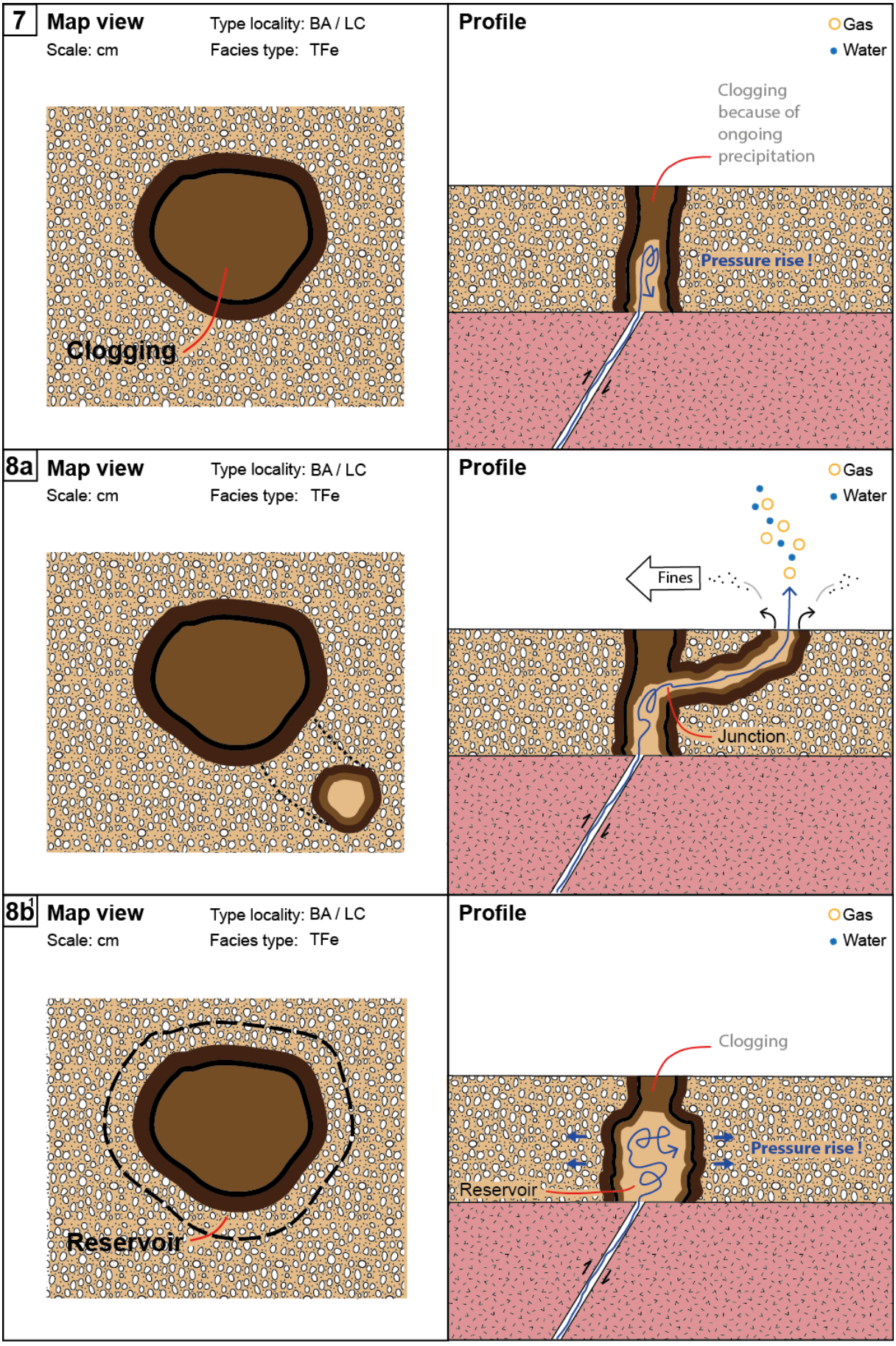

Figure 56: Genetic model of tubes – Stages 7 to 8b[1].

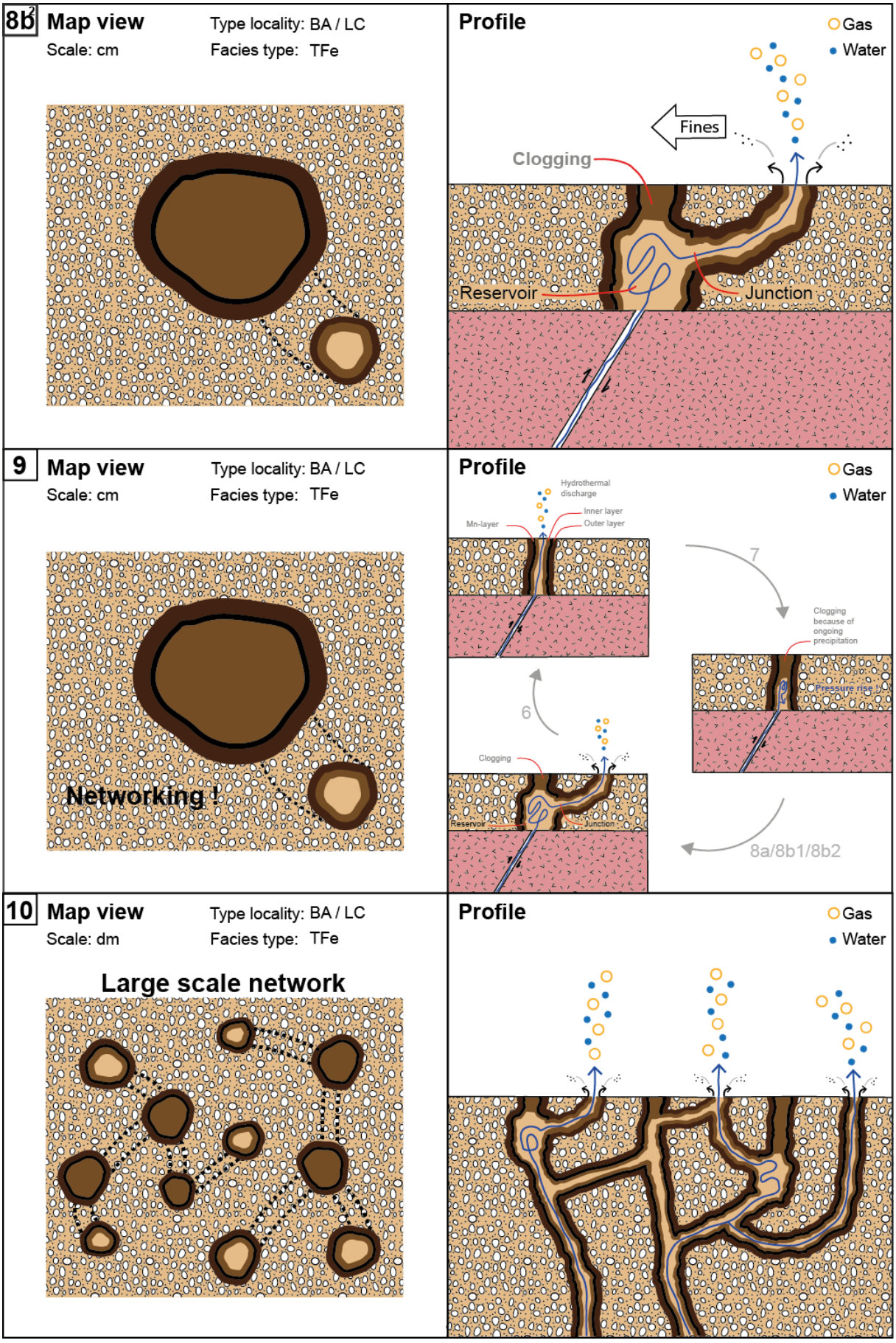

Figure 57: Genetic model of tubes – Stages 8b^2 to 10.

Stage 9: forming of networks

The permanent iteration of stages 6, 7, 8a, $8b^1$ and $8b^2$ leads to the formation of tube network structures.

Dominant process: mineral precipitation

Type locality: Basiluzzo, La Calcara

Stage 10: final stadium: large scale networks

The processes of tube-formation result in most cases in large-scale networks of several meters in extend. Within the networks, complex variations of these processes may take place, depending on the micro-conditions within the network and possible shifting in the source of hydrothermal discharge (e.g. closure of fractures; neotectonics).

Dominant process: mineral precipitation, fluid erosion

Type locality: Basiluzzo, La Calcara

Tube formation is possible by pure geogenesis. However, the presence of certain plants such as *Posidonia sp.* may trigger their formation what is witnessed by common occurrences of plant detritus within the cements.

The following scheme supplements the previously given processes to describe formation with a dominant biogenic influence or trigger (Figures 58 - 59 and pages 135 - 137):

Stage 1: colony of plants above a discharging fracture – starting point
A colony of plants with tubular roots, such as *Posidonia sp.*, grows in the sediments above a discharging fracture in the basement. Roots of dead specimen may act as pathways for hydrothermal fluid discharge.

Dominant process: hydrothermal discharge

Type locality: Bottaro West, Area 26

Stage 2: first precipitation on living plants
Hydrothermal discharge causes mineral precipitation along the roots which act as biological pathways through the sediment. Plants are predominantly still alive, although rising pH values (due to hydrothermal discharge) make it hard to survive.

Dominant process: hydrothermal discharge, mineral precipitation

Type locality: Area 26, Point 21, Basiluzzo

Stage 3: exitus of plants
Ongoing hydrothermal discharge and resulting low pH values kill the plants. Only the solid parts such as roots, and tissues remain. Tube-shaped roots form excellent frames for the development of tubular hydrothermal discharge features. Mostly this process was documented with types TFe and TS.

Dominant process: mineral precipitation

Type locality: Area 26, Point 21, Basiluzzo

Stage 4: decay of plant remains and articulation of multi-layer-tubes
Over time, remaining parts of dead plants decay or become eroded by fluid flow. The only hint on preexisting plant colonies may be root remains within the sediment. Ongoing tube-formation forms articulated multi-layer-tubes as explained before (stages 1-10).

Dominant process: decay, mineral precipitation

Type locality: Area 26, Point 21, Basiluzzo

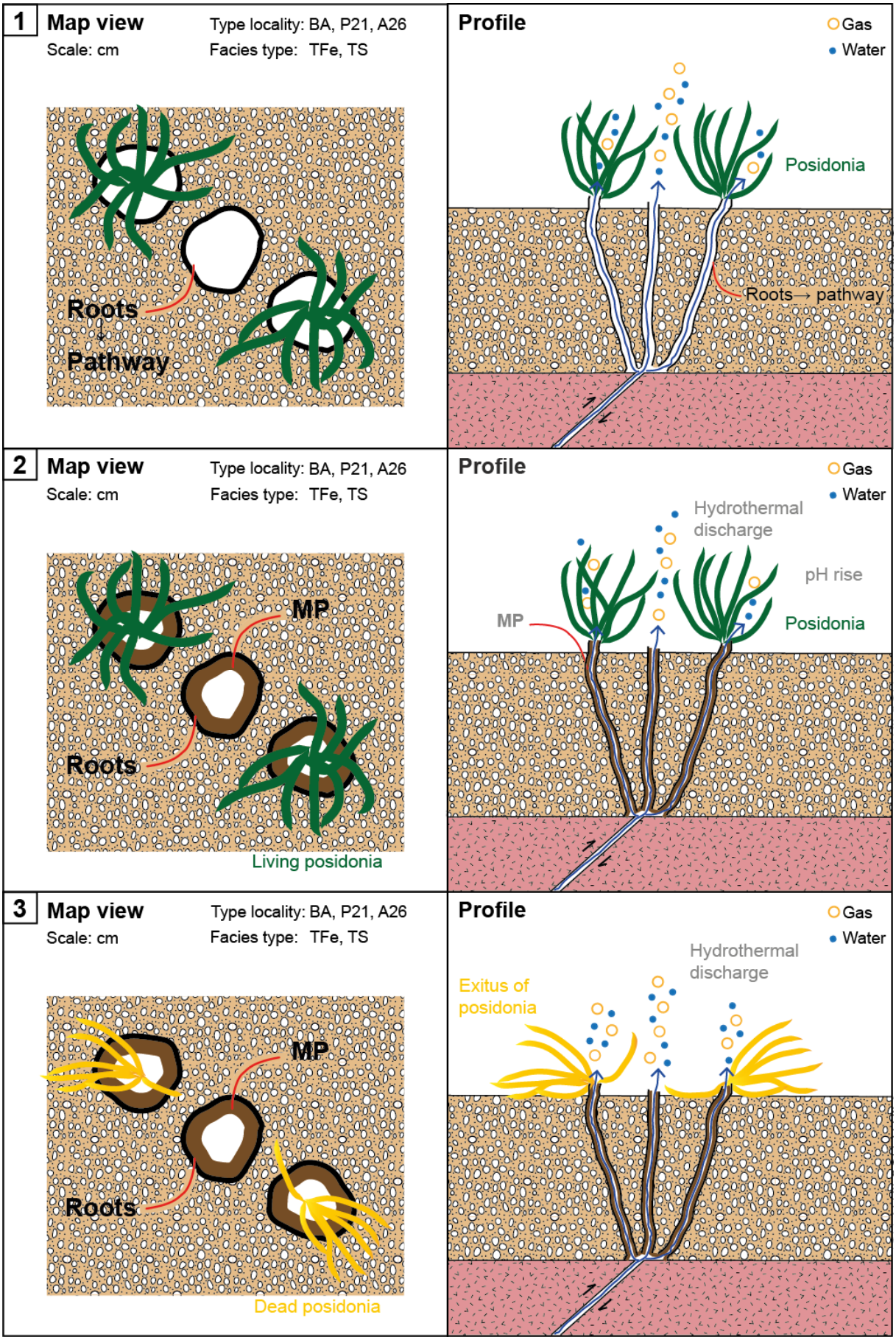

Figure 58: Genetic model on the bio-influence of *Posidonia sp.* on tube formation – Stages 1 to 3.

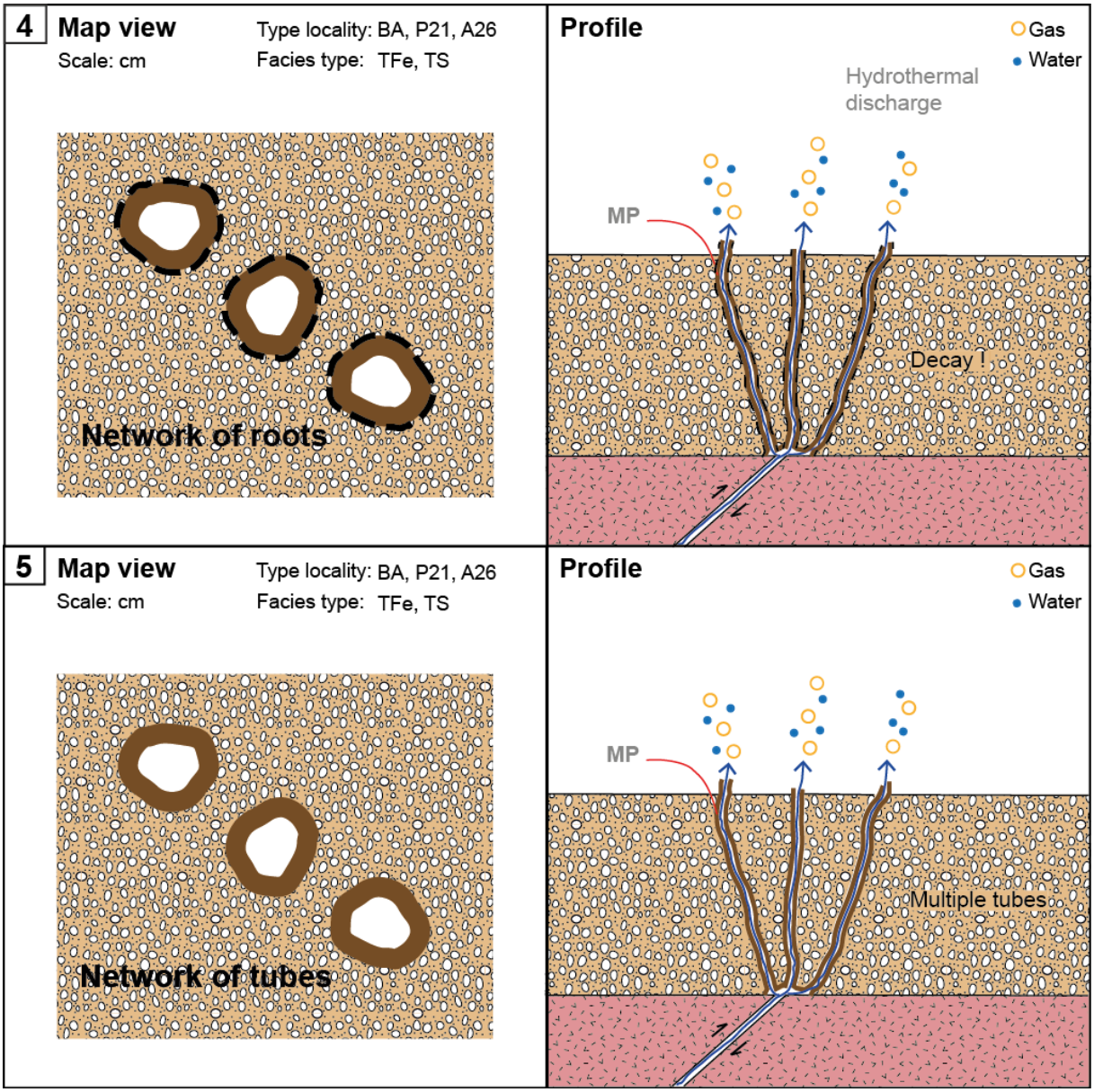

Figure 59: Genetic model on the bio-influence of *Posidonia sp.* on tube formation – Stages 4 to 5.

Stage 5: tube formation and networking

After the complete decay of most of the plant remains, a simple network of typical tubes has developed. Mixed forms of stage 4a and 5a are common. Tube formation may go on from here as described in stages 5 to 10, depending on the named frame conditions.

Dominant process: mineral precipitation

Type locality: Area 26, Point 21, Basiluzzo

All described stages of tube formation may form together with the stages given on pages 128 - 134. They integrate from stage 1 to stage 4. Overlap and parallel development are likely.

6.2. Preservation potential and paleo-record

Paleo-evidences for hydrothermal systems are reported from different locations worldwide. Features such as stromatolites (microbial mats) are known to occur lithified (a.o. NOFFKE 2000, 2007, 2009 and 2010; NOFFKE et al. 2001a, 2001b, 2003b; REITNER & THIEL 2011 and AN ADÓN et al. 2013). Geophysical approaches on the characterization of paleo-hydrothermal system are described by GRAB et al. (2015) on the example of an icelandic system. DI BELLA et al. (2019) and FERRETTI et al. (2019) report from recently forming iron-bearing precipitates from the hydrothermal system of Panarea, which potentially are showing a high preservation potential. Their genetic process seems to be similar to the formation of hydrothermal discharge features (type TFe) described by STANULLA et al. (2017a).
The here presented hydrothermal discharge features from Panarea show prominent shapes and characteristic appearances. They are powerful tools for the interpretation of geological strata providing paleo-hydrothermal systems. The comparison of yet undefined sedimentary structures with the here investigated recent hydrothermal features may potentially solve open questions and facilitate the interpretation of such geologic sequences. All genetic schemes given in this thesis do not consider processes of preservation until this chapter. Fossilization may start at any point of their evolution.

Most hydrothermal features generally show a high preservation potential. Especially parts, that are solidified by mineral precipitates undergo the same processes of lithification and fossilization as typical fossils. The type of preservation depends on the depositional regime. Possible options are imprints, stone cores or fillings.

Additionally, preservable bioindicators such as microbial mats (stromatolites) or the paleo-occurrence of certain species like Spiculosiphon oceana (foraminifera; cf. ESPOSITO et al., 2019) may be helpful features while approaching paleo-hydrothermal systems.

The preservation of hydrothermal discharge features in Panarea is proven by the appearance of the paleo-lineament facies in subaerial 1 and the paleo-tube facies in subaerial 2 (Figure 60).

Findings from the quaternary Laacher See thephra, structures in the permian Leukersdorf formation near Chemnitz and yet unidentified tubular structures in the Zechstein limestones of Thuringia (Kamsdorf) are examples from other environments and strengthen these statements (Figure 61; cf. STANULLA 2012).

However, it must be distinguished between subaquatic and subaerial/semiaquatic formations. The given examples from Panarea imply a subaquatic formation followed by tectonic activity (cf. sea level fluctuations/uplift, chapter 3.1. – Regional Geology). Subaerial/semiaquatic formations from Volcano Island and Iceland respectively seem to follow at least comparable, if not the same, genetic processes (cf. STANULLA 2012).

Further investigations will thus attempt the development of an interdisciplinary tool describing recently forming hydrothermal features concerning the prevailing environmental conditions plus further specific observations. Approaching paleo-systems considering the knowledge about recently active systems will give new insights on their paleo-evolution and allow insights on their genetic history. A catalogue of both, paleo and recent features, will give a compilation of defined structures and characteristic patterns of recently observed and investigated ecosystems. That information can comparatively be used for environmental reconstruction of lithified systems having had similar environmental conditions in the earth's history.

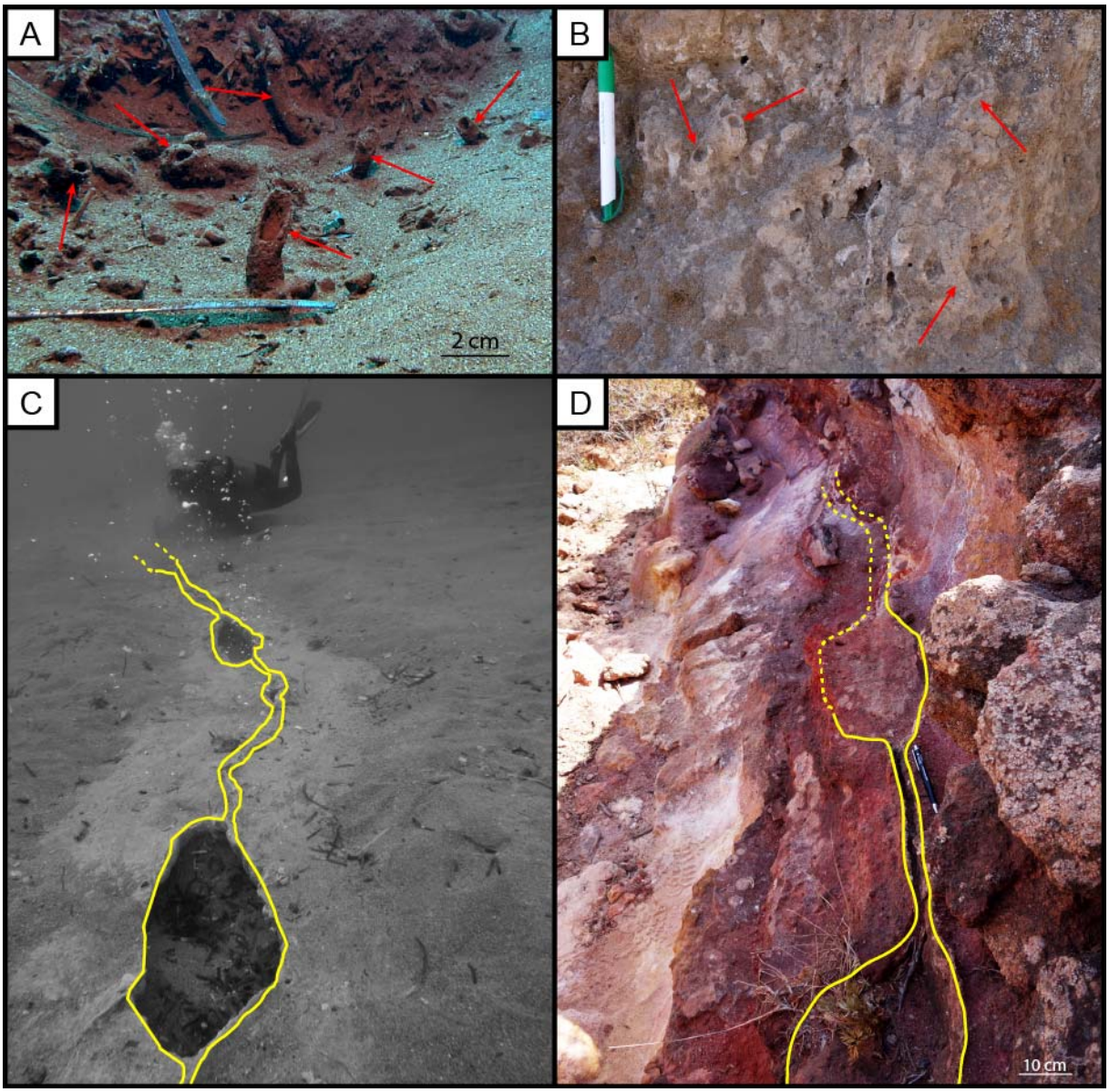

Figure 60: Comparison of recent and paleo structures. **A –** Network of *TFe* type *tubes* in Basiluzzo. The red arrows mark selected prominent specimen. **B –** Network of *Tpal* type *tubes* in subaerial 2. The comparison to the Basiluzzo sample witnesses a nearly identical habitus. The red arrows mark selected prominent specimen. **C –** *Lineament Structure* in Area 26. The yellow line highlights the general shape. **D –** Preserved lineament structure of type *Lpal* at subaerial 1. The yellow line highlights the general shape. The substantial similarity to the underwater specimen from Area 26 in C cannot be neglected.

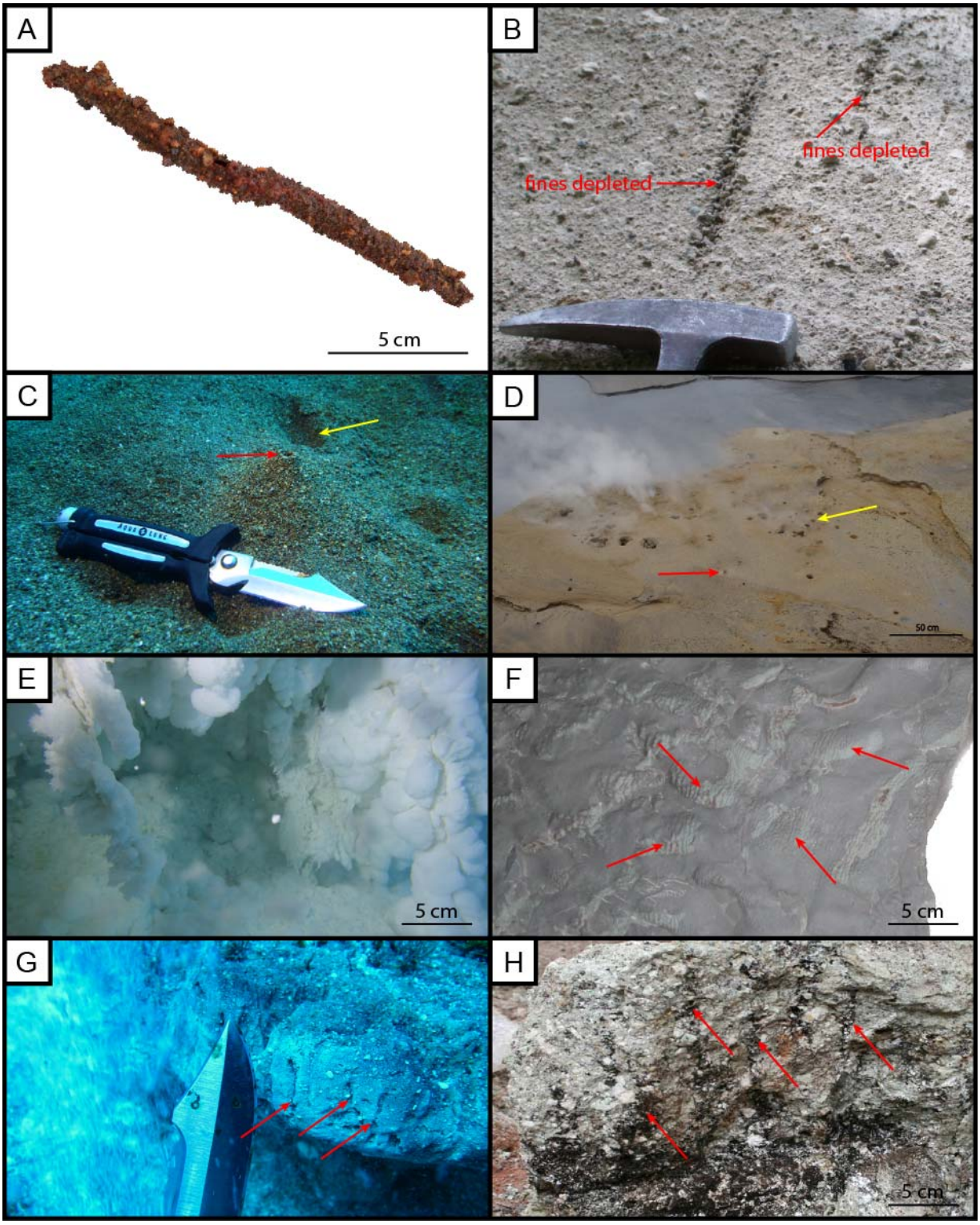

Figure 61: Comparison of recent and paleo structures. Right row modified after STANULLA (2012). **A –** Small, recent TFe tube from La Calcara. **B –** Degassing tubes in the Laacher See tephra. Red arrows mark degassing channels. **C –** Cu in La Calcara. Red arrow marks a typical Cu specimen. The yellow arrow marks negatively reliefed emanation point. **D –** Semiaquatic Cu in the Krysuvik hydrothermal field in Iceland. Same indicators as in C. **E –** Massive growth of microbial mats in the grotto at Cave. **F –** Fossilized microbial mats from the Permian Goldlauter Formation near Tabarz (Thuringia, Germany). Red arrows mark prominent occurrences. **G –** Gas erosion channels (red arrows) at *Lava Tongue* in Area 26. **H –** Degassing structures in the volcanic sediments of the Leukersdorf Formation of Chemnitz, Germany (Zeisigwald-Tuff-Horizon). Post-depositional manganese impregnation causing dark colors. Photography: J.W. Schneider (2011).

7. Conclusion and Discussion

7.1. General context of the formation of hydrothermal discharge features in Panarea

The formation of hydrothermal discharge features is controlled by a number of influencing factors (Figure 62). Besides the geological framework, i.e. the type of bedrock or the degree of alteration of both, sediments and secondary mineralizations, hydrological and (geo-)chemical parameters are among the main controlling variables. Furthermore, physical parameters and bio-influences affect their formation. The type of discharge feature will always be the result of the interaction of all these criteria. It strongly depends on *where* and *how* a hydrothermal discharge feature emerges.

This fact is exceptionally well proven by the example of the tube facies described for the Panarea system. At least six completely different types of tubes develop in quite comparable environments (TFe, TS, Tore, etc.). However, all of them differ regarding their geological background (e.g. type of sediment, host rock) and the fluid dynamics on-spot (flowrates and -volumes). The same facts account for the persistent development of single discharge features and their preservation potential.

Due to the multitude of influencing variables, a general statement on the evolutionary timescale cannot be provided.

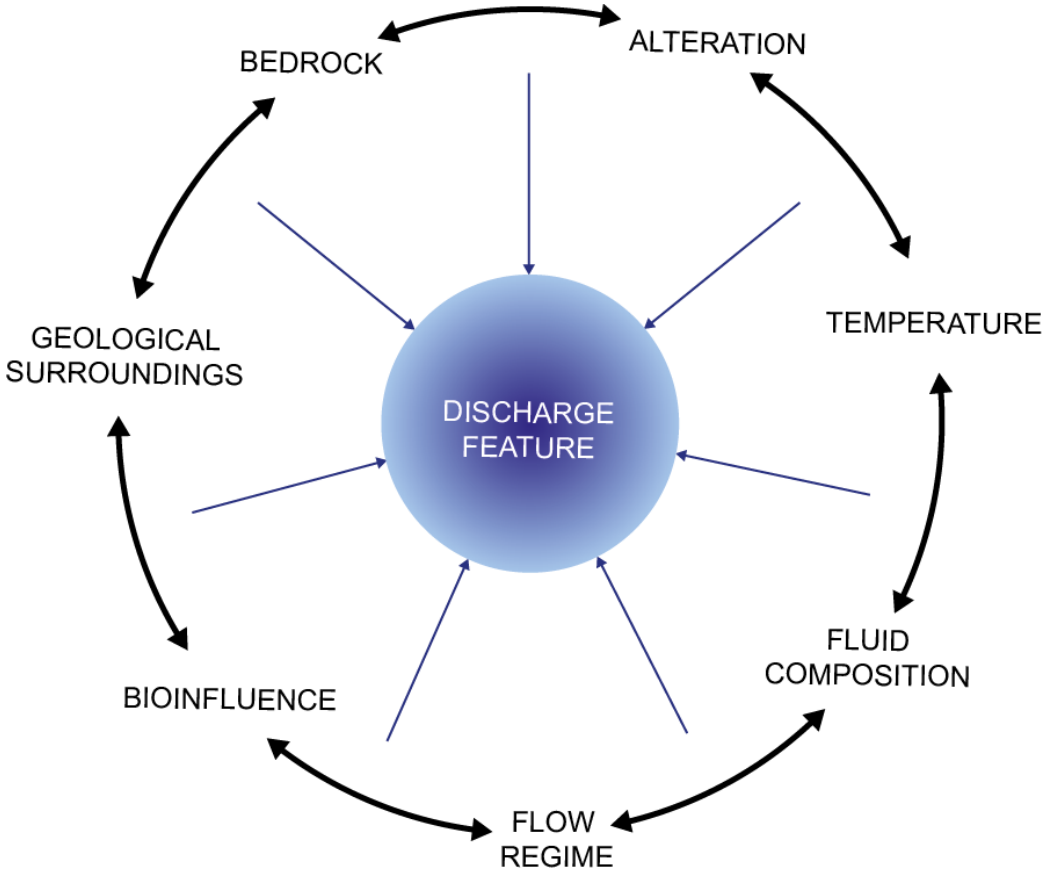

Figure 62: Schematic sketch approaching the main influencing factors on the formation of hydrothermal discharge features.

7.2. Evolution of hydrothermal discharge features in Panarea

A development scheme for discharge features in the Panarea system is proposed in Figure 63. The figure combines schematic illustrations and images of typical features in the Panarea volcanic system. A typical location, where the feature occurs, is given, referring to the documented underwater investigation site (type locality). The data supposes at least six evolutionary stages, that are mainly controlled by an interplay of destructive and constructive processes. A cyclic change in domination causes rhythmic laminations.

constructive processes ↔ destructive processes

A sustained domination of one side of this relation may lead to the further development to the next stage. In contrast, extreme conditions such as massive gas discharge (e.g. at the main vents of Point 21 or Bottaro North) may hinder the development of susceptible or fragile types of discharge features due to excessive energetic conditions. Obviously, the best evolutionary rate is reached in settings, where moderate conditions prevail, and the controlling factors interact in an optimal way for the particular discharge feature facies. Additionally, an affinity of hydrothermal discharge features to sediments and sedimentary rocks is likely, as nearly all types of discharge features presented in this thesis occur in sedimentary environments. However, a progressive evolution may not take place and the discharge feature remains in its current development stage obtaining a greater maturity.

Stage 1: initial state

The assumption is, that an initial fracture prevails, being caused by (neo-) tectonics. It potentially widens due to erosive processes such as abrasion of high gas flowrates or chemical erosion by aggressive hydrothermal fluids (Figure 63-1).

Type locality: Point 21

Stage 2: facies type - *fracture*

In addition to the erosive processes described in (1), mineral precipitation takes place narrowing the profile of the fracture.

An interplay of constructive and destructive processes evolves, forming different opening widths of the fracture (near surface). The discharge feature type *fracture* develops at centimeter scale (Figure 63-2).

Type locality: Point 21, Area 26

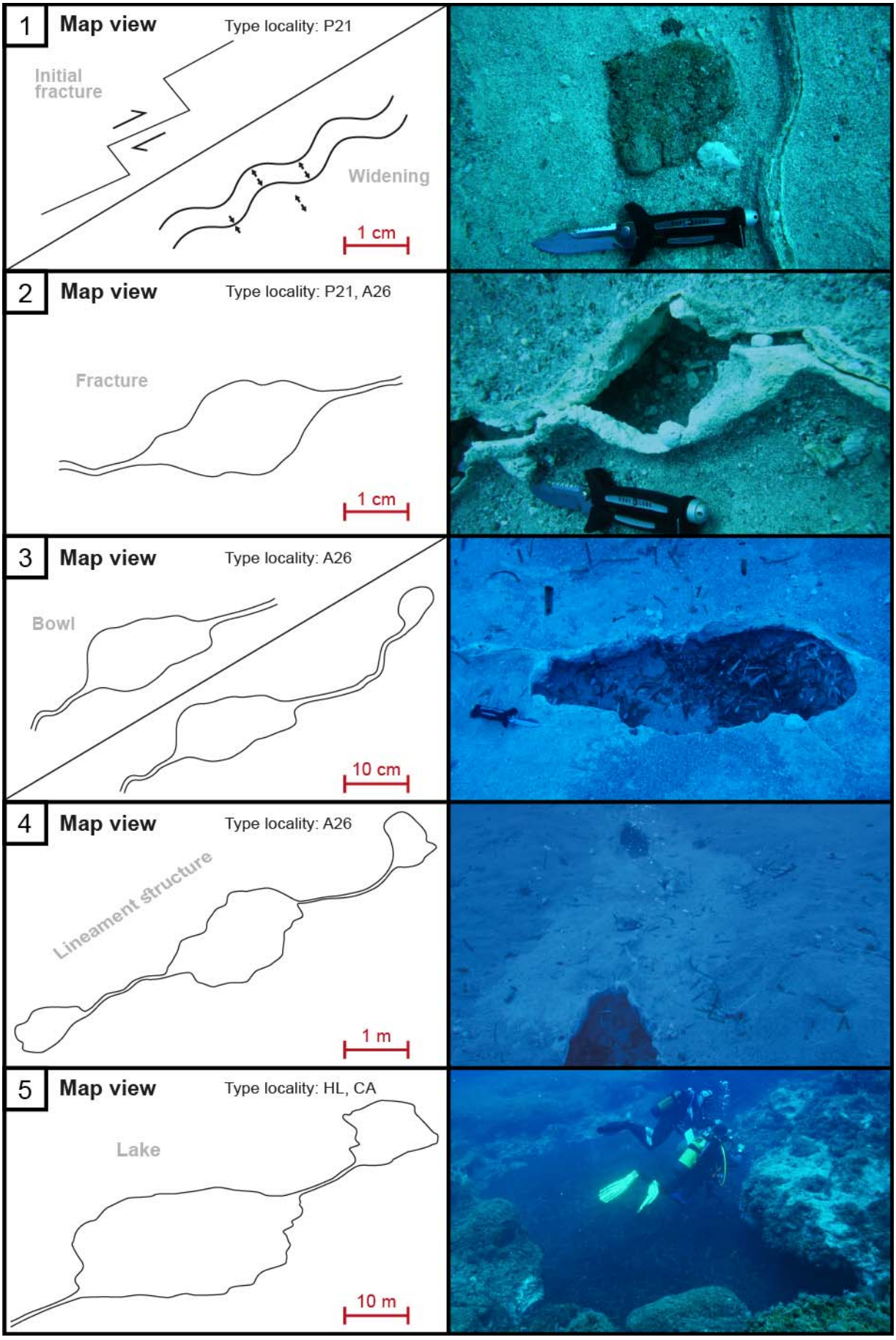

Figure 63: Schematic sketch on the evolution of hydrothermal discharge features in Panarea.

Stage 3: facies type - *bowl*

Depending on the boundary conditions, the destructive processes might predominate at least for a certain time. The resulting further widening forms the discharge feature type *bowl* (scale: cm to dm; Figure 63-3).

A repeatedly domination of one of the processes causes a cyclic evolution of the discharge feature. The geologic record shows a cyclic lamination at micro and macro scale.

Type locality: Area 26

Stage 4: facies type - *lineament*

Resulting in the fact that all bowls evolved on the same basis (the fracture), an arrangement along the fracture lines is common. In case the *bowls* are connected by the widened fracture, the facies type *lineament* is formed (Figure 63-4). These meter-scaled structures combine the facies *fracture* and *bowl* to form a new stage of development. Due to the described cyclic evolution, a geochronological characterization is complicated by means of relative ages. A well-developed, mature *bowl* is potentially older than a relatively young, immature *lineament*.

Type locality: Area 26

Stage 5: facies type - *lake*

Further development of the discharge features may lead to the formation of “super” *bowls* – so called *lakes* (Figure 63-5). The discharge feature type *lake* may reach up to several tens of meters in extend.

Analog to the development of *lineaments*, also “super”-*lineaments* may evolve, connecting a number of *lakes* by *fractures* or *lineaments*.

Type locality: Cave, Hot Lake

Stage 6: final state

As the development of discharge features is directly connected to hydrothermal activity, it will end at the latest at the time the venting ends. The destructive processes will finally dominate, and standard processes of erosion will abstract the hydrothermal discharge feature. In combination with possible commonalities to abstracted submarine explosion craters as described by MONECKE et al. (2012), this makes this stage of development hard to identify. It has therefore not been securely identified in the Panarea system up to now. However, MARTORELLI et al. (2016) report of “cone shaped features” and “elongated pockmarks” near Zannone Island. These could potentially be analogue forms of the final stage of development.

7.3. Comprehensive summary

The conducted investigations bring knowledge about the geological and sedimentary settings as well as the interior structures of hydrothermal discharge features, their genesis and facies variations. The complex interaction of host rock, physico-chemical conditions, biota, hydrothermal fluids, and discharge behavior forms unique hydrothermal features, that are still undescribed in scientific literature up to now.

Considering this context, the thesis aims to answer four central hypotheses given in the introduction. The new insights on the materials and processes involved in the development of the sea-bottom-interface of the hydrothermal system of Panarea allow to answer these research questions as follows:

Hypothesis 1:

“The seabed interface of the hydrothermal system of Panarea Island is composed of at least 11 lithofacies types of various properties and a complex spatial distribution. Secondary mineralization forms different types of cement.”

The thesis presents a rough inventory of the prevailing lithologies in the system, without claiming a complete geological or sedimentological characterization.

The **three hardrock facies** include a **Dacite/Andesite**, that is forming the major bedrock in the area. The volcanite is severely affected by hydrothermal alteration what makes the differentiation between Dacite and Andesite impossible with the applied techniques. It is intersected by several dykes, that show characteristic alterations and discharge structures. These rocks are referred to as **Dykite**. Furthermore, fall deposits form massive **Tuffites** being the host rock for a number of hydrothermal discharge features.

The **seven sedimentary rock facies** mainly consist of **sandstones**, **conglomerates** and **fanglomerates**, each showing **varying cements**.

Secondary mineral precipitation forms four different types of cement that may also occur as mineral precipitates in coatings or fillings. The documented types can be composed of massive sulfide ores or iron-bearing, sulfurous, or clayish mineral facies. All of them are mostly internally laminated what hints on a rhythmic deposition.

Most of these rock facies are covered by one of the **five** different **sedimentary facies**. The work presents examples from different locations comprising **medium grained sands and gravel** showing varying influences of secondary mineral precipitation (see above; cements). Doubtless, a more intense sedimentological investigation will approve a more detailed facies differentiation.

At all, the thesis presents **a suite of 15 lithofacies** in the investigated underwater locations of Panarea.

Hypothesis 2:

“The development of secondary structures and fluid discharge features follows only one complex genetic scheme just varying in the outer shape according to the facies of the discharge feature, the characteristics of the hydrothermal fluids and the type of host rock material.”

The Panarea system comprises a broad variety of hydrothermal discharge features developing under different environmental conditions. Thus, a comprehensive facies model is developed, distinguishing **six major groups of discharge features**: ***channels, fractures, tubes, cones, bowls*, and *lineaments*.**

The investigation of different maturity stages showed that ***channel* and *tube* formation** follow their **own genetic model**, respectively. Especially in the rather complex formation of *tubes* a number of influencing factors such as the presence of certain biota (i.e. *Posidonia sp.*) or the amount of mineral precipitation affect the development of single *tube* specimen.

The investigations of **fractures, cones, bowls, and lineaments** suggest, that each of these facies represents distinct **evolutionary stages of one single genetic process**. Assuming optimal boundary conditions, the described discharge features develop from simple, small-scale, near discharge structures to complex patterns of larger scale embedding numerous outlets and smaller structures. However, the continuous development might not be completed and thus the discharge feature may remain in a certain evolutionary stage forming structures of proceeding maturity over time.

Hypothesis 3:

“The occurrence of fluid discharges and secondary structures is controlled by regional tectonics in the back-arc basin.”

All developed genetic models base on the assumption that there is an initial fracture which acts as pathway for hydrothermal fluids. The hydrothermal features can only evolve during times of active hydrothermal discharge. The migrating fluids may modify the initial fracture (for example widen it) what is the basis for their further development. However, all discharge features show a prominent affinity to the local (neo-) tectonic system, what makes them a powerful proxy and indicator for tectonic investigations. Most of the discharge features are arranged along the structural elements on-spot. The evolutionary stage of hydrothermal discharge features therefore often corresponds to the prevailing host rock material and the local tectonic regime.

However, hydrothermal discharge features were documented in all investigated locations in Panarea. A concise investigation on the relation between evolutionary stage of the discharge feature and (neo-) tectonic influences should be attempted in further investigations.

Hypothesis 4:

“Secondary structures and fluid discharge features show a high preservation potential and represent unique marker structures suggesting preserved hydrothermal systems in the paleo rock record.”

The main focus of this thesis is set on the investigation of submerged locations in Panarea. However, also selected outcrops on land were investigated in terms of potentially preserved secondary structures and hydrothermal discharge features. Especially two subaerial locations in Panarea give evidence of preserved hydrothermal discharge features as documented in the underwater locations. Particularly *tubes* and *lineaments* could be investigated in subaerial settings up to ~130 m asl.

Despite, the underwater locations show both, active and inactive or ancient hydrothermal discharge features. The latter may be classified as an early stage fossilized form of the discharge feature. A distinct characterization proved to be difficult because of ongoing strong hydrothermal activity as ancient discharge features might be reactivated in case of changing discharge behavior of the outlet. Further examples from other locations worldwide strengthen these findings, although showing facies variations.

However, the processes of lithification and development of already fossilized structures have not been attempted in this work. The work documents preserved discharge features in Panarea. They witness the potential of fossilization but cannot prove or describe the detailed processes involved yet. This can be traced back in central parts on the still problematic identification of other fossilized hydrothermal systems of a comparable type, their accessibility, and the temporal and financial frame of this work. Nevertheless, these central points should be approached by further investigations, as a concise catalogue of comparable structures will facilitate the identification of lithified analogues to the described hydrothermal features enormously.

F. References

Acocella, V.; Neri, M.; Walter, T. R. (2009): Structural features of Panarea volcano in the frame of the Aeolian Arc (Italy): Implications for the 2002–2003 unrest. Journal of Geodynamics 47, pp. 288-292.

Adamek, J.; Stanulla, R.; Pohl, T.; Kürzinger, V. (2019): Geological and structural mapping of holocene small-scaled secondary subrosion structures at Area 26, Panarea, Italy. 5th European Conference on Scientific Diving, Sopot, Poland, April 2019.

Adamek, J. (2021): Investigation of neotectonic and structural characteristics of the subaerial and submarine system of Panarea Island, Italy. Master's Thesis. TU Bergakademie Freiberg - Institute of Geology, Chair of Tectonics, unpublished.

Aliani, S.; Meloni, R.; Dando, P. R. (2004): Periodicities in sediment temperature time-series at a marine shallow water hydrothermal vent in Milos Island (Aegean Volcanic arc, Eastern Mediterranean). Journal of Marine Systems 46(1-4), pp. 109-119.

Aliani, S.; Bortoluzzi, G.; Caramanna, G.; Raffa, F. (2010): Seawater dynamics and environmental settings after November 2002 gas eruption off Bottaro (Panarea, Aeolian Islands, Mediterranean Sea). Continental Shelf Research 30(12), pp. 1338-1348.

Amils, R.; Ellis-Evans, J. C.; Hinghofer-Szalkay, H. (eds) (2007): Life in extreme environments. Dordrecht: Springer, p. 450.

Anastasakis, G. & Piper, D. J. W. (2005): Late Neogene evolution of the western South Aegean volcanic arc: sedimentary imprint of volcanicity around Milos. Marine Geology 215(3-4), pp. 135-158.

An Adón, P.; Canet, C.; Friedrich, W. L. (2013): Aragonite stromatolitic buildups from Santorini (Aegean Sea, Greece): Geochemical and palaeontological constraints of the caldera palaeoenvironment prior to the Minoan eruption (ca 3600 yr BP). Sedimentology 60(5), pp. 1128-1155.

Andaloro, F.; Romeo, T.; Renzi, M.; Guerranti, C.; Perra, G.; Consoli P.; Perzia, P.; Focardi, S. E. (2010): Trace Elements Levels in Aeolian Archipelago (Central Mediterranean Sea) following an Episode of Intense Volcanic Activity. In: Italiano, F. (ed) (2010): Second international workshop on research in shallow marine and freshwater systems. Palermo, pp. 9-10.

Anzidei, M.; Esposito, A.; Bortoluzzi, G.; De Giosa, F. (2005): The high-resolution bathymetric map of the exhalative area of Panarea (Aeolian Islands, Italy). Annals of Geophysics 48(6), pp. 899-921.

Anzidei, M.; Esposito, A.; Benini, A. (2014): Evidence of active subsidence at Basiluzzo island (Aeolian islands, southern Italy) inferred from a Roman age wharf. Quaternary International 332, pp.143-150.

Bagnato, E.; Oliveri, E.; Acquavita, A.; Covelli, S.; Petranich, E.; Barra, M.; Italiano, F.; Parello, F.; Sprovieri, M. (2017): Hydrochemical mercury distribution and air-sea exchange over the submarine hydrothermal vents off-shore Panarea Island (Aeolian arc, Tyrrhenian Sea). Marine Chemistry 194, pp. 63-78. DOI: 10.1016/j.marchem.2017.04.003.

Barth, G.; Müller, C.; Merkel, B. J. (2010): Development of Methods to Determine the Geothermal State of Shallow Submarine Geothermal Systems. In: Italiano, F. (ed) (2010): Second international workshop on research in shallow marine and freshwater systems. Palermo, pp. 13-16.

Bauer, K.; Bauer, D.; Fütterer; W.; Kleutges, J. (2009): Flow rate measurements at submarine volcanic gas emissions. In: Merkel, B. J. & Schipek, M. (eds) (2009): Research in Shallow Marine and Freshwater Systems. 1st International Workshop - Proceedings, FOG 22, pp. 112-117.

Becke, R. (2009): Mineralogische & Geochemische Untersuchung von submarinen, vulkanogen-hydrothermalen Mineralpräzipitaten im back-arc-basin des Tyrrhenischen Meeres am Beispiel von Panarea, Äolischer Inselbogen, Italien. Diploma Thesis. Universität Leipzig, Institut für Geophysik und Geologie & TU Bergakademie Freiberg, Department of Hydrogeology and Environmental Geology, Scientific Diving.

Becke, R.; Merkel, B.; Pohl, T. (2009): Mineralogical and geochemical characteristics of the shallow-water massive sulfide precipitates of Panarea, Aeolian Islands, Italy. In: Merkel, B. J. & Schipek,

M. (eds) (2009): Research in Shallow Marine and Freshwater Systems. 1st International Workshop - Proceedings, FOG 22, pp. 94-100.

Bell, K. L. C.; Elliott, K.; Martinez, C.; Fuller, S. A. (eds) (2012): New Frontiers in Ocean Exploration, the E/V Nautilus and NOAA Ship Okeanos Explorer 2011 Field Season. Oceanography 25(1), Supplement 03/2012, pp. 1-72.

Benjamin, J.; Rovere, A.; Fontana, A.; Furlani, S.; Vacchi, M.; Inglis, R. H.; Galili, E.; Antonioli, F.; Sivan, D.; Miko, S.; Mourtzas, N.; Felja, I.; Meredith-Williams, M.; Goodman-Tchernov, B.; Kolaiti, E.; Anzidei, M.; Gehrels, R. (2017): Late Quaternary sea level changes and early human societies in the central and eastern Mediterranean Basin: An interdisciplinary review. Quaternary International 449, pp. 29-57.

Biasi, A. M.; Bianchi, C. N.; Aliani, S.; Periano, A.; Dando, P. R.; Morri, C. (2004): Epibenthic communities in a marine shallow aerea with hydrothermal vents (Milos Island, Aegean Sea). Chemistry and Ecology 20(1), pp. 89-105.

Binns, R. A. (2014): Bikpela: A Large Siliceous Chimney from the PACMANUS Hydrothermal Field, Manus Basin, Papua New Guinea. Economic Geology109(8), pp. 2243-2259.

Blumenberg, M. (2010): Microbial Chemofossils in Specific Marine Hydrothermal and Methane Cold Seep Settings. In: Kiel, S. (ed) (2010): The vent and seep biota. From microbes to ecosystems, Bd. 33. Heidelberg, London, New York: Springer, pp. 73-106.

Bortoluzzi, G.; Romeo, T.; La Cono, V.; La Spada, G.; Smedile, F.; Esposito, V.; Sabatino, G.; Di Bella, M.; Canese, S.; Scotti, G.; Bo, M.; Giuliano, L.; Jones, D.; Golyshin, P. N.; Yakimov, M. M.; Andaloro, F. (2017): Ferrous iron- and ammonium-rich diffuse vents support habitat-specific communities in a shallow hydrothermal field off the Basiluzzo Islet (Aeolian Volcanic Archipelago). Geobiology 15(5), pp. 664-677.

Botz, R.; Stüben, D.; Winckler, G.; Bayer, R.; Schmitt, M.; Faber, E. (1996): Hydrothermal gases offshore Milos Island, Greece. Chemical Geology 130, pp. 161-173.

Brümmer, F.; Fritz, G. B.; Pfannkuchen, M. (2013): DOBB: water sampling device for SCUBA divers to obtain in situ data. Berichte aus dem MARUM und dem Fachbereich Geowissenschaften der Universität Bremen 292, pp. 54-57.

Butterfield, D. A. (2000): Deep ocean hydrothermal vents. In: Sigurdsson, H.; Houghton, B. F.; McNutt, S. R.; Rymer, H.; Stix, J. (eds) (2010): Encyclopedia of Volcanoes. Academic Press, San Diego, California, pp. 857-875.

Calanchi, N.; Capaccioni, B.; Martini, M.; Tassi, F.; Valentini, L. (1995): Submarine gas emission from Panarea Island Aeolian Archipelago: distribution of inorganic and organic compounds and inferences about source conditions. Acta Vulcanologica 7, pp. 43-48.

Calanchi, N.; Tranne, C. A.; Lucchini, F.; Rossi, P. L.; Villa, I. M. (1999): Explanatory notes to the geological map (1:10.000) of Panarea and Basiluzzo islands (Aeolian arc. Italy), Acta Vulcanologica 11(2), pp. 223– 243.

Calanchi, N.; Peccerillo, A.; Tranne, C. A.; Lucchini, F.; Rossi, P. L.; Kempton, P.; Barbieri, M.; Wu, T. W. (2002): Petrology and geochemistry of volcanic rocks from the island of Panarea: implications for mantle evolution beneath the Aeolian island arc (southern Tyrrhenian sea). Journal of Volcanology and Geothermal Research 115, pp. 67-395.

Campbell, K. A. (2006): Hydrocarbon seep and hydrothermal vent paleoenvironments and paleontology: Past developments and future research directions. Palaeogeography, Palaeoclimatology, Palaeoecology 232(2-4), pp. 362-407.

Canzler, W. (2012): Charakterisierung von ausgewählten submarinen geothermischen Aktivitätsflächen vor Panarea. Bachelor's Thesis. TU Bergakademie Freiberg - Institute of Geology, Chair of Hydrogeology, unpublished.

Capaccioni, B.; Tassi, F.; Vaselli, O.; Tadesco, D.; Poreda, R. (2007): Submarine gas burst at Panarea Island (southern Italy) on 3 November 2002: A magmatic versus hydrothermal episode. Journal of Geophysical Research 112, B05201. DOI: 10.1029/2006JB004359.

Capaccioni, B.; Tassi, F.; Vaselli, O. (2010): Geochemistry of thermal waters and gases from the submarine fumarolic field of Panarea Island (Aeolian archipelago, Italy). In: Italiano, F. (ed)

(2010): Second international workshop on research in shallow marine and freshwater systems. Palermo, p. 20.

Caracausi, A.; Ditta, M.; Italiano, F.; Longo, M.; Nuccio, P. M.; Paonita, A. (2005a): Massive submarine gas output during the volcanic unrest off Panarea Island (Aeolian arc, Italy): Inferences for explosive conditions. Geochemical Journal 39(5), pp. 459-467.

Caracausi, A.; Ditta, M.; Italiano, F.; Longo, M.; Nuccio, P. M.; Paonita, A.; Rizzo, A. (2005b): Changes in fluid geochemistry and physico-chemical conditions of geothermal systems caused by magmatic input: The recent abrupt outgassing off the island of Panarea (Aeolian Islands, Italy). Geochimica et Cosmochimica Acta 69, pp. 3045-3059. DOI: 10.1016/j.gca.2005.02.011

Cas, R.; Giordano, G.; Balsamo, F.; Esposito, A.; Lo Mastro, S. (2011): Hydrothermal Breccia Textures and Processes: Lisca Bianca Islet, Panarea Volcano, Aeolian Islands, Italy. Economic Geology 106(3), pp. 437-450.

Caso, C.; Signanini, P.; De Santis, A.; Favali, P.; Iezzi, G.; Marani, M. P.; Paltrinieri, D.; Rainone, M. L.; Di Sabatino, B. (2010): Submarine Geothermal Systems in Southern Tyrrhenian Sea as Future Energy Resource: The Example of Marsili Seamount. Proceedings World Geothermal Congress 2010 Bali, Indonesia (25-29 April 2010).

Chiocci, F. L. & Romagnoli, C. (2004): Submerged depositional terraces in the Aeolian Islands (Sicily). Memorie Descrittive della Carta Geologica d'Italia 58, pp. 49-64.

Chiodini, G.; Caliro, S.; Caramanna, G.; Granieri, D.; Minopli, C.; Morretti, R.; Perotta, L.; Ventura, G. (2006): Geochemistry of the submarine gaseous emissions of Panarea (Aeolian Islands, Southern Italy): Magmatic vs. hydrothermal origin and implications for volcanic surveillance. Pure and Applied Geophysics 163, pp. 759-780.

Christidis, G. E. (1998): Comparative study of the mobility of mayor and trace elements during alteration of an andesite and a rhyolite to bentonite, in the islands of Milos and Kimolos, Aegean, Greece. Clays and Clay Minerals 46(4), pp. 379-399.

Corliss, J. B.; Dymond, J.; Gordon, L. I.; Edmond, J. M.; Von Herzen R. P.; Ballard, R. D.; Green, K.; Williams, D.; Bainbridge, A.; Crane, K.; Van Andel, T. H. (1979): Submarine thermal springs on the Galapagos Rift. Science 203, pp. 1073-1083.

Conte, A. M. & Caramanna, G. (2010): Preliminary characterisation of a shallow water hydrothermal sulphide deposit recovered by scientific divers (Aeolian Islands, southern Tyrrhenian Sea). International Journal of the Society for Underwater Technology 29(3), pp 109-115.

Converse, D. R.; Holland, H. D.; Edmond, J. M. (1984): Flow rates in the axial hot springs of the East Pacific Rise (21° N): Implications for the heat budget and the formation of massive sulfide deposits. Earth and Planetary Science Letters 69(1), pp. 159-175.

Cuadrado, D. G.; Carmona, N. B.; Bournod, C. (2011): Biostabilization of sediments by microbial mats in a temperate siliciclastic tidal flat, Bahia Blanca estuary (Argentina). Sedimentary Geology 237(1-2), pp. 95-101.

Dando, P. R. (2010): Biological communities at marine shallow-water vent and seep sites. In: Kiel, S. (ed) (2010): The vent and seep biota: aspects from microbes to ecosystems, Bd. 33. Heidelberg, London, New York: Springer, pp. 33-378.

Dando, P. R.; Hughes, J. A.; Leahy, Y.; Niven, S. J.; Taylor, L. J.; Smith, C. (1994): Gas venting rates from submarine hydrothermal areas around the island of Milos, Hellenic Volcanic Arc. Continental Shelf Research 15(8), pp. 913-929.

Dando, P. R.; Hughes, J. A.; Leahy, Y.; Taylor, L. J.; Zivanovic, S. (1995): Earthquakes increase hydrothermal venting and nutrient inputs into the Aegean. Continental Shelf Research 15(6), pp. 655-662.

Dando, P. R., Stüben, D.; Varnavas, S. P. (1999): Hydrothermalism in the Mediterranean Sea. Progress in Oceanography 44(1-3), pp. 333-367.

Dando, P. R.; Aliani, S.; Arab, H.; Bianchi, C. N.; Brehmer, M.; Cocito, S.; Fowlers, S. W.; Gundersen, J.; Hooper, L. E.; Kölbh, R.; Kuevere, J.; Linke, P.; Makropoulosr, K. C.; Meloni, R.; Miquel, J.-C.; Morri, C.; Müller, S.; Robinson, C.; Schlesner, H.; Sieverts, S.; Störr, R.; Stüben, D.; Thormm, M.; Varnavas, S. P.; Ziebiss, W. (2000): Hydrothermal Studies in the Aegean Sea. Physics and Chemistry of the Earth 25(1), pp. 1-8.

De Astis, G.; Ventura, G.; Vilardo, G. (2003): Geodynamic significance of the Aeolian volcanism (Southern Tyrrhenian Sea, Italy) in light of structural, seismological and geochemical data. Tectonics 22 (4), pp. 14/1-14/17.

Dekov, V. M. & Savelli, C. (2004): Hydrothermal activity in the SE Tyrrhenian Sea: an overview of 30 years of research. Marine Geology 204(1-2), pp. 161-185. DOI: 10.1016/S0025-3227(03)00355-4.

Dekov, V. M.; Kamenov, G. D.; Abrasheva, M. D.; Capaccioni, B.; Munnik, F. (2013): Mineralogical and geochemical investigation of seafloor massive sulfides from Panarea Platform (Aeolian Arc, Tyrrhenian Sea). Chemical Geology 335, pp. 136-148. DOI: 10.1016/j.chemgeo.2012.10.048.

Di Bella, M.; Sabatino, G.; Quartieri, S.; Ferretti, A; Cavalazzi, B.; Barbieri, R.; Foucher, F.; Messori F.; Italiano, F. (2019): Modern Iron Ooids of Hydrothermal Origin as a Proxy for Ancient Deposits. Scientific Reports 9(7107). DOI: 10.1038/s41598-019-43181-y

Doherty, A. L.; Cannatelli, C.; Raia, F.; Belkin, H. E.; Albanese, S.; Lima, A.; De Vivo, B. (2015): Geochemistry of selected lavas of the Panarea volcanic group, Aeolian Arc, Italy. Miner Petrol 109, pp. 597-610.

Dragantis, E. & Noffke, N. (2004): Siliciclastic stromatolites and other microbially induced sedimentary structures in an early devonian barrier-island environment (Muth-Formation, NW-Himalayas). Journal of Sedimentary Research 74(2), pp. 191-202.

Espa, S.; Caramanna, G.; Bouché, V. (2010): Field study and laboratory experiments of bubble plumes in shallow seas as analogues of sub-seabed CO_2 leakages. Applied Geochemistry 25, pp. 696-704.

Esposito, A.; Giordano, G.; Anzidei, M. (2006): The 2002–2003 submarine gas eruption at Panarea volcano Aeolian Islands, Italy: volcanology of the seafloor and implications for the hazard scenario. Marine Geology 227, pp. 119-134.

Esposito, A.; Anzidei, M.; Atzori, S.; Devoti, R.; Giordano, G.; Pietrantonio, G. (2010): Modeling ground deformations of Panarea volcano hydrothermal/geothermal system (Aeolian Islands, Italy) from GPS data. Bull Volcanol 72(5), pp. 609-621.

Esposito, V.; Andaloro, F.; Canese, S.; Bortoluzzi, G.; Bo, M.; Di Bella, M.; Italiano, F.; Sabatino, G.; Battaglia, P.; Conoli, P.; Giordano, P.; Spagnoli, F.; La Cono, V.; Yakimov, M. M.; Scotti, G.; Romeo, T. (2018): Exceptional discovery of a shallow-water hydrothermal site in the SW area of Basiluzzo islet (Aeolian archipelago, South Tyrrhenian Sea): An environment to preserve. PLOS ONE 13(1). DOI: 10.1371/journal.pone.0190710.

Esposito, V.; Canese, S., Scotti, G.; Bo, M.; De Vittor, C.; Andaloro, F.; Romeo, T. (2019): Spiculosiphon oceana (foraminifera) and its affinity to intermediate stress conditions in the Panarea hydrothermal complex (Mediterranean Sea). Marine Biodiversity Records 12 (23). DOI: 10.1186/s41200-019-0183-4.

Fabris, M.; Baldi, P.; Anzidei, M.; Pesci, A.; Bortoluzzi, G.; Aliani, S. (2010): High resolution topographic model of Panarea Island by fusion of photogrammetric, lidar and bathymetric. The Photogrammetric Record 25(132), pp. 382-401. DOI: 10.1111/j.1477-9730.2010.00600.x.

Favalli, M.; Karátson, D.; Mazzuoli, R.; Pareschi, M. T.; Ventura, G. (2005): Volcanic geomorphology and tectonics of the Aeolian archipelago (Southern Italy) based on integrated DEM data. Bull Volcanol 68(2), pp. 157-170.

Ferretti, A.; Messori, F.; Di Bella, M.; Sabatino, G.; Quartieri, S.; Cavalazzi, B.; Italiano, F.; Barbieri, R. (2019): Armoured sponge spicules from Panarea Island (Italy): Implications for their fossil preservation. Palaeogeography, Palaeoclimatology, Palaeoecology 536, DOI: 10.1016/j.palaeo.2019.109379.

Fink, L. K. Jr. (1972): Bathymetric and geologic studies of the Guadeloupe region, Lesser Antilles Island Arc. Marine Geology 12, pp. 267–288.

Fitzsimons, M. F.; Dando, P. R.; Hughes, J. A.; Thiermann, F.; Akoumianaki, I.; Pratt; S. M. (1997): Submarine hydrothermal brine seeps off Milos, Greece: Observations and geochemistry. Marine Chemistry 57, pp. 325-340.

Fontaine, F. J.; Rabinowicz, M.; Boulègue, J. (2003): Hydrothermal processes at Milos Island (Greek Cyclades) and the mechanisms of compaction-induced phreatic eruptions. Earth and Planetary Science Letters 210(1-2), pp. 17-33.

Fouquet, Y.; Knott, R.; Cambon, P.; Fallick, A.; Rickard, D.; Desbruyeres, D. (1996): Formation of large sulfide mineral deposits along fast spreading ridges: Example from off-axial deposits at 12°43'N on the East Pacific Rise. Earth Planet Science Letters 144, pp. 147-162.

Francheteau, J.; Needham, H. D.; Choukroune, P. Juteau, T.; Seguret, M.; Ballard, R. D.; Fox, P. J.; Normark, W.; Carranza, A.; Cordoba, D.; Guerrero, J.; Rangin, C.; Bougault, H.; Cambon, P.; Hekinian, R. (1979): Massive deep-sea sulphide ore deposits discovered on the East Pacific Rise. Nature 77(5697), pp. 523-528.

Frey, S. E.; Gingras, M. K.; Dashtgard, S. E. (2009): Experimental Studies of Gas-Escape and Water-Escape Structures: Mechanisms and Morphologies. Journal of Sedimentary Research 79(11), pp. 808-816.

Früh-Green, G. L. (2003): 30,000 Years of Hydrothermal Activity at the Lost City Vent Field. Science 301(5632), pp. 495-498.

Fytikas, M. (1989): Updating the geological and geothermal research on Milos Island. Geothermics 18(4), pp. 485-496.

Gabbianelli, G.; Gillot, P. Y.; Lanzafame, G.; Romasgnolli, C.; Rossi, P. L. (1990): Tectonic and Volcanic Evolution of Panarea (Aeolian Islands, Italy). Marine Geology (92), pp. 313-326.

Gabbianelli, G.; Romasgnolli, C.; Rossi, P. L.; Calanchi, N. (1993): Marine geology of Panarea–Stromboli area, Aeolian Archipelago, South-eastern Tyrrhenian Sea. Acta Vulcanologica 3, pp. 11-20.

Gamberi, F.; Marani, M.; Savelli, C. (1997): Tectonic, volcanic and hydrothermal features of a submarine portion of the Aeolian arc (Tyrrhenian Sea). Marine Geology 140, pp. 167-181.

Ganß, R. (2013): Geochemische und kleinmorphologische Untersuchungen an Sulfidablagerungen im hydrothermalen System von Panarea, Italien. Bachelor‘s Thesis, unpublished. TU Bergakademie Freiberg.

Gerdes, G.; Klenke, T.; Noffke, N. (2000): Microbial signatures in peritidal siliclastic sediments: a catalogue. Sedimentology 47, pp. 279-308.

Gingras, M. (2002): Microbially induced sedimentary structures - A new category within the classification of primary sedimentary structures - Discussion. Journal of Sedimentary Research 72(4), pp. 587-588.

Grab, M.; Zürcher, B.; Maurer, H.; Greenhalgh, S. (2015): Seismic velocity structure of a fossilized Icelandic geothermal system: A combined laboratory and field study. Geothermics 57, pp. 84-94.

Gros, J.; Schmidt, M.; Dale, A. W.; Linke, P.; Vielstädte, L.; Bigalke, N.; Haeckel, M.; Wallmann, K.; Sommer, S. (2019): Simulating and Quantifying Multiple Natural Subsea CO_2 Seeps at Panarea Island (Aeolian Islands, Italy) as a Proxy for Potential Leakage from Subseabed Carbon Storage. Environmental Science & Technology 53 (17), pp. 10258-10268, DOI: 10.1021/acs.est.9b02131.

Gugliandolo, C.; Italiano, F.; Maugeri, T. (2006): The submarine hydrothermal system of Panarea (Southern Italy): biogeochemical processes at the thermal fluids-sea bottom interface. Annals of Geophysics 49(2/3), pp. 783-792.

Gugliandolo, C.; Lentini, V.; Bunk, B.; Overmann, J.; Italiano, F.; Maugeri, T. L. (2015): Changes in prokaryotic community composition accompanying a pronounced temperature shift of a shallow marine thermal brine pool (Panarea Island, Italy). Extremophiles 19, pp. 547-559. DOI: 10.1007/s00792-015-0737-2.

Guilini, K.; Weber, M.; de Beer, D.; Schneider, M.; Molari, M.; Lott, C.; Bodnar, W.; Mascart, T.; De Troch, M.; Vanreusel, A. (2017): Response of Posidonia oceanica seagrass and its epibiont communities to ocean acidification. Plos one 12(8): e0181531. DOI: 10.1371/journal.pone.0181531

Hamel, M. (2010): Investigation and modelling of the geochemical processes in the hydrothermal system of Panarea, Italy. Diploma Thesis. TU Bergakademie Freiberg - Institute of Geology, Chair of Hydrogeology. FOG 25.

Hannington, M. D.; de Ronde, C. E. J.; Petersen, S. (2005): Sea-Floor Tectonics and Submarine Hydrothermal Systems. Economic Geology 100th Anniversary Volume. Society of Economic Geologists, Littelton, Colorado, USA, pp. 111-141.

Hannington, M.; Jamieson, J.; Monecke, T.; Petersen, S.; Beaulieu, S. (2011): The abundance of seafloor massive sulfide deposits. Geology 39 (12), pp. 1155-1158, DOI: 10.1130/G32468.1.

Hannington, M.; Petersen, S.; Krätschell A. (2017): Subsea mining moves closer to shore. Nature Geoscience 10, pp. 158-159, DOI: 10.1038/ngeo2897.

Heinicke, J.; Italiano, F.; Maugeri, R.; Merkel, B.; Pohl, T.; Schipek, M.; Braun, T. (2009): Evidence of tectonic control on active arc volcanism: The Panarea-Stromboli tectonic link inferred by submarine hydrothermal vents monitoring (Aeolian arc, Italy). Geophysical Research Letters 36(4), L04301, pp. 1-6. DOI: 10.1029/2008GL036664.

Heinicke, J.; Italiano, F.; Maugeri, R.; Merkel, B.; Pohl. T.; Schipek, M. (2010): Long-term Submarine Gas Flow Continuous Monitoring at Panarea (Aeolian Islands, Italy): Preliminary Results of the September 2008 – September 2010 Monitoring Period (2010). In: Italiano, F. (ed) (2010): Second international workshop on research in shallow marine and freshwater systems. Palermo, pp. 39-40.

Hekinian, R.; Fevrier, M.; Bischoff, J. L.; Picot, P.; Shanks, W. C. III (1980): Sulfide deposits from the East Pacific rise near 21°N: A mineralogical study. Science 207, pp. 1433-1444.

Heubeck, C. (2009): An early ecosystem of Archean tidal microbial mats (Moodies Group, South Africa, ca. 3.2 Ga). Geology 37(10), pp. 931-934.

Humphris, S. E.; Herzig, P. M.; Miller, D. J.; Alt, J. C.; Becker, K.; Brown, D.; Bruegmann, G.; Chiba, H.; Fouquet, Y.; Gemmell, J. B.; Guerin, G.; Hannington, M. D.; Holm, N. G.; Honnorez, J. J.; Iturrino, G. J.; Knott, R.; Ludwig, R.; Nakamura, K.; Petersen, S.; Reysenbach, A. L.; Rona, P. A.; Smith, S.; Sturz, A. A.; Tivey, M. K.; Zhao, X. (1995): The internal structure of an active sea-floor massive sulphide deposit. Nature 377, pp. 713-716.

Ingrassia, M.; Beaubien, S.; Bosman, A.; Chiocci, F.L.; Conte, A. M; Di Bella, L.; Frezza, V.; Graziani, S.; Italiano, F.; Macelloni, L.; Martorelli, E.; Sposato A. (2020): Il sistema idrotermale sottomarino a largo dell'Isola di Zannone (Arcipelago Pontino occidentale, Mar Tirreno). Memorie descrittive della Carta Geologica d'Italia 105, pp. 51-54.

Italiano, F. & Nuccio, P. M. (1991): Geochemical investigations of submarine volcanic exhalations to the east of Panarea, Aeolian Islands, Italy. Journal of Volcanology and Geothermal Research 46, pp. 125-141.

Italiano, F. (2009): Hydrothermal fluids vented at shallow depths at the Aeolian islands: relationships with volcanic and geothermal systems. In: Merkel, B. J. & Schipek, M. (eds) (2009): Research in Shallow Marine and Freshwater Systems. 1st International Workshop - Proceedings, FOG 22, pp. 55-60.

Italiano, F. (ed) (2010): Second international workshop on research in shallow marine and freshwater systems. Instituto Nazional di Geofisica e Vulcanologia. Palermo, pp. 90.

Italiano, F.; Romano, D.; Caruso, C.; Longo, M.; Corbo, A.; Lazzaro, G. (2019): Magmatic Signature in Submarine Hydrothermal Fluids Vented Offshore Ventotene and Zannone Islands (Pontine Archipelago, Central Italy). Geofluids, DOI: 10.1155/2019/8759609.

Joseph, E. P.; Fournier, N.; Lindsay, J. M.; Fischer, T. P. (2011): Gas and water geochemistry of geothermal systems in Dominica, Lesser Antilles island arc. Journal of Volcanology and Geothermal Research 206(1-2), pp. 1-14.

Jogler, C.; Wiegand, S.; Boedeker, C.; Heuer, A.; Peeters, S. H.; Jogler, M.; Jetten, M. S. M.; Rohde, M.; Kallscheuer, N. (2020): Tautonia plasticadhaerens sp. nov., a novel species in the family Isosphaeraceae isolated from an alga in a hydrothermal area of the Eolian Archipelago. Antonie van Leeuwenhoek. DOI: 10.1007/s10482-020-01424-3

Juniper, K. S. & Tebo, B. M. (1995): Microbe-Metal Interactions and Mineral Deposition at Hydrothermal Vents. In: Karl, D. M. (ed) (1995): The microbiology of deep-sea hydrothermal vents. Boca Raton: CRC Press. p. 299.

Kakuk, F. (2014): Characterization of the sediment on the location of La Calcara (Panarea, Aeolian Islands) with the priority on precipitates in the sediment. Bachelor's Thesis. TU Bergakademie Freiberg - Institute of Geology, Chair of Hydrogeology, unpublished.

Kakuk, F. (2016): Entstehung der Präzipitate im Geothermalgebiet La Calcara (Panarea, Italien). Master's Thesis. TU Bergakademie Freiberg - Institute of Geology, Chair of Hydrogeology, unpublished.

Kallscheuer, N.; Wiegand, S.; Heuer, A.; Rensink, S.; Boersma, A. S.; Jogler, M.; Boedeker, C.; Peeters, S. H.; Rast, P.; Jetten, M. S. M.; Rohde, M.; Jogler, C. (2020): Blastopirellula retiformator sp. nov. isolated from the shallow-sea hydrothermal vent system close to Panarea Island. Antonie van Leeuwenhoek. DOI: 10.1007/s10482-019-01377-2.

Karageorgis, A.; Anagnostou, C.; Sioulas, A.; Chronis, G.; Papathanassiou, E. (1998): Sediment geochemistry and mineralogy in Milos bay, SW Kyklades, Aegean Sea, Greece. Journal of Marine Systems 16, pp. 269-281.

Karl, D. M. (ed) (1995a): The microbiology of deep-sea hydrothermal vents. Boca Raton: CRC Press. p. 299.

Karl, D. M. (1995b): Ecology of Free-Living, Hydrothermal Vent Microbial Communities. In: Karl, D. M. (eds) (1995a): The microbiology of deep-sea hydrothermal vents. Boca Raton: CRC Press, pp. 35-124.

Kelly, D. S.; Karson, J. A.; Früh-Green, G. L.; Yoerger, D. R. (2005): A Serpentinite-Hosted Ecosystem: The Lost City Hydrothermal Field. Science 307(5714), pp. 1428-1434.

Kelly, D. S.; Früh-Green, G. L.; Karson, J. A.; Ludwig, K. A. (2007): The Lost City Hydrothermal Field Revisited. Oceanography 20(4), pp. 90-99.

Khimasia, A.; Rovere, A.; Pichler, T. (2020): Hydrothermal areas, microbial mats and sea grass in Paleochori Bay, Milos, Greece, Journal of Maps, 16:2, pp. 348-356, DOI: 10.1080/17445647.2020.1748131

Kiel, S. (ed) (2010): The vent and seep biota: aspects from microbes to ecosystems, Bd. 33. Heidelberg, London, New York: Springer.

Kiel, S. & Tyler, P. A. (2010): Chemosynthetically driven ecosystems in the deep-sea. In: Kiel, S. (ed) (2010): The vent and seep biota. From microbes to ecosystems, Bd. 33. Heidelberg, London, New York: Springer, pp. 1-15.

Koschinsky, A.; Seifert, R.; Knappe, A.; Schmidt, K.; Halbach, P. (2007): Hydrothermal fluid emanations from the submarine Kick'em Jenny volcano, Lesser Antilles island arc. Marine Geology 244(1-4), pp. 129-141.

Krumbein, W. E.; Buchholz, H.; Franke, P.; Giani, D.; Giele, C.; Wonneberger, K. (1979): O_2 and H_2S Coexistence in Stromatolites. Naturwissenschaften 66, pp. 381-389.

Krumbein, W. E. (2008): Biogenerated Rock Structures. In: Space Science Reviews 135(1-4), pp. 81-94.

Kürzinger, V. (2019): Determination and Differentiation of the Hydrothermal Precipitates of Panarea, Italy. Master's Thesis. TU Bergakademie Freiberg - Institute of Geology, FOG 54, pp. 90.

Lauritano, C.; Ruocco, M.; Dattolo, E.; Buia, M. C.; Silva, J.; Santos, R.; Olivé, I.; Costa, M. M.; Procaccini, G. (2015): Response of key stress-related genes of the seagrass Posidonia oceanica in the vicinity of submarine volcanic vents. Biogeosciences 12, pp. 4185-4194, DOI: 10.5194/bg-12-4185-2015.

Le Bris, N. & Gaill, F. (2010): Microbial Habitats Associated with Deep-Sea Hydrothermal Vents Invertebrates: Insights from Microanalysis and Geochemical Modelling. In: Kiel, S. (ed) (2010): The vent and seep biota. From microbes to ecosystems, Bd. 33. Heidelberg, London, New York: Springer, pp. 51-72.

Lentini, V.; Gugliandolo, C.; Bunk, B.; Overmann, J.; Maugeri, T. L. (2014): Diversity of Prokaryotic Community at a Shallow Marine Hydrothermal Site Elucidated by Illumina Sequencing Technology. Current Microbiology 69, pp. 457-466, DOI 10.1007/s00284-014-0609-5.

Li, J.; White, P.; Roche, B.; Bull, J.; Davis, J.; Leighton, T.; Deponte, M.; Gordini, E.; Cotterle, D. (2019): Natural seabed gas leakage - variability imposed by tidal cycles. Conference IEEE OCEANS 2019 MTS/IEEE Seattle, US (27-31 October 2019), pp. 1-6, DOI: 10.23919/OCEANS40490.2019.8962746.

Liakopoulos, A.; Katerinopoulos, A.; Markopoulos, T.; Boulegue, J. (1991): A mineralogical, petrographic and geochemical study of samples from wells in the geothermal field of Milos Island (Greece). Geothermics 20(4), pp. 237-256.

Losito, R. (1989): Stratigrafia, caratteri deposizionali e aree sorgente dei tufi bruni delle Isole Eolie. PhD thesis, University of Bari, unpublished. 85 p.

Lucchi, F.; Tranne, C. A.; Calanchi, N.; Rossi, P. L.; Keller, J. (2007a): The stratigraphic role of marine deposits in the geological evolution of the Panarea volcano (Aeolian Islands, Italy). Journal of the Geological Society, London 164, pp. 983-996.

Lucchi, F.; Tranne, C. A.; Calanchi, N.; Rossi, P. L. (2007b): Late Quaternary deformation history of the volcanic edifice of Panarea, Aeolian Arc, Italy. Bulletin of Volcanology 69 (3), pp. 239-257. DOI: 10.1007/s00445-006-0070-9

Lucchi, F.; Tranne, C. A.; De Astis, G.; Keller, J.; Losito, R.; Morche, W. (2008): Stratigraphy and significance of Brown Tuffs on the Aeolian Islands (southern Italy). Journal of Volcanology and Geothermal Research 177(1), pp. 49-70. DOI: 10.1016/j.jvolgeores.2007.11.006.

Lucchi, F.; Peccerillo, A.; Keller, J.; Tranne, C. A.; Rossi, P. L. (eds) (2013a): The Aeolian Islands Volcanoes. Geological Society, London, Memoirs 37, pp. 510. DOI: 10.1144/M37.1.

Lucchi, F.; Tranne, C. A.; Peccerillo, A.; Keller, J.; Rossi, P. L. (2013b): Geological history of the Panarea volcanic group (eastern Aeolian archipelago). In: Lucchi, F.; Peccerillo, A.; Keller, J.; Tranne, C. A.; Rossi, P. L. (eds) (2013a): The Aeolian Islands Volcanoes. Geological Society, London, Memoirs 37, pp. 351-395. DOI: 10.1144/M37.12.

Lüdmann, T. & Wong, H. K. (2003): Characteristics of gas hydrate occurrences associated with mud diapirism and gas escape structures in the northwestern Sea of Okhotsk. Marine Geology 201(4), pp. 269-286.

Marani, M.P.; Gamberi, F.; Savelli, C. (1997): Shallow-water polymetallic sulfide deposits in the Aeolian island arc. Geology 25 (9), pp. 815-818.

Marini, L.; Gambardella, B.; Principe, C.; Arias, A.; Brombach, T.; Hunziker, J. C. (2002): Characterization of magmatic sulfur in the Aegean island arc by means of the $\delta^{34}S$ values of fumarolic H_2S, elemental S, and hydrothermal gypsum from Nisyros and Milos islands. Earth and Planetary Science Letters 200, pp. 15-31.

Martorelli, E.; Italiano, F.; Ingrassia, M.; Macelloni, L.; Bosman, A.; Conte, A. M.; Beaubien, S. E.; Graziani, S.; Sposato, A.; Chiocci, F. L. (2016): Evidence of a shallow water submarine hydrothermal field off Zannone Island from morphological and geochemical characterization: Implications for Tyrrhenian Sea Quaternary volcanism. Journal of Geophysical Research: Solid Earth 121 (12), pp. 8396-8414, DOI: 10.1002/2016JB013103.

McCarthy, K. T.; Pichler, T.; Price, R. E. (2005): Geochemistry of Champagne Hot Springs shallow hydrothermal vent field and associated sediments, Dominica, Lesser Antilles. Chemical Geology 224(1-3), pp. 55-68.

McDonough, W. F. & Sun, S. (1995): The composition of the Earth. Chemical Geology 120, pp. 223-253.

McLoughlin, N.; Staudigel, H.; Furnes, H.; Eickmann, B.; Ivarsson, M. (2010): Mechanisms of microtunneling in rock substrates: distinguishing endolithic biosignatures from abiotic microtunnels. Geobiology 8(4), pp. 245-255.

Meinardus, F. (2016): Chemical investigations of groundwater and submarine hydrothermal fluid exhalations at Panarea, Italy. Master's Thesis. TU Bergakademie Freiberg - Institute of Geology. FOG 48, pp. 161.

Merkel, B. J. & Schipek, M. (eds) (2009): Research in Shallow Marine and Freshwater Systems. 1st International Workshop - Proceedings, TU Bergakademie Freiberg, Institute of Geology, Chair of Hydrogeology. FOG 22, pp. 143.

Merkel, B. J.; Kummer, N. S.; Planer-Friedrich, B.; Pohl, T.; Schipek, M. (2011): Development of a gas sampling technique for determining trace elements in submarine volcanic exhalations. Procedia Earth and Planetary Science 4, pp. 50-56.

Molari, M.; Guilini, K.; Lins, L.; Ramette, A.; Vanreusel, A. (2019): CO_2 leakage can cause loss of benthic biodiversity in submarine sands. Marine Environmental Research 144, pp. 213-229. DOI: 10.1016/j.marenvres.2019.01.006.

Monecke, T.; Petersen, S.; Hannington, M.; D.; Anzidei, M.; Esposito, A.; Giordano, G.; Garbe-Schönberg, D.; Augustin, N.; Melchert, B.; Hocking, M. (2012): Explosion craters associated with shallow submarine gas venting off Panarea island, Italy. Bulletin of Volcanology 74, pp. 1937-1944, DOI: 10.1007/s00445-012-0651-8.

Monecke, T.; Petersen, S.; Hannington, M. D. (2014): Constraints on Water Depth of Massive Sulfide Formation: Evidence from Modern Seafloor Hydrothermal Systems in Arc-Related Settings. Economic Geology 109 (8), pp. 2079-2101, DOI: 10.2113/econgeo.109.8.2079.

Müller, C. (2011): Geothermal state of shallow submarine geothermal systems and isotopic signatures of Panarea, Aeolian Islands (Italy). Diploma Thesis. TU Bergakademie Freiberg - Institute of Geology. FOG 30, pp. 154.

Naden, J.; Kilias, S. P.; Leng, M. J.; Cheliotis, I.; Shepherd, T. J. (2003): Do fluid inclusions preserve $\delta^{18}O$ values of hydrothermal fluids in epithermal systems over geological time? Evidence from paleo- and modern geothermal systems, Milos island, Aegean Sea. Chemical Geology 197(1-4), pp. 143-159.

Naden, J.; Kilias, S. P.; Darbyshire, D. P. F. (2005): Active geothermal systems with entrained seawater as modern analogs for transitional volcanic-hosted massive sulfide and continental magmato-hydrothermal mineralization: The example of Milos Island, Greece. Geology 33(7), pp. 541-544.

Nelson, D. C. & Fisher, C. R. (1995): Chemoautotrophic and Methanoautotrophic Endosymbiontic Bacteria at Deep-Sea. In: Karl, D. M. (ed) (1995): The microbiology of deep-sea hydrothermal vents. Boca Raton: CRC Press.

Noè, S.; Bellavia, C.; Calvo, S.; Mazzola, A.; Pirrotta, M.; Sciandra, M.; Vizzini, S.; Tomasello, A. (2020): Resilience of the seagrass Posidonia oceanica following pulse-type disturbance. Marine Environmental Research 159, DOI: 10.1016/j.marenvres.2020.105011.

Noffke, N. & Krumbein, W. E. (1999): A quantitative approach to sedimentary surface structures contoured by the interplay of microbial colonization and physical dynamics. Sedimentology 46, pp. 417-426.

Noffke, N. (2000): Extensive microbial mats and their influences on the erosional and depositional dynamics of a siliciclastic cold-water environment (Lower Arenigian, Montange Noire, France). Sedimentary Geology 136, pp. 207-215.

Noffke, N.; Gerdes, G.; Klenke, T.; Krumbein, W. E. (2001a): Microbially induced sedimentary structures - A new category within the classification of primary sedimentary structures. Journal of Sedimentary Research 71, pp. 649-656.

Noffke, N.; Gerdes, G.; Klenke, T.; Krumbein, W. E. (2001b): Microbially Induced Sedimentary Structures Indicating Climatological, Hydrological and Depositional Conditions within Recent and Pleistocene Coastal Facies Zones (Southern Tunisia). Facies 44, pp. 23-30.

Noffke, N. & Knoll, A. (2002): Sedimentary Controls on the Formation and Preservation of Microbial Mats in Siliciclastic Deposits: A Case Study from the Upper Neoproterozoic Nama Group, Namibia. Palaios 17, pp. 533-544.

Noffke, N.; Hazen, R.; Nhleko, N. (2003a): Earth's earliest microbial mats in a siliciclastic marine environment (2.9 Ga Mozaan Group, South Africa). Geology 31, pp. 673-676.

Noffke, N.; Gerdes, G.; Klenke, T. (2003b): Benthic cyanobacteria and their influence on the sedimentary dynamics of peritidal depositional systems (siliciclastic, evaporitic salty, and evaporitic carbonatic). Earth-Science Reviews 62(1-2), pp. 163-176.

Noffke, N.; Eriksson, K. A.; Hazen, R. M.; Simpson, E. L. (2006a): A new window into Early Archean life: Microbial mats in Earth's oldest siliciclastic tidal deposits (3.2 Ga Moodies Group, South Africa). Geology 34(4), pp. 253-256.

Noffke, N.; Beukes, N.; Gutzmer, J.; Hazen, R. (2006b): Spatial and temporal distribution of microbially induced sedimentary structures: A case study from siliciclastic storm deposits of the 2.9Ga Witwatersrand Supergroup, South Africa. Precambrian Research 146(1-2), pp. 35-44.

Noffke, N. (2007): Microbially induced sedimentary structures in Archean sandstones: A new window into early life. Gondwana Research 11(3), pp. 336-342.

Noffke, N. & Paterson, D. (2008): Microbial interactions with physical sediment dynamics, and their significance for the interpretation of Earth's biological history. Geobiology 6(1), pp. 1-4.

Noffke, N. (2009): The criteria for the biogeneicity of microbially induced sedimentary structures (MISS) in Archean and younger, sandy deposits. Earth-Science Reviews 96(3), pp. 173-180.

Noffke, N. (2010): Geobiology: Microbial mats in sandy deposits from the Archean era to today. Berlin, Heidelberg: Springer Berlin Heidelberg, p.200.

Norton, D. L. (1984): Theory of Hydrothermal Systems. Earth and Planetary Science 12, pp. 155-177.

Norton, D. L. & Dutrow, B. L. (2001): Complex behavior of magmahydrothermal processes: role of supercritical fluid. Geochimica et Cosmochimica Acta 65, pp. 4009–4017.

Okrusch, M.; Matthes, S. (2005): Mineralogie - Eine Einführung in die spezielle Mineralogie, Petrologie und Lagerstättenkunde. 7. edition, Springer, Berlin, Heidelberg, New York, p. 526.

Ordrusch, A. (2016): Field Report – Scientific Diving Excursion Panarea 2016. TU Bergakademie Freiberg, Scientific Diving Center, unpublished.

Pansini, M.; Morri, C.; Bianchi, C. N. (2000): The Sponge Community of a Subtidal Area with Hydrothermal Vents: Milos Island, Aegean Sea. Estuarine, Coastal and Shelf Science 51(5), pp. 627-635.

Peccerillo, A.; De Astis, G.; Faraone, D.; Forni, F.; Frezzotti, M. L. (2013): Compositional variations of magmas in the Aeolian arc: implications for petrogenesis and geodynamics. In: Lucchi, F.; Peccerillo, A.; Keller, J.; Tranne, C. A.; Rossi, P. L. (eds) (2013a): The Aeolian Islands Volcanoes. Geological Society, London, Memoirs 37, pp. 491-510. DOI: 10.1144/M37.15.

Peccerillo, A. (2017): Cenozoic Volcanism in the Tyrrhenian Sea Region. Advances in Volcanology, Springer. DOI: 10.1007/978-3-319-42491-0_1.

Peckmann, J.; Walliser, O. H.; Riegel, W.; Reitner, J. (1999): Signatures of Hydrocarbon Venting in a Middle Devonian Carbonate Mound (Hollard Mound) at the Hamar Laghdad (Antiatlas, Morocco). Facies 40(1), pp. 281-296.

Penninio, V.; Sulli, A.; Caracausi, A.; Grassa, F.; Interbartolo, F. (2014): Fluid escape structures in the north Sicily continental margin. Marine and Petroleum Geology 55, pp. 202-213. DOI: 10.1016/j.marpetgeo.2014.02.007.

Pepe, F.; Bertotti, G.; Cella, F.; Marsella, E. (2000): Rifted margins formation in the Southern Tyrrhenian Sea: A high-resolution seismic profile across the north Sicily continental margin. Tectonics 19, pp. 241-257.

Peters, M.; Strauss, H.; Petersen, S.; Kummer, N. A.; Thomazo, C. (2011): Hydrothermalism in the Tyrrhenian Sea: Inorganic and microbial sulfur cycling as revealed by geochemical and multiple sulfur isotope data. Chemical Geology 280(1-2), pp. 217-231.

Petersen, S.; Herzig, P. M.; Hannington, M. D. (2000): Third dimension of a presently forming VMS deposit: TAG hydrothermal mound, Mid-Atlantic Ridge, 26 °N. Mineralium Deposita 35, pp. 233-259, DOI: 10.1007/s001260050018.

Petersen, S. & Monecke, T. (2009): FS Meteor, Cruise Report M73/2: Shallow drilling of hydrothermal sites in the Tyrrhenian Sea (PALINDRILL), Genoa – Heraklion 14.08.2007 – 30.08.2007, 30, 10-14 & 43.

Petersen, S.; Monecke, T.; Westhues, A.; Hannington, M. D.; Gemmell, J. B.; Sharpe, R.; Peters, M.; Strauss, H.; Lackschewitz, K.; Augustin, N.; Gibson, H.; Kleeberg, R. (2014): Drilling Shallow-Water Massive Sulfides at the Palinuro Volcanic Complex, Aeolian Island Arc, Italy. Economic Geology 109 (8), pp. 2129-2157, DOI: 10.2113/econgeo.109.8.2129.

Petersen, S.; Krätschell, A.; Augustin, N.; Jamieson, J.; Hein, J. R.; Hannington, M. D. (2016): News from the seabed – Geological characteristics and resource potential of deep-sea mineral resources. Marine Policy 70, pp. 175-187.

Petersen, S.; Lehrmann, B.; Murton, B. J. (2018): Modern Seafloor Hydrothermal Systems: New Perspectives on Ancient Ore-Forming Processes. Elements 14, pp. 307-312.

Pohl, T.; Becke, R.; Ganß, R.; Stanulla, R.; Merkel, B. (2010): Small Scale Recent Sulfide Mineralization in a Shallow Submarine Environment. In: Italiano, F. (ed) (2010): Second international workshop on research in shallow marine and freshwater systems. Palermo, pp. 64-66.

Ponepal, M.; Barth, G.; Fütterer, W.; Schipek, M.; Merkel, B. J. (2010): Discharge Measuring of Massive Gas Emissions at Panarea, Italy. In: Italiano, F. (ed) (2010): Second international workshop on research in shallow marine and freshwater systems. Palermo, pp. 66-71.

Ponepal, M. (2011): Konstruktion und Test einer Volumenstrommessanlage für submarine Gasaustritte sowie deren Ertüchtigung für Langzeitmessungen. Student research project. TU Bergakademie Freiberg - Institute of Mechanical Engineering, unpublished.

Prautzsch, A. (2012): Geochemical-mineralogical investigation of degassing structures caused by recent volcanic hydrothermalism; Case study: La Calcara at Panarea, Aeolian islands (Italy). Bachelor's Thesis. TU Bergakademie Freiberg - Institute of Geology, Chair of Hydrogeology, unpublished.

Price, R. E.; Savov, I.; Planer-Friedrich, B.; Bühring, S. I.; Amend, J.; Pichler, T. (2013a): Processes influencing extreme As enrichment in shallow-sea hydrothermal fluids of Milos Island, Greece. Chemical Geology 348, pp. 15-26, DOI: 10.1016/j.chemgeo.2012.06.007.

Price, R.; Lesniewski, R.; Nitzsche, K.; Meyerdierks, A.; Saltikov, C.; Pichler, T.; Amend, J. (2013b): Archaeal and bacterial diversity in an arsenic-rich shallow-sea hydrothermal system undergoing phase separation. Frontiers in Microbiology 4, DOI: 10.3389/fmicb.2013.00158.

Price, R. E.; LaRowe, D. E.; Italiano, F.; Savov, I.; Pichler, T.; Amend, J. P. (2015): Subsurface hydrothermal processes and the bioenergetics of chemolithoautotrophy at the shallow-sea vents off Panarea Island (Italy). Chemical Geology 407-408, pp. 21-45, DOI: 10.1016/j.chemgeo.2015.04.011.

Rößler, R.; Annacker, V.; Kretzschmar, R.; Mehlhorn, S. (2009): Auf Schatzsuche in Chemnitz - Wissenschaftliche Grabungen `09. Veröffentlichungen des Museums für Naturkunde Chemnitz 32, pp. 25-46.

Reitner, J. & Thiel, V. (eds) (2011): Encyclopedia of geobiology. Dordrecht: Springer, pp. 943.

Romano, D.; Gattuso, A.; Longo, M.; Caruso, C.; Lazzaro, G.; Corbo, A.; Italiano, F. (2019): Hazard Scenarios Related to Submarine Volcanic-Hydrothermal Activity and Advanced Monitoring Strategies: A Study Case from the Panarea Volcanic Group (Aeolian Islands, Italy). Geofluids. DOI: 10.1155/2019/8728720

Romagnoli, C.; Casalbore, D.; Bosman, A.; Braga, R.; Chiocci, F. L. (2013): Submarine structure of Vulcano volcano (Aeolian Islands) revealed by high-resolution bathymetry and seismo-acoustic data. Marine Geology 338, pp. 30-45. DOI: 10.1016/j.margeo.2012.12.002.

Sandargo, B.; Jeske, O.; Boedeker, C.; Wiegand, S.; Wennrich, J.-P., Kallscheuer, N.; Jogler, M.; Rohde, M.; Jogler, C.; Surup, F. (2020): Stieleriacines, N-Acyl Dehydrotyrosines From the Marine Planctomycete Stieleria neptunia sp. nov. Frontiers in Microbiology 11, DOI: 10.3389/fmicb.2020.01408.

Savelli, C.; Marani, M.; Gamberi, F. (1999): Geochemistry of metalliferous, hydrothermal deposits in the Aeolian arc (Tyrrhenian Sea). Journal of Volcanology and Geothermal Research 88, pp. 305-323.

Schieber, J. (1998): Possible indicators of microbial mat deposits in shales and sandstones: examples from the Mid-Proterozoic Belt Supergroup, Montana, USA. Sedimentary Geology 120, pp. 105-124.

Schieber, J.; Bose, P.K.; Eriksson, P.G.; Banerjee, S.; Sarkar, S.; Altermann, W.; Catuneau, O. (eds) (2007): Atlas of microbial mat features preserved within the Siliciclastic rock record. Amsterdam: Elsevier. pp.288

Schipek, M. & Merkel, B. J. (2011): Continuous monitoring of dissolved CO_2 and H_2S: Technical application in the submarine hydrothermal system of Panarea, Italy. Procedia Earth and Planetary Science 4, pp. 74-79.

Seebauer, L. (2015): Seegraswiesen (Posidonia oceanica) bei Panarea (Äolische Inseln, Italien) – Vegetationsstruktur und der Einfluss von Gas- und Fluidaustritten. Master's Thesis. TU Bergakademie Freiberg - Institute of Biosciences, unpublished.

Serpelloni, E.; Vannucci, G.; Pondrelli, S.; Argnani, A.; Casula, G.; Anzidei, M.; Baldi, P.; Gasperini, P. (2007): Kinematics of the Western Africa-Eurasia plate boundary from focal mechanisms and GPS data. Geophysical Journal International 169(3), pp. 1180-1200. DOI: 10.1111/j.1365-246X.2007.03367.x.

Seyfried, W. E. Jr. & Mottl, M. J. (1995): Geological Setting and Chemistry of Deep-Sea Hydrothermal Vents. In: Karl, D. M. (ed) (1995): The microbiology of deep-sea hydrothermal vents. Boca Raton: CRC Press, pp. 1-34.

Shakirov, R.; Obzhirov, A.; Suess, E.; Salyuk, A.; Biebow, N. (2004): Mud volcanoes and gas vents in the Okhotsk Sea area. In: Geo-Marine Letters 24(3), pp.140-149.

Shanks, W. C. III & Bischoff, J. L. (1980): Geochemistry, sulfur isotope composition, and accumulation rates of Red Sea geothermal deposits. Econ Geology 74, pp. 445-459.

Shanks, W. C. III (2019): Stable isotopes in seafloor hydrothermal systems: Vent fluids, hydrothermal deposits, hydrothermal alteration, and microbial processes. Mineralogy and Geochemistry 43(1), pp. 469-525.

Sieland, R. (2009): Chemical and isotopic investigations of submarine hydrothermal fluid discharges from Panarea, Aeolian Islands, Italy. Diploma Thesis. TU Bergakademie Freiberg - Institute of Geology. FOG 21.

Sievert, S. M. (1999): Microbial communities at a shallow submarine hydrothermal vent in the Aegean Sea (Milos, Greece). Dissertation. Universität Bremen.

Sigurdsson, H.; Houghton, B. F.; McNutt, S. R.; Rymer, H.; Stix, J. (eds) (2000): Encyclopedia of Volcanoes. Academic Press, San Diego, California, p. 1417.

Spiess F. N.; Macdonald, K. C.; Atwater, T; Ballard, R.; Carranza, A.; Cordoba, D.; Cox, C.; Garcia, V. M.; Francheteau, J.; Guerrero, J.; Hawkins, J.; Haymon, R.; Hessler, R.; Juteau, T.; Kastner, M.; Larson, R.; Luyendyk, B.; Macdougall, J. D.; Miller, S.; Normark, W.; Orcutt, J.; Rangin, C. (1980): East Pacific Rise: Hot springs and geophysical experiments. Science 207(4438), pp. 1421-1432.

Spagnoli, F.; Andaloro, F.; Canese, S.; Capaccioni, B.; Esposito, V.; Giordano, P.; Romeo, T.; Bortoluzzi, G. (2019): Nuove recenti conoscenze sul sistema idrotermale del complesso vulcanico dell'Isola di Panarea (Arcipelago delle Eolie, Mar Tirreno Meridionale). Memorie descrittive della Carta Geologica d'Italia 105, pp. 85-90.

Stanulla, R. (2012): Geological record of submarine hydrothermal gas and water escape structures – morphology and geochemistry of the recent volcanic system of Panarea, Italy. Master's Thesis. TU Bergakademie Freiberg - Institute of Geology, Chair of Hydrogeology, unpublished.

Stanulla, R.; Barth, G.; Ganß, R.; Reich, M.; Merkel, B. (2016): Development of a mobile airlift pump for Scientific Divers and its application in sedimentological underwater research. Underwater Technology, 34(1), pp. 39-43. DOI: 10.3723/ut.34.039.

Stanulla, R.; Pohl, T.; Müller, C.; Merkel, B. (2017a): Geological record of (sub-) recent gas- and water escape structures in the shallow marine hydrothermal system of Panarea, Italy. Environmental Earth Sciences 76, pp. 404-430. DOI: 10.1007/s12665-017-6714-6.

Stanulla, R.; Stanulla, C.; Pohl, T.; Merkel, B. (2017b): Structural and mineralogical study of active hydrothermal fluid discharges at Strýtan hydrothermal chimney, Akureyri Bay, Eyjafjörður region, Iceland. Geothermal Energy 5, pp. 8-19. DOI: 10.1186/s40517-017-0065-0.

Stanulla, R.; Kakuk, F.; Pohl, T.; Merkel, B. (2017c): Geochemical and mineralogical investigations on hydrothermal lithologies in La Calcara, Panarea Island, Italy. 3rd European Conference on Scientific Diving, Funchal, Portugal, March 2017.

Steinbrückner, D. (2009): Quantification of submarine degassing of Panarea Volcano in the Aeolian archipelago, Italy. Diploma Thesis. TU Bergakademie Freiberg - Institute of Geology. FOG 23, pp. 126.

Stewart, A. L. & McPhie, J. (2004): An Upper Pliocene coarse pumice breccia generated by a shallow submarine explosive eruption, Milos, Greece. Bulletin of Volcanology 66(1), pp. 15-28.

Stewart, A. L. & McPhie, J. (2006): Facies architecture and Late Pliocene – Pleistocene evolution of a felsic volcanic island, Milos, Greece. Bulletin of Volcanology 68(7-8), pp. 703-726.

Sur, S.; Schieber, J.; Banerjee, S. (2006): Petrographic observations suggestive of microbial mats from Rampur Shale and Bijaigarh Shale, Vindhyan basin, India. Journal of Earth System Science 115(1), pp. 61-66.

Tarasov, V. G.; Gebruk, A. V.; Mironov, A. N.; Moskalev, L. I. (2005): Deep-sea and shallow-water hydrothermal vent communities: Two different phenomena? Chemical Geology 224(1-3), pp. 5-39.

Tassi, F.; Capaccioni, B.; Caramanna, G.; Cinti, D.; Montegrossi, G.; Pizzino, L.; Quattrocchi, F.; Vaselli, O. (2009): Low-pH waters discharging from submarine vents at Panarea Island (Aeolian Islands, southern Italy) after the 2002 gas blast: Origin of hydrothermal fluids and implications for volcanic surveillance. Applied Geochemistry 24, pp. 246-254.

Tassi, F.; Capaccioni, B.; Vaselli, O. (2014): Compositional spatial zonation and 2005–2013 temporal evolution of the hydrothermal-magmatic fluids from the submarine fumarolic field at Panarea Island (Aeolian Archipelago, southern Italy). Journal of Volcanology and Geothermal Research 277, pp.41–50, DOI: 10.1016/j.jvolgeores.2014.03.010.

Tinti, S.; Maramai, A.; Armigliato, A.; Graziani, L.; Manucci, A.; Pagnoni, G.; Zaniboni, F. (2005a): Observations of physical effects from tsunamis of December 30, 2002 at Stromboli volcano, southern Italy. Bull Volcanol 68, pp. 450-461.

Tinti, S.; Pagnoni, G.; Zaniboni, F. (2005b): The landslides and tsunamis of the 30th of December 2002 in Stromboli analysed through numerical simulations. Bull Volcanol 68, pp. 462-479.

Tivey, M. K. (1995): Modeling chimney growth and associated fluid flow at seafloor hydrothermal vent sites. In: karl, S. E.; Zierenberg, R. A.; Mullineaux, L. S.; Thomson, R. E. (eds) (1995): Seafloor Hydrothermal Systems: Physical, Chemical, Biological, and Geological Interactions. American Geophysical Union, Washington DC. Monograph Series 91, pp. 158-177. DOI: 10.1029/GM091p0158.

Tudino, T.; Aliani, S.; Bortoluzzi, G. (2013): Shallow water gaseohydrothermal plume studies after massive eruption at Panarea, Aeolian Islands, Italy. Journal of Marine Systems 131, pp. 1-9, DOI: 10.1016/j.jmarsys.2013.10.001.

Ugur, A.; Miquel, J. C.; Fowler, S. W.; Appleby, P. (2003): Radiometric dating of sediment cores from a hydrothermal vent zone off Milos Island in the Aegean Sea. The Science of the Total Environment 307, pp. 203-214.

Valsami-Jones, E.; Baltatzis, E.; Bailey, E. H.; Boyce, A. J.; Alexander, J. L.; Magganas, A.; Anderson, L.; Waldron, S.; Ragnarsdottir, K. V. (2005): The geochemistry of fluids from an active shallow submarine hydrothermal system: Milos island, Hellenic Volcanic Arc. Journal of Volcanology and Geothermal Research 148, pp. 130-151, DOI: 10.1016/j.jvolgeores.2005.03.018.

Varnavas, S. P. & Cronan, D. S. (2005): Submarine hydrothermal activity off Santorini and Milos in the Central Hellenic Volcanic Arc: A synthesis. Chemical Geology 224(1-3), pp. 40-54.

Ventura, G. (2013): Kinematics of the Aeolian volcanism (Southern Tyrrhenian Sea) from geophysical and geological data. In: Lucchi, F.; Peccerillo, A.; Keller, J.; Tranne, C. A.; Rossi, P. L. (eds) (2013a): The Aeolian Islands Volcanoes. Geological Society, London, Memoirs 37, pp. 3-11. DOI: 10.1144/M37.2.

Vizzini, S.; Tomasello, A.; Di Maida, G.; Pirrotta, M.; Mazzola, A.; Calvo, S. (2010): Effect of explosive shallow hydrothermal vents on $\delta^{13}C$ and growth performance in the seagrass Posidonia oceanica. Journal of Ecology 98, pp. 1284-1291. DOI: 10.1111/j.1365-2745.2010.01730.x.

Voltattorni, N.; Sciarra, A.; Caramanna, G.; Cinti, D.; Pizzino, L.; Quattrocchi, F. (2009): Gas geochemistry of natural analogues for the studies of geological CO_2 sequestration. In: Applied Geochemistry 24(7), pp. 1339-1346.

Von Damm, K. L. (1990): Seafloor hydrothermal activity: Black Smoker chemistry and chimneys. Annual Review of Earth and Planetary Sciences 18, pp. 173-204.

Vrijenhoek, R. C. (2010): Genetics and Evolution of Deep-Sea Chemosynthetic Bacteria and Their Invertebrate Host. In: Kiel, S. (ed) (2010): The vent and seep biota. From microbes to ecosystems, Bd. 33. Heidelberg, London, New York: Springer, pp. 15-50.

Walter, T. R.; Wang, R.; Acocella, V.; Neri, M.; Grosser, H.; Zschau, J. (2009): Simultaneous magma and gas eruptions at three volcanoes in southern Italy: An earthquake trigger? Geology 37(3), pp. 251-254.

White, D. E. (1964): Deep geothermal brine near Salton Sea, California. Bulletin Volcanologique 27(1), pp. 369-370.

Witte, K.; Wölfel, J.; Karsten, U. (2004): Das Vorkommen mikrobieller Matten an der deutschen Ostseeküste und die saisonale Sukzession in Mikrobenmatten am Beispiel des Windwatts "Großer Werder". Rostocker Meeresbiologische Beiträge 12, pp. 61-70.

Zierenberg, R. A.; Fouquet, Y.; Miller, D. J.; Bahr, J. M.; Baker, P. A.; Bjerkgard, T.; Brunner, C. A.; Duckworth, R. C.; Gable, R.; Gieskes, J. M.; Goodfellow, W. D.; Groeschel-Becker, H. M.; Guerin, G.; Ishibashi, J.; Iturrino, G. J.; James, R. H.; Lackschewitz, K. S.; Marquez, L. L.; Nehlig, P.; Peter, J. M.; Rigsby, C. A.; Schultheiss, P. J.; Shanks, W. C. III; Simoneit, B. R. T.; Summit, M.; Teagle, D. A. H.; Urbat, M.; Zuffa, G. G. (1998): The deep structure of a sea-floor hydrothermal deposit. Nature 392, pp. 485-488.

G. List of Figures

H. List of Tables

I. Appendices

I Photo documentation

II Video documentation

Appendices can be made available on request via science@geowid.de.